Nanoscale and Bio-inspired Communication Techniques for the Internet of Bio-Nano Things

by

Murat Kuşcu

A Dissertation Submitted to the
Graduate School of Sciences and Engineering
in Partial Fulfillment of the Requirements for
the Degree of

Doctor of Philosophy

in

Electrical and Electronics Engineering



November 2017

Nanoscale and Bio-inspired Communication Techniques for the Internet of Bio-Nano Things

Koç University

Graduate School of Sciences and Engineering

This is to certify that I have examined this copy of a doctoral dissertation by

Murat Kuşcu

and have found that it is complete and satisfactory in all respects,
and that any and all revisions required by the final
examining committee have been made.

Committee Members:

_____

Prof. Özgür B. Akan

_____

Prof. A. Murat Tekalp

_____

Prof. Fatih Alagöz

_____

Prof. Alper T. Erdoğan

_____

Assoc. Prof. Berk Canberk

Date: _____

To my parents Fikriye and Süreyya Kuşcu

ABSTRACT

Internet of Bio-Nano Things (IoBNT) is a novel ICT framework, in which nanomachines and biological entities, such as nanobiosensors, living cells, engineered bacteria, are connected with each other and with conventional macroscale networks to cooperatively perform sensing, actuation and processing. The framework has an enormous potential to transform the way we connect with and understand the world "at the bottom" by enabling new methods of interfering with the processes inside living organisms at the single-molecular level, and extending the human consciousness and control with bio-nano things collaboratively sensing and acting upon the environments never explored by any other paradigm before. Realization of IoBNT, however, demands novel engineering solutions to overcome unique challenges regarding miniaturization and connectivity subject to peculiarities of nanoscale-physics and limited capabilities of bio-nano things. These challenges call for novel approaches to devise solutions for a set of modeling, analysis and implementation problems on a highly interdisciplinary domain covering engineering, nanotechnology and biophysics.

This thesis is focused on the challenges regarding the physical layer of IoBNT. To this end, communication techniques that can enable high-speed and reliable wireless communication in nanonetworks and at the same time provide a seamless interface between the nanonetworks and the macroscale cyber networks are investigated. The first part of the thesis is concentrated on the use of fluorescent molecules, i.e., fluorophores, to enable wireless communication at nanoscale through a quantum mechanical phenomenon, which is Förster Resonance Energy Transfer (FRET). Communication and information theoretical models for FRET-based, graphene plasmon-assisted FRET-based and multi-step FRET-based propagation channels are developed. Accounting for the natural optical interface between the nanoscale and macroscale worlds pro-

vided by the intrinsic characteristics of fluorophores, the novel concept of Internet of Molecular Things is introduced to further extend the coverage of IoBNT with networks of sub-100nm primitive molecular devices, such as fluorophore-based molecular logic gates, sensors and actuators. Moreover, the first practical realization of a wireless nanoscale communication network is achieved with a network of single molecular fluorescent transceivers.

The second part is focused on molecular communications, which has been extensively studied from various aspects including channel and noise models. Different from the existing literature, the feasibility of designing a molecular receiver, in a physical domain other than synthetic biology, meeting the basic requirements of nanonetwork applications and also serving the needs of an electromagnetic nano-macro interface between the chemical domain of nanonetworks and the electrical domain of the cyber networks is thoroughly examined. Based on the advancements in the biosensing literature, Field Effect Transistor-based Biosensors (BioFETs) is proposed as the most viable solution to design a molecular receiver, which can transduce molecular messages into electrical signals. A communication theoretical model for Silicon Nanowire (SiNW) bioFET-based MC receiver is developed and the noise statistics at the receiver output is derived. The performance of this receiver is evaluated with common ICT metrics such as Signal to Noise Ratio (SNR), Symbol Error Probability (SEP) and information theoretical capacity.

ÖZETÇE

Biyo-Nano Nesnelerin İnterneti (BNNİ), nanobiyosensörler, biyolojik sensörler, canlı hücreler, sentetik bakteriler gibi nanomakinelerin ve biyolojik varlıkların birbirleriyle ve konvansiyonel haberleşme ağlarıyla kooperatif algılama, hesaplama gibi işlemleri gerçekleştirmek adına bağlantı kurmasıyla oluşturdukları ağları tanımlayan yeni bir bilişim ve iletişim teknolojisidir. BNNİ, canlı hücrelerin içindeki süreçlere tekil molekül seviyesinde hassasiyet ile müdahelenin ve daha önce hiçbir teknoloji ile temas edilememiş ortamlarda çalışabilen sensör ve aktör ağlarıyla insan bilincini ve kontrolünü geliştirmenin yolunu açmasıyla, nano boyutlardaki dünyayla iletişimizi ve onu anlama yöntemlerimizi dönüştürmek adına çok önemli bir potensiyele sahiptir. Ancak, BBNİ'nin pratik olarak gerçekleştirilebilmesi, nano boyutlardaki fizik kuralları ve bio-nano nesnelerin limitli yeteneklerine bağlı olarak ortaya çıkan yeni problemlerin aşılmasını gerektirmektedir. Bu problemlerin çözümü ise modelleme, analiz ve uygulama alanlarında yeni ve oldukça disiplinlerarası yaklaşımların üretilmesine ihtiyaç duymaktadır.

Bu tezde, BNNİ'nin önündeki fiziksel katman problemleri üzerine odaklanılmıştır. Bu amaçla, nano-haberleşme ağlarında yüksek hızlı ve güvenilir kablosuz bilgi aktarımını gerçekleştirebilen ve aynı zamanda nano ve makro ölçekli siber ağlar arasında kesintisiz bir arabirim sağlayabilen iletişim teknikleri araştırılmıştır. Tezin ilk bölümünde, nano-haberleşme ağlarında, kuantum mekanik bir fenomen olan Förster Rezonans Enerji Transferi ile kablosuz bilgi aktarımını sağlayabilmek adına flüoresan moleküllerin kullanımı üzerinde yoğunlaşılmıştır. FRET temelli, grafen plazmon destekli FRET temelli, ve çok kademeli FRET temelli haberleşme kanalları için haberleşme ve bilgi kuramsal modeller geliştirilmiştir. Bu çalışmanın bir diğer fazında, flüoresan moleküllerin özünde optik nano-makro arayüz olması temel alınarak, Mole-

küllerin İnterneti adında, BBNİ'nin kapsama yeteneğini 100nm ve daha küçük boyutlardaki basit moleküler aygıtların oluşturduğu jaberleşme ağlarını da kapsayacak şekilde genişleten yeni bir teknoloji tanıtılmıştır. Ayrıca, bu doğrultuda, flüoresan moleküllerin alıcı-verici olarak kullanılmasıyla, pratik olarak literatürde ilk kez kablosuz bir nano-haberleşme ağı deneysel olarak gösterilmiş ve analizleri gerçekleştirilmiştir.

Tezin ikinci bölümü, çeşitli kanal ve gürültü modelleri de dahil olmak üzere halihazırda çeşitli yönlerden kapsamlı olarak incelenmiş olan moleküler iletişim üzerine odaklanmıştır. Mevcut literatürden farklı olarak, nano-haberleşme uygulamalarının temel gereksinimlerini ve moleküler nano-haberleşme ağları ile konvensiyonel elektromanyetik makro-ağlar arasında arayüz işlevi görebilecek yetenekte bir moleküler alıcı tasarımı üzerine çalışılmıştır. İlk olarak biosensör alanındaki en gelişmiş teknolojiler temel alınarak, moleküllerin ortamdaki konsantrasyonuna kodlanmış bilgileri elektrik sinyallerine dönüştürebilen bir moleküler alıcı tasarlamak adına Alan Etkili Transistör Biyosensörler (BioFETs) en uygun başlangıç noktası olarak önerilmiştir. Silikon Nanotel (SiNW) bioFET temelli moleküler haberleşme alıcı aygıtı için kapsamlı bir haberleşme kuramsal model geliştirilmiş ve alıcı çıkışındaki gürültü istatistikleri elde edilmiştir. Bu alıcının performansı, sinyal-gürültü oranı (SNR), sembol hata olasılığı (SEP) ve bilgi kuramsal kapasitesi gibi metrikler ile analiz edilmiştir.

ACKNOWLEDGMENTS

I would like to express my gratitudes and sincere thanks to my supervisor, Prof. Özgür Barış Akan, who led me into this exciting area of Internet of bio-nano things. I am indebted to Prof. Akan for his continued support, guidance and understanding. I would like to express my sincere thanks to Prof. Fatih Alagöz and Prof. A. Murat Tekalp for accepting to supervise this thesis and to drive it further with their valuable comments throughout the process. My cordial thanks also extend to Prof. Alper T. Erdoğan and Prof. Berk Canberk for taking part in my thesis committee, for critical reading of this thesis and for their valuable suggestions and comments.

I would like to express my gratitude to the members of the Next-generation and Wireless Communications Laboratory for their support in the last four years. My special thanks are due to Kardelen Çepni, who has been more of a good friend than a colleague.

I must also acknowledge the profound love and support of my beloved ones, Melis, Zeynep, and Lucy. I am deeply thankful to them for their magical cuddles and purrs.

I also gratefully acknowledge the support of The Scientific and Technological Research Council of Turkey (TÜBİTAK) and Koç University.

And, last but foremost, I am eternally grateful to my parents and sisters for all their support, love and patience.

TABLE OF CONTENTS

List of Tables **xv**

List of Figures **xvi**

Nomenclature **xxv**

Chapter 1: Introduction **1**

1.1 Nanoscale Communications and Internet of Bio-Nano Things 1

1.2 Fundamental Contributions 4

1.3 Thesis Outline 5

Chapter 2: A Communication Theoretical Analysis of FRET-Based Mobile Ad Hoc Molecular Nanonetworks **8**

2.1 Introduction 8

2.2 Theory of FRET 12

2.3 FRET-Based Mobile Molecular Nanonetworks 14

2.3.1 FRET-Based Mobile Molecular Sensor/Actor Network 15

2.3.2 FRET-Based Mobile Ad Hoc Molecular Network 21

2.4 Performance Analysis of FRET-Based Mobile Molecular Nanonetworks 26

2.4.1 Performance Analysis of FRET-MSAN 27

2.4.2 Performance Analysis of FRET-MAMNET 30

2.5 Conclusion 33

Chapter 3: Coverage and Throughput Analysis for FRET-Based Mobile Molecular Sensor/Actor Nanonetworks **38**

3.1 Introduction 38
3.2 Theory of FRET 40
3.3 FRET-Based Mobile Molecular Sensor/Actor Network (FRET-MSAN) 42
3.4 Performance Analysis 46
3.4.1 Simulation Setup 46
3.4.2 Results 49
3.5 Conclusion 54

Chapter 4: An Information-Theoretic Model and Analysis of Graphene Plasmon-Assisted FRET-Based Nanocommunication Channel 55

4.1 Introduction 55
4.2 Channel Model 59
4.2.1 Probability of Energy Transfer 60
4.2.2 Graphene Plasmon Wavenumber and Plasmon Travel Length . 62
4.2.3 Transition Probabilities and Channel Capacity 63
4.3 Numerical Analysis 65
4.3.1 Effect of Intermolecular Distance 67
4.3.2 Effect of Electron Scattering Rate 67
4.3.3 Effect of QD-Graphene Distance 69
4.3.4 Effect of Donor's Radiative Lifetime 69
4.3.5 Effect of Excitation Pulse Length 70
4.4 Conclusion 70

Chapter 5: Fluorescent Molecules as Transceiver Nanoantennas: The First Practical and High-Rate Information Transfer over a Nanoscale Communication Channel based on FRET 72

5.1 Introduction 72
5.2 Methods 76

5.2.1 Experimental Setup 76
5.2.2 3-Cube Method for Signal Extraction 82
5.3 Results and Discussions 84
5.3.1 FRET Efficiency 84
5.3.2 Random Data Transmission 84
5.4 Conclusion 87

Chapter 6: The Internet of Molecular Things Based on FRET 88
6.1 Introduction 88
6.2 Overview of Fluorophores and FRET 90
6.3 FRET-Based Nanoscale Communications 93
6.3.1 Architecture 93
6.3.2 Networking Opportunities 96
6.4 Applications 104
6.4.1 Molecular Information Processing 105
6.4.2 Collaborative Sensing and Actuating 106
6.4.3 Application to Molecular Communications 108
6.5 Theoretical Modeling Approaches 108
6.5.1 Theory of FRET 109
6.5.2 Communication with Single-Exciton Encoding 113
6.5.3 Communication with Multi-Exciton Encoding 115
6.6 Experimental Approaches and Implementation Challenges 117
6.7 Conclusion 121

Chapter 7: On the Physical Design of Molecular Communication Receiver Based on Nanoscale Biosensors 123
7.1 Introduction 123
7.2 Molecular Communications Receiver 126
7.3 Overview of Biosensing Mechanisms 128

7.4 FET-Based Molecular Receiver 132
7.4.1 Signal Flow and Noise Sources 135
7.4.2 Performance Metrics 137
7.5 Design Options 140
7.5.1 Semiconductor Channel 140
7.5.2 Bioreceptors and Ligands 142
7.6 A Modeling Approach for SiNW FET-Based MC Receiver 147
7.6.1 Model of Biorecognition Unit 148
7.6.2 Model of Transducer Unit 150
7.6.3 Performance Analysis 155
7.6.4 Sensitivity Analysis 159
7.6.5 SNR Analysis 160
7.7 Advanced Design Issues 162
7.7.1 Molecular Division Multiple Access (MDMA) and MoSK . . . 162
7.7.2 Diversity Combining 164
7.7.3 Energy Efficiency Schemes 165
7.7.4 Tunable Kinetics 166
7.7.5 EM-Molecular Hybrid Operation 166
7.8 Challenges 167
7.8.1 Fabrication Challenges 167
7.8.2 Scaling and Integration Challenges 168
7.8.3 Application Challenges 169
7.9 Future Research Avenues 170
7.10 Conclusion 172

Chapter 8: Modeling and Analysis of SiNW FET-Based Molecular Communication Receiver 174

8.1 Introduction 174

8.2 Principles of BioFETs . . . 180
8.3 SiNW FET-Based Receiver Model . . . 181
8.3.1 Model Description . . . 181
8.3.2 Molecular Transport in Microfluidic Channel . . . 184
8.3.3 Received Signal . . . 185
8.3.4 Biorecognition Block and Binding Noise . . . 187
8.3.5 Transducer Block . . . 191
8.3.6 Output Block and $1/f$ Noise . . . 194
8.3.7 Overall Noise PSD and Output SNR . . . 196
8.4 Gaussian Approximation and Symbol Error Probability . . . 197
8.4.1 Gaussian Approximation for Noise Processes . . . 197
8.4.2 Derivation of SEP for M-CSK Modulation . . . 198
8.5 Performance Analysis . . . 200
8.5.1 Receiver Response and Noise Power . . . 202
8.5.2 SNR Analysis . . . 206
8.5.3 SEP Analysis . . . 210
8.6 Conclusion . . . 213

Chapter 9: On the Capacity of Diffusion-Based Molecular Communications with SiNW FET-Based Receiver 216

9.1 Introduction . . . 216
9.2 MC System Model . . . 217
9.3 Capacity . . . 223
9.4 Results . . . 227
9.5 Conclusion . . . 229

Chapter 10: Conclusion 230

10.1 A Communication Theoretical Analysis of FRET-Based Mobile Ad Hoc Molecular Nanonetworks . . . 231

10.2 Coverage and Throughput Analysis for FRET-Based Mobile Molecular Sensor/Actor Nanonetworks 231
10.3 An Information-Theoretic Model and Analysis of Graphene Plasmon-Assisted FRET-Based Nanocommunication Channel 232
10.4 Fluorescent Molecules as Transceiver Nanoantennas: The First Practical and High-Rate Information Transfer over a Nanoscale Communication Channel based on FRET 232
10.5 The Internet of Molecular Things Based on FRET 232
10.6 On the Physical Design of Molecular Communication Receiver Based on Nanoscale Biosensors 233
10.7 Modeling and Analysis of SiNW FET-Based Molecular Communication Receiver 234
10.8 On the Capacity of Diffusion-Based Molecular Communications with SiNW FET-Based Receiver 234

Bibliography **235**

LIST OF TABLES

2.1 Simulation Parameters for FRET-MSAN 27
2.2 Simulation Parameters for FRET-MAMNET 31
3.1 Simulation Parameters for FRET-MSAN 49
4.1 Simulation Parameters 66
5.1 Optimal Sampling Settings and Resultant BER and SNR 85
7.1 Simulation Parameters 152
8.1 Default Values of Simulation Parameters 202
9.1 Default Values of Simulation Parameters 225

LIST OF FIGURES

2.1 Information flow in FRET-MSAN. 16

2.2 Markov chain model of FRET-MSAN. 17

2.3 Information flow in FRET-MAMNET. 22

2.4 Markov chain model of FRET-MAMNET. 23

2.5 The successful detection probability, mean extinction time of excitons, and average system throughput for one-bit message transmission in FRET-MSAN. 35

2.6 Mutual information between the generated message on nanosensors and detected message by the nanoactors in FRET-MSAN. 36

2.7 The successful detection probability of one-bit message, mean extinction time of excitons, capacity of the channels, and achievable communication rates in FRET-MAMNET. 37

3.1 Jablonski diagram demonstrating the energy flow for the cases of (a) fluorescence and (b) FRET. 40

3.2 Two dimensional demonstration of an example FRET-MSAN. The arrows indicate the rates for exciton activity, and the circles denote the transfer range for an excited node. 42

3.3 Simulation algorithm for the exciton jump process on the Brownian mobile nodes. Simulation ends when $t = 250$ns. 47

3.4 The mean network throughput T and mean first passage times of excitons T_f as a function of R for varying diffusion constant D with fitted exponential curves. 50

3.5 The mean network throughput T and mean first passage times of excitons T_f as a function of R for varying Förster radius R_0 with fitted exponential curves. 52
3.6 The mean network throughput T and mean first passage times of excitons T_f as a function of R for varying mean excited state lifetime τ_0 with fitted exponential curves. 53
3.7 The mean network throughput T and mean first passage times of excitons T_f as a function of R for varying total concentration C_T with fitted exponential curves. 53

4.1 The conceptual design of plasmon-assisted FRET-based communication channel on a graphene sheet. Arrow (1) denotes the excitation power, (2) denotes the total power transferred to the graphene, (3) is the power of the generated GPs traveling through graphene, (4) is the power transferred to the acceptor QD by the GPs, (5) is the transferred power through direct FRET mechanism. 57
4.2 Channel capacity for different electron scattering rates γ with varying R_{ad}. 68
4.3 Channel capacity for different graphene to QD distances $z_a = z_d$ with varying R_{ad}. 68
4.4 Channel capacity for different mean excited state lifetimes μ_τ with varying R_{ad}. 71
4.5 Channel capacity for different excitation pulse lengths τ_P with varying R_{ad}. 71

5.1 Block diagram for a digital communication system. 77
5.2 Block diagram for the experimental setup. 77
5.3 Normalised absorption (A) and emission (E) spectra of Fluorescein (Fl) and Rhodamine B (RhB), and the calculated overlap function. 80

5.4 Eye diagrams of S_{DA} and S_{FRET} signals for several information transmission rates. 86

6.1 FRET between an excited-state donor fluorophore and a ground-state acceptor fluorophore. θ_T denotes the angle between the emission transition dipole of the donor **D** and the absorption transition dipole of the acceptor **A**, θ_D and θ_A denote the angles between these dipoles and the vector joining the donor and acceptor. R is the intermolecular distance. 91

6.2 Multihop FRET-based communication schemes: (a) 1-d unidirectional photonic wire on DNA scaffold consisting of spectrally different fluorophores; (b) 1-d unidirectional photonic wire consisting of identical relay fluorophores between a transmitter and a receiver node; (c) 1-d bidirectional photonic wire consisting of identical fluorophores acting as transmitter, relay, and receiver nodes; (d) 3-d multihop link consisting of randomly deployed relay nodes between a transmitter-receiver node pair. 97

6.3 Working principles of main switching mechanisms feasible for FRET-based nanonetworks: (a) Quenching of acceptor's absorption under visible light leading to optical switching; (b) Shift of donor's emission spectrum under electric field leading to electrical switching; (c) 1-d translational movement of macrocyclic ring of *[2]rotaxane* depending on the pH of environment leading to chemical switching; (d) Ligand-receptor binding leading to biological switching. 99

6.4 Conceptual drawings of some applications of FRET-based communications. Molecular logic network and sensor network are connected to Internet via macroscale gateways comprising optical source and detectors whereas molecular sensor/actor network is envisioned to operate in autonomous manner under continuous excitation of a remote optical source. 104

6.5 Probability of FRET for an excited donor with varying donor-acceptor distance R_0 and Förster radius R_0. 111

6.6 Capacity of a point-to-point channel for different Förster radii R_0 and varying internodal distance R. 113

6.7 Capacity of a multihop communication channel for different relay concentrations C_R and varying transmitter-receiver distance. Data were obtained through Monte Carlo simulations using Algorithm 1 for $T_{pulse} = 1\mu s$ and $R_0 = 6nm$. 116

6.8 Markov process model of bit-1 transmission for rapid-diffusion case: (a) Birth-death Markov process model valid for $t \leq T_{pulse}$; (b) Pure-death Markov process model valid for $t > T_{pulse}$. 119

7.1 Molecular communications between a pair of nanomachines. 126

7.2 Functional units of a molecular communications receiver. 128

7.3 Conceptual design of FET-based MC receiver. 133

7.4 Expected time domain response of a p-type doped FET-based MC receiver in terms of drain-to-source current in the transducer channel, when (a) no information molecule is present in the reception space, (b) a negatively charged information molecule binds to a surface receptor, (c) the bound molecule leaves the recognition unit. 134

7.5 Signal flow diagram of an MC receiver antenna. The triangles and circles denote the information and interferer molecules, respectively. . 137

7.6 FET-based MC receiver with different type of transducer channels: (a) SiNW channel, (b) SWCNT chanel, (c) graphene channel. 142

7.7 Equivalent circuit model for the transducer of the SiNW FET-based MC receiver [Deen et al., 2006] [Kuscu and Akan, 2015] [Georgakopoulou et al., 2015]. *REF* denotes the reference electrode, which stabilizes the gate voltage V_G. 151

7.8 Receiver response in terms of difference in threshold voltage, i.e., $\Delta V_T = \Delta I_{DS}/g_m$, as a function of ligand concentration c_i for (a) different mean number of electrons per ligand N_e, (b) different ionic concentration c_{ion}, (c) different concentration of surface receptors c_R (note that $N_R = c_R WL$), (d) different oxide layer thickness t_{ox}. 153

7.9 The results of experiments conducted in [Duan et al., 2012] for the detection of DNA concentration by a SiNW FET functionalized with HMGB1 proteins: (a) Threshold voltage ΔV_T vs. time data for the detection of DNA with HMGB1 receptors on the same SiNW bioFET device for different concentrations of DNA. Each DNA delivery is followed by 1 M NaCl buffer to accelerate the desorption of bound DNAs from the surface. (b) ΔV_T as a function of DNA concentration. The dissociation constant K_D for DNA-HMGB1 ligand-receptor pair is determined by the authors as 105 ± 6 nM. 157

7.10 Receiver sensitivity with input concentration c_i normalized by K_D. Sensitivity with (a) varying concentration c_i of information-carrying ligands, (b) varying ionic concentration c_{ion}, (c) varying receptor length L_R, and (d) varying oxide layer thickness t_{ox}. 158

7.11 SNR as a function of (a) ligand concentration c_i, (b) ionic concentration c_{ion}, (c) receptor length L_R, and (d) trap density N_t. 162

7.12 Receiver antennas for MDMA and MoSK schemes. 164

7.13 (a) Multiplexed detection of cancer biomarkers with three SiNW bioFETs constructed on a common substrate [Zheng et al., 2005]. Each bioFET is functionalized with distinct monoclonal antibody receptors (**NW1** with PSA antibody, **NW2** with CEA antibody, **NW3** with mucin-1 antibody) specific to the three different biomarkers (PSA, CEA, mucin-1). (b) Conductance measurements for the simultaneous detection of biomarkers which are sequentially delivered to the array as follows: (1) 0.9 ng/ml PSA, (2) 1.4 pg/ml PSA, (3) 0.2 ng/ml CEA, (4) 2 pg/ml CEA, (5) 0.5 ng/ml mucin-1, (6) 5 pg/ml mucin-1. The biomarker solutions are followed by buffer solutions which are delivered at the time points indicated by black arrows. 165

8.1 (a) Functional units of an MC receiver, and (b) SiNW FET-based MC receiver antenna. Insulating SiO_2 layer entirely covering the SiNW is not shown in (b) for better visualization of the transducer. 179

8.2 (a) 3D and (b) 2D dimensional view of microfluidic propagation channel. The locations of the transmitter and receiver, and the plug of ligands, which is dispersed as it flows towards the receiver location, are shown. 182

8.3 Block diagram of microfluidic MC system with SiNW FET-based MC receiver. 183

8.4 Cross-sectional view of SiNW FET-based MC receiver buried at the bottom of the microfluidic channel, (a) when the channel is empty; (b) when the receiver is exposed to the electrolyte solution with ligands flowing along the x-axis. We show only the receptors at the top surface of the SiNW, since we assume that the ligands can bind only to these receptors. The top part of the diffusion layer resulting from the counterions attracted to the insulating SiO_2 layer, and the corresponding SiNW double layer emerged inside the SiNW are also shown in (b). The region of interest is the zone lying above the dashed line, which is the effective part of the receiver for ligand detection. 190

8.5 Equivalent circuit model for the transducer of the SiNW FET-based MC receiver [Gao et al., 2009], [Shoorideh and Chui, 2014]. *REF* denotes the reference electrode. 192

8.6 Expected output current μ_{I_m} as a function of number of ligands N_m released by transmitter and transmitter-receiver distance d. 201

8.7 PSD of noise effective on the output current of SiNW FET-based MC receiver. The plot reveals the individual contributions of binding and $1/f$ noise. 203

8.8 Output current noise PSD at the frequency range of receiver's operation with varying N_m. 203

8.9 Effect of the communication system parameters on the SNR at the electrical output of the receiver. SNR as a function of (a) number of transmitted ligands N_m, (b) transmitter-receiver distance $d = x_R - x_T$, (c) ion concentration c_{ion} of the electrolyte medium, (d) average flow velocity u inside the microfluidic channel. 205

8.10 Effect of the molecular parameters on the SNR at the electrical output of the receiver. SNR as a function of (a) intrinsic diffusion coefficient of ligands D_0, (b) intrinsic binding rate of ligands k_1, (c) surface receptor length l_{SR}, (d) number of free electrons per ligand molecule N_e^-. . . . 206
8.11 Effect of the receiver design parameters on the SNR at the electrical output of the receiver. SNR as a function of (a) SiNW radius r_R, (b) surface receptor concentration ρ_{SR} (c) SiO_2 layer thickness t_{OX}, and (d) oxide trap density N_t in SiNW. 207
8.12 Symbol error probability (SEP) for M-CSK modulation. SEP as a function of (a, c) transmitter-receiver distance d, (b, e) maximum number K of ligands that transmitter can release, (c, f) constellation exponent s.214
8.13 Symbol error probability (SEP) for M-CSK modulation. SEP as a function of (a, c) ion concentration c_{ion} of the electrolyte medium, (b, e) receptor length l_{SR}, (c, f) oxide trap density N_{ot} in SiNW. 215

9.1 (a) Functional units of an MC receiver, and (b) SiNW FET-based MC receiver antenna. 219
9.2 Capacity-achieving input distribution with $N_{tx}^{min} = 10^8$ and $N_{tx}^{max} = 10^9$.227
9.3 Capacity with (a) varying maximum number N_{tx}^{max} of transmitted molecules, (b) varying TX-RX distance d, (c) varying ionic concentration c_{ion}, and (d) varying oxide trap density N_{ot}. 228

NOMENCLATURE

AF	Acceptor Filter
ASBT	Acceptor's Spectral Bleed-Through
BEP	Bit Error Probability
BER	Bit Error Rate
bioFET	Field Effect Transistor based Biosensor
CNT	Carbon Nanotube
CSK	Concentration Shift Keying
CTMC	Continuous Time Markov Chain
CVD	Chemical Vapor Deposition
DAQ	Data Acquisition Card
DF	Donor Filter
DSBT	Donor's Spectral Bleed-Through
EM	Electromagnetic
EOM	Electro-Optic Modulator
FET	Field Effect Transistor
Fl	Fluorescein
FRET	Förster Resonance Energy Transfer
FWHM	Full-Width Half-Maximum
GP	Graphene Plasmon
HVA	High-Voltage Amplifier
IoBNT	Internet of Bio-Nano Things
IoMT	Internet of Molecular Things
IoT	Internet of Things
ISI	Intersymbol Interference
MC	Molecular Communications

MDMA	Molecular Division Multiple Access
MIMO	Multiple-Input and Multiple-Output
ML	Maximum Likelihood
MoS_2	Molybdenum Disulfide
MoSK	Molecular Shift Keying
MSAN	Mobile Molecular Sensor/Actor Nanonetwork
MAMNET	Mobile Ad Hoc Molecular Nanonetwork
NW	Nanowire
SEP	Symbol Error Probability
SIR	Susceptible, Infected, Recovered
SiNW	Silicon Nanowire
SNR	Signal-to-Noise Ratio
SPR	Surface Plasmon Resonance
SWCT	Single-Walled Carbon Nanotube
OOK	On-Off Keying
PBS	Polarizing Beam Splitter
PDT	Photodynamic Therapy
PSD	Power Spectral Density
QCSE	Quantum Confined Stark Effect
QD	Quantum Dot
RhB	Rhodamine B
RN	Receiver Nanomachine
smFRET	Single-Molecule FRET
SPP	Surface Plasmon Polariton
TN	Transmitter Nanomachine
TTL	Transistor-Transistor Logic

Chapter 1

INTRODUCTION

1.1 Nanoscale Communications and Internet of Bio-Nano Things

Nanomachines are envisioned as very basic operational units with nanoscale dimensions, which are individually capable of performing simple actuating, sensing and computing tasks. Enabling nanomachines to communicate with each other, and hence, form nanonetworks to overcome the limitations of an individual nanomachine would have unprecedented impact especially on life sciences with groundbreaking applications such as smart drug delivery and intra-body continuous health monitoring.

The emerging field of nanoscale communications and nanonetworks has witnessed tremendous advancements in the last decade. Since classical communication paradigms are not applicable in nanonetworks, a great deal of effort has been devoted to develop novel nanocommunication techniques, such as bio-inspired molecular communications and THz-band nanoscale electromagnetic communications. Interconnecting these nanonetworks to the wider Internet is expected to greatly extend the application domain of nanonetworks. This in turn would transform the Internet of Things (IoT) with another dimension: the Internet of Bio Nano Things (IoBNT). IoBNT is proposed as the basis of numerous future applications, such as those in the military, healthcare, and security fields, where the nanothings, thanks to their limited size, can be easily concealed, implanted, and scattered in the environment, and cooperatively perform sensing, actuation, processing, and networking. However, connecting nanonetworks to the Internet would bring along unique challenges such as developing new techniques for enabling an interface between the nanonetworks and macroscale

networks which in general have heterogenous characteristics.

This thesis is focused on the physical layer issues for the realization of IoBNT. In particular, we investigate communication techniques that can enable high-speed and reliable wireless communication in nanonetworks and at the same time provide a seamless interface between the nanonetworks and the macroscale cyber networks. In the first part, we study the use of fluorescent molecules, i.e., fluorophores, to enable wireless communication at nanoscale through Förster Resonance Energy Transfer (FRET). Communication and information theoretical models for FRET-based and multi-step FRET-based propagation channels are developed. We also investigate the feasibility of realizing FRET-based mobile nanonetworks. Using functionalized fluorophores as network nodes, we propose two different FRET-based mobile ad hoc sensor-actor nanonetwork architectures, and examined their coverage and throughput performance. In another part of this thesis, we approach the problem of limited communication range from a different perspective and propose the use of graphene plasmons as mediators of FRET-based information transfer between two Quantum Dots (QDs), and develop the first end-to-end channel model. The graphene plasmon-assisted FRET-based technique extends the communication range up to 500nm with an acceptable reliability, thus, it is promising especially for on-chip nanocommunication. Moreover, using Fluorescein and Rhodamine B dyes as nanotransceiver antennas, we achieved to practically realize the first wireless high-rate data transfer between fluorescent molecules, proving the feasibility of wireless communications at nanoscale. This part of this thesis is the first to experimentally demonstrate that it is possible to transfer information between primitive molecular devices at very high rates up to 250kbps. These studies underline the potential and practicality of FRET as a high-rate and reliable nanocommunication method among molecular scale devices, and all of them opened new research avenues in this emerging field. Furthermore, accounting for the natural optical interface between the nanoscale and macroscale worlds provided by the intrinsic characteristics of fluorophores, the novel concept of Internet of Molecular Things is introduced to further extend the coverage of IoBNT

with networks of sub-100nm primitive molecular devices, such as fluorophore-based molecular logic gates, sensors and actuators.

The second part of this thesis is focused on molecular communications, where molecules are used to encode, transmit, and receive information for the coordination of nanoscale devices. This bio-inspired communication paradigm has been extensively studied from various aspects, including channel modelling and noise analysis. Comparatively little attention has been given to the physical design of molecular receiver and transmitter, envisioning biological synthetic cells with intrinsic molecular reception and transmission capabilities as the future nanomachines. However, this assumption leads to a discrepancy between the envisaged applications requiring complex communication interfaces and protocols, and the very limited computational capacities of the envisioned biological nanomachines. As the first step to overcome this discrepancy, we examine the feasibility of designing a molecular receiver, in a physical domain other than synthetic biology, meeting the basic requirements of nanonetwork applications and also serving the needs of an EM nano-macro interface between the bio-chemical domain of nanonetworks and the electrical domain of the cyber networks. We first present a comprehensive review of the state-of-the-art biosensing approaches to determine whether they can inspire a receiver design, and we reveal that nanoscale field effect transistor based electrical biosensor technology (bioFET) is a particularly useful starting point for designing a molecular receiver. Focusing on bioFET-based molecular receivers with a conceptual approach, we provide a guideline elaborating on their operation principles, performance metrics and design parameters. Moreover, we develop a comprehensive model for silicon nanowire (SiNW) FET-based MC receivers by integrating the underlying processes in MC and bioFET to provide a unified analysis framework. Furthermore, we derive closed-form expressions for the noise statistics, the signal-to-noise ratio (SNR) at the receiver output, and the symbol error probability (SEP), and performed extensive analyses to reveal the effects of individual system parameters on the detection performance of the proposed MC receiver. Using the receiver model, we also derive closed-form expressions for the capacity and capacity-

achieving input distribution for a memoryless MC channel with a SiNW FET-based MC receiver, which would find use in optimizing the information flow in MC systems equipped with nanobioelectronic receivers.

1.2 Fundamental Contributions

The contributions of this thesis in the field of Internet of Bio-Nano Things can be listed as follows:

- Design, modeling and analysis of FRET-based mobile ad hoc molecular networks
- Development of simulation algorithms for extracting spatial features of FRET-based mobile nanonetworks
- Information theoretical modeling of graphene plasmon assisted FRET-based nanoscale communication channel
- First practical realization of a FRET-based nanonetwork
- Proposal of a novel molecular-scale fluorophore-based IoBNT framework named Internet of Molecular Things
- Investigation of the state-of-the-art biosensing solutions for implementing a molecular communication receiver
- Analytical modeling and analysis of a molecular communication receiver based on silicon nanowire field effect transistor biosensor (SiNW bioFET)
- Information theoretical modeling of molecular communication channels with bioFET-based receivers

1.3 Thesis Outline

The thesis is organized as follows.

Part 1: Internet of Molecular Things Based on FRET

Chapter 2: In this chapter, for the first time in the literature, we investigate the network of *mobile* nanomachines communicating through FRET. We introduce two novel mobile molecular nanonetworks: *FRET-based mobile molecular sensor/actor nanonetwork (FRET-MSAN)* which is a distributed system of mobile fluorophores acting as sensor or actor node; and *FRET-based mobile ad hoc molecular nanonetwork (FRET-MAMNET)* which consists of fluorophore-based nanotransmitter, nanoreceivers and nanorelays. We model the single message propagation based on birth-death processes with continuous time Markov chains. We evaluate the performance of FRET-MSAN and FRET-MAMNET in terms of successful transmission probability and mean extinction time of the messages, system throughput, channel capacity and achievable communication rates.

Chapter 3: In this chapter, we focus on the spatial characteristics of FRET-Based Mobile Molecular Sensor/Actor Nanonetworks (FRET-MSAN) by investigating the network performance in terms of communication coverage, network throughput and information propagation rate through extensive Monte Carlo simulations. The effect of fundamental system parameters related to FRET and to the mobility of the network nodes on the network performance are revealed. The results of the simulations indicate that the throughput and propagation rate as a function of distance from the information source are well-fitted by exponential curves. We also observe that the impact of FRET mechanism suppresses the effect of Brownian motion of network nodes on the exciton mobility.

Chapter 4: In this chapter, we propose to exploit Graphene Plasmons (GPs) incorporated with excitons as the information carriers between two distant fluorescent molecules. The interaction between the optical excitons and graphene plasmons is a newly explored phenomenon, and this is the first study that approaches this phenomenon from the communication theoretical perspective. In this paper, we derive

an analytical expression for the point-to-point channel capacity, and investigate the effect of fundamental system parameters on the channel performance. We show that information can be transmitted reliably through distances over 500nm with acceptable communication rates.

Chapter 5: In this chapter, further to the extensive theoretical studies, we demonstrate the first information transfer through a FRET-based nanocommunication channel. We implement a digital communication system combining macroscale transceiver instruments and a bulk solution of fluorophore nanoantennas. The performance of the FRET-based Multiple-Input and Multiple-Output (MIMO) nanocommunication channel between closely located mobile nanoantennas in the sample solution is evaluated in terms of Signal-to-Noise Ratio (SNR) and Bit Error Rate (BER) obtained for the transmission rates of 50kbps, 150kbps and 250kbps. The results of the performance evaluation are very promising for the development of high-rate and reliable molecular communication networks at nanoscale.

Chapter 6: In this chapter, we provide an in-depth architectural view of FRET-based nanoscale communication paradigm with a focus on its peculiarities, fundamental principles and design requirements by comprehensively surveying the theoretical and experimental positions and ideas. We give an overview of networking opportunities offered by the intrinsic capabilities of fluorophores under the novel concept of *Internet of Molecular Things*. We present the prospective applications, theoretical modeling approaches and experimental opportunities, and finally discuss the implementation challenges.

Part 2: BioFET-Based Molecular Communication Receiver

Chapter 7: In this chapter, we examine the feasibility of designing a molecular receiver, in a physical domain other than synthetic biology, meeting the basic requirements of nanonetwork applications. We first review the state-of-the-art biosensing approaches to determine whether they can inspire a receiver design. We reveal that nanoscale field effect transistor based electrical biosensor technology (bioFET) is a particularly useful starting point for designing a molecular receiver. Focusing on

bioFET-based molecular receivers with a conceptual approach, we provide a guideline elaborating on their operation principles, performance metrics and design parameters. We then provide a deterministic model for signal flow in silicon nanowire (SiNW) FET-based molecular receiver and investigate its response and sensitivity for different settings of system parameters. Lastly, we discuss the practical challenges of implementing the receiver and present the future research avenues from a communication theoretical perspective.

Chapter 8: In this chapter, we introduce a comprehensive model for silicon nanowire (SiNW) FET-based MC receivers by integrating the underlying processes in MC and bioFET to provide a unified analysis framework. We derive closed-form expressions for the noise statistics, the signal-to-noise ratio (SNR) at the receiver output, and the symbol error probability (SEP). Performance evaluation in terms of SNR and SEP reveals the effects of individual system parameters on the detection performance of the proposed MC receiver.

Chapter 9: In this chapter, we derive analytical closed-form expressions for the capacity and capacity-achieving input distribution for a memoryless MC channel with a silicon nanowire (SiNW) FET-based MC receiver. The resulting expressions could be used to optimize the information flow in MC systems equipped with nanobioelectronic receivers.

Chapter 2

A COMMUNICATION THEORETICAL ANALYSIS OF FRET-BASED MOBILE AD HOC MOLECULAR NANONETWORKS

2.1 Introduction

Nanomachines are envisioned as nanoscale-sized machines with basic operation capabilities such as computing, sensing, actuating. The capabilities of these nanomachines can be improved by enabling communication among them. These nanonetworks are envisaged to accomplish more complex tasks ranging from nuclear defense to treatment of many diseases [Akyildiz et al., 2008]. Many efforts have been devoted to develop communication methods for future nanonetworks. Electromagnetic and molecular communications are the most promising approaches [Akyildiz and Jornet, 2010a, Nakano et al., 2005]. Recently, we have proposed a radically different molecular communication method based on the energy transfer between fluorescent molecules, i.e., fluorophores, which provides high communication rates at the molecular level [Kuscu and Akan, 2011].

Fluorophores, e.g., organic dyes, fluorescent proteins, and quantum dots (QDs), are special molecules that are able to be excited by optical, electrical, chemical or biological energy, and individually relax to the ground state after a random time, i.e., excited-state lifetime, by fluorescing, i.e., releasing a single photon with a wavelength at the range of their emission spectrum [Lakowicz, 1999]. There are many quenching mechanisms that can suppress the fluorescence of the excited-state donor. For example, collision of the excited donor with another molecule can result in quenching of the fluorescence. In case of a collision, the excited energy of the donor is dissipated

through heat without radiation of photon. Förster resonance energy transfer (FRET) is another quenching mechanism that defines the migration of the excited-state energy in the form of exciton from the donor molecule to a ground-state acceptor molecule. In the case of FRET, the donor does not fluoresce, and the acceptor non-radiatively becomes excited, i.e., sensitized, by receiving the donor's exciton.

FRET occurs non-radiatively when the donor and acceptor are close to each other with intermolecular distances less than 10nm [Förster, 1948]. It is a pairwise energy transfer phenomenon, therefore, an exciton can be transferred to a single acceptor at a time. It is based on the near-field Coulomb interaction of the emission transition dipole moment of the donor with the acceptor's absorption transition dipole moment. Therefore, the phenomenon requires a significant overlap between the donor's emission spectrum and the acceptor's absorption spectrum which increases the resonance probability.

Due to the strong dependence of transfer probability on the intermolecular distance, FRET is extensively exploited as a spectroscopic ruler in biotechnological research [Stryer, 1978]. Protein binding events, molecular anisotropy and proximity can be efficiently observed through FRET [Joo et al., 2008]. There exist several nanoscale biosensors based on FRET mechanism which signal the existence of certain targets in the sensor's proximity [Medintz et al., 2003, Zhou et al., 2008]. The phenomenon is also naturally observed in photosynthesis during the efficient transmission of absorbed optical energy to the reaction centers [Ritz et al., 2002], thus, FRET constitutes the main focus for the design of synthetic light-harvesting devices [Hardin et al., 2009].

FRET has been proposed as a means of short-range nanocommunications for the first time in [Kuscu and Akan, 2011]. The idea was mainly based on encoding the information into the excited-states of fluorophores, and transferring the information via FRET mechanism between a donor fluorophore as the nanotransmitter antenna and an acceptor fluorophore as the nanoreceiver antenna. In [Kuscu and Akan, 2012], employing a laser with a wavelength in the range of donor's absorption spectrum as the remote information source and using on-off keying (OOK) modulation scheme by

representing single bit of information with the presence or absence of a single exciton, we information theoretically analyzed the capacity of the channel between them. We also investigated the pulsed excitation scheme in which the information is encoded into multiple excitons to increase the reliability of the channel [Kuscu and Akan, 2014c]. We showed that the high rate of energy transfer between fluorophores (10^6-10^9 Hz) can provide high rate and reliably nanocommunications. Lastly, with a Monte Carlo approach, we simulated the information transmission through point-to-point channel in a three dimensional aqueous medium comprising a varying concentration of relay fluorophores, and showed that information can be reliably transmitted through 200 *nm* distance at a rate over 10 *Mbps* [Kuscu and Akan, 2013b]. Due to the high degree of randomness intrinsic to the FRET mechanism, all of these studies assumed that the fluorophores are stationary, and the relative orientation of the fluorophores is constant during the excited-state lifetime, therefore, we applied the classical Förster theory which is not valid for mobile diffusing fluorophores. However, most of the applications that nanonetworks promise, such as in-body target detection and drug delivery, need to employ mobile nanomachines. Therefore, this study aims to investigate the FRET-based communication between *mobile nanonodes* by approaching the problem from a perspective radically different from classical Förster theory. f In case that the fluorophores with sufficiently long excited-state lifetimes are used, a donor and acceptor pair with long intermolecular distance at the time of excitation can get into proximity during the lifetime of the donor molecule. Therefore, the probability for an excited donor to get into proximity with more ground-state acceptors during its lifetime increases. As a result of these conditions, the classical Förster theory fails to express the FRET probability for a mobile excited state fluorophore. Fortunately, Stryer et al. derived an expression for the transfer rate of the fluorophores with long lifetimes diffusing in a three dimensional environment [Thomas et al., 1978].

In this study, using the expressions derived in [Thomas et al., 1978], [Stryer et al., 1982], we investigate the performance of FRET-based communication between mobile nanonodes for two network scenarios: *i*) *FRET-based mobile molecular*

sensor/actor network (FRET-MSAN); and *ii*) *FRET-based mobile ad hoc molecular network (FRET-MAMNET)*. In FRET-MSAN, bioluminescent molecules which are special kind of fluorophores that are excited upon binding a target molecule are considered as the sensor nodes. There are also actuators in the network that can realize a specific task upon receiving an exciton. This deployment can be used for autonomous sensing and actuating tasks at the molecular level. FRET-MAMNET consists of transmitter, relay and receiver nanonodes which are also fluorophores. The single nanotransmitter in the network receives a pulsed excitation signal from an information source and sequentially transmits the excitons to the relay nodes or directly to the nanoreceivers in a probabilistic manner.

In order to model the single message propagation in both networks, in the earlier version of this study [Kuscu and Akan, 2013a], we exploit the SIR model of epidemics [Newman, 2002] to analytically derive the message transmission probability in FRET-MSAN, and the transmission delay in FRET-MAMNET assuming that a continuous excitation pulse is applied until the detection. However, SIR model is incapable of expressing the transmission probability for FRET-MAMNET with finite-time excitation pulses, and the message transmission delay for FRET-MSAN. In this study, instead of using the SIR models, we benefit from the birth-death processes with continuous time Markov chain models, and extend our previous study by investigating the transmission delay, system throughput and mutual information for FRET-MSAN. Considering that a finite-time excitation pulse is applied, we analyze the message transmission probability, transmission delay, the information theoretical capacity of the channel between the nanotransmitter and the nanoreceivers, and achievable communication rates for FRET-MAMNET. The performance evaluation is carried out by the Monte Carlo simulations of Markov chain models for both mobile nanonetworks.

The remainder of this paper is organized as follows. In Section II, we review the FRET theory and rapid-diffusion criterion for mobile fluorophores. In Section III, we present the Markov chain models for single message propagation in FRET-MSAN and FRET MAMNET. The results of Monte Carlo simulations for performance evaluation

are given in Section IV. Finally, the concluding remarks are given in Section V.

2.2 Theory of FRET

FRET is a fundamental excited state process observed among fluorescent molecules. It is the transfer of excited state energy in the form of exciton from an excited molecule, called the donor, to a ground-state molecule, called the acceptor, in close proximity of each other. The theory of FRET between immobile fluorophores is established in Theodor Förster's seminal work [Förster, 1948], and then, fundamentally validated by an extensive number of experimental studies [Stryer, 1978].

When there exists no quenching mechanism such as molecular collisions or FRET, the excited-state donor is expected to return to ground-state after a randomly short time by fluorescing, i.e., releasing a photon. The excited state lifetime τ, i.e., the time interval between the excitation and relaxation of a molecule, is an exponential random variable of which mean is generally in the range between 2ns-1μs [Lakowicz, 1999]. The reciprocal of the mean excited-state lifetime gives the natural fluorescence rate k_0 of a fluorophore, i.e., $k_0 = 1/\mu_0$. k_0 is the number of photons released at a unit time when there is no quencher. The existence of a quenching mechanism provides additional pathways for the excited-state donor to relax to the ground-state, and thus, significantly reduces the lifetime of excitons by increasing the relaxation rate of the donor.

As a fundamental quenching mechanism, FRET can be realized if the following conditions are satisfied: *i*) the excited fluorophore must be in close proximity (0-10 nm) with at least one ground-state acceptor; *ii*) the emission spectrum of the donor and the absorption spectrum of the acceptor must overlap; and *iii*) the relative orientation of transition dipole moments of the donor and the acceptor fluorophores must not be orthogonal. If all requirements are met, the rate of the energy transfer as a function of the natural fluorescence rate of the donor k_0 and in terms of number

of excitons transferred per unit time is given as

$$k_t = k_0(\frac{R_0}{R})^6 \tag{2.1}$$

where R is the intermolecular distance, and R_0 is the Förster radius which incorporates the effects of some intrinsic and environmental parameters. Since information is encoded into the excitons, the exciton transfer rate k_t is the most crucial parameter for the performance of FRET-based communications. It is a measure of how fast the information can be transferred between fluorophore-based nanonodes. Förster radius R_0 can be expressed by

$$R_0 = (8.8 \times 10^{22}\kappa^2 n^{-4} Q_D J)^{-\frac{1}{6}} \tag{2.2}$$

where κ^2 is the relative orientation factor, Q_D is the quantum yield of the donor, n is the refractive index of the medium, and J is the degree of the spectral overlap. R_0 ranges between 4 - 10 nm [Lakowicz, 1999].

In the case of mobile fluorophores, the situation is radically different in the sense that during the excited state lifetime of the donor, the intermolecular distances and the relative orientation of the dipole moments of fluorophores are not constant. Furthermore, the excited donor fluorophore can get in close proximity with a varying number of acceptors if the donor lifetime or the diffusion coefficient of the fluorophores is sufficiently long. Considering that the excitons randomly walk in a random lattice consisting of diffusing fluorophores, giving a closed form expression for the transfer rate requires some assumptions. Stryer et al. postulated the governing rate equations for the energy transfer from a single excited donor to a single ground-state acceptor in a three dimensional environment assuming that the fluorophores are in the rapid-diffusion limit [Stryer et al., 1982]:

$$k_{rd} = \frac{4\pi k_0 R_{0,d-a}^6}{3V a_{d-a}^{-3}} \tag{2.3}$$

where $R_{0,d-a}$ is the Förster radius between the donor and the acceptor, and V is the volume of the three dimensional medium. a_{d-a} is the possible closest distance between the centers of the donor and the acceptor. When there are more than one acceptor molecules, the total FRET rate between the donor and the acceptors becomes

$$k_t = k_{rd} N_a \tag{2.4}$$

where N_a is the number of available, i.e., ground-state, acceptor molecules in the environment. The rapid-diffusion criterion is given as

$$\frac{D\tau_0}{s^2} \gg 1 \tag{2.5}$$

where D is the sum of diffusion coefficients of the donor and the acceptor, τ_0 is the natural excited state lifetime of the donor, i.e., $\tau_0 = 1/k_0$, and s is the mean intermolecular distance between donor-acceptor fluorophores [Stryer et al., 1982], [Kinosita Jr et al., 1987].

The rapid diffusion limit can be achieved by using fluorophores with moderate diffusion coefficients and long lifetimes such as $1 - 2\ \mu s$ [Kinosita Jr et al., 1987].

2.3 FRET-Based Mobile Molecular Nanonetworks

FRET-based nanocommunication channel has been previously modeled with different configurations assuming that the communicating nanomachines are immobile during the communication. However, most of the applications, especially in-body applications, that nanonetworks promise, require for nanomachines to be mobile. Along with this motivation, in this section, we focus on the network of mobile nanomachines communicating through FRET. We model the single message propagation both in FRET-MSAN and FRET-MAMNET based on Continuous Time Markov Chains (CTMCs) assuming that the nanonetwork nodes are freely and randomly diffusing in a three dimensional aqueous environment satisfying the rapid-diffusion criterion.

The performance of the proposed nanonetworks are investigated based on the re-

sults of the Monte Carlo simulations on Markov chain models. For FRET-MSAN, we obtain the successful transmission probability of a single message generated on the nanosensors to the nanoactors randomly diffusing in the environment. The temporal characteristics of the network are analyzed based on the average delay between the generation of a single message on the nanosensors and its reception by the nanoactors. We derive the average system throughput using the delay parameter and the number of nanoactors that receive the message. We also information theoretically investigate the mutual information between nanosensors and nanoactors with varying event probability. For FRET-MAMNET, the information theoretical capacity of the communication channel between the nanotransmitter and nanoreceivers is obtained through the successful transmission probability of a single message for varying system parameters. We also investigate the achievable communication rate on the mobile network based on the transmission delay.

2.3.1 FRET-Based Mobile Molecular Sensor/Actor Network

Bioluminescent molecules define a class of fluorescent molecules which are excited upon binding a target molecule [Lakowicz, 1999]. Since they do not need a remote excitation source, e.g., optical laser, they are extensively used in biotechnological research as biomolecular sensors optically indicating the presence of a certain kind of molecule [Contag and Bachmann, 2002]. For example, *aequorin*, a bioluminescent protein, reacts with calcium ions, and relaxes through releasing a photon, thus, it is extensively used to measure $Ca2+$ concentration [Allen and Blinks, 1978].

Fluorescent molecules also find applications in photodynamic therapy (PDT) of cancer as actuators. In QD-based PDT, QDs are excited by optical energy from a remote source and then transfer its exciton to the conjugated photosensitizing agent which synthesizes a reactive singlet oxygen via energy transfer [Samia et al., 2003]. The produced singlet oxygen initiates the apoptosis of nearby cancer cells. However, the reactive singlet oxygen is also harmful for normal cells, therefore, the spatial precision of the activation of singlet oxygen is crucial.

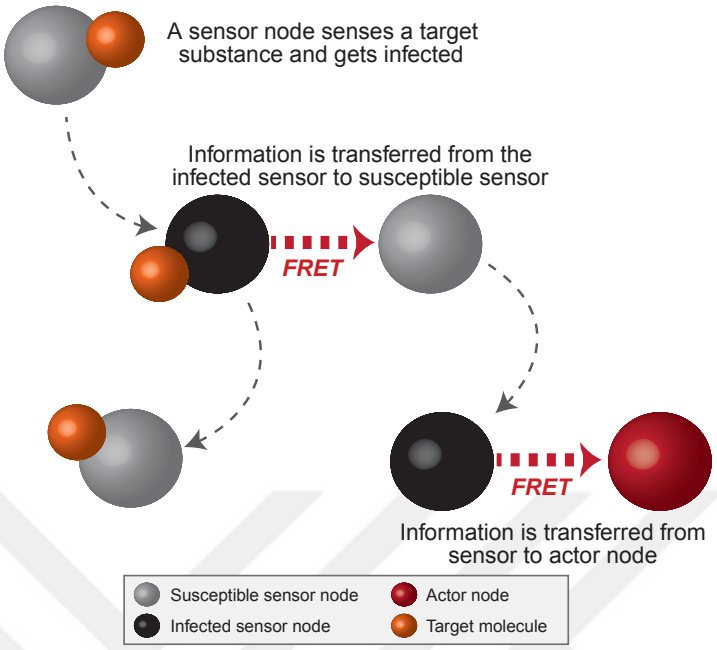


Figure 2.1: Information flow in FRET-MSAN.

Here, we focus on a molecular sensor and actor network, namely FRET-MSAN, composed of mobile bioluminescent sensors and fluorophore-based actors that can collect the information from the sensors and perform an appropriate action upon the environment. The investigated scenario in this section can pave the way for designing autonomous networks of nanomachines which are able to collaboratively sense the presence of tumor cells, and act precisely for the apoptosis of them. The information flow in FRET-MSAN is demonstrated in Fig. 2.1.

The generated message by the nanosensors is a one-bit message which is an exciton indicating whether the nanosensors bound to a target molecule or not. The target can be a macromolecule, e.g., biopolymer, and thus, it is possible that more than one sensor nodes bind to the same target. In this case, each nanosensor can generate excitons signaling the existence of the target, therefore, more than one excitons can flow on the network at the same time. We assume that the nanoactors are not capable of the detecting the target and generating excitons individually. The initially generated excitons occupy on the detecting nanosensors during an exponentially random time,

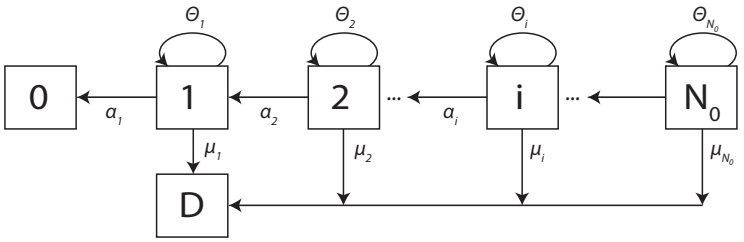


Figure 2.2: Markov chain model of FRET-MSAN.

and then transferred to the other sensors or actors in the ground-state, i.e., randomly walk on a random lattice, or they can be removed from the system by fluorescence.

We assume that the detection is realized with a varying number of nanosensor nodes at the same, and during the transmission of the detection message, no other detection occurs. Therefore, the initially generated excitons set an upper bound on the number of excitons on the network, and the number of excitons is a monotonically decreasing function. During this discrete fade away of the excitons, if at least one nanoactor receive an exciton from an excited sensor node, the message is successfully transferred. These characteristics of the network imply that the single message transmission resembles a death process which can be modeled with a continuous time Markov chain demonstrated in Fig. 2.2.

In the model, the states demonstrate the number of excitons that are available on the network. The transition rates depend on the state of the network, i.e., number of excitons that randomly walk throughout the network. There are two absorbing states in this Markov chain, i.e., state-0 and state-D. The state-0 represents the complete extinction of the excitons in the network. Detection cannot be realized once the extinction occurs since no other exciton is generated. If none of the nanoactors receive an exciton until the extinction, the message is lost, and the transmission fails. The state-D represents the successful detection of the message which occurs when a nanoactor receives an exciton. All of the states except the state-0 are connected to the state-D. The model is based on the following assumptions:

- Initially N_0 number of sensors are in the excited state, i.e., N_0 number of sensors

detect the target.

- No additional exciton is generated during the message propagation.
- The number of sensor nodes, N_s, and the number of actor nodes, N_a, and the total number of the network nodes, $N = N_s + N_a$, in the closed environment are constant.
- An excited sensor node gets rid of the excitation and returns to the ground-state without an exciton transfer at a rate of k_0. Note that, this is the natural fluorescence rate of the bioluminescent fluorophores used as molecular sensors.
- An excited sensor node transfers the infection to a ground-state sensor node making it excited while returning to the ground-state with a rate of k_{ss}.
- An excited sensor node transfers its excitation to an actor, and return to the ground-state with a rate of k_{sa}.
- The exciton transfer is pairwise, i.e., an excited nanonode can transfer its excitation to only a single nanonode at a time.

The information transfer rate between a rapidly-moving excited sensor node to a ground-state, i.e., available, sensor node in the environment, i.e., k_{ss}, is given using (2.3) as follows

$$k_{ss} = \frac{4\pi k_0 R_{0,ss}^6}{3V a_{ss}^{-3}} \tag{2.6}$$

where $R_{0,ss}$ is the Förster radius between sensor nodes, and a_{ss} is the intermolecular distance of closest approach of two sensor nodes. We assume that the bioluminescent sensors are spherical with radius r_s, therefore, $a_{ss} = 2r_s$. Similarly, the rate of the information transfer from an excited sensor node to an actor node is given by

$$k_{sa} = \frac{4\pi k_0 R_{0,sa}^6}{3V a_{sa}^{-3}} \tag{2.7}$$

where $R_{0,sa}$ is the Förster radius between a sensor node and an actor node, and a_{sa} is the intermolecular distance of closest approach of a sensor node with an actor node. Assuming that the actor nodes are also spherical with radius r_a, $a_{sa} = r_s + r_a$.

Based on the listed assumptions, and using the transfer rates in rapid-diffusion, we derive the transition rates of the Markov chain. The state-dependent death rate, α_i, is the overall fluorescence rate on the network, and it can be given by

$$\alpha_i = ik_0 \tag{2.8}$$

where i is the number of excitons, i.e., number of excited sensor nodes, on the network, and k_0 is the natural fluorescence rate of the fluorophores which we assume identical for each fluorophore. The exciton transfers between sensor nodes do not alter the state of the network, since the number of excitons does not change. The overall transfer rate between nanosensors is given in terms of number of excited state sensors and ground-state sensors as

$$\theta_i = i(N_s - i)k_{ss} \tag{2.9}$$

where N_s is the total number of sensor nodes. The rate of transfer from the excited sensor nodes to the actor nodes can be given by

$$\mu_i = iN_a k_{sa} \tag{2.10}$$

where N_a is the number of actor nodes.

Considering the infeasibility of deriving analytical expressions for the performance metrics for this death process, we simulate the model by dividing the time into small intervals, i.e., Δt, in which we assume only one event, e.g., exciton transfer or fluorescence, can occur. For this time interval, the transition probabilities can be given

as

$$P_{i,i-1} = P(S_{t+\Delta t} = i-1 | S_t = i) \approx \alpha_i \Delta t \tag{2.11}$$

$$P_{i,i+1} = P(S_{t+\Delta t} = i+1 | S_t = i) = 0 \tag{2.12}$$

$$P_{i,D} = P(S_{t+\Delta t} = D | S_t = i) \approx \mu_i \Delta t \tag{2.13}$$

$$P(S_{t+\Delta t} = i | S_t = i) \approx 1 - P_{i,i-1} - P_{i,D} \tag{2.14}$$

where $i = 1, 2, ...N_0$, and S_t demonstrates the state of the network at time t. Using the transition probabilities and setting a sufficiently small time interval Δt, we conduct a Monte Carlo simulation in Matlab to obtain the successful detection probability of a single message, $Pr(success)$ and average message delivery delay, $E[T_d]$ for different system parameters. The detection probability is calculated as the number of successful transmission to the number of extinctions without detection. The simulation is run until the detection probability converges to a finite value. In the simulations, we also obtain the average number of actor nodes that receive an exciton for each cycle of message transmission, i.e., n. Using this parameter and the mean delay as the average extinction time of the excitons, we derive the average system throughput as

$$T_{avg} = \frac{n}{E[T_d]} \tag{2.15}$$

If there is sufficient interval between each target detection, intersymbol interference (ISI) does not occur. Since we assume that no other excitons except the initial excitons are generated during the transmission, no-target message, i.e., bit-0, is always successfully detected if there is no-ISI. Considering that only the transmission of bit-1 is problematic, the communication channel between nanosensors and nanoactors is information theoretically a Z-channel. Therefore, considering X as the transmitted bit by the sensor nodes, and Y as the received bit by the actor nodes, the mutual

information between X and Y can be expressed as

$$I(X;Y) = H(P_E\ Pr(Success)) - P_E\ H(1 - Pr(Success)), \tag{2.16}$$

where $H(.)$ is the binary entropy function, and P_E is the event probability.

The derived metrics based on the simulations are sufficient to evaluate the performance of the FRET-MSAN with different system parameters. The results of the simulation and the network performance based on the varying parameters are discussed in the Section 7.4.2.

2.3.2 FRET-Based Mobile Ad Hoc Molecular Network

In FRET-MAMNET, there are three kinds of fluorophore-based nanonodes randomly dispersed in the same environment: *i*) nanotransmitter; *ii*) nanorelays; and *iii*) nanoreceivers. The single nanotransmitter in the network is continuously excited by an information source, e.g., a remote optical source or a nearby electrical source, with a pulse of duration T_p. The excited transmitter node generates excitons randomly during T_p. We can assume that the nanotransmitter is always occupied by an exciton, therefore, it is always in the excited-state. The relay nodes are not directly excited by an information source. The excitons generated on the nanotransmitter follow random hopping with sequential transfers through the relay nodes, and carry the message from the nanotransmitter to the nanoreceivers. The nanoreceivers are assumed to realize a specific task, e.g., singlet oxygen sensitization, when they receive an exciton. This configuration is similar to the scenario simulated in [Kuscu and Akan, 2013b], however, here we assume that the characteristics of the network nodes satisfy the rapid-diffusion limit, therefore, we are able to derive closed form expression for transfer rates among fluorophores. The information flow in FRET-MAMNET is demonstrated in Fig. 2.3.

We model the single message propagation from the nanotransmitter to a nanoreceiver until an exciton is first received by an receiver node. Different from the FRET-

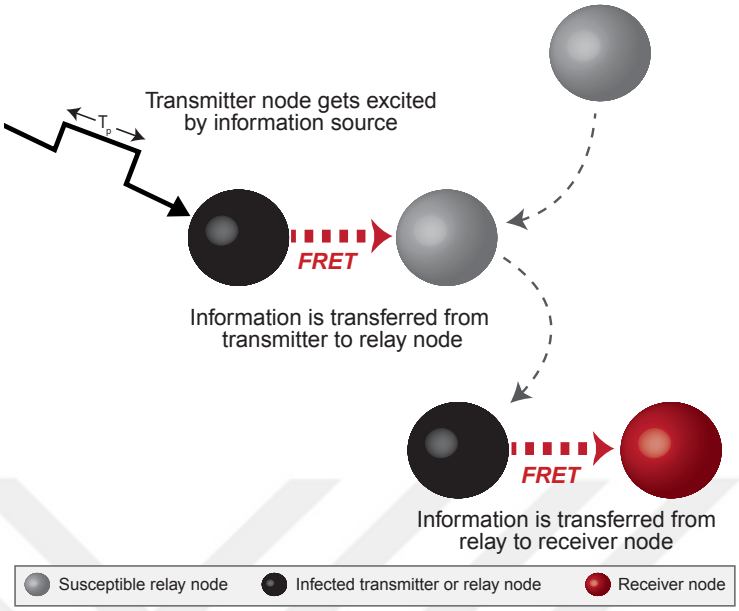


Figure 2.3: Information flow in FRET-MAMNET.

MSAN, in this network excitons are generated by the information source. Therefore, the transmission of a single message during the application of the excitation pulse is a birth-death process which can be modeled by the Markov chains demonstrated in Fig. 2.4(a). The upper limit for the number of excitons in this model can be given as the total number of relay and transmitter nodes, i.e., N_h. The Markov chain in Fig. 2.4(b) models the message propagation for the time from the cut-off of excitation pulse until the complete extinction of the excitons. This second model describing the no-pulse situation is similar to the Markov chain model of FRET-MSAN, where no exciton generation occurs. The upper limit for the second model is the number of excitons that exists on the network at the time of pulse cut-off, i.e., N_p. Note that, the message can be detected during the excitation pulse, i.e., before the second model is applied. However, the network never goes into state-0 during the pulse, since the nanotransmitter is always excited by the excitation pulse.

The model is based on the following assumptions:

- Transmitter and relay nodes are of same type of fluorophores, i.e., they have the

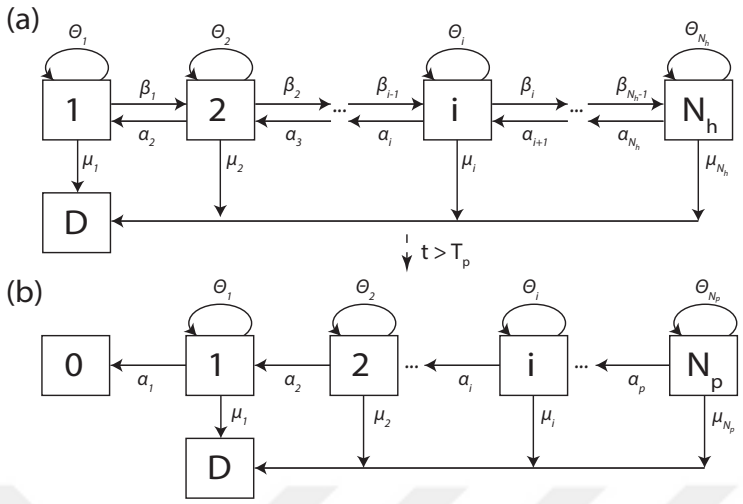


Figure 2.4: Markov chain model of FRET-MAMNET.

same fluorescence rate (k_0), Förster radius ($R_{0,hh}$) and molecular radius (r_h).

- There is only a single nanotransmitter that can receive excitation signal from the information source.

- An excited nanonode gets rid of the excitation and returns to the ground-state without transfer of exciton at a rate of k_0.

- An excited nanonode transfers the excitation to a ground-state nanonode with a rate of k_{hh}.

- An excited nanonode transfers the excitation to a nanoreceiver with a rate of k_{hr}.

- During the pulse, excitons are generated on the transmitter node with a rate of k_g.

- The total number of transmitter and relay nodes, N_h, and the number of receiver nodes, N_r, are constant.

On the nanotransmitter, when an exciton is removed either by self relaxation, i.e., fluorescence, or by transfer to another node, another exciton is generated immediately during the application of the excitation pulse. Therefore, the exciton generation rate on the nanotransmitter is given by

$$k_g(t) = k_0 + k_{hh}(N_h - N_{h,e}(t)) \tag{2.17}$$

where $N_{h,e}(t)$ is the number of excited nanotransmitters and nanorelays at time t. k_{hh} is the transfer rate between a single transmitter-relay (or relay-relay) pair, that can be expressed using (2.3) as

$$k_{hh} = \frac{4\pi k_0 R_{0,hh}^6}{3V a_{hh}^{-3}} \tag{2.18}$$

where R_{hh} is the Förster radius between transmitter-relay (or relay-relay) pair, and a_{hh} is the intermolecular distance at the closest approach of a relay node with a relay or transmitter node. In a similar way, the exciton transfer rate between an excited relay (or transmitter) and a receiver node is given as

$$k_{hr} = \frac{4\pi k_0 R_{0,hr}^6}{3V a_{hr}^{-3}} \tag{2.19}$$

where R_{hr} is the Förster radius between a nanoreceiver and a nanotransmitter or nanorelay, and a_{hr} is the intermolecular distance at the closest approach of a nanoreceiver with a nanorelay or nanotransmitter.

The state-dependent transition rates on the Markov chain can be expressed in terms of the exciton transfer, generation, and fluorescence rates as follows

$$\alpha_i = ik_0 \tag{2.20}$$

$$\theta_i = i(N_h - i)k_{hh} \tag{2.21}$$

$$\mu_i = iN_r k_{hr} \tag{2.22}$$

where i always denotes the number of excitons on the network. The birth rate during the excitation pulse can be expressed as the generation rate of the excitons, i.e,

$$\beta_i = k_{g,i} = k_0 + k_{hh}(N_h - i) \tag{2.23}$$

Assuming again that the time is divided by sufficiently small intervals, Δt, the transition probabilities can be expressed as follows

$$P_{i,i-1} = P(S_{t+\Delta t} = i - 1 | S_t = i) \approx \alpha_i \Delta t \tag{2.24}$$

$$P_{i,i+1} = P(S_{t+\Delta t} = i + 1 | S_t = i) \approx \beta_i \Delta t \tag{2.25}$$

$$P_{i,D} = P(S_{t+\Delta t} = D | S_t = i) \approx \mu_i \Delta t \tag{2.26}$$

$$P(S_{t+\Delta t} = i | S_t = i) \approx 1 - P_{i,i-1} - P_{i,i+1} - P_{i,D} \tag{2.27}$$

where $i = 1, 2, ...N_h$.

Using the transition probabilities for the time interval Δt, we again conduct Monte Carlo simulation to obtain the successful detection probability of the information generated on nanotransmitter, and the mean extinction time of the excitons which we name as the mean delay, i.e., $E[T_d]$. Based on the obtained transmission probabilities, we also investigate the information theoretical capacity of the channel between nanotransmitter and the nanoreceivers. Assuming a sufficient time interval between successive generation of messages on the nanotransmitter, we can neglect the ISI. Therefore, the channel shows Z-channel characteristics as in the FRET-MSAN, and its capacity can be expressed as the maximum mutual information over all input distributions, i.e.,

$$C = \max_{P_1} I(\mathbf{X}; \mathbf{Y}) \tag{2.28}$$

where P_1 is the probability that the information source generates bit-1. Since this time we have control over the information source different from the case of FRET-

MSAN where targets can be detected randomly, the capacity can be achieved. We derive the achievable transmission rates for the channel between nanotransmitter and nanoreceivers as follows,

$$R = \frac{C}{E[T_d]} \tag{2.29}$$

assuming that a bit interval of $E[T_d]$, i.e., mean extinction time of excitons, is sufficient to neglect ISI.

2.4 Performance Analysis of FRET-Based Mobile Molecular Nanonetworks

In this section, we evaluate the performance of the two network scenario described in Section III. We conduct Monte-Carlo simulations to obtain the successful detection probability of a single message and the mean extinction time of excitons in FRET-MSAN and FRET-MAMNET with varying network and node parameters to understand the effect of each parameter on the network performance and gain insight on the feasibility of the FRET-based mobile nanonetworks.

Note that the Markov chain models developed in the previous section are not adequate to reveal the spatial properties of these mobile nanonetworks such as communication coverage, since they are based on the number of excitons on the whole network regardless of their location assuming that the rapid-diffusion criterion is satisfied. The spatial properties of information flow can be observed by computationally expensive algorithms that do not necessitate rapid diffusion and incorporate the random Brownian motion of network nodes. This is left as a future work. Nevertheless, we know from the work in [Kuscu and Akan, 2013b] that when the network nodes are assumed to be immobile the information can be transferred over a range of 200nm.

Table 2.1: Simulation Parameters for FRET-MSAN

Radius of nanosensors (r_s)	0.25 (nm)
Radius of nanoactors (r_a)	0.25 (nm)
Natural fluorescence rate of sensor and actor nodes (k_0)	10^6 (sec^{-1})
Volume (V)	1 (μm^3)
Number of initially excited sensor nodes (N_0)	5
Total number of sensor nodes (N_s)	100
Number of actor nodes (N_a)	20
Förster radius of nanosensor-nanosensor pair ($R_{0,ss}$)	8 (nm)
Förster radius of nanosensor-nanoactor pair ($R_{0,sa}$)	8 (nm)

2.4.1 Performance Analysis of FRET-MSAN

In this section, we present the performance of the FRET-MSAN based on the simulation results for single message propagation. We analyze the single-message transmission probability, mean transmission delay as the mean extinction time of excitons, average system throughput and mutual information between the generated and the detected message for varying number of nanoactors and initially excited nanosensors, varying Förster radius between nanosensors and nanoactor, and varying size of nanomachines. Note that, the number of initially ground-state nanosensors, the Förster radius of nanosensor-nanosensor pair, and the fluorescence rate of the nanonodes do not affect the detection probability. The default values of parameters used in the numerical simulations are presented in Table 3.1.

Probability of Successful Detection

The effect of the number of initially infected nanosensors on the detection probability is shown in Fig. 2.5b with varying number of nanoreceivers. Since we assume that no other external infection occurs, and the infection is only transferred between the network nodes, the number of infected nanosensors is a decreasing function of time. Therefore, the initial number of infection is an important parameter for the detection performance. It is observed that the detection probability significantly increases even with a small increase in the number of initially infected nanosensors.

The probability of detection with varying number of nanoactors, N_a, for different values of Förster radius of nanosensor-nanoactor pair, $R_{0,sa}$, is shown in Fig. 2.5a. We observe that the detection probability significantly increases with increasing number of actors, since the chance for an infected nanosensor to be in the communication range of an actor node at any time increases.

In Fig. 2.5c, Pr(success) with varying $R_{0,sa}$ for different number of receiver nodes is presented. It is shown that as $R_{0,sa}$ increases, the probability of detection is significantly enhanced. In fact, Förster radius is analogous of the communication range of a network node in traditional networks. Therefore, with a large communication range of a nanosensor, more nanoactors as acceptors become available for the energy transfer. As a result, the transfer probability of excitons on each node increases with a decrease in the removal probability of excitons by fluorescence. We also observe that for small values of $R_{0,si}$, a large number of nanoreceivers are required to successfully detect the message of nanosensors. However, by employing nanosensor-nanoactor pairs with relatively large $R_{0,sa}$, less than 50 receiver nodes will be enough for successful detection.

The size of nanomachines also significantly affects the successful detection probability, since the extent of the distance of closest approach has a direct effect on the energy transfer rate between nanonodes. The detection probability for varying radii of nanosensors and nanoactors is shown in Fig. 2.5d. The selected values for radii are in the range of size of common fluorophores, e.g., fluorescent dyes. We observe that, using small-size nodes significantly increases the detection probability.

Mean Extinction Time of Excitons

Mean extinction time of the exciton determine the average time that the generated message (bit-1) propagates through the network. Since the actor nodes can get the excitation even when there is a single exciton existing in the network, the mean extinction time, $E[T_d]$ can be regarded as the mean delay for the message transmission, therefore it is one of the main characteristics of the mobile network.

In Fig. 2.5d, the mean extinction time is demonstrated with varying N_0 for different Förster radii. As expected, when the message is encoded into higher number of initial excitons, the extinction time increases, since the initial state of the network is further from the extinction state, i.e., state-0, when there are more initial excitons.

Förster radius between sensor nodes, $R_{0,ss}$, has no effect on the average decay time of the excitons, since it only has a contribution in the rate of the exciton transfer between sensor nodes which does not alter the state of network, i.e., the number of excitons. However, Förster radius between sensor and actor nodes, $R_{0,sa}$ has a significant effect on the extinction time. This is because, increasing $R_{0,sa}$ increases the exciton transfer rate from sensor nodes to actor nodes, i.e., k_{sa}. Since an exciton that is transferred to an actor node is assumed to be lost during the decoding process, the number of excitons decreases more rapidly, when k_{sa} increases. This is directly related to the result presented in Fig. 2.5e which demonstrates that the mean extinction time decreases with increasing number of actor nodes which also increases k_{sa}.

System Throughput

System throughput is a significant factor which determines how many actor nodes can receive the one-bit message per unit time. To calculate the system throughput, the number of actor nodes that achieve to receive excitation until the extinction of the excitons, is observed in the Monte Carlo simulations. The average system throughput that is calculated using (2.15) is demonstrated in Fig. 2.5f and Fig. 2.5g with varying N_0, N_a and Förster radii.

When the initial number of excitons increases, the extinction time of the excitons also increases, therefore it is more likely that more actor nodes get into close proximity of excited sensor nodes and get an excitation. Increasing the number of actor nodes and the Förster radius between sensor and actor nodes, the exciton transfer rate from excited sensor nodes to the actor nodes increases. This results in a higher detection probability at any time interval. Therefore, excitons can be transferred to more actor nodes during a single message transmission.

Mutual Information

Mutual information between the transmitted message and the detected message is a measure of the reliability of the communication. It is a function of the probability distribution of the transmitted message. In FRET-MSAN, the input message is the target detection signal which is encoded into excitons. We refer to detection message as bit-1. Bit-0 denotes the no-target information, and assuming that no other excitation except the initial ones occurs during the transmission, the correct transmission probability of bit-0 is always 1. However, the probability of the correct transmission of bit-1, i.e., target information, depends on the system parameters.

Here, we investigate the mutual information between the transmitted and received alphabets for varying number of initial excitons and actor nodes, and for different molecular sizes of nanosensors and nanoactors. When the number of initial excitons and actor nodes increase and the size of the nanonodes is reduced, the successful transmission probability of bit-1 significantly increases. As a result the mutual information also increases as is seen in Fig. 2.6.

2.4.2 Performance Analysis of FRET-MAMNET

In this section, we present the results of numerical simulations to investigate the performance of FRET-MAMNET in terms of probability of successful transmission of bit-1, mean extinction time of excitons, information theoretical channel capacity and achievable communication rates. We evaluate the effect of varying number network nodes, varying Förster radii of different pairs, varying lifetime of the nanosensors, varying size of nanonodes, and varying pulse length on these performance metrics. Note that, different from FRET-MSAN, the number of ground-state nanosensors and the excited state lifetime of nanosensors have effect on the performance of FRET-MAMNET through their effect on the generation rate of excitons. The default values of the system parameters used in the simulations are given in Table 2.2.

Table 2.2: Simulation Parameters for FRET-MAMNET

Radius of nanotransmitters and nanorelays (r_h)	0.25 (nm)
Radius of nanoreceivers (r_r)	0.25 (nm)
Excitation pulse length (T_p)	2 (μs)
Natural fluorescence rate of nanotransmitter, nanorelay and nanoreceivers (k_0)	10^6 (sec^{-1})
Volume (V)	1 (μm^3)
Total number of transmitter and relay nodes (N_h)	100
Number of receiver nodes (N_r)	20
Förster radii of nanotransmitter-nanorelay and nanorelay-nanorelay pairs ($R_{0,hh}$)	8 (nm)
Förster radii of nanorelay-nanoreceiver and nanotransmitter-nanoreceiver pairs ($R_{0,hr}$)	8 (nm)

Probability of Successful Detection of Bit-1

Here, we investigate the effect of pulse length, mean excited state lifetime of the fluorophores, the number of relay nodes, and the Förster radii between fluorophores on the detection probability of bit-1.

The result presented in Fig. 2.7a reveals that the pulse length has a significant effect on the success probability. This is because it determines the number of transmitted excitons into the network. As the pulse length increases, the excitons stay longer time on the network which increases the probability for a receiver node to get into the range of an excited relay or transmitter node. As a result, the receivers can detect the message with a higher probability. The increasing Förster radius between the relay and transmitter fluorophores, $R_{0,hh}$ increases the transfer rate from the nanotransmitter to the nanorelays, therefore, excitons are generated more rapidly on the nanotransmitter. This results in a higher number of excitons existing on the network at the same time which increases the detection probability. When the Förster radius between relay and receiver nodes $R_{0,hr}$ increases, the transfer probability of the excitons from the excited relay nodes to the receiver nodes increases, i.e., detection probability increases.

The effect of excited state lifetime of the nanonodes, τ_0, is shown in Fig. 2.7b for

different N_h. It is shown that increasing the lifetime decreases the detection probability. The lifetime has a significant effect on the transmitter side, such that, it directly affects the exciton generation rate. Lifetime gives a measure of average occupation time of an exciton on a nanonode. When the lifetime is short, the excitons are generated more frequently on the nanotransmitter, therefore, the number of excited nanonodes on the network at time t increases, as a result the detection probability increases. It is also clearly shown that the detection probability significantly increases with increasing number of nanorelays. Increasing the concentration of the relay nodes increases the number of ground-state nodes in the range of an excited relay node, thus, increases the transfer rate for each of the nanonode, and excitons stay longer time in the network. Keeping the number of excitons high increases the probability for a receiver to encounter an excited nanonode in its range, and thus increases the detection probability of bit-1.

Mean Extinction Time of Excitons

Mean extinction time is investigated for varying pulse length and varying excited state lifetime of the fluorophores. Fig. 2.7c reveals that the mean extinction time almost linearly increases with the increasing pulse length. This is expected because the excitation pulse prevents the network from entering into the extinction state, such that, the transmitter always has an exciton during the application of the pulse. However, when the pulse is cut-off, the number of excitons quickly decay and extinction occurs.

Fig. 2.7d demonstrates that the mean extinction time linearly increases with increasing lifetime of the fluorophores. When the lifetime increases, excitons occupy longer time on the network nodes, and the fluorescence rate decreases reciprocally. As a result, the removal rate of the excitons from the network decreases, and excitons survive longer on the network.

Channel Capacity

The channel capacity is the maximum mutual information over all input distributions, and it is related to the reliability of the message transmission. Assuming the bit interval satisfies the no-ISI criterion, the capacity of the communication channel between the nanotransmitter and the nanoreceivers is directly related to the successful transmission probability of bit-1. The channel capacity for varying pulse length and mean lifetime of the fluorophores is shown in Fig. 2.7e and Fig. 2.7f, and the correlation between the transmission probability of bit-1 presented in Fig. 2.7a and Fig. 2.7b is clearly demonstrated.

Achievable Rates

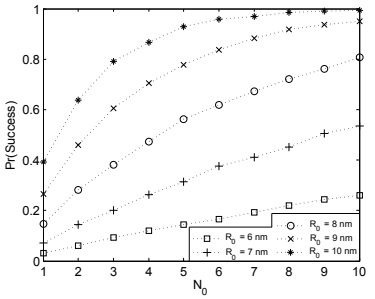
Considering that setting the bit interval as equal to the mean extinction time of excitons, we can neglect the ISI, such that the successive transmissions of messages do not lead to ambiguity in the detection of the messages. Therefore, the achievable rates for varying system parameters are calculated according to (2.29). Fig. 2.7g and Fig. 2.7h demonstrates the communication rates for different pulse lengths and mean excited state lifetimes. The results reveal that communication can be realized at a rate of 50 *kbps* over FRET-MAMNET. Note that, the pulse length has almost no effect on the communication rate. Although, increasing pulse length significantly increases the channel reliability, it also linearly increases the extinction time, i.e., bit interval.

2.5 Conclusion

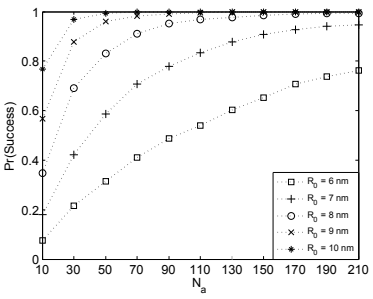
In this chapter, based on our recent studies, we introduce FRET-based mobile molecular nanonetworks for the first time in the literature. We present continuous time Markov chain models for FRET-based mobile molecular sensor and actor networks (FRET-MSAN) and FRET-based mobile ad hoc molecular networks (FRET-MAMNET) benefiting from birth-death processes. We analyze the performance of both nanonet-

works in terms of reliable transmission probability, message transmission delay, system throughput, mutual information, information theoretical channel capacity and achievable rates assuming that the network nodes satisfy the rapid-diffusion criterion. The simulation results reveal that it is possible to achieve reliable communication at high-rates with FRET-based mobile molecular networks.

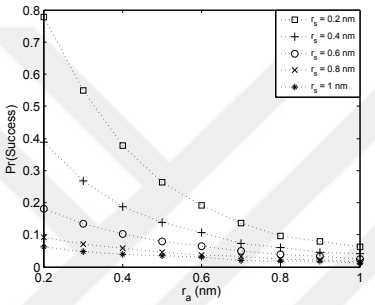
The deployment of bioluminescent sensor fluorophores and photoactive actor fluorophores makes FRET-MSAN promise autonomous applications of target detection and acting at nanoscale such as highly precise PDT applications with singlet oxygen sensitizer fluorophores as actor nodes. FRET-MAMNET provides the opportunity of remotely controlling the operation of nanonetworks by an optical information source. This optical link can be made bidirectional if the fluorescence outputs of nanoreceivers are observed by photodetectors, and therefore, it can provide a connection between nanonetworks and larger communication networks, which is currently not possible for other molecular networks proposed so far.



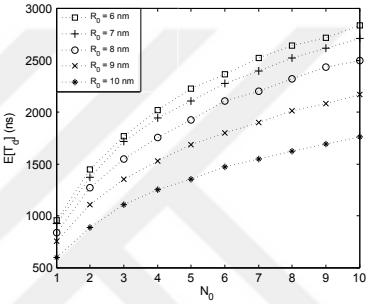
(a) $Pr(success)$ with varying N_0 for different $R_{0,ss} = R_{0,sa} = R_0$.



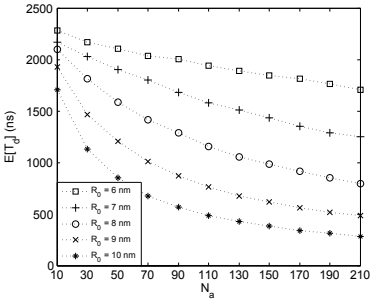
(b) $Pr(success)$ with varying N_a for different $R_{0,ss} = R_{0,sa} = R_0$.



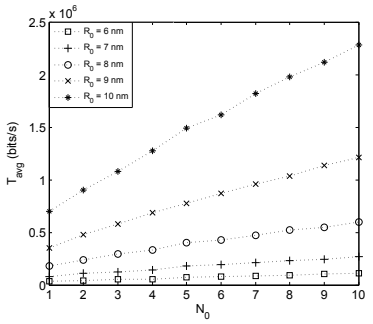
(c) $Pr(success)$ with varying r_a for different r_s.



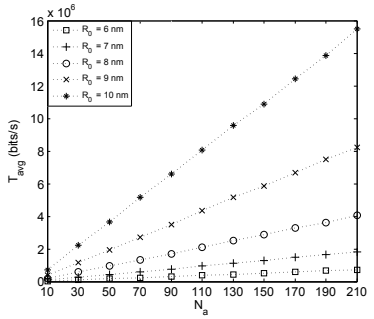
(d) $E(T_d)$ with varying N_0 for different $R_{0,ss} = R_{0,sa} = R_0$.



(e) $E(T_d)$ with varying N_a for different $R_{0,ss} = R_{0,sa} = R_0$.

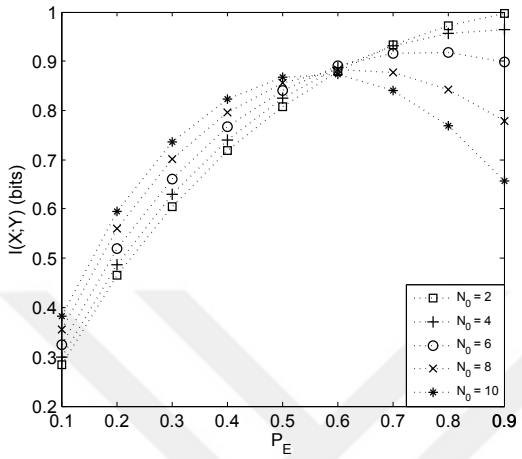


(f) T_{avg} with varying N_0 for different $R_{0,ss} = R_{0,sa} = R_0$.

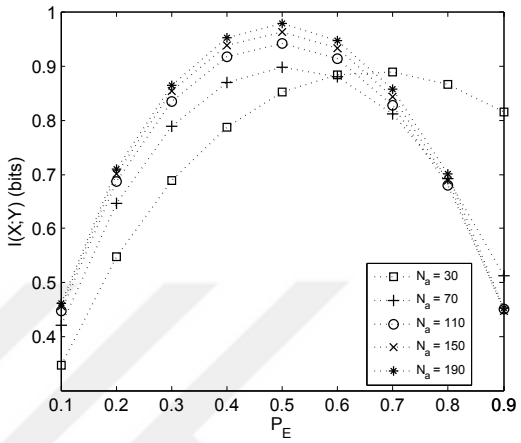


(g) T_{avg} with varying N_a for different $R_{0,ss} = R_{0,sa} = R_0$.

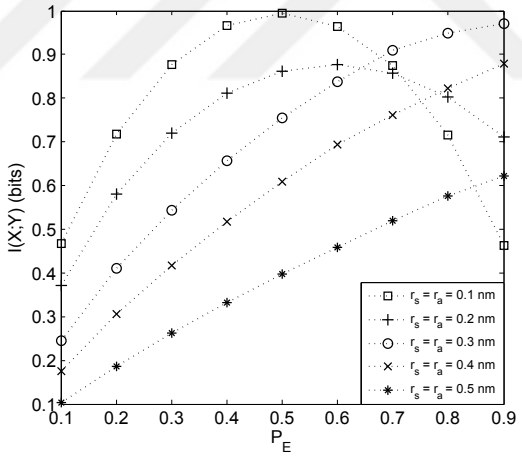
Figure 2.5: The successful detection probability, mean extinction time of excitons, and average system throughput for one-bit message transmission in FRET-MSAN.



(a) $I(X;Y)$ with varying P_E for different N_0.

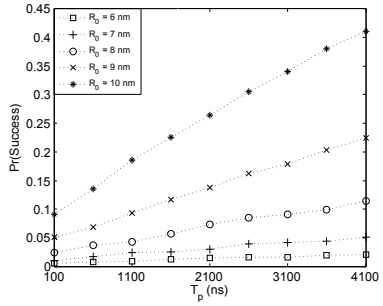


(b) $I(X;Y)$ with varying P_E for different N_a.

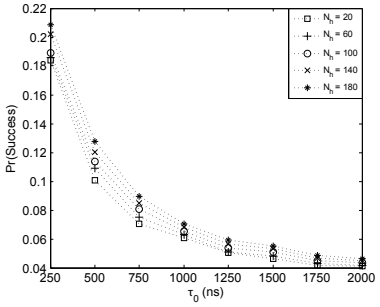


(c) $I(X;Y)$ with varying P_E for different r_s, r_a.

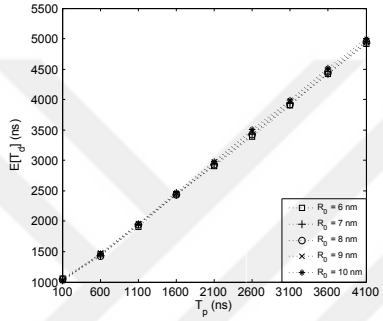
Figure 2.6: Mutual information between the generated message on nanosensors and detected message by the nanoactors in FRET-MSAN.



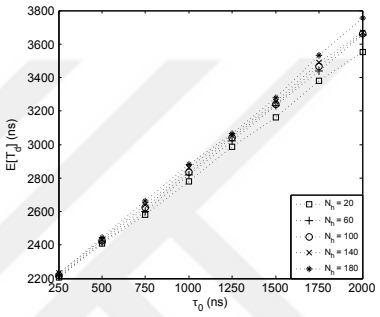
(a) $Pr(success)$ with varying T_p for different R_0.



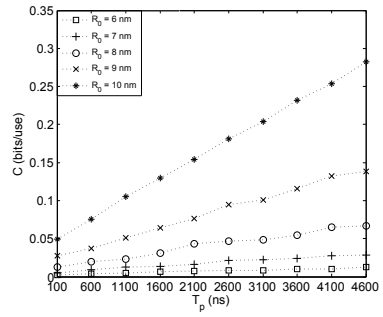
(b) $Pr(success)$ with varying τ_0 for different N_h.]



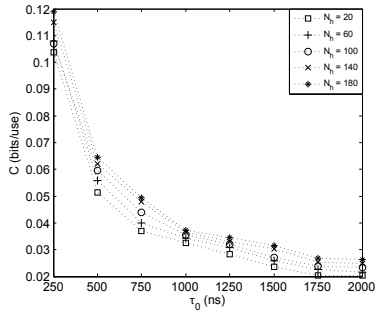
(c) $E(T_d)$ with varying T_p for different $R_{0,hh} = R_{0,hr} = R_0$.



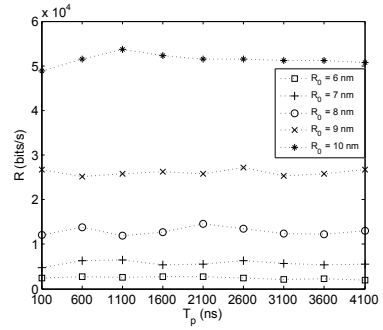
(d) $E(T_d)$ with varying τ_0 for different N_h.



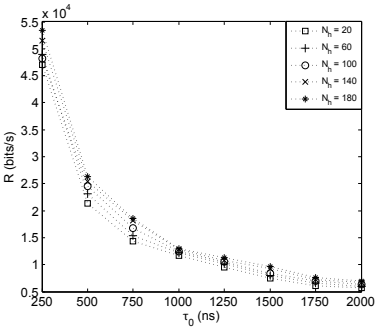
(e) C with varying T_p for different $R_{0,hh} = R_{0,hr} = R_0$.



(f) C with varying τ_0 for different N_h.



(g) R with varying T_p for different R_0.



(h) R with varying τ_0 for different N_h.

Figure 2.7: The successful detection probability of one-bit message, mean extinction time of excitons, capacity of the channels, and achievable communication rates in FRET-MAMNET.

Chapter 3

COVERAGE AND THROUGHPUT ANALYSIS FOR FRET-BASED MOBILE MOLECULAR SENSOR/ACTOR NANONETWORKS

3.1 Introduction

Nanomachines are envisioned as nano-sized functional units with basic operational capabilities such as computing, sensing, actuating. The limited capabilities of these tiny machines can be enhanced by enabling communication between them. Establishing collaborative nanonetworks among diversely specialized nanomachines is the key to realize advanced applications that nanotechnology promises such as continuous health monitoring, smart drug delivery and cancer therapy with molecular precision [Akyildiz et al., 2008]. Several attempts have been devoted to design practical and reliable nanocommunication methods such as THz-band electromagnetic and bio-inspired molecular communications [Akyildiz and Jornet, 2010a], [Nakano et al., 2005]. Recently, we have proposed a radically different molecular communication mechanism exploiting the excited-state transfer phenomenon of fluorescent molecules, i.e., Förster Resonance Energy Transfer (FRET) [Kuscu and Akan, 2012].

FRET is the non-radiative resonant transfer of excitons from an excited donor fluorophore to a ground-state fluorophore based on the near-field Coulomb interactions between them [Lakowicz, 1999]. The phenomenon has been extensively used in biotechnological applications ranging from fluorescence microscopy to biosensing and nanomedicine [Jares-Erijman and Jovin, 2003], [Samia et al., 2003]. FRET has been proposed as a communication mechanism for the first time in [Kuscu and Akan, 2012] based on the idea of encoding the information to the excited-states of fluorescent

molecules, and its performance for several channel configurations such as point-to-point, broadcast and relay have been analyzed extensively in [**?**], [Kuscu and Akan, 2013b].

Recently, we have studied FRET-based mobile molecular sensor/actor nanonetworks (FRET-MSAN) composed of bioluminescent fluorophores as the sensor nodes and photoactive florophores as the actor nodes which collaboratively perform a common task, and showed its potential for in-vivo automated biosensing/acting applications [Kuscu and Akan, 2013a]. We have modeled the information transmission propagation in these mobile nanonetworks exploiting the SIR model of epidemic disease spreading, and derived analytical expressions for the successful transfer of sensing information to an actor node in the environment by assuming that the fluorophore nodes are rapidly diffusing and have a very long excited-state lifetimes. However, using the SIR model, we ignored the spatial characteristics of the information propagation which are crucial especially for in-vivo medical applications.

In this paper, we analyze the FRET-MSAN based on the fundamental performance metrics related to spatial characteristics of the network such as the communication coverage, the network throughput as a function of distance from the information source, and the propagation rate. The exciton mobility combined with the Brownian motion of network nodes are well-observed through realistic Monte Carlo simulations. The effect of the system parameters related both to the exciton transfer mechanism and to the diffusion of the nodes on the exciton mobility are clearly revealed from the simulation results. Through the discussions, we aim to pave the way for the practical design of application-specific sensor/actor nanonetworks by configuring the easily controllable system parameters.

The remainder of this paper is organized as follows. In Section II, we present the fundamentals of FRET theory. In Section III, we introduce the FRET-MSAN and describe the analyzed network scenario. The performance analysis based on the simulation results is presented Section IV. Finally, the concluding remarks are given in Section V.

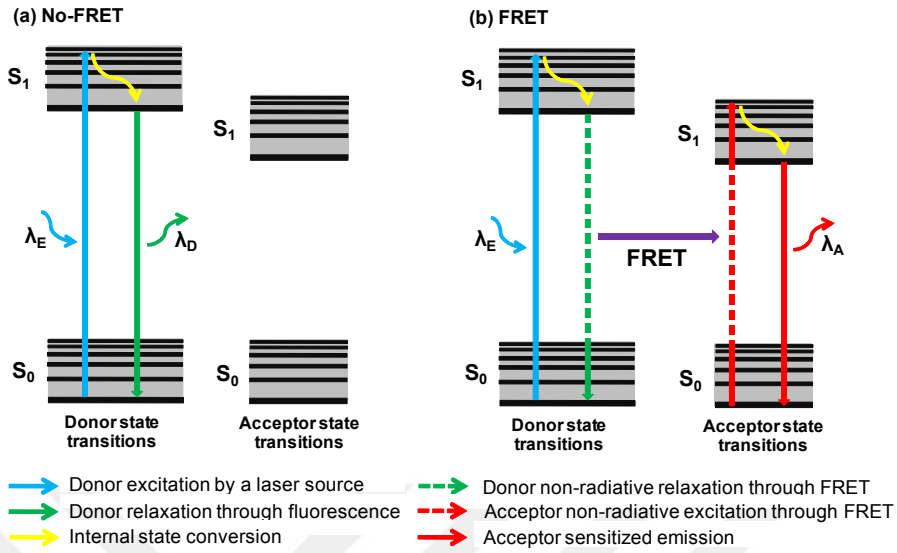


Figure 3.1: Jablonski diagram demonstrating the energy flow for the cases of (a) fluorescence and (b) FRET.

3.2 Theory of FRET

FRET phenomenon has a well-established theory which is fundamentally validated by an extensive number of experimental studies over the years [Förster, 1948]. In this section, we present the governing rate equations and briefly introduce the FRET mechanism.

When a fluorescent molecule is excited through an optical source, it relaxes after a random time either through fluorescing, i.e., releasing a photon, or through a non-radiative quenching mechanism. The natural fluorescing rate of a fluorophore k_0 is the reciprocal of its mean excited-state lifetime, i.e., $k_0 = 1/\tau_0$. The lifetime denotes the average time that the molecule stays in the excited-state before relaxing to the ground-state, and it is generally in the range of 2ns-1μs [Lakowicz, 1999]. There are several quenching mechanisms that can shorten the lifetime of an exciton on a fluorophore such as collisional quenching and transfer to a nearby ground-state fluorophore through FRET. Fig 6.1 demonstrates the Jablonski diagram for the case when FRET is the only possible quenching mechanism.

Mainly two conditions are required for FRET to occur. The spectral characteristics of donor, which is the excited fluorophore, and acceptor in the ground-state must have significant similarity, i.e., the emission spectrum of the donor and the absorption spectrum of the acceptor must overlap. The spectral similarity is proportional to the resonance probability of the molecules' transition dipoles, therefore, it increases the transfer rate. Moreover, the molecules must be in a close proximity such as 0-10 nm. When these conditions are satisfied, FRET competes with fluorescence and other quenching processes. FRET rate between a pair of excited donor and a ground-state acceptor molecule with the intermolecular distance R is given by

$$k_T = k_0 \left(\frac{R_0}{R} \right)^6 \tag{3.1}$$

where R_0 is the Förster radius denoting the distance between the molecules when $k_T = k_0$. R_0 relates the FRET rate with environmental and intrinsic parameters and can be expressed by

$$R_0 = (8.8 \times 10^{22} \kappa^2 n^{-4} Q_D J)^{-\frac{1}{6}} \tag{3.2}$$

where κ^2 is the dipole orientation factor, Q_D is the quantum yield of the donor and n is the refractive index of the medium. J denotes the degree of overlap between the donor's emission spectrum and the acceptor's absorption spectrum, and it is given by

$$J = \int_0^\infty f_D(\lambda) \epsilon_A(\lambda) \lambda^4 \mathrm{d}\lambda \tag{3.3}$$

where f_D is the normalized emission spectral function of the donor, ϵ_A is the acceptor's molar absorptivity, and λ is the wavelength. The dipole orientation factor κ^2 is expressed by

$$\kappa^2 = (\cos\theta_T - 3\cos\theta_D \cos\theta_A)^2 \tag{3.4}$$

where θ_T is the angle between the donor's emission dipole and the acceptor's absorp-

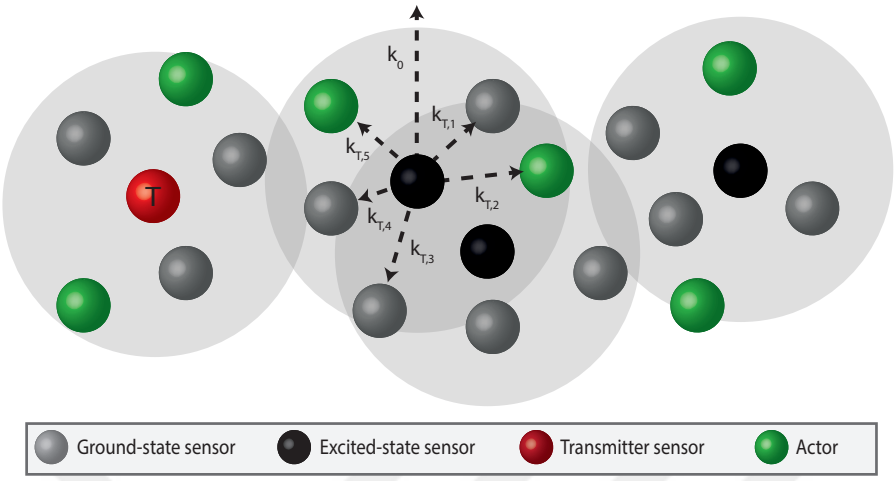


Figure 3.2: Two dimensional demonstration of an example FRET-MSAN. The arrows indicate the rates for exciton activity, and the circles denote the transfer range for an excited node.

tion dipole moment, θ_D and θ_A are the angles between these dipole moments and the axis where donor and acceptor jointly located [Lakowicz, 1999]. It is commonly assumed that $\kappa^2 = 2/3$ which is the mean value when the molecules have isotropic and unrestricted distributions.

3.3 FRET-Based Mobile Molecular Sensor/Actor Network (FRET-MSAN)

The sensor/actor nanonetwork considered in this paper consists of single fluorophore-based sensor and actor nodes which realize three dimensional random movements based on Brownian motion. The aim of this nanonetwork is to execute a proper action with the actor nodes upon the detection of a target molecule or an event by the fluorescent sensor nodes. This advanced task which can be realizable by the collaboration of differently specialized fluorophore nodes exceeds the limits of a single fluorophore's capabilities, and constitutes an excellent example for the future applications of nanocommunications.

The fluorescent sensor nodes employed in this scenario are assumed to change their spectral characteristics when they bind to a specific target molecule. We also assume

that the whole system is illuminated by an optical source which continuously releases photons with a certain wavelength. The signaling mechanism of a fluorescent sensor node can be described as follows: (i) The absorption spectrum of the nanosensor does not overlap with the wavelength of the optical source when it is not bound to any target molecule, therefore, it is not excited and stays in the ground-state. (ii) When the sensor node is bound to a target molecule, the resultant spectral shift causes an overlap of its absorption spectrum with the source wavelength, therefore, it becomes excited by absorbing a photon. After an exponentially random lifetime, it fluoresces indicating the existence of the target, if there is not any non-radiative quencher in its close vicinity. Through this mechanism, a sensor node acts as fluorescent switch which is turned on and off depending on the existence of a target molecule [de Silva et al., 2001].

The actor nodes are assumed to consist of photosensitive molecules which are specialized to realize an action upon receiving an exciton. The photosynthesizing agents, e.g., porphyrin, used in the photodynamic therapy (PDT) of cancer are appropriate examples of single molecular exciton-activated actors [Bonnett, 1995]. Under an illumination with a proper wavelength, these agents synthesize singlet oxygen which is extremely harmful for the living organisms, and therefore, they are used to initiate the apoptosis of the targeted cancer cells with the control of a remote optical excitation source. Recently, it has been experimentally proved that photosynthesizing agents can also be activated by FRET through a conjugation with a Quantum Dot (QD) [Samia et al., 2003].

In this study, we consider a scenario, demonstrated in Fig. 6.2, in which a single nanosensor, which we call as the transmitter sensor node, is bound to a target molecule. The transmitter is always in the excited-state during the application of the optical pulse, and the remaining sensor nodes stay in the ground-state since they are not bound to any target. The transmitter sensor node is assumed to be immobilized through the bound to the target molecule, while all the remaining nodes in the nanonetwork are mobile with Brownian motion. During the application of the

excitation pulse with a length of $T_p > \tau_0$, many ground-state sensor and actor nodes can enter into proximity of the excited transmitter, therefore, they frequently quench it through FRET or collisions. As long as the optical pulse is applied, the transmitter is immediately excited after it is quenched to ground-state or relaxed through fluorescence, therefore, we expect that a high number of excitons are generated on the transmitter. If a generated exciton is transmitted to an actor node through FRET, it is assumed that the actor node immediately consumes the exciton to realize its action. When the generated excitons are received by the ground-state sensor nodes through homo-FRET, i.e., FRET between identical fluorophores [[Lakowicz, 1999]], they may remove the exciton from the system by relaxing through fluorescence or collisional quenching, or they may transfer it to another ground-state sensor node or to an actor node in their close vicinity. In a properly configured system, by the consecutive exciton transfers through the sensor nodes acting like relays, the detection information can spread to a considerable region, and many actor nodes can achieve to receive the information and collaboratively increase the impact of their action.

Since the nanonetwork nodes except the transmitter are mobile, the region covered by the excitons are expected to be larger compared to the network composed of immobile nodes. However, the Brownian motion of the network nodes can have an adverse effect on the mobility of excitons, since it also increases the rate of collisions between nodes and succeeding collisional quenchings, especially when the molecular density of the environment is high. At this point, to determine the effect of main system parameters related to FRET mechanism and Brownian process on the communication coverage and diffusion rate of excitons is very crucial to design a powerful application.

In our previous work [Kuscu and Akan, 2013a], we have modeled the FRET-MSAN exploiting the Suspected-Infected-Recovered (SIR) model of epidemic disease spreading assuming that the network nodes are highly mobilized and have very long excited-state lifetimes which are greater than $1\mu s$. We have achieved to derive closed-form expressions for the probability of a transmitter sensor node to successfully transmit

its information to an actor node. However, using the SIR model, we have ignored the spatial characteristics of the information spreading which are very valuable for the applications like PDT. Since the main purposes of the cancer therapies including PDT are both to be effective on a focused region where the target is located, and not to harm the cells which function properly, the throughput of the designed system as a function of distance from the target is also important. However, to derive closed-form expressions for these spatial properties of the system is very difficult considering that the system has a very high degree of randomness which is resultant from the following characteristics:

- The sojourn times of excitons on the network nodes including the transmitter are exponentially random variables with mean values depending on the distance and the number of ground-state network nodes in the close vicinity.

- The excitons have random lifetimes on the system, and the probability for each exciton to be removed from the system by collisional quenching, fluorescing, or reception by an actor node at each time instant varies depending on the system state.

- The network nodes, that constitute the lattice for the excitons' random jumps, randomly move based on Brownian dynamics, and the state of the nodes, e.g., excited or ground-state, frequently changes with the random jump of the excitons.

Due to the difficulty to analytically model the spatial properties of the system, in the next section, we design a Monte Carlo algorithm to realistically simulate the information propagation on the system, and reveal the main characteristics like communication coverage, throughput, and propagation rate for varying system parameters.

3.4 Performance Analysis

We conduct extensive Monte Carlo simulations to determine the effect of fundamental system parameters on the characteristics of exciton mobility in FRET-MSAN. In this section, we describe the simulation setup and present the results with discussions.

3.4.1 Simulation Setup

The simulations are performed in MATLAB by dividing the whole process into small time intervals and assuming that an exciton realizes only one activity, e.g., FRET, fluorescence, during a simulation timestep. The simulation algorithm is demonstrated in Fig. 6.3. The following list summarizes the assumptions made and governing equations for the simulations:

1. The excited-state lifetimes τ_0 and the diffusion constant D of all the nodes are assumed to be identical. The Förster radii between each network node R_0 are also taken as the same.

2. The simulation timestep is determined in proportion to the excited-state lifetime of the network nodes, $\Delta t = 0.001\tau_0$, to almost guarantee no more than single exciton activity in a timestep.

3. The initial positions of the network nodes are randomly determined for each run of simulation following a uniform probability distribution on a three dimensional cubic lattice with edge length of 400nm. Periodic boundary conditions are applied for the motion of network nodes.

4. The transmitter sensor node which is bound to a point target, is always in the excited-state during the application of optical pulse.

5. The length of the optical pulse T_p is assumed to be 200ns, and the simulations are run for a duration of 250ns which almost ensures that all of the generated excitons are removed from the system at the end of the simulation.

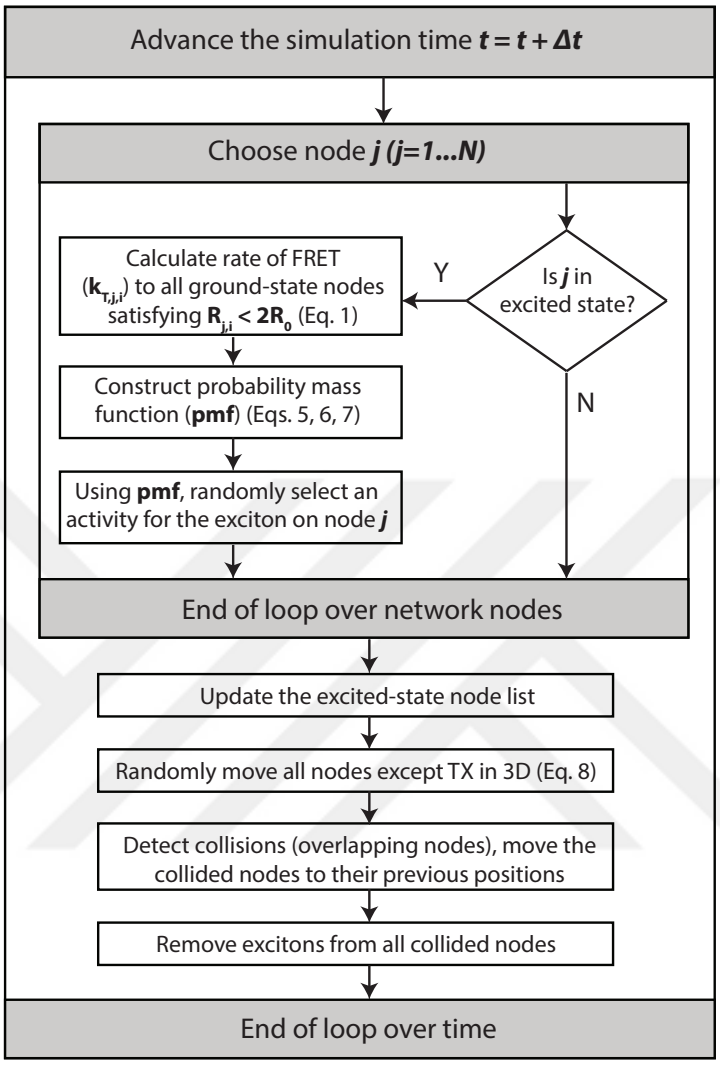


Figure 3.3: Simulation algorithm for the exciton jump process on the Brownian mobile nodes. Simulation ends when $t = 250$ns.

6. The dipole orientation factor κ^2 is taken as 2/3 which is the average value assuming free rotation of network nodes.

7. The network nodes are modeled as non-interacting hard spheres with diameters $d = 1.5$nm.

8. FRET rate between two node becomes very low when the internodal distance

exceeds $2R_0$. Therefore, in the simulations, the transfer range for an excited node is assumed to be $2R_0$; hence, the transfer probabilities to the nodes which are located at distances greater than $2R_0$ from the excited node are not calculated.

9. The transition probabilities for an exciton occupied on a sensor node given that the node does not collide with another network node during a timestep are as follows:

   (i) The transfer probability to a ground-state sensor node or to an actor node:

   $$P_{j,i} = k_{T,j,i}\Delta t \qquad i = 1, \ldots, k \tag{3.5}$$

   where j is the index of the occupied node, i is the index of the node to be transferred, and $1, \ldots, k$ are the indices of ground-state, i.e., available, sensor and actor nodes in the transfer range of occupied node. $k_{T,j,i}$ is the transfer rate from node j to node i, and calculated using (6.1).

   (ii) The probability of removal through fluorescence:

   $$P_{j,0} = k_0\Delta t \tag{3.6}$$

   (iii) The probability of remaining at the same state, i.e., on the same node:

   $$P_{j,j} = 1 - P_{j,0} - \sum_{i=1}^{k} P_{j,i} \tag{3.7}$$

10. All of the network nodes except the transmitter are assumed to realize random motion. We use Brownian dynamics which is computationally inexpensive to describe their movement and neglect the acceleration of the nodes. Their positional increments at each timestep are randomly assigned according to the

Table 3.1: Simulation Parameters for FRET-MSAN

Excited state lifetime (τ_0)	10ns
Förster radius (R_0)	6nm
Total molecular concentration (C_T)	1.44mM
Concentration ratio (C_A/C_S)	1
Diffusion constant (D)	$0.4\text{nm}^2/\text{ns}$

following normal distribution [Cinlar, 2013]:

$$dx_{\Delta t} = dy_{\Delta t} = dz_{\Delta t} = \mathcal{N}(0, \sqrt{2D\Delta t}) \tag{3.8}$$

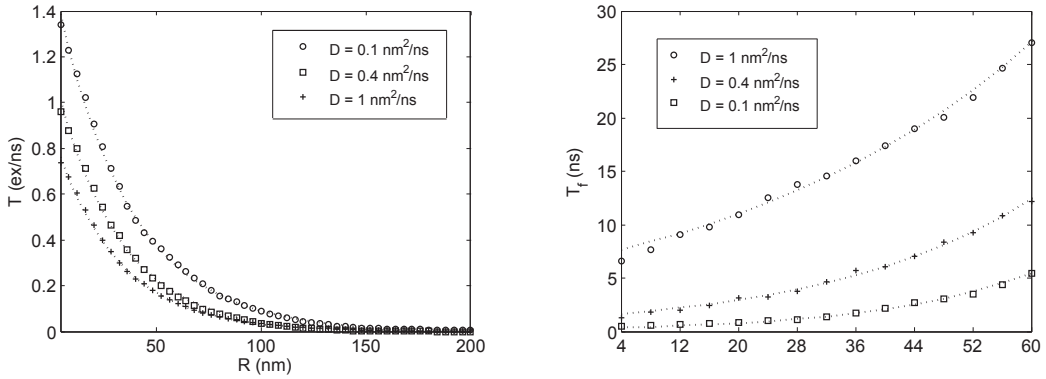
where D is the diffusion coefficient of the network nodes, and dx, dy, dz are the positional increments through x, y, z directions, respectively.

11. Since we neglect the acceleration of the nodes, the collision has to be described in a simplified manner. If an overlap between network nodes is detected as a result of their motion, the nodes are assumed to collide and move back to their position at the previous timestep. If any of the collided nodes are in the excited-state, the excitons are removed from the system as a consequence of collisional quenching. At each timestep, this is repeated until there is no overlapping node in the system.

The simulations are conducted for varying system parameters such as the excited-state lifetime, the diffusion coefficient, the Förster radii, and the concentration of molecules, and repeated for each configuration until the observed parameters converge to finite values (∼10000 repetitions for each parameter change). The default values for the main system parameters are listed in Table 3.1.

3.4.2 Results

The throughput of the FRET-MSAN is the overall transfer rate of information to the actor nodes, and it is equal to the rate at which the actor nodes perform their



(a) T with varying R for different D. (b) T_f with varying R for different D.

Figure 3.4: The mean network throughput T and mean first passage times of excitons T_f as a function of R for varying diffusion constant D with fitted exponential curves.

task, e.g., production of singlet oxygen in a PDT application. Therefore, throughput is one of the fundamental performance metrics. In the Monte Carlo simulations, we observe the number of actor node excitations with the spatial information at the resolution of 4nm for different diffusion coefficients, Förster radii, excited-state lifetimes and molecular concentrations. The throughput T as a function of distance from the transmitter is calculated as the ratio of the excitations of the actor nodes located outside the sphere with radius R and centered at the transmitter's location to the excitation pulse length $T_p = 200$ns. The results also reveal the network coverage, i.e., the region where the throughput is focused on.

We also observe the mean first passage times of excitons T_f through the spheres with radius R and centered at the transmitter's location to reveal the propagation rate of the detection information. All of the simulated parameters significantly affect the performance, and in the following sections, we discuss the reasons behind each outcome. It is to be noted that, the obtained throughput and first passage time data as a result of extensive number of simulations are well-expressed with decreasing and increasing exponential functions, respectively. In each plot demonstrating the outcomes for different parameters, we also give the well-fitted exponential curves.

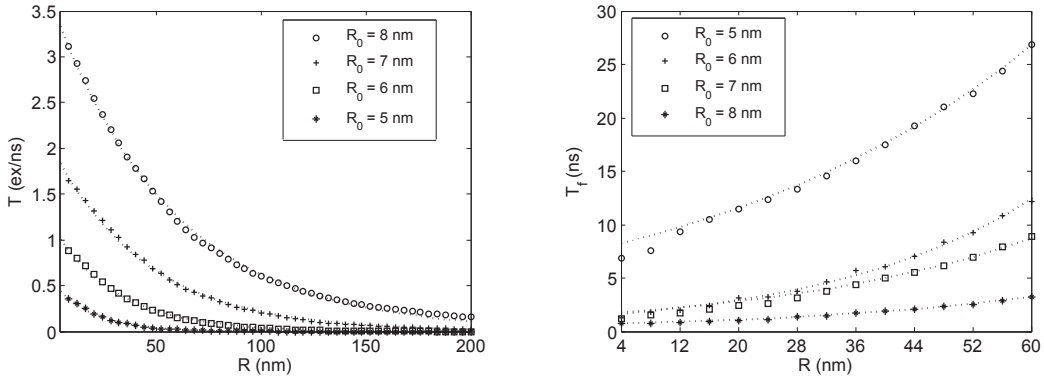
Effect of Diffusion Constant

For the first analysis, we observe the effect of node mobility on the throughput, coverage, and propagation rate. The diffusion constant D is varied in a range between 0.1-0.1nm^2/ns, which is common for fluorescent molecules in aqueous environments [Lakowicz, 1999]. The simulation results for throughput in Fig. 3.4a are quite interesting, since the high mobility of network nodes, i.e., the increased diffusion constant, results in a decrease of the throughput and the effective range. Actually, the process of exciton transfer is very fast compared to the Brownian motion of the nodes, therefore, the slightly increased node mobility cannot effectively increase the exciton mobility. Moreover, the higher collision rate with the greater diffusion constant, results in higher rate of collisional quenching of excitons, therefore, it decreases the number of excitons on the system averaged over time, and results in narrower coverage. We reveal from the results that the exciton activity is effective up to 100nm-distance from the transmitter while $D = 0.1$nm^2/ns.

The same reasons are valid for the increased mean first passage times when the diffusion constant gets greater, as shown in Fig 3.4b. Since the average number of excitons on the system decreases with the increasing collisional quenching rate, the mean time for the smaller number of excitons that achieve surviving to reach a certain distance from the transmitter also increases.

Effect of Förster Radius

Fig. 3.5a demonstrates the effect of Förster radius R_0 on the throughput performance of the network. As is seen, the higher R_0 results in higher throughput and significantly larger coverage. The increased R_0 extends the transfer range for a single exciton. Moreover, the FRET rate is strongly enhanced with the increased R_0. As a consequence, excitons are more frequently generated on transmitter, and more frequently transferred between sensor nodes. Therefore, the chance for an exciton to survive at larger distances increases, and the chance for an actor node to receive an exciton through FRET from an excited sensor also increases which results in higher



(a) T with varying R for different R_0. (b) T_f with varying R for different R_0.

Figure 3.5: The mean network throughput T and mean first passage times of excitons T_f as a function of R for varying Förster radius R_0 with fitted exponential curves.

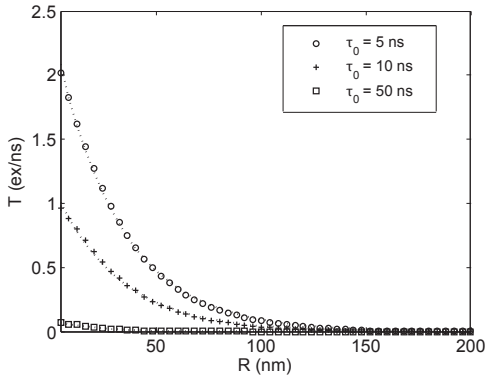
throughput for greater R_0.

The propagation rate is also strongly affected by the varying R_0 as is seen in Fig. 3.5b. The high exciton mobility obtained by increasing R_0 significantly decreases the mean first passage time of excitons through certain distances. For $R_0 = 8$nm, in a very short time less than 10ns, the volume of radius 60nm is covered by the excitons signaling the existence of the target.

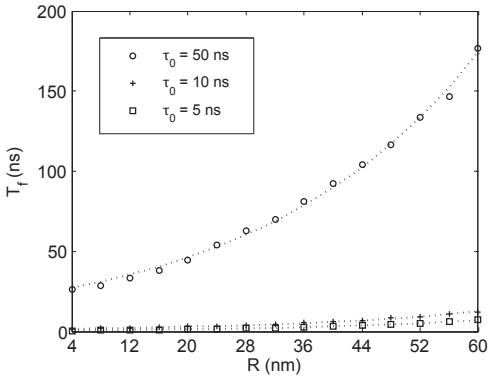
Effect of Excited State Lifetime

The excited-state lifetime τ_0 strongly affects the throughput as seen in Fig. 3.6a. As the lifetime increases, the network throughput significantly decreases. This is mainly resultant from the fact that when the lifetime increases, the exciton generation rate on the transmitter decreases, since each generated exciton stays longer time on transmitter. Moreover, the FRET rate decreases with greater sojourn times, and therefore, at each timestep, the probability for an exciton to be removed from the system through collisional quenching or fluorescence increases.

The increased lifetime also decreases the propagation rate of the excitons as demonstrated in Fig. 3.6b. In fact, most of the simulations for $\tau_0 = 50$ns resulted

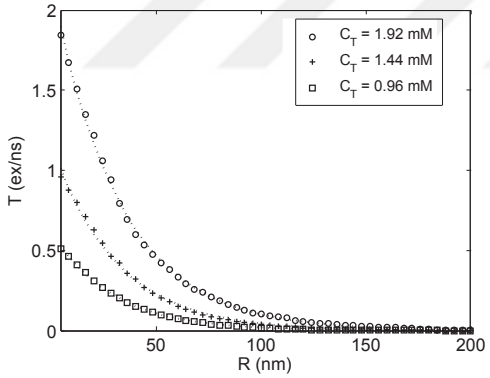


(a) T with varying R for different τ_0.

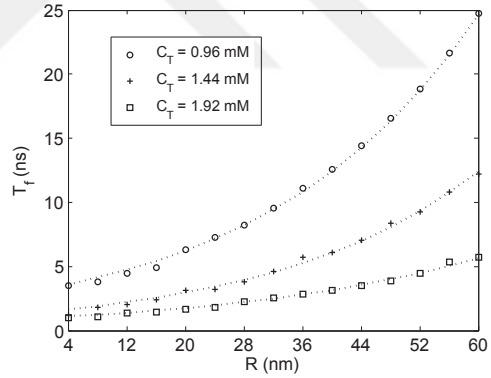


(b) T_f with varying R for different τ_0.

Figure 3.6: The mean network throughput T and mean first passage times of excitons T_f as a function of R for varying mean excited state lifetime τ_0 with fitted exponential curves.



(a) T with varying R for different C_T.



(b) T_f with varying R for different C_T.

Figure 3.7: The mean network throughput T and mean first passage times of excitons T_f as a function of R for varying total concentration C_T with fitted exponential curves.

with the extinction of excitons before reaching to 60nm-barrier. Therefore, it is a wise strategy to employ short-lifetime molecules for applications requiring fast information dissemination over greater volumes.

Effect of Molecular Concentration

In order to investigate the impact of nodal density on the throughput and propagation rate, we simulate the system increasing the total molecular concentration and by keeping the individual concentrations of sensor and actor nodes as equal to each other. The results presented in Fig. 3.7a are not considerably different from the expected, such that, the throughput increases for the denser network. In fact, the higher concentration causes a decrease of the average intermolecular distances between network nodes, which results in the higher transfer rate, therefore, the exciton mobility increases. The exciton generation rate at the transmitter node is also increases, since the generated excitons are more frequently transmitted to the system through energy transfers. On the other hand, the increased nodal density causes higher collisional quenching rate. However, this time, the increased quenching rate cannot suppress the increase in the exciton mobility.

The result of the simulations for the propagation rate, given in Fig. 3.7b, clearly demonstrates that when the concentration is lower, it takes longer time on average to reach a certain distance from the transmitter, underlining the reduced exciton mobility resultant from the decreased density.

3.5 Conclusion

In this chapter, we analyze the fundamental spatial properties of information propagation in FRET-MSAN performing extensive Monte Carlo simulations. We investigate the effect of main system parameters on the coverage, network throughput and propagation rate, and conclude that the exciton mobility can be described by the FRET mechanism rather than the diffusion of network nodes. We show that excitons signaling the existence of a single target molecule can rapidly propagate and activate actor nodes over significant distances compared to their sizes when the system parameters are properly set.

Chapter 4

AN INFORMATION-THEORETIC MODEL AND ANALYSIS OF GRAPHENE PLASMON-ASSISTED FRET-BASED NANOCOMMUNICATION CHANNEL

4.1 Introduction

Nanotechnology has enabled manufacturing of nano-size machines such as nano-robots, nanosensors, nano-logic gates which are able to perform simple actuating, sensing and computing operations. Forming nanonetworks by enabling coordination through communication among them is envisioned to significantly enhance their operational capabilities. Therefore, realizing communication at nanoscale is of crucial importance for groundbreaking medical, environmental and industrial nanotechnology applications. Nanocommunications have been approached from several perspectives such as molecular [Akyildiz et al., 2011], acoustic [Hogg and Freitas Jr, 2012], or electromagnetic [Akyildiz and Jornet, 2010a], some of which are bio-inspired. In addition to these approaches, we proposed a radically different communication technique based on Förster Resonance Energy Transfer (FRET) observed among fluorescent molecules, e.g., organic dyes, fluorescent proteins, and Quantum Dots (QDs) [Kuscu and Akan, 2012].

FRET is a well-known quantum mechanical phenomenon which defines the non-radiative resonant transfer of excitons from an excited donor fluorophore to a ground state fluorophore based on the near-field Coulomb interaction between them [Lakowicz, 1999]. It is widely observed in photosynthesis during the coherent transmission of absorbed optical energy to reaction center [Van Amerongen et al., 2000]. The phenomenon has been extensively used in biotechnological applications ranging from

fluorescence microscopy to biosensing and nanomedicine. For example, based on the FRET mechanism, QDs have been proposed as efficient photosensitizers for photodynamic therapy (PDT) of cancer [Samia et al., 2003]. Moreover, single molecular logic gates have been designed exploiting the FRET phenomenon, which underlines its potential for molecular information processing [Li et al., 2007]. Recently, we proposed to use FRET as a communication means between single-fluorophore-based nanomachines, and analyzed its performance for several channel configurations such as point-to-point, broadcast and relay [**?**]-[Kuscu and Akan, 2013b]. We also studied FRET-based mobile ad hoc nanonetworks, and showed its potential for in-vivo biosensing applications [Kuscu and Akan, 2013a]. However, the range of FRET and FRET-based nanocommunication is very limited since it is based on the weak Coulomb interaction of fluorophores, which strongly degrades for intermolecular distances larger than Förster radius, e.g., 2-10nm.

Our approaches from the communications perspective to resolve this problem theoretically resulted in a communication range of approximately 200nm by applying longer excitation pulses, and employing a large concentration of fluorescent molecules as the relay nodes [Kuscu and Akan, 2013b]. Besides our studies, several attempts have been made to increase the range of FRET. A large body of work has been focused on the enhancement of transfer efficiency and range near the metal interfaces. The underlying mechanism of this phenomenon is the intermediation of the Surface Plasmon Polaritons (SPPs) to carry the exciton energy over larger distances [Komarala et al., 2008]. In other words, an excited donor fluorophore in the close vicinity of a metal-air interface excites SPPs, and the excited SPPs traveling through the two dimensional interface transfer their energy to a nearby acceptor fluorophore through a near-field interaction. However, the ohmic losses intrinsic to the metallic interfaces limits this enhancement of range. Recently, this phenomenon is revisited by employing Graphene Plasmons (GPs) as the intermediaries of energy transfer, and it is theoretically demonstrated that the transfer efficiency can be increased by a factor of 10^4 over distances larger than 500nm [Velizhanin and Shahbazyan, 2012].

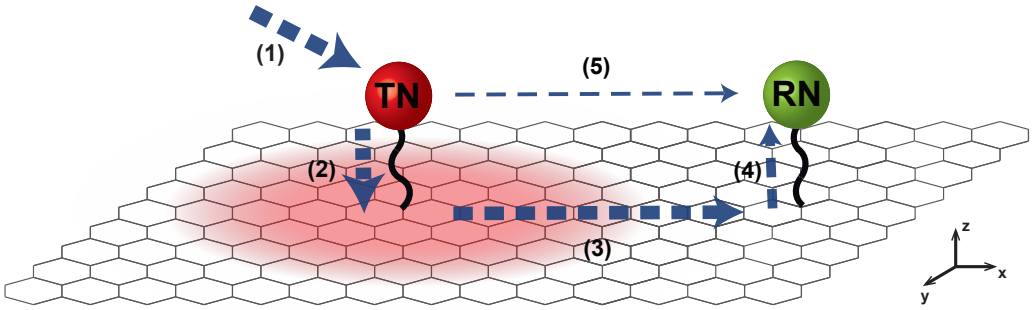


Figure 4.1: The conceptual design of plasmon-assisted FRET-based communication channel on a graphene sheet. Arrow (1) denotes the excitation power, (2) denotes the total power transferred to the graphene, (3) is the power of the generated GPs traveling through graphene, (4) is the power transferred to the acceptor QD by the GPs, (5) is the transferred power through direct FRET mechanism.

Graphene plasmonics is a newly emerging research area, and fundamentally differs from the metal plasmonics by offering significant advantages in terms of lower plasmonic losses resulted from the weaker electron-phonon interactions [Luo et al., 2013]. Another intrinsic advantage of GPs over metalic SPPs is the adjustability of the extent of strong electromagnetic energy confinement through electrical gating or chemical doping. However, a fundamental problem arises from the weak coupling of freely propagating photons to graphene plasmons which does not allow the direct optical excitation of plasmons [Jablan et al., 2013]. The very first studies on the exciton-GP interactions originates from this limitation, such that, using semiconductor fluorescent molecules like Quantum Dots (QDs) as nanoscale tips was proposed to excite GPs through near-field interaction, and the strong coupling between GPs and excitons was underlined [Velizhanin and Efimov, 2011]. Moreover, the long-range coupling of QD emitters near the graphene interface was also demonstrated in [Huidobro et al., 2012]. Furthermore, GPs begin to find applications in nanocommunications by allowing the design of graphene-based nanoantennas for communication in THz band [Jornet and Akyildiz, 2013].

In this article, for the first time in the literature, we investigate the phenomenon of exciton-GP coupling from the information theoretical perspective. We propose and

analytically model a point-to-point nanocommunication channel between a single pair of QD molecules immobilized on a two-dimensional chemically doped graphene sheet through aptamers. We assume that binary ON/OFF Keying modulation is utilized, and the information is represented by finite optical pulses. Employing GPs as the intermediaries for information transfer from a donor QD as the nanotransmitter to an acceptor QD as the nanoreceiver which are distantly located, we derive an analytical expression for the capacity of this communication channel. Based on the channel capacity, we analyze the channel's performance for varying system design parameters such as the excitation pulse length and intermolecular distance, and intrinsic parameters of graphene and QDs such as the QD's radiative lifetime and electron scattering rate of graphene. We aim to reveal the effect of each controllable parameter on the communication performance. We arrive at the conclusion that reliable communication is possible through intermolecular distances over 500nm with relatively high communication rates by properly adjusting the system parameters.

The proposed communication channel promises for a wide variety of nanotechnology applications. For example, the outputs of a number of fluorescent biosensors which are capable of detecting single molecular targets, and dispersed on a graphene surface can be rapidly transfered to a reaction center, e.g., fluorophore-based singlet oxygen synthesizers, for real-time acting. Moreover, it can enable high-rate information processing through nanoscale FRET-based logic gates when the system is powered by a remote optical source. It also constitutes an optical interface between nanoscale and macroscale operations.

The remainder of the paper is organized as follows. In Section II, we present the system model, and derive the channel capacity. Numerical analyses for channel performance are presented in Section III. Finally, the concluding remarks are given in Section IV.

4.2 Channel Model

The proposed nanocommunication channel is conceptually demonstrated in Fig. 4.1. A QD pair is located in the close proximity of the graphene. The QDs have different but similar optical characteristics, such that, one of them is acting as energy donor, and the other one is acting as energy acceptor. The emission spectrum of the donor and the absorption spectrum of the acceptor have a considerable overlap such that resonant energy transfer between them is possible. We consider that binary ON/OFF Keying modulation is employed. The information is encoded into the excited state of the QDs, such that excited state represents bit-1, and ground state represents bit-0.

The donor QD is the nanotransmitter of the system which is powered by a remote optical source with a wavelength belongs to its absorption spectrum. The optical source can be either an information source which sends the information to the donor QD, i.e., nanotransmitter, by means of finite length optical pulses, or a power source which continuously excites the donor and allows it to switch on and off in the context of biosensing operation. The excited nanotransmitter is expected to generate longitudinal plasmons on the graphene surface which can travel a certain distance depending on the system parameters. The plasmons that succeed to arrive to the proximity of the acceptor QD, i.e., nanoreceiver, are expected to excite the acceptor. The donor QD can also directly excite the acceptor QD through the classical FRET mechanism, or it can relax through fluorescence. We assume that the nanoreceiver can detect bit-1 when it receives at least one exciton during the transmission of bit-1.

In the following, we analytically model information transmission through the channel, and derive the information theoretic capacity. The transmission of bit-1 relies on the transfer of the generated excitons on the nanotransmitter to the nanoreceiver through the plasmonic channel. In order to express the probability of successful transmission of bit-1, it is imperative to begin with the derivation of the transfer probability of single generated exciton.

4.2.1 Probability of Energy Transfer

An excited fluorescent molecule, e.g., QD, relaxes to the ground state after a random duration through radiative or non-radiative energy loses. While radiative loses are directly related to the intrinsic characteristics of the fluorophore, e.g., fluorescence rate, non-radiative loses mostly depend on the electromagnetic interactions within the molecular proximity [Lakowicz, 1999]. For the nanotransmitter in our system, the excitation power is dissipated through three distinct ways:

$$P_{Total}(w) = P_0(w) + P_G(w) + P_{FRET}(w) \tag{4.1}$$

where w is the angular frequency, $P_0(w)$ is the radiative power loss of the donor in the form of released photons. $P_G(w)$ denotes the power dissipated in the graphene, and $P_{FRET}(w)$ is the power transferred to the acceptor. The acceptor can receive the excitation power from the donor in two different ways, it can be either directly excited by the classical FRET as a result of the Coulomb interaction via free space, or indirectly through the plasmonic channel:

$$P_{FRET}(w) = P_{FRET,D}(w) + P_{FRET,G}(w) \tag{4.2}$$

$P_{FRET,D}(w)$ and $P_{FRET,G}(w)$ represent the received power by the acceptor through direct FRET, and through graphene plasmons, respectively. The overall efficiency of the energy transfer can be calculated by integrating the ratio of the power received by the acceptor to the initial excitation power, which equals to the total dissipated power, over all frequencies.

$$E_{FRET} = \int \frac{P_{FRET}(w)}{P_{Total}(w)} f_d(w) \mathrm{d}w \tag{4.3}$$

Here, $f_d(w)$ is the normalized emission spectral function of the donor QD.

Considering at the quantum level, the probability of a single exciton generated on the donor to be transferred to the acceptor is equal to the transfer efficiency, i.e.,

$Pr[FRET] = E_{FRET}$ [Kuscu and Akan, 2012].

The radiative loss of the donor can be given by

$$P_0(w) = \frac{\mu_d^2 w^4}{3c^3 Q_d} \tag{4.4}$$

where, μ_d is the amplitude of the donor's transition dipole moment, Q_d is the quantum yield of the donor, and c is the speed of light. The power non-radiatively dissipated in the graphene is given in [Velizhanin and Shahbazyan, 2012] by

$$P_G(w) = \frac{\mu_d^2 w q_p^3}{3\kappa} e^{-2q_p|z_d|} \tag{4.5}$$

where q_p is the wavenumber, κ is the effective dielectric constant of the medium, and z_d is the distance of the donor QD to the graphene surface.

The power transferred to the acceptor as a result of direct FRET is given by

$$P_{FRET,D}(w) = \frac{w}{3}\mu_D^2 \mathrm{Im}[\alpha_a(w)] R_{ad}^{-6} \tag{4.6}$$

where R_{ad} is the intermolecular distance between the donor and acceptor QDs, $\alpha_a(w)$ is the dipole polarizability of the acceptor. The imaginary part of the dipole polarizability can be related to the absorption cross section of the acceptor σ_a by

$$\mathrm{Im}[\alpha_a(w)] = \frac{3c\sigma_a}{4\pi w} \tag{4.7}$$

For intermolecular distances exceeding the characteristic Förster radius, the energy transfer occurs mainly through the plasmonic channel. The transferred power by the graphene plasmons is expressed in [Velizhanin and Shahbazyan, 2012] as

$$\begin{aligned} P_{FRET,G}(w) = \; & \frac{8\pi\mu_d^2 w \mathrm{Im}[\alpha_a(w)] q_p^5}{9\kappa^2 R_{ad}} \\ & \times e^{-(R_{ad}/R_p) - 2q_p(|z_a| + |z_d|)} \end{aligned} \tag{4.8}$$

where z_a is the distance between the acceptor QD and the graphene, and R_p is the

characteristic travel length of the graphene plasmons.

4.2.2 Graphene Plasmon Wavenumber and Plasmon Travel Length

Plasmon wavenumber and travel length are the key parameters that determine the extent of the exciton transfer probability, however, for doped graphene, to the best of our knowledge no exact analytical expressions for them have been derived so far. In this paper, we compute them numerically based on the density correlation function of the doped graphene.

The bare density correlation function of the graphene is expressed as

$$\begin{aligned}\Pi(q,w) = &-\frac{g_s g_v \epsilon_F}{2\pi\hbar^2 v_F^2} - i\pi\frac{F(q,w)}{\hbar^2 v_F^2} + \frac{F(q,w)}{\hbar^2 v_F^2} \\ &\times\left\{G\left(\frac{\hbar w + 2\epsilon_F}{\hbar v_F q}\right) - \Theta\left(\frac{2\epsilon_F - \hbar w}{\hbar v_F q} - 1\right)\right. \\ &\times\left[G\left(\frac{2\epsilon_F - \hbar w}{\hbar v_F q}\right) - i\pi\right] \\ &\left.-\Theta\left(\frac{\hbar w - 2\epsilon_F}{\hbar v_F q} + 1\right) \times G\left(\frac{\hbar w - 2\epsilon_F}{\hbar v_F q}\right)\right\}\end{aligned} \tag{4.9}$$

where g_s is the spin degeneracy, g_v is the valley degeneracy, $\hbar$ is the reduced Planck constant, v_F and ϵ_F are the Fermi velocity and Fermi level, respectively [Wunsch et al., 2006]. $\Theta(.)$ stands for the Heaviside step function, and the functions $G(.)$ and $F(.)$ are defined as

$$F(q,w) = \frac{g}{16\pi}\frac{\hbar v_F^2 q^2}{\sqrt{w^2 - v_F^2 q^2}} \tag{4.10}$$

$$G(x) = x\sqrt{x^2-1} - \ln\left(x + \sqrt{x^2-1}\right) \tag{4.11}$$

The Fermi velocity is calculated using

$$v_F = \frac{3at}{2\hbar} \tag{4.12}$$

where $a = 0.142$nm is the carbon-carbon bond length for graphene, $t = 2.7$eV is the

nearest neighbor hopping energy, and resulting $v_F = 8.73 \times 10^5$m/s [Wunsch et al., 2006].

In order to account for the losses due to electron scattering in doped graphene, adapting the Mermin procedure, the modified bare density correlation function can be written as [Velizhanin and Shahbazyan, 2012]

$$\Pi_\gamma(q,w) = \frac{(1+i\gamma/w)\Pi(q,w+i\gamma)}{1+(i\gamma/w)\Pi(q,w+i\gamma)/\Pi(q,0)} \tag{4.13}$$

where γ is the electron scattering rate. The full density correlation function of graphene within the Random Phase Approximation (RPA) is then given by

$$\Pi_{RPA}(q,w) = \frac{\Pi_\gamma(q,w)}{1-v(q)\Pi_\gamma(q,w)} \tag{4.14}$$

where $v(q) = e^2/2\kappa q$ is the in-plane Coulomb potential.

Using the same procedure in [Velizhanin and Shahbazyan, 2012], the plasmon wavenumber $q_p(w)$ is calculated as the value that makes the denominator of (4.13) equal to zero. Using the found $q_p(w)$ for infinitely small frequency intervals, the plasmon travel length $R_p(w)$ is calculated by numerically solving the following equation

$$R_p(w) = -\frac{\frac{\partial}{\partial q}\left\{v(q)\mathrm{Re}\left[\Pi_\gamma(q,w)\right]\right\}\Big|_{q=q_p(w)}}{v\left(q_p(w)\right)\mathrm{Im}\left[\Pi_\gamma\left(q_p(w),w\right)\right]} \tag{4.15}$$

4.2.3 Transition Probabilities and Channel Capacity

After we find the transfer probability of single exciton, we now proceed by investigating the collective behavior of excitons. Before doing that, we need to express the number of generated excitons for an optical pulse with a given length.

An excited fluorescent molecule cannot be re-excited until it relaxes to the ground state. The occupation time of the excitons on a fluorescent molecule, i.e., the excited state lifetime or the time between two consecutive generations of excitons, is an exponential random variable [Lakowicz, 1999]. Additionally, we know that ex-

citon generations are independent events [Lakowicz, 1999]. Therefore, the exciton generation is described by a Poisson process.

The generation rate is equal to the total loss rate of the excitons. Therefore, for the donor QD in our system, the generation rate of excitons can be expressed as the sum of the exciton loss rates through three distinct pathways

$$k_e = k_0 + k_G + k_{FRET} \tag{4.16}$$

where k_0 is the intrinsic radiative relaxation rate, k_G is the loss rate of excitons in the graphene, and k_{FRET} is the exciton transfer rate to the acceptor QD. The mean of the excited state lifetime is then given as $\mu_\tau = 1/k_e$.

The intrinsic radiation rate is specific to the employed donor molecule, however, the loss rates of excitons to graphene and to acceptor rely on the system parameters. The total dissipation rate of excitons can be derived from the given radiation rate as follows

$$k_0/k_e = Pr[Fluo] = \int \frac{P_0(w)}{P_{Total}(w)} f_d(w) \mathrm{d}w \tag{4.17}$$

where $Pr[Fluo]$ is the probability of radiation, i.e., fluorescence, for a single exciton.

Since the exciton generation is a Poisson process, the number of generated excitons N_e under an excitation with a pulse length τ_P is a random variable with Poisson distribution, of which mean is $\mu_e = \tau_p k_e$. Therefore, its probability mass function (pmf) can be expressed by

$$Pr[N_e(\tau_P) = n] = \frac{e^{-\mu_e}(\mu_e)^n}{n!} \tag{4.18}$$

Using pmf for the number of generated excitons and the transfer probability expression for a single exciton, we can now derive the successful transmission probability of bit-1, i.e., $Pr[Y = 1|X = 1]$. Since the transfer of at least one exciton to the acceptor is sufficient for the successful detection of bit-1, for a given number of generated

excitons n, the conditional detection probability can be expressed by

$$Pr[Y = 1|X = 1, N_e = n] = 1 - (1 - Pr[FRET])^n \tag{4.19}$$

and the detection probability of bit-1 is given as

$$\begin{aligned} &Pr[Y = 1|X = 1] \\ &\quad = \sum_{n=0}^{\infty} Pr[Y = 1|X = 1, N_e = n] Pr[N_e(\tau_P) = n] \\ &\quad = \sum_{n=0}^{\infty} (1 - (1 - Pr[FRET])^n) \frac{e^{-\mu_e}(\mu_e)^n}{n!} \end{aligned} \tag{4.20}$$

For the transmission of bit-0, the donor QD is not excited for a specified bit interval which equals to the length of the pulse used for bit-1, i.e., τ_P. We assume that there is no other excitation source in the system except the optical source. Therefore, it is not possible for the acceptor QD to be excited during the transmission of bit-0, and we can conclude that $Pr[Y = 0|X = 0] = 1$.

Given the transition probabilities and system characteristics, the channel is information-theoretically well-defined as a discrete memoryless Z-channel [Cover and Thomas, 2012].

The capacity of the channel is the mutual information maximized over all input distributions, and can be analytically expressed as

$$C_Z(p) = \log_2 \left(1 + 2^{-s(p)}\right) \tag{4.21}$$

where $p = 1 - P[Y = 1|X = 1]$ is the probability of failure [Tallini et al., 2002]. $s(p) = h(p)/(1 - p)$, where $h(.)$ is the binary entropy function.

4.3 Numerical Analysis

As seen in the derivation of channel capapacity, the communication performance of the plasmon-FRET channel relies on several parameters such as the intrinsic character-

Table 4.1: Simulation Parameters

Electron scattering rate (γ)	10ps^{-1}
Dielectric coefficient (κ)	1
Fermi level (ϵ)	0.6eV
Donor's and acceptor's distance to graphene (z_d, z_a)	3nm
Intrinsic radiative lifetime of donor	5ns
Quantum yield of donor (Q_d)	10^{-2}
Absorption cross section of acceptor (σ_a)	0.02nm^2
Length of pulse representing bit-1 (T_p)	1μs)
Central frequency of donor's emission ($w_{c,d}$)	$0.60\text{eV}/\hbar$
Central frequency of acceptor's absorption ($w_{c,d}$)	$0.55\text{eV}/\hbar$
FWHM (Δ_d, Δ_a)	$0.10\text{eV}/\hbar$
Spin/valley degeneracy for graphene (g_s, g_v)	2

istics of the employed fluorescent molecules and graphene, or the system parameters related to the applied optical pulse and the location of transmitter and receiver nodes relative to each other and to the graphene.

In this section, we analyze the channel performance by means of information theoretical capacity with varying critical design parameters. Note that, the plasmon travel length and wavenumber are numerically calculated for each configuration.

The default system setting used in the simulations is summarized in Table 4.1. We assume that PbSe QDs with different spectral characteristics are employed for the nanotransmitter and nanoreceiver. The spectral density functions of the QDs are approximated by Lorentzian line shape:

$$f_i(w) = \frac{1}{1 + \left(\frac{w - w_{c,i}}{\Delta_i/2}\right)^2} \tag{4.22}$$

where $w_{c,i}$ is the central frequency, and Δ_i is the Full-Width Half-Maximum (FWHM) of the spectrum, for $i \in \{d, a\}$ denoting the donor and acceptor. For the selected values in Table 4.1, Förster radius between donor and acceptor R_0 is approximately 8nm which is a common result for semiconductor fluorescent molecules [Lakowicz, 1999].

4.3.1 Effect of Intermolecular Distance

We begin our analysis by investigating the effect of the most critical system parameter, i.e., intermolecular distance between the nanotransmitter and nanoreceiver QDs R_{ad}. In Figs. 4.2-4.5, for different settings, the channel capacity with varying R_{ad} is demonstrated.

The near-field Coulomb interaction between the donor and acceptor QDs strongly degrades over a certain critical distance whose extent mainly relies on the spectral similarity. The Förster theory on the resonance energy transfer states that the probability of energy transfer depends on the inverse sixth power of the intermolecular distance [Förster, 1948]. Therefore, pure FRET mechanism can be effective up to $2R_0$, which is approximately 16nm for the employed fluorophores. For intermolecular distances over $2R_0$, the energy transfer is dominated by the graphene plasmons excited by the donor QD, and the ultimate energy transfer range strongly depends on the plasmonic characteristics of the system such as the plasmon travel length R_p, and the electron scattering rate γ and the doping level ϵ_F of graphene.

In the following analyses, we see that as the plasmon travel length is improved by the system parameters, the range of the information transfer also increases, which make it possible for nanotransmitter and nanoreceiver to communicate over greater distances.

4.3.2 Effect of Electron Scattering Rate

Electron scattering rate is a measure of how fast the excited carriers in the form of plasmons lose their energy. Therefore, it sets a limit on the graphene carrier mobility. It is one of the intrinsic characteristics of graphene, and directly related to the impurities and defects on the graphene surface, and the frequency of electron-plasmon coupling, and interactions with the acoustical or optical phonons [Jablan et al., 2013].

The electron scattering rate of graphene strongly affects the characteristic travel length of plasmons. High scattering rates result in significant loss of graphene plas-

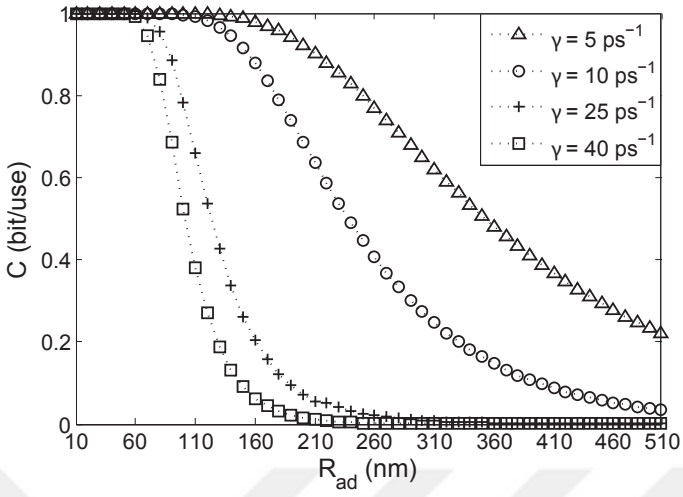


Figure 4.2: Channel capacity for different electron scattering rates γ with varying R_{ad}.

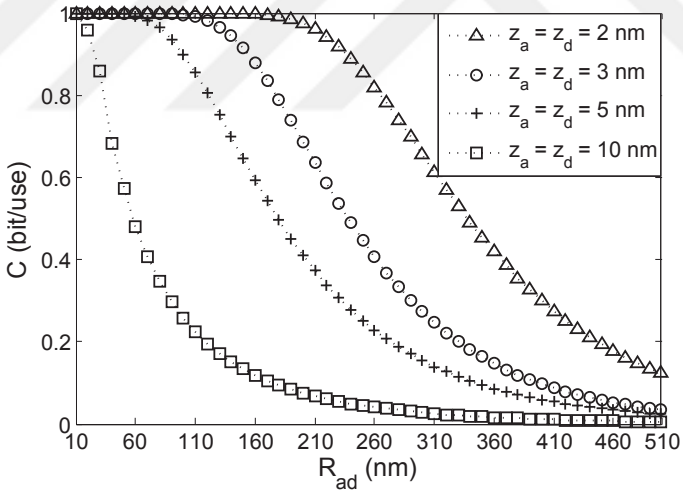


Figure 4.3: Channel capacity for different graphene to QD distances $z_a = z_d$ with varying R_{ad}.

mons excited by the donor QD before reaching to the acceptor's proximity. Therefore, the probability of exciton transfer is reduced, and the channel's reliability decreases. This can be easily deduced from Fig. 4.2. For an intermolecular distance of 160nm, the capacity decreases to 0.05bit/use from 1bit/use, when the graphene's scattering

rate is increased by 8-fold. Hence, employing clean samples of graphene, and properly choosing the geometrical parameters resulting in low scattering rates is of great importance for communication purposes.

4.3.3 Effect of QD-Graphene Distance

Another important system parameter is the distance of the donor and acceptor QDs to the graphene sheet. The effect of the QD-graphene distance on the channel capacity is demonstrated in Fig. 4.3. As is seen, the increased distance significantly decreases the channel capacity. The reason behind this is twofold.

As can be deduced from the power dissipation equations, the extent of the electromagnetic interaction between the graphene and QDs increases when QDs get into the proximity of the graphene. Stronger interaction indicates that donor QD can excite more plasmons on the graphene, and the probability of generated graphene plasmons to excite the ground-state acceptor increases with the decreased distance.

As the graphene and donor QD get into closer proximity of each other, the energy loss of the donor to the graphene also increases, therefore, the lifetime of the generated excitons on the donor decreases. Thus, more excitons are generated on the donor during a single pulse which results in the increase of successful transmission probability of bit-1.

4.3.4 Effect of Donor's Radiative Lifetime

The intrinsic excited state lifetime of the donor QD determines the occupation time of the generated excitons on the donor. Since more than one exciton cannot exist at the same time on the same molecule, an excited fluorophore needs to return to the ground state to accept the next exciton. Therefore, as the excited state lifetime of the donor decreases, the generation rate of the excitons increases. Since more excitons are generated on the system given a pulse length, the transition probability of bit-1 increases, which also extends the channel capacity.

The effect of the lifetime can be seen in Fig. 4.4. The selected values lies in the

range of common fluorophore lifetimes. As is seen, the channel capacity is significantly improved with the reduced lifetime, i.e., increased exciton generation rate.

4.3.5 Effect of Excitation Pulse Length

The length of the optical pulse representing bit-1, i.e., τ_P directly affects the number of generated excitons. For longer excitations, more excitons are generated on the donor QD which extends the reliable transition probability of bit-1.

In Fig. 4.5, the capacity of the channel for varying R_{ad} with different pulse lengths, ranging from 10ns to 100μs, is demonstrated. As is seen, the channel capacity is significantly improved by applying longer pulses. While the range of the noiseless communication is approximately 150nm for $\tau_P = 1\mu$s, it increases up to 510nm for $\tau_P = 100\mu$s. However, as the pulse length is increased, the information transmission rate decreases. As in the most of the communication systems, this trade-off between the reliable and high-rate communication should be carefully considered depending on the requirements of the application.

Assuming the bit interval is equal to the pulse length, it is possible for nanonodes in the proximity of graphene to reliably communicate through 150nm at a rate of 1Mbps, and through 510nm at a rate of 10kbps. These rates achievable with the combined plasmon-exciton system are significantly higher than one of free-space FRET-based nanocommunication channel [**?**].

4.4 Conclusion

In this chapter, we propose and analysis an FRET-based nanocommunication channel exploiting graphene plasmons as the intermediaries for information transfer. We analyze the performance of the channel with varying channel parameters by means of information theoretical capacity, and theoretically prove that the reliable communication range can be extended to distances over 500nm with an acceptable communication rates by properly selecting configuring the system parameters.

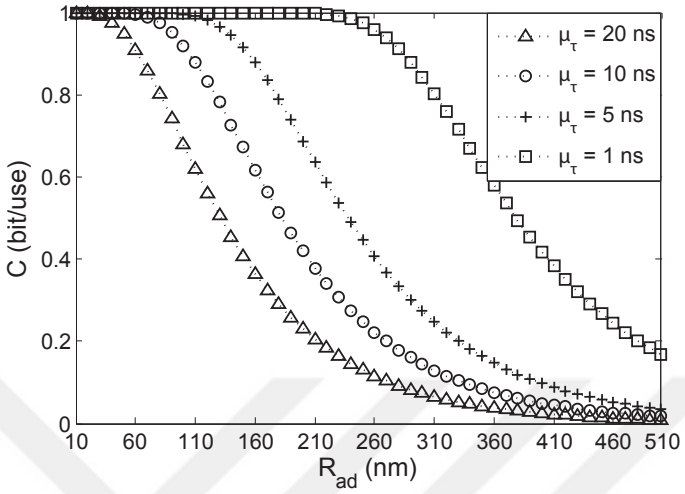


Figure 4.4: Channel capacity for different mean excited state lifetimes μ_τ with varying R_{ad}.

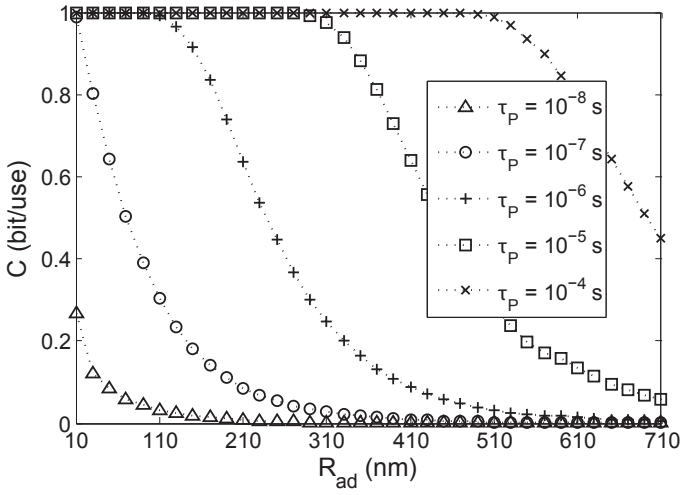


Figure 4.5: Channel capacity for different excitation pulse lengths τ_P with varying R_{ad}.

Chapter 5

FLUORESCENT MOLECULES AS TRANSCEIVER NANOANTENNAS: THE FIRST PRACTICAL AND HIGH-RATE INFORMATION TRANSFER OVER A NANOSCALE COMMUNICATION CHANNEL BASED ON FRET

5.1 Introduction

Nanotechnology has opened up the opportunity to manipulate individual molecules to design molecular-size machines, i.e., nanomachines, that can perform very basic tasks such as sensing, actuating, computing and data storing. However, the limited operational capabilities of individual nanomachines are not sufficient to realise advanced applications that nanotechnology promises such as real-time health monitoring and precise drug-delivery. To extend the application range, it is crucial to provide coordination through communication among nanomachines with different capabilities as well as between nanonetworks and macroscale remote controller units [Akyildiz et al., 2011]. But the rather unique characteristics of nanoscale environments hinder the implementation of conventional communication techniques, and thus, lead researchers to investigate the feasibility of bio-inspired nanocommunication methods such as molecular communications.

Molecular communications is based on the idea of using molecules as information carriers [Nakano et al., 2012]. Following a bio-inspired approach, it is envisioned that information can be encoded into concentration or type of molecules, and molecular messages can be delivered through diffusion in a fluid medium. However, as the case for most of the biological processes, transmission, propagation and reception of

molecules are very slow, which results in very-low rate communications and limits the range of possible applications. Moreover, implementing molecular communications requires cell-like complex nanomachines to be devised. Therefore, it is not surprising that studies on molecular nanonetworks so far have been limited to theoretical investigations.

The progress in nanotechnology has also enabled the design of several photoactive nanomachines, some of which are single molecular, such as photosynthesizers [Samia et al., 2003], fluorescence biosensors [Medintz et al., 2003], all optical molecular transistors [Hwang et al., 2009], photochromic memory units [Tsujioka and Kondo, 2003], excitonic logic gates and switches, e.g., bistable [2]rotaxane [Im Jun et al., 2000]. The functionalities of these devices mainly rely on the trade of optical excitation energy among nanounits, or between nanounits and macroscale controllers such as laser source [Browne and Feringa, 2006]. These developments have led us to investigate the feasibility of a radically different molecular communication technique which can reveal the cooperative functions of these nanomachines. The proposed communication paradigm is based on Förster Resonance Energy Transfer (FRET) [Förster, 1948], which is the exchange of excited state energies between fluorescent units in resonance and promising for enabling communication between simple, even single molecular, photoactive nanomachines, without the need of designing complex device architectures and communication protocols.

FRET is a pairwise non-radiative energy transfer process observed among fluorescent molecules, i.e., fluorophores, such as organic dyes, fluorescent proteins, and semiconductor nanoparticles, e.g., Quantum Dots (QDs), which have spectral similarities and are located in close proximity [Lakowicz, 1999]. The phenomenon has been widely used in biotechnological research including fluorescence microscopy, molecular biology and optical imaging, since it provides a significant amount of structural and spatial information about molecules by means of optical signals with nanoscale resolution [Jares-Erijman and Jovin, 2003]. FRET also intrinsically meets the very basic requirement of any communication system, i.e., the transportation of energy between

distant functional units. Basically, FRET requires three conditions to be satisfied: (i) spectral similarity between the fluorophores, i.e., the emission spectrum of the donor and the absorption spectrum of the acceptor should have sufficient overlap; (ii) proximity of the fluorophores, i.e., the energy donor and acceptor should be in close proximity such as 0-10 nm; (iii) the transition dipole moments of the donor and acceptor should not be orthogonal to each other. If the conditions are satisfied, the donor is expected to transfer the excited state energy to a nearby acceptor.

FRET-based nanocommunications, firstly proposed in [Kuscu and Akan, 2012], is based on encoding information into the energy states of fluorescent molecules, which are ground and excited state. The exchange of energy states between an excited and a ground-state fluorophore through FRET establishes a short-range nanocommunication. Our initial studies focused on the information theoretical analysis of the communication channel for different configurations such as point-to-point, broadcast and relay [Kuscu and Akan, 2012], [Kuscu and Akan, 2013b], [Kuscu and Akan, 2014c]. The rate of communication is ultimately limited by the energy transfer rate which is on the order of $10^7 - 10^9 \mathrm{s}^{-1}$ depending on the system parameters like fluorescence lifetime of the molecules, intermolecular distance and Förster radius [Lakowicz, 1999]. This was validated by our realistic Monte Carlo simulations which we obtained very high data transmission rates on the order of 10Mbps for practical cases including the effect of Inter-Symbol Interference (ISI) [Kuscu and Akan, 2013b], [Kuscu and Akan, 2014c]. The results underlined that FRET-based nanocommunications can pave the way for high-speed molecular information processors and computers. We also investigated the FRET-based mobile molecular ad hoc sensor/actor networks in which information is propagated in a stochastic manner among mobile fluorescent molecules with basic sensing and actuating functionalities [Kuscu and Akan, 2014a], [Kuscu and Akan, 2014b]. The main design principle of these networks is to take the intelligence from the network nodes, which have limited capabilities, to the external control units that communicate with the nanonetwork through an optical interface. The communication theoretical studies showed that this type of collaboration between mobile

functional units without the need of any protocol can provide significant practical advantages especially for *in vivo* applications, such as target detection and removal, in terms of extended coverage range and throughput.

In this study, we aim to experimentally validate the feasibility of FRET-based nanocommunications. We implement a communication system composed of macroscale instruments, which are connected to Internet, and FRET-based nanoscale communication channel. The channel is established in an ethanol solvent with a high concentration of Fluorescein (Fl) and Rhodamine B (RhB) dye molecules as the transmitter and receiver nanoantennas (TNs and RNs), respectively. The molecules are densely deployed and randomly moving. The TNs receive an On-Off Keying (OOK) modulated optical signal from a laser source and transmit the information into the channel in the form of excitons, i.e., excited state. RhB molecules, as the RNs, receive the transmitted information through the FRET mechanism, and send the detected information to a distant photodetector, which is a macroscale receiver hardware, in the form of fluorescence signals. The topology of the channel connections with multiple TNs and RNs distributed randomly is analogous to the collaborative Multiple-Input and Multiple-Output (MIMO) scheme which is extensively implemented in conventional wireless communications [Wang et al., 2010]. However, it is not possible to analytically model the behavior of the channel due to the high level of randomness originated from both the transfer characteristics intrinsic to FRET as well as the mobile and complex topology of the channel connections. Nevertheless, this study aims to empirically analyse the performance of the nanocommunication channel focusing on the resultant transmission errors and SNR for communication rates of 50kbps, 150kbps and 250kbps. The unique contributions of this work can be summarised as follows

- To the best of our knowledge, this is the first demonstration of a controlled information transfer through a molecular nanocommunication channel.

- The study is also the first experimental investigation of FRET phenomenon

from a communication theoretical perspective.

- The paper provides the experimental setup and the methodology to analyse a FRET-based nanocommunication channel, which can pave the way for the design, test and implementation of future nanonetwork applications.

- This study also introduces an optical interface between a macroscale network and a nanonetwork, which has not been implemented before.

5.2 Methods

5.2.1 Experimental Setup

A digital communication system is composed of basically three major components: sender, channel and receiver. The overall aim of the system is to transfer any kind of information from the source node to the destination node through the communication channel with minimum error. Fig. 5.1 demonstrates the basic functional units of each communication block. The source encoder encodes the information into a binary data sequence which is then transmitted to the channel encoder which adds redundancy bits to combat with the possible transmission errors. Based on a predefined modulation scheme, the modulator shapes a carrier signal according to the bit-stream modified by the channel encoder. The transmitter antenna, which is the interface between the transmitter hardware and the channel, converts the modulated signal into a suitable energy form that can be transmitted through the physical channel. The transmitted waveforms propagate along the channel and presumably reach to the receiver antennas with additional noise whose extent mostly depends on the physical characteristics of the channel. The waveforms detected at the receiver antennas are transmitted to the demodulator which converts the signal into a binary bit stream according to a predefined demodulation scheme. The function of the channel decoder is the removal of the redundant bits. The source decoder converts the binary stream into the symbols, and transmits them to the destination as the recovered information.

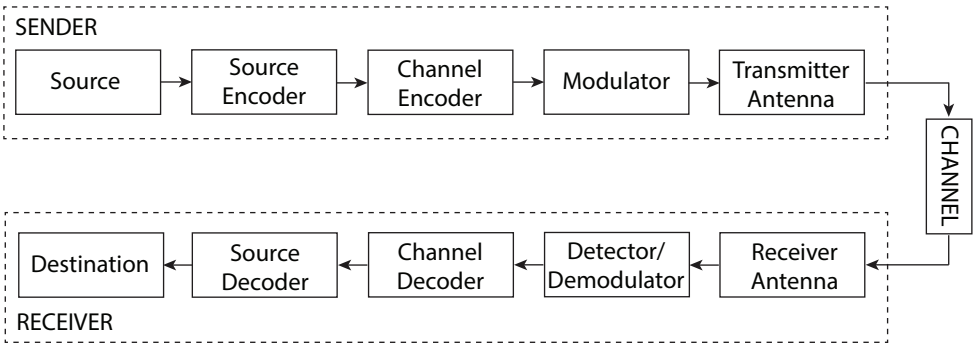


Figure 5.1: Block diagram for a digital communication system.

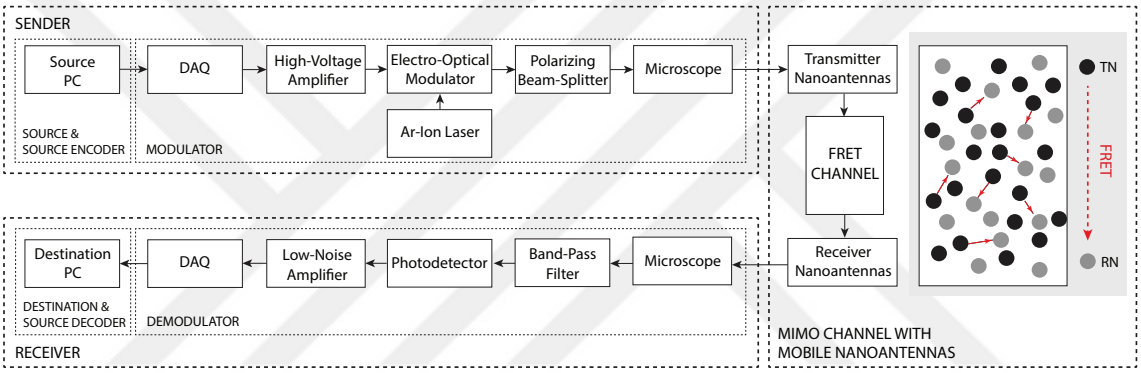


Figure 5.2: Block diagram for the experimental setup.

For the aim of demonstrating the feasibility and evaluating the performance of a FRET-based nanocommunication channel, we implement a simple and yet practical communication system whose block diagram is presented in Fig. 5.2. Note that we do not implement any channel coding mechanism to explicitly reveal the information transfer characteristics of the channel. Each functional block of the system is expressed in detail as follows

Source and Source Encoder

In the source PC, the information to be transmitted through the channel is prepared in the form of continuous binary (digital) sequence. If the information is analog, then it requires to be converted into digital by the source encoder based on a predefined

quantisation scheme.

Modulator

The bit sequence generated in the source encoder is received by the Data Acquisition Card (DAQ) through serial communications, and stored at this unit. Once triggered by the user through the instrument control program NI-LabVIEW, the DAQ generates Transistor-Transistor-Logic (TTL) signal at its digital output representing Bit-1 by 5V-level, and Bit-0 by 0V-level, and transmits it to the High-Voltage Amplifier (HVA) at a user-defined transmission rate. The HVA amplifies the modulating TTL signal to the voltage level required for the input of the Electro-Optic Modulator (EOM). The operation of EOMs are based on the electro-optic effect, i.e., Pockels effect, which defines the modulation of the refractive index of crystal materials by the applied electric field. The modulation of the refractive index is reflected by the EOM into the polarization of the optical input. We use a visible-spectrum broadband electro-optic amplitude modulator (New Focus, model 4102) which operates with 0-195V digital modulating input and supports operation frequencies ranging from DC to 200MHz. The optical input of the EOM is supplied by an Argon-Ion laser whose emission is at 488nm (with ∼30mW optical power), which is close to the maximum absorption wavelength of the Fluorescein molecules employed as the FRET donors, i.e., TNs. The input laser beam is vertically polarized, and thus, the EOM changes the polarization from vertical to horizontal when high-voltage signal representing Bit-1, i.e., 195V, is applied to its modulation input. The Polarizing Beam Splitter (PBS) located at the output of the EOM is aligned to allow the passage of only horizontally polarized beams, thus, it reflects the laser beams whose polarization is not altered by the EOM. This setup provides an ON/OFF Keying modulation of the laser output based on the binary information supplied by the DAQ. The modulated optical output of the PBS is transferred at the same rate to the optical microscope through the band-pass filter which filters out the undesired optical contributions. The function of the microscope is to condense the optical input passed through the filter and send it directly to

the molecular sample, i.e., nanocommunication channel, consisting of the donor and acceptor molecules, i.e., TNs and RNs, respectively.

Nanoantennas and Communication Channel

The overall communication link from the sender to the receiver is completed through the FRET channel between the TNs and the RNs, which constitutes the main focus of this study. The function of the TNs is to represent the modulated optical signal by the molecular energy states (ground state for Bit-0 and excited state for Bit-1), which are then transferred via FRET. The RNs do the inverse, i.e., they convert the excited state of the acceptors, which are sensitised through FRET if Bit-1 is transmitted, into fluorescence which is then collected by an external photodetector. In the case of Bit-0 transmission, the TNs stay in the ground-state, and thus, the RNs are not sensitised and do not release any photon.

For the TNs and RNs, we use a commonly used FRET pair, i.e., Fluorescein (Fl) and Rhodamine B (RhB), whose emission and absorption spectra with the resonance overlap between them are shown in Fig. 5.3. We prepare a bulk ethanol solution of these organic dyes with the concentrations of 3mM for each type of molecule. The single molecular nanoantennas are not bound to any structure, thus, they freely translocate and rotate in the solution. The high spectral overlap between the emission of Fl and the absorption of RhB results in a Förster radius of 5.7nm [Kurian et al., 2005]. Note that the configuration of the channel in this work is substantially different from the ones in the previous theoretical studies which consider the communication between a single donor (TN) and a single acceptor (RN) molecule [Kuscu and Akan, 2012], [Kuscu and Akan, 2013b], [Kuscu and Akan, 2014c]. We prefer using bulk solution of fluorophores instead of a single pair of donor-acceptor molecules due to the very low time resolution of single-molecule FRET (smFRET) measurements with the state-of-the-art instruments which limit the sampling rate of fluorescence signals to the range of 1-10kHz [Roy et al., 2008]. Employing multiple donor and acceptors increases the resultant fluorescence intensity, and allows sampling at higher frequencies up

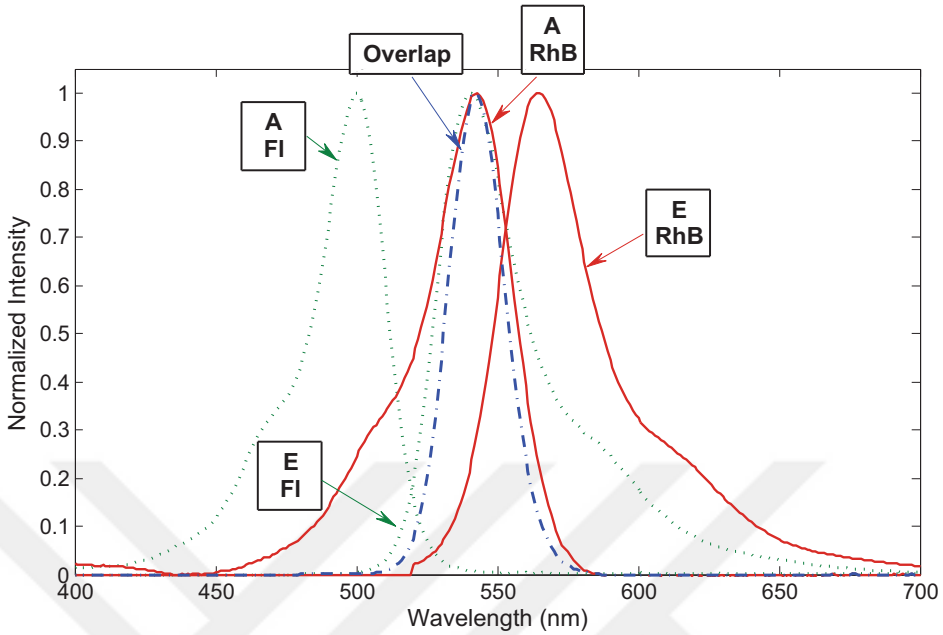


Figure 5.3: Normalised absorption (A) and emission (E) spectra of Fluorescein (Fl) and Rhodamine B (RhB), and the calculated overlap function.

to MHz, which we require for demonstrating a real-time communication with data transmission rates on the order of kbps.

The FRET mechanism, which is one of the relaxation pathways for the excited donors, constitutes a virtual communication channel between the TNs and RNs. The topology with multiple transmitter and receiver antennas which are randomly mobile is analogous to the cooperative MIMO scheme applied for electromagnetic wireless communications where multiple transmitter antennas collaborate to transmit the same information. However, the information transmission through the MIMO channel in this experiment has a high degree of randomness which results in significant amplitude and timing distortions over the transmitted signal and makes it impossible to analytically model the received signal. In addition to the stochastic nature of FRET and the inevitable noise originated from the hardware, the signal distortions are mainly resultant from the following characteristics of the channel:

- The molecules, i.e., nanoantennas, are freely moving and rotating in the solu-

tion. Therefore, the intermolecular distances, the relative orientations of the molecular transition dipole moments, and the number of possible relaxation pathways for the TNs, all of which have significant effects on the extent of the energy transfer, are rapidly fluctuating.

- The donor molecules (TNs) are not expected to be simultaneously excited by the laser. Moreover, they can be randomly excited and relaxed multiple times during a single Bit-1 transmission, especially if the symbol duration is larger than the mean donor lifetime.

- The received signal is the superposition of the fluorescence signals of multiple acceptors (RNs). The acceptor molecules cannot be expected to concurrently get excited through FRET and fluoresce. Moreover, they can get excited and fluoresce multiple times during a single symbol transmission. Furthermore, due to the diversity in the direction of the photon release, it is not possible to detect all of the fluorescence resultant from the sensitisation of RNs.

- Organic dyes are known to photobleach after approximately 10^5-10^6 excitation-relaxation cycles [Lakowicz, 1999]. Therefore, especially for long data transmissions, photobleaching of molecules can contribute to the distortions.

- Since the solution includes high concentration of molecules, random collisional quenchings, which result in the loss of information carrying excitons on the excited molecules, are expected to contribute to fluctuation of the received signal.

Demodulator

The fluorescence of the system resultant from the transmission is collected by the microscope and transmitted optically to the photodetector after passing through the band-pass filter. The photodetector converts the optical signal to electrical signal which is then amplified by a low-noise amplifier. DAQ samples the continuous analog output of the amplifier at a predefined frequency and demodulates the sampled signal

based on OOK modulation scheme by comparing the voltage level to a threshold. If the signal amplitude is higher than the threshold voltage, it decides Bit-1; otherwise, it decides Bit-0. The generated binary information sequence as a result of the demodulation is sent serially to the destination PC for source decoding.

Source Decoder and Destination

Source decoding is performed at the destination PC, and the binary sequence received from the DAQ is converted to an analog signal based on the uniform quantisation scheme applied in the source PC.

5.2.2 3-Cube Method for Signal Extraction

The first step in experimenting FRET is to excite a sample solution consisting of donor and acceptor fluorophores with an optical signal, the wavelength of which is in the absorption spectrum of the donor. The second step is to detect the resultant fluorescence signal of the acceptor after passing it through a band-pass filter whose pass-band overlaps with the emission spectrum of the acceptor. In most cases, especially when the donor and the acceptor have very similar optical characteristics, the absorption spectra of the donor and acceptor may overlap. The same situation may apply to their emission spectra as well. If there is an overlap of the absorption spectra, the acceptors in the system may also be directly excited with the optical input. In a similar way, any overlap in the emission spectra results in ambiguity between the acceptors' sensitised emission resultant from FRET, and the natural fluorescence of the donor molecules without any contribution of FRET. These contaminations are termed the Acceptor's Spectral Bleed-Through (ASBT) and the Donor's Spectral Bleed-Through (DSBT) to the FRET signal for the former and latter cases, respectively, and both complicate the detection of the contribution of FRET on the resultant fluorescence signal [Elangovan et al., 2003]. Fortunately, with a proper methodology including a post signal processing on the received fluorescence, the FRET signal can be revealed.

In this work, in order to remove the spectral bleed-through, we apply the 3-cube method which is regarded as the most effective procedure in the literature [Gordon et al., 1998]. In the 3-cube method, three solutions, i.e., three cubes, which contain only donor (C_D), only acceptor (C_A) and both donor and acceptor (C_{DA}) should be prepared. Each solution is separately excited by the same laser source with a wavelength which is close to the maximum absorption wavelength of the donor [Gordon et al., 1998]. The resultant fluorescence signals are then transmitted through one of two different optical band-pass filters selected based on the type of the excited sample. One of the band-pass filters is the Donor Filter (DF) which allows only the signals with the wavelengths near the maximum emission wavelength of the donor to pass. The other filter is named the Acceptor Filter (AF), and allows the signals with the wavelengths close to the maximum emission wavelength of acceptor to pass. In this experiment with the donor-acceptor pair of Fl-RhB, the pass-bands of the filters are determined as 525/50nm and 607/67nm for the DF and AF, respectively. The fluorescence signals that achieve to pass through filters are then observed by a photodetector and recorded for the post signal processing. Using the data obtained, the contribution of FRET can be extracted based on the following equation

$$S_{FRET} = S_{DA,AF} - S_{A,AF} - S_{D,AF}\frac{I_{DA,DF}}{I_{D,DF}} \tag{5.1}$$

where $S_{DA,AF}$, $S_{A,AF}$ and $S_{D,AF}$ are the continuous fluorescence signals received from the samples C_{DA}, C_A and C_D, respectively, through the filter AF. $I_{DA,DF}$ and $I_{D,DF}$ are the fluorescence intensities for the samples C_{DA} and C_D, respectively, detected through the optical filter DF. To apply the 3-cube method, we prepared ethanol solutions of 3mM Fl as the sample C_D, 3mM RhB as the sample C_A, and 3mM Fl + 3mM RhB as the sample C_{DA}.

5.3 Results and Discussions

5.3.1 FRET Efficiency

We first observe the overall energy transfer efficiency of the system to evaluate its suitability for the further communication experiments. Donor's fluorescence intensity in the absence of any acceptor decreases when acceptor molecules are introduced to the sample because of the energy transfer. The level of decrease in the donor's fluorescence reveals the efficiency of FRET which can be calculated as follows

$$E_{FRET} = 1 - \frac{I_{DA,DF}}{I_{D,DF}} \tag{5.2}$$

We obtained the fluorescence intensities by exciting each sample, i.e., C_{DA} and C_D, with a stationary optical pulse. We observed the resultant fluorescence signal through photodetector by recording its electrical voltage output which is proportional to the fluorescence intensity of the corresponding sample. The output voltages are measured as 0.130V and 0.715V for the samples C_{DA} and C_D, respectively. Using equation (5.2), we calculate the FRET efficiency of the system as $\sim 81.7\%$.

The high efficiency is expected because in the sample C_{DA}, where the TNs and RNs communicate through FRET, an individual donor is presumably surrounded by more than one acceptor in its close proximity, which significantly increases the probability of FRET for an excited donor compared to a single-pair FRET system. Therefore, our system with the specified molecular concentrations provides a very efficient, thus suitable, environment to test the information transmission characteristics of FRET.

5.3.2 Random Data Transmission

The performance of a serial digital communication system is best evaluated by observing its eye diagram which is the superposition of all Bit-0 to Bit-1 and Bit-1 to Bit-0 transitions, as well as the constant Bit-0 and Bit-1 levels. Eye diagrams provides a rich set of information about the transmission characteristics of the channel such as the noise level and the jitter caused by the random fluctuations in the fall and rise

Table 5.1: Optimal Sampling Settings and Resultant BER and SNR

Transmission Rate (*kbps*)	Optimal Threshold (V)	Optimal Sample Point	SNR (dB)	BER (bit^{-1})
50	0.248	3/8	12.16	1.9074×10^{-6}
150	0.202	5/8	7.10	5.7221×10^{-5}
250	0.167	7/8	3.34	3.0449×10^{-2}

times.

To generate the eye diagram, we prepare a pseudorandom binary sequence with 2^{19} bits at the source PC to be transmitted through the channel at various transmission rates, i.e., 50kbps, 150kbps and 250kpbs. Following the 3-cube method, for each rate, the binary sequence is transmitted through each of the three samples, and the resulting fluorescence signals are detected by the photodetector after they pass through the appropriate bandpass filter (see Section II). The amplified electrical outputs of the photodetector are sampled by the DAQ at the sampling rates of 400kHz, 1.2MHz and 2MHz (8 samples per bit) for 50kbps, 150kbps and 250kbps transmission rates, respectively; and recorded at the destination PC. Note that no source encoding/decoding scheme is applied, because the generated pseudorandom information sequence is already binary.

The obtained eye diagrams which store 1000 traces of 4 bit-length sequences for the observed signal S_{DA} and the calculated signal S_{FRET} are demonstrated in Fig. 5.4, for different transmission rates. Note that the pure FRET signal S_{FRET} is obtained using the 3-cube equation (5.1). To increase the resolution of the eye diagrams, the sampling rates of the observed signals are increased 32 times through lowpass interpolation in MATLAB; however, further analysis of BER and SNR are realised on the original waveform without interpolation.

The eye diagrams clearly demonstrate the transitions among all sequential combinations of Bit-1 and Bit-0's. If the signal had been ideally transmitted, i.e., without noise and any time distortion, the waveforms would have looked like sequential rectangular boxes. However, as in all communication systems, the stochastic nature of

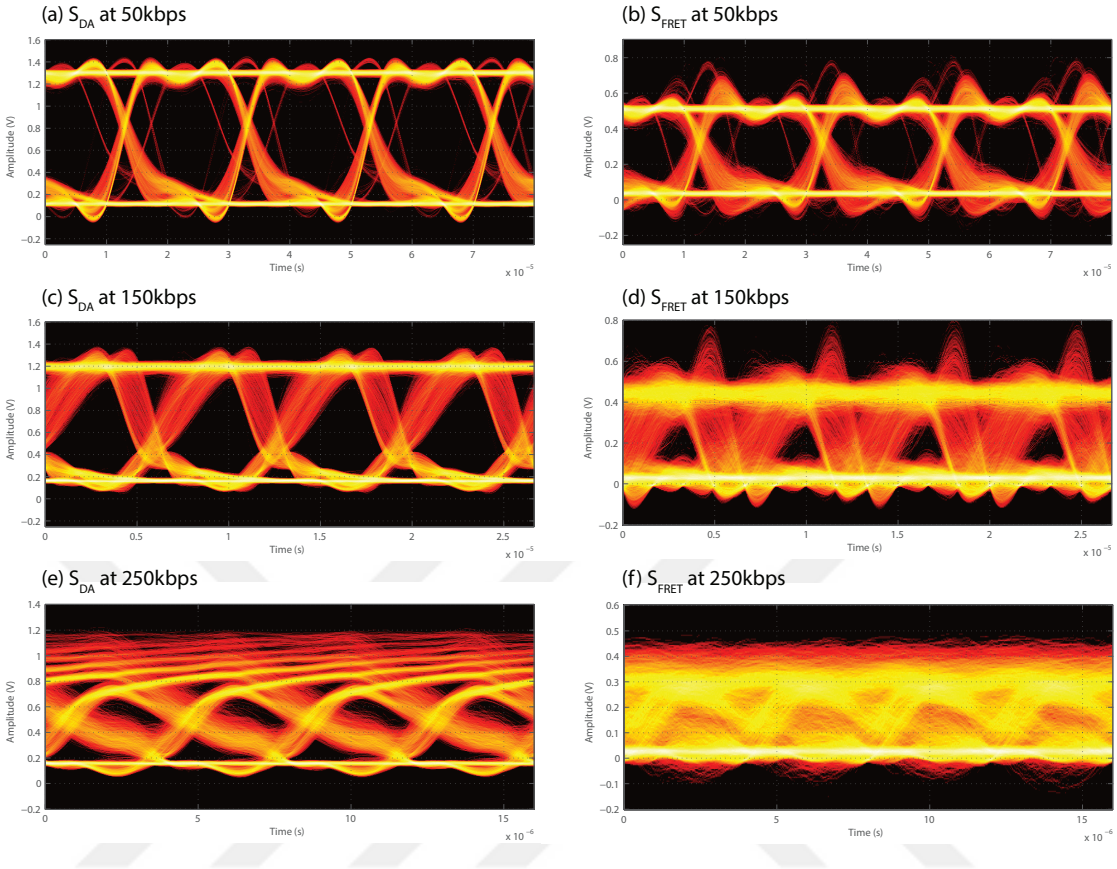


Figure 5.4: Eye diagrams of S_{DA} and S_{FRET} signals for several information transmission rates.

the communication channel together with the thermal noise of the employed hardware causes amplitude and timing distortions, i.e., jitter, in the received signal. The extent of the distortion in the amplitude can be revealed from the eye closure in the vertical axis; and the timing distortions can be observed through the eye closure in the horizontal axis. As is seen in Fig. 5.4, all of the received waveforms at each transmission rate contain both type of the distortions in some extent. As the transmission rate increases from 50kbps to 250kbps, jitter resultant from the distortions in the finite fall and rise times of the fluorescence signal completely closes the eyes, and thus, complicates the detection. The jitter is mainly originated from the high level of randomness in the timing of the excitation of the donors and the emission of the acceptors. We also observe that the amplitude of the waveforms decreases as the transmission rate

increases. This is because the decreasing bit interval does not allow the fluorescence intensity reach to higher levels.

Comparing to the transmitted binary sequence, we also obtain the optimal decision threshold voltage and optimal sampling point, i.e., decision point out of 8 sampling times per bit, which minimise the errors at the end of the demodulation process for each transmission rate. Table 5.1 presents the results of this analysis with the corresponding BER and SNR values. At the rate of 50kbps, the communication is realised with an average of 1.9bit errors per 1Mbits transmission, and with an SNR of approximately 12dB, which makes the channel very suitable for the envisioned nanonetwork applications. At the rate of 150kbps, the channel is in a fairly good condition with an acceptable SNR of 7dB. However, as the transmission rate increases to 250kbps, SNR decreases to 3dB, which makes the communication very problematic. This can be validated by the low BER value such that on average, 3% of the transmitted bits are erroneously decoded.

5.4 Conclusion

In this chapter, we realise the first data transfer exploiting FRET as a communication means at nanoscale. We implemente a practical communication system in which macroscale devices are connected over a nanoscale MIMO communication channel between fluorophore-based nanoantennas. The performance of the channel is evaluated by transmitting pseudorandom binary bit sequences and observing the resultant BER and SNR for different transmission rates. The experiments reveal that the FRET-based communication channel provides acceptable reliability for nanonetworks up to 150kbps transmission rates, even when the location of nanoantennas are not fully controllable. The easy-to-implement test setup and the simple methodology presented in this paper will surely benefit the nanocommunications literature for designing, testing and improving the nanonetworks based on FRET, and developing high-rate and reliable nanonetwork applications.

Chapter 6

THE INTERNET OF MOLECULAR THINGS BASED ON FRET

6.1 Introduction

Fluorophores are a special class of molecules, including fluorescence proteins, organic dyes, quantum dots (QDs), which can be optically excited and fluoresce at visible wavelengths, thus, serve as interface between nanoscale and macroscale worlds [Lakowicz, 1999]. Their use in biological imaging started the era of fluorescence microscopy which then evolved to the fluorescence nanoscopy with nanometer resolution, the development of which was awarded the 2014 Nobel Prize in Chemistry [Hell, 2009]. Besides their extensive use as molecular beacons, they have been also functionalized to serve as binary logical switches which are controllable by several kinds of stimuli [De Silva et al., 1997], [Cusido et al., 2009], and memory units [Kawata and Kawata, 2000], as well as actuators [Samia et al., 2003]. Connecting these molecular devices with each other and with macroscale networks in a controllable manner is envisaged to enable advanced applications including molecular all-optical information processing and small scale sensor-actor nanonetworks performing cooperative theranostic tasks which are far beyond the capabilities of individual devices.

Prominent approaches to nanoscale communications, such as the use of molecules or THz-band electromagnetic waves as information carriers [Akyildiz and Jornet, 2010b], [Balasubramaniam and Kangasharju, 2013], do not provide a feasible solution for implementing networks of molecular scale devices, because they include overly complex communication mechanisms which obviously cannot be handled by these primitive devices consisting of single or a few molecules with dimensions lower

than 100nm. In the quest to find an alternative approach, we proposed to exploit FRET as a nanoscale wireless communication mechanism between fluorophore-based devices [Kuscu and Akan, 2012].

FRET is the nonradiative exchange of electronic states between an excited-state fluorophore serving as donor and a ground-state fluorophore serving as acceptor when they are in close proximity, i.e., 0-10nm, of each other [Förster, 1948]. As a result of FRET, the donor returns to its ground-state whereas the acceptor becomes excited. In addition to the proximity condition, FRET also requires for the donor-acceptor pair to be spectrally similar to enable resonance. The probability and rate of transfer strongly depend on the degree of fulfillment of these criteria, and also on the intrinsic properties of participating fluorophores. The phenomenon has a well-established theory which is validated over years of prevalent use in biotechnology applications as spectroscopic rulers.

We have envisioned FRET as a communication mechanism between fluorophore-based molecular devices through encoding information into the electronic states of molecules. Toward realizing this vision, we have initially focused on developing theoretical models for possible network configurations. In [Kuscu and Akan, 2012], we provided the physical channel model between a single pair of fluorophores, and derived its information theoretical capacity. A robust encoding scheme using multiple molecular excitons as information carriers was introduced and analyzed for point-to-point and point-to-multipoint channels in [Kuscu and Akan, 2014c]. In the same work, we also investigated potential mechanisms of external control on the communication pathways. A multihop relay topology extending the range of information transfer to a few hundred nanometers was provided in [Kuscu and Akan, 2013b]. Using functionalized fluorophores as network nodes, we proposed a mobile ad hoc sensor-actor nanonetwork in [Kuscu and Akan, 2014a], and examined its coverage and throughput performance in [Kuscu and Akan, 2014b]. Finally, to prove the feasibility of FRET-based nanocommunications, in [Kuscu et al., 2015], we demonstrated the first practical data transfer between organic dye fluorophores at the transmitting rates of

50, 150 and 250kbps with very low error rates. These studies underlined the potential and practicality of FRET as a high-rate and reliable nanocommunication means among molecular scale devices.

In this paper, our objective is to provide an in-depth coverage of the basic principles of FRET-based communications. We first present a conceptual view of the envisioned architecture, and elaborate on the design options for each phase of communication. We examine the networking opportunities, offered by fluorophore and FRET technologies, by reviewing the related theoretical and empirical positions and ideas. We then investigate the feasibility of interfacing FRET-based nanonetworks with macroscale networks to realize the internet of molecular things, and give an overview of prospective applications. We present the theoretical modeling approaches together with the simulation algorithms developed for different network configurations. We lastly discuss the experimental opportunities and implementation challenges.

The remainder of the paper is organized as follows. In Section II, we give an overview of FRET phenomenon together with the main properties of fluorophores. In Section III, we provide the conceptual architecture of FRET-based nanocommunications and discuss the networking opportunities. In Section IV, we present the prospective applications. Theoretical modeling approaches are given in Section V. Experimental opportunities and implementation challenges are discussed in Section VI. Finally, the concluding remarks are given in Section VII.

6.2 Overview of Fluorophores and FRET

Fluorophores are chemical compounds that can emit a photon upon the excitation by an optical stimulation. The emitted photon is generally of lower energy than the excitation photon due to the energy loss in vibrational energy states. Time between the excitation and relaxation of a fluorophore is exponentially random, mean of which is termed as excited-state lifetime, and is on the order of nanoseconds for common fluorophores [Lakowicz, 1999]. Organic dyes, fluorescent proteins, semiconductor QDs are the most frequently used fluorophores as molecular probes in fluorescence spec-

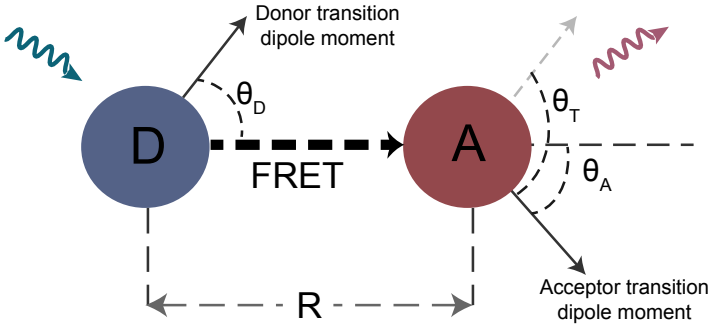


Figure 6.1: FRET between an excited-state donor fluorophore and a ground-state acceptor fluorophore. θ_T denotes the angle between the emission transition dipole of the donor **D** and the absorption transition dipole of the acceptor **A**, θ_D and θ_A denote the angles between these dipoles and the vector joining the donor and acceptor. R is the intermolecular distance.

troscopy.

Releasing a photon, i.e., fluorescing, is not the only relaxation pathway for an excited fluorophore. The radiative relaxation could be hindered by a competing quenching mechanism. For example, collision or reaction of the excited fluorophore with another molecule may result in the dissipation of excited-state energy as heat leading to the quenching of the fluorophore. However, probability of molecular collision or any pairwise reaction during the lifetime of excited-state is very low even in bulk solutions, therefore, these relaxation pathways are generally neglected [Lakowicz, 1999]. Another fundamental excited-state process is FRET, which defines the nonradiative transfer of excited-state energy to a nearby ground-state fluorophore. As a result of FRET, while the emission of initially excited fluorophore, serving as energy donor, is being quenched; another flurophore, serving as energy acceptor, is excited leading to sensitized emission with a red-shifted wavelength as demonstrated in Fig. 6.1. The phenomenon is resultant from the long-range dipole-dipole Coulomb interactions of excited- and ground-state fluorophores.

FRET is feasible only when the following conditions are met: *i*) the donor fluorophore should be in close proximity (0-10 nm) with at least one ground-state accep-

tor; *ii*) the absorption spectrum of the acceptor should have a considerable overlap with the emission spectrum of the donor; and *iii*) the absorption transition dipole moment of the acceptor should not be orthogonal to the emission transition dipole of the donor. When these conditions are satisfied, FRET becomes a possible relaxation pathway for the excited-state donor and competes with the natural fluorescence process. Through this competition, FRET decreases the excited-state lifetime and the fluorescence probability of the fluorophore. The probability of FRET depends on the degree of fulfillment of these conditions together with the intrinsic properties of the donor and acceptor.

To abstract the excited-state processes, it is beneficial to consider the excited-state of fluorophores as particle-like molecular excitons [Berney and Danuser, 2003], which can be generated on fluorophores as a result of excitation or sensitization, converted to a photon via fluorescence, or transferred among fluorophores via FRET. In this way, FRET becomes a process defining the hopping of excitons on a lattice consisting of fluorophore nodes. The rules governing the exciton dynamics can be summarized as follows:

- A fluorophore node can be occupied by at most one exciton. Thus, to accept an exciton transfer from another fluorophore, it should lose its exciton, if any, and return to the ground-state.

- An exciton has a short and random lifetime, i.e., sojourn time, on a fluorophore. When there are multiple relaxation pathways for the fluorophore leading to multiple competing processes, the lifetime further decreases.

- Excitons do not have transferable properties, since they only represent the state of being excited on the occupied fluorophore.

- Once converted into a photon or transferred to another fluorophore, an exciton is removed from the initially occupied fluorophore without any trace.

- Excitons cannot be copied or stored on a fluorophore.

6.3 FRET-Based Nanoscale Communications

Being the short-range but high-rate transfer of excitons between fluorophores, FRET could be exploited as a nanoscale wireless communication method to connect individual molecular devices by encoding information into excitons. This section provides a conceptual architecture for this communication method having very interesting peculiarities due to the quantized nature of excitons, and elaborates on the networking opportunities.

6.3.1 Architecture

A communication process can be viewed as comprising basically five consecutive phases: encoding, transmitting, propagation, receiving, and decoding. FRET-based nanoscale communications, due to the lack of an actual propagation channel and the instantaneous nature of exciton transfer, consists of encoding and decoding phases, and an additional transfer phase combining the transmitting, propagation and receiving processes. We explain each phase in detail as follows:

Encoding Phase

In the encoding phase, information is translated into a representation by excitons which can be transmitted through FRET channel. This requires for the controllable generation of excitons on the transmitter node. The excitation source could be an external optical device such as a laser which can emit photons with wavelengths matching to the absorption spectrum of the transmitter fluorophore. The device could be the direct source of information if it is regulated by an additional computing device or connected to a macroscale network, or it could be used only for the purpose of continuously powering the transmitter to generate excitons for encoding information related to a nanoscale phenomenon such as a sensing event. If the transmitter is a bio/chemoluminescent molecule, then, a chemical reaction resulting in excitation of the transmitter could be both power and information source [Pinto da Silva and Esteves da Silva, 2012].

Depending on the excitation source and method, a proper modulation scheme should be applied. Given the fact that a single exciton as information carrier represents only the state of the occupied fluorophore and does not possess transferable properties such as amplitude or frequency, the number of feasible modulation methods are very limited. The only appropriate amplitude modulation scheme is On-Off Keying (OOK), which can be implemented by encoding logical bit-1 and bit-0 into the presence and absence of excitons for a predefined time interval [Kuscu and Akan, 2012]. If an optical laser is employed as the power or information source, depending on the length of optical pulses, single excitons or sequentially generated multiple excitons can represent bit-1 [Kuscu and Akan, 2013b]. If the excitation is realized through an irreversible chemical reaction, then encoding into single exciton is the only way of representing information. For the optical excitation case, pulse modulation methods such as pulse-width modulation, pulse-duration modulation and pulse-frequency modulation are also feasible for FRET-based communications [Proakis and Salehi, 2007].

Transfer Phase

Different from the electromagnetic and molecular communications, FRET-based communications, due to the nonradiative nature of FRET, does not include a propagation phase, in which information carriers propagate from a transmitter to a receiver [Lakowicz, 1999]. Moreover, transmission of information-carrying signals by a transmitter and their reception by a receiver are simultaneous processes, since excitons are instantly transferred. Therefore, transmitting, propagating and receiving phases can be jointly viewed as a single transfer phase.

Transfer phase requires for the FRET criteria to be satisfied such that there should be at least one suitable receiver in the transfer range of the transmitter. If the criteria are met, an information-carrying exciton generated on the transmitter is transferred to the receiver node at a random time. The time interval between the generation and transfer of a single exciton cannot be controlled by the transmitter, and solely de-

pends on the extent and number of the present relaxation pathways. For example, as the receiver node gets closer to the transmitter, exciton generation and transfer rates are increased along with the decreasing sojourn time of excitons on the transmitter. Since fluorescence is an intrinsic relaxation pathway, there is always a chance that a generated exciton is recombined into a photon before transferred. This implies the loss of information if it is encoded by a single exciton. From this aspect, multi-exciton scheme that uses longer excitation pulses to encode information into sequentially generated multiple excitons is more robust compared to single-exciton schemes, although it reduces the communication rate [Kuscu and Akan, 2014c].

It is to be noted here that there is an exceptional case for the propagation process, which is the usage of a plasmonic waveguide as the intermediary of exciton transfer [Toppari et al., 2013], [Velizhanin and Shahbazyan, 2012]. In this configuration, a pair of transmitter and receiver is immobilized on the surface of a plasmonic nanostructure, e.g., two-dimensional doped graphene [Kuscu, 2014]. Internodal distance between the transmitter and receiver can be set larger than the FRET range. An exciton generated on the transmitter is first transferred to the propagation channel by resonantly exciting a surface plasmon. The excited plasmon propagates through the waveguide and carries the information radiatively. If it succeeds in arriving at the receiver location, the receiver can be resonantly excited by the surface plasmon. In this way, the information can be transferred much longer distances with the collaboration of exciton transfer and surface plasmon propagation.

Decoding Phase

In the decoding phase, received excitons are transduced into another signal form, which can be processed or used for realizing a proper action in the context of a nanonetwork application. The receiving node has no control over the decoding phase, and realizes its predefined functionality in an autonomous manner. As it receives excitons from the transmitter, it can fluoresce to optically transmit the information to an external observer. In addition, transduction of received excitons into electrical

signals at the nanoscale can also be feasible with the use of semiconductor nanowire photodiodes [Bulgarini et al., 2012]. Moreover, if the receiver node is a photosensitizer fluorophore, excitons could be used to sensitize singlet oxygens in photodynamic therapy of cancer [Samia et al., 2003], which will be further discussed in Section 6.4.

6.3.2 Networking Opportunities

Most of the envisioned nanotechnology applications require more than two molecular devices to communicate with each other, thus, to form nanonetworks that can accomplish advanced tasks [Akyildiz et al., 2011]. Due to the inability of individual fluorophore nodes to process signals and self-control, FRET-based nanonetworks are envisaged to be passive-networks with predefined autonomous or externally-controllable functionalities [Kuscu and Akan, 2014a]. In this section, we give an overview of the feasible networking opportunities offered by the intrinsic capabilities of fluorophores and FRET.

Multihop Communication

Limited range of FRET-based communications can be extended via multihop FRET, which is the sequential transfer of an exciton through cascaded FRET channels [Heilemann et al., 2004]. Cascade of channels can be realized deploying a relay node between the transmitter and receiver nodes, with an absorption spectrum overlapping the emission spectrum of the transmitter, and an emission spectrum overlapping the absorption spectrum of the receiver [Kuscu and Akan, 2012]. In this way, an information carrying exciton generated on the transmitter is first transferred to the relay node. Then the relay node, without any amplification mechanism, autonomously transfers the exciton to the receiver node if the FRET criteria are satisfied for both connections. Likewise, we can employ multiple relay nodes to further extend the communication range by increasing the number of cascaded channels, all of which satisfy the FRET criteria [Kuscu and Akan, 2013b]. If each of the utilized relay fluorophores is of different type, their emission and absorption spectra should be red-shifted as

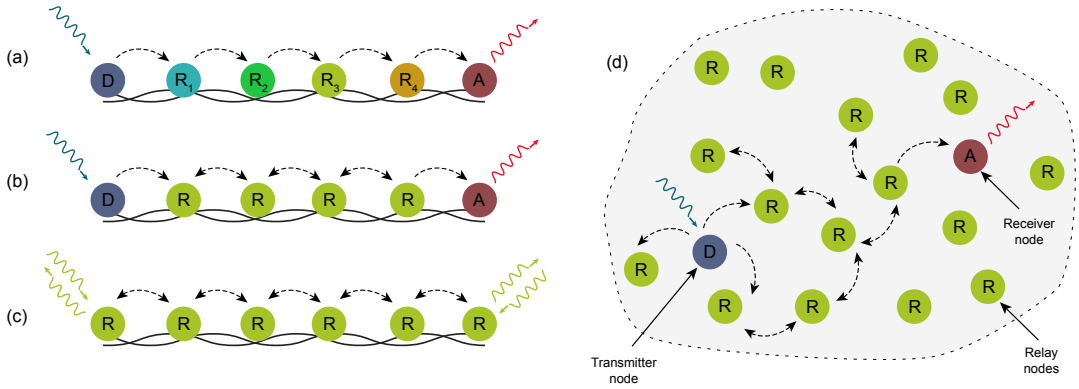


Figure 6.2: Multihop FRET-based communication schemes: (a) 1-d unidirectional photonic wire on DNA scaffold consisting of spectrally different fluorophores; (b) 1-d unidirectional photonic wire consisting of identical relay fluorophores between a transmitter and a receiver node; (c) 1-d bidirectional photonic wire consisting of identical fluorophores acting as transmitter, relay, and receiver nodes; (d) 3-d multihop link consisting of randomly deployed relay nodes between a transmitter-receiver node pair.

their location approaches to the receiver node to ensure the directionality of the information flow as shown in Fig. 6.2(a). Relays can also be identical if their emission and absorption spectra do a significant overlap (see Fig. 6.2(b)). In this case, the transfer between identical fluorophores is termed homoFRET [Lakowicz, 1999]. If the overall network nodes including the transmitter and receiver are all identical, homoFRET among them can enable communication in both direction in a half-duplex manner (see Fig. 6.2(c)).

Depending on the application and the required communication range, relays can be deployed in numerous configurations. They can be immobilized on a one dimensional structure to obtain a one dimensional photonic wire. DNA and zeolite L are the examples of one dimensional host molecules allowing the deployment of organic dyes on prescribed locations [Heilemann et al., 2004], [Ramachandra et al., 2011]. Relays can also be mobile randomly moving in a three dimensional fluidic environment as demonstrated in Fig. 6.2(d). The excitons randomly hop along a random lattice comprised of mobile relays, and communication is realized in an ad hoc manner [Kuscu and Akan, 2013b]. This type of deployment requires for a high concentration

of identical relay nodes to be employed in the communication environment and for information to be represented by a high number of excitons using sufficiently long optical pulses. The generated excitons for one bit of information diffuse through the channel, and if any of them reaches to the receiver, it is decoded into the original information. Communication range depends on the FRET characteristics, as well as the mobility of the relay fluorophores and their concentration in the communication channel. As the excited-state lifetimes and the mobility of the deployed relays are increased, the communication range is also expected to increase [Kuscu and Akan, 2013b].

Switching

Control over the communication pathways on a nanonetwork is crucial for diversifying the applications. Although pathways can be predefined by exploiting the strong distance dependence of FRET [Stein et al., 2011], it is also possible to dynamically regulate the information flow on the nanonetwork through external control signals which can modulate one of the characteristics of the employed relay nodes, or act on the network topology by altering the geometry of nanostructures on which the communicating nodes are deployed. Switching of communication pathways can be realized by optical, electrical, chemical or biological means which are explained in detail as follows:

- ***Optical switching*** makes use of the photochromic molecules which are photoactive fluorophores that undergo reversible transformation between two states of different absorption spectral characteristics depending on the wavelength of irradiation [Lakowicz, 1999]. While irradiation at visible wavelengths (400nm-700nm) switches their absorption at their characteristic spectrum off, ultraviolet (UV) irradiation switches their absorption back on. In this way, the extent of optical absorption is able to be reversibly modulated by an additional control signal. Since they do not change their states until the next stimulation, they have been widely exploited as molecular memory units [Kawata and Kawata,

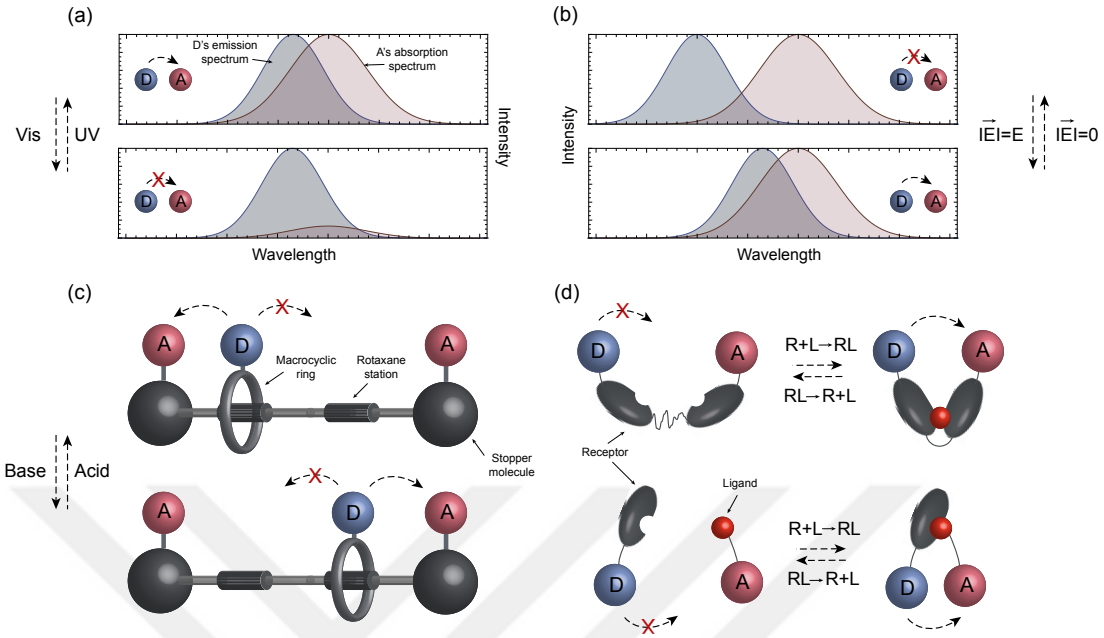


Figure 6.3: Working principles of main switching mechanisms feasible for FRET-based nanonetworks: (a) Quenching of acceptor's absorption under visible light leading to optical switching; (b) Shift of donor's emission spectrum under electric field leading to electrical switching; (c) 1-d translational movement of macrocyclic ring of *[2]rotaxane* depending on the pH of environment leading to chemical switching; (d) Ligand-receptor binding leading to biological switching.

2000]. Photochromic fluorophores have also found use in FRET-based molecular switches [Raymo and Tomasulo, 2005], being employed as FRET acceptors adjacent to a spectrally similar donor fluorophore. Depending on the control signal, which is flipped between UV and visible wavelengths, the spectral overlap between the donor and photochromic acceptor is switched on and off leading to the modulation of FRET. This implies that a communication pathway relying on the flow of excitons could be optically controlled by employing photochromic molecules.

- ***Electrical switching*** is based on the Quantum Confined Stark Effect (QCSE) which defines the red-shift of the emission spectrum of a semiconductor fluorophore as proportional to the magnitude of the applied electric field [Empedo-

cles and Bawendi, 1997]. Given the fact that QCSE is not observed in organic fluorophores, it can enable the modulation of the overlap between the emission spectrum of a semiconductor donor fluorophore and the absorption spectrum of an organic acceptor fluorophore with a varying electrical field supplied from an external source [Becker et al., 2006]. Modulation of spectral overlap leads to the control of communication pathways as the information flow from a semiconductor transmitter to an organic receiver fluorophore could be switched on and off depending on their spectral overlap controlled through electric field. If a semiconductor node is placed in between two organic nodes with proper spectral characteristics, information on the semiconductor node flows either toward the first node or toward the second node depending on the electric field [Kuscu and Akan, 2014c].

- ***Chemical switching*** relies on the use of chemically active supramolecules, the physical forms of which change depending on a chemical input [Ashton et al., 1998]. One of the examples is *[2]rotaxane* which comprises a macrocyclic ring trapped on the axis of a dumbbell-like component containing two recognition sites on top of it. Two stopper molecules are placed at the both ends of the dumbbell [Pease et al., 2001]. Depending on the pH of the environment, the ring on the axis undergoes a reversible translational movement between two recognition sites as a bistable molecular shuttle. When two fluorophores acting as acceptor are placed on the stopper molecules, and a donor flurophore is placed on the ring, due to the strong distance dependence of FRET, the flow of excitons from the donor to the acceptors is modulated with the pH level [Li et al., 2005]. If this configuration is deployed in a nanonetwork, the information coming to the transmitter node on the ring flows either to the receiver node at the first recognition site or to the receiver at the second site. In this way, chemical switching of the communication pathways could be enabled [Kuscu and Akan, 2014c]. Rotaxane-like switches can also be built using DNA [Ackermann et al., 2010], which could be better adapted into the FRET-based nanonetworks

implemented on DNA chains.

- ***Biological switching*** can be realized based on the modulation of intermolecular distance between donor and acceptor or the addition of another acceptor to the network through ligand-receptor binding [Ibraheem and Campbell, 2010]. It is the underlying mechanism of FRET-based biosensors which find extensive use in bioimaging applications. If a network node is placed on a receptor, and a strong acceptor fluorophore is bound to the corresponding ligand, binding of the ligand to the receptor brings the acceptor into the close proximity of the network node creating a new pathway for the excitons flowing through the network. Thus, the information flow in the initial pathway is switched on and off with the reversible binding of a ligand. Another strategy can be the placement of two network nodes on a receptor molecule, the structure of which changes upon binding of a ligand. This way, the nodes get closer to each other when a ligand binds to the receptor, allowing excitons to flow from one node to another. In this way, depending on the network topology, new communication pathways could be generated, or the existing pathways could be switched off with the presence of ligands on the communication environment.

Point-to-Multipoint Communication

A single transmitter node can communicate to multiple receiver nodes if the individual transmitter-receiver pairs satisfy the FRET criteria [Kuscu and Akan, 2014c]. However, this is only possible when one of the multi-exciton schemes is applied for the modulation, since a single exciton can only be transferred to a single receiver at a time and cannot be copied on the transmitter [Berney and Danuser, 2003]. Representing the information with a finite length pulse, multiple excitons are generated on the transmitter and transferred to the receivers in a random manner. However, this does not guarantee that all of the receivers can get the information at the end of bit interval. If a receiver is closer to the transmitter than the other receivers, then, it has higher probability of receiving the information because of the stronger Förster

coupling.

Broadcasting of information from the transmitter is also possible for the multihop communication case where identical relays are randomly distributed in a fluidic environment, and the information carrying excitons are diffusing through the lattice of relay nodes similar to the diffusion of molecules in molecular communication [Kuscu and Akan, 2013b]. If there are multiple receivers with absorption spectra overlapping with the emission spectra of the relays, then they can receive the broadcasted information when they are in the diffusion range of excitons.

Multiple Access

As was discussed in the previous section, FRET is based on the pairwise coupling of fluorophores, and FRET-based communications does not include an actual propagation channel. Therefore, we cannot envision a multiple access scheme for single-hop FRET-based communications. This functionality on a nanonetwork can be realized if a multihop communication is performed [Kuscu and Akan, 2013b]. Since the transferred excitons individually cannot carry an addressing information, multiple-access is possible only through time-division multiplexing.

Other than the multiple access schemes, simultaneous communication of multiple transmitter-receiver pairs on the same medium can also be realized if different groups of relay nodes with divergent spectral properties are deployed with a high concentration [Kuscu and Akan, 2013b]. In this way, excitons carrying the information of different transmitters hop through the different relays without interfering with each other, and independently reach to their target receivers. This is realized through wavelength-division multiplexing; however, the scheme is fundamentally different from the conventional wavelength-division multiple access, because the communicating pairs do not share the same physical channel, rather, they communicate through different multihop FRET links created on relay fluorophores with divergent spectral characteristics. The extent of co-channel interference in this deployment depends on the spectral similarity of the relay nodes employed on separate links.

Macro-Nano Interface

Fluorophores, being able to be optically excited and fluoresce, intrinsically behave as optical interfaces between macroscale and nanoscale worlds. Therefore, every node in a FRET-based nanonetwork actually acts as a macro-nano interface. In this sense, the characteristic absorption and emission spectra of an interface can be viewed as its natural addresses for sending and receiving optical messages. However, deploying fluorophores with different spectral addresses for every node is impractical for large-scale nanonetworks, considering that the spectrum, in which fluorophores can absorb and emit, is a limited source. Moreover, addresses cannot be defined by a single wavelength but a wavelength range, which decreases the maximum number of uniquely definable addresses in a nanonetwork. Hence, grouping large number of nodes based on their functionality in an application may be required [Balasubramaniam and Kangasharju, 2013].

Utilizing a tunable-wavelength laser as a gateway unidirectionally connecting a macroscale network to a nanonetwork, information can be sent to a specific group of nodes using the group's absorption address. On the other hand, information flow from a nanonetwork to a macroscale network can be realized by using a photodetector as a gateway [Kuscu et al., 2015]. Decoding of the information can be performed based on the wavelength of the detected fluorescence. In that way, bidirectional communication could be established between macroscale and nanoscale networks. Using a wavelength division multiplexing scheme in both link, the communication capacity of the macro-nano interface can be substantially improved.

For *in vivo* applications of FRET-based nanonetworks, tissue penetration depth of the light used for the excitation should also be considered. Two-photon excitation scheme developed for biological imaging applications enables the use of near-infrared (NIR) light, which provides substantially improved tissue penetration compared to visible light exploiting the near-infrared window in biological tissues [Pawlicki et al., 2009]. The scheme is based on the excitation of a donor fluorophore through successive absorption of two photons with lower energy than the donor's normal absorption

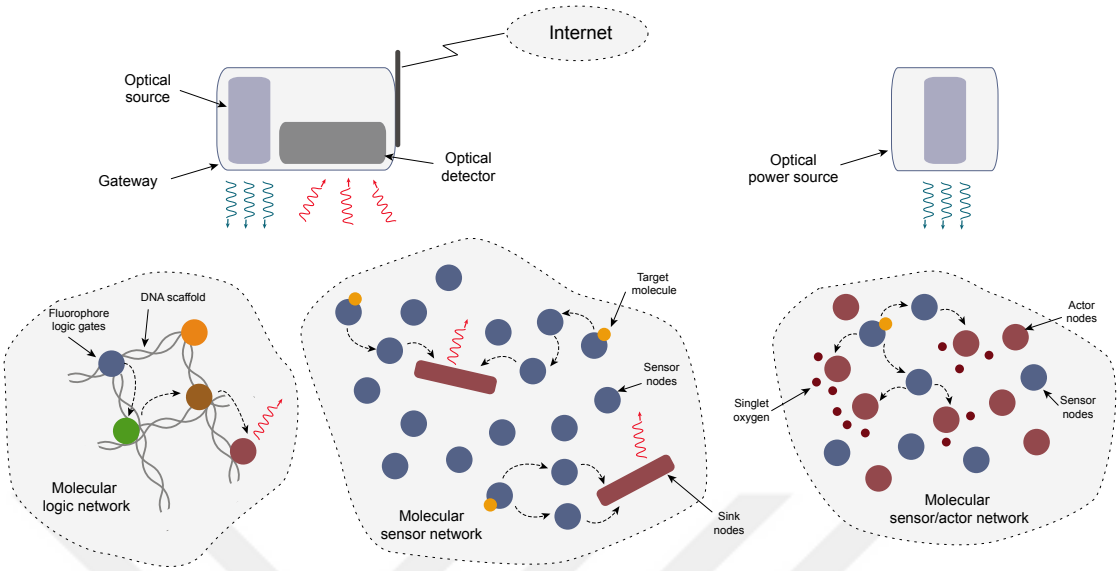


Figure 6.4: Conceptual drawings of some applications of FRET-based communications. Molecular logic network and sensor network are connected to Internet via macroscale gateways comprising optical source and detectors whereas molecular sensor/actor network is envisioned to operate in autonomous manner under continuous excitation of a remote optical source.

spectrum. In this way, a fluorophore normally absorbing at visible wavelengths can be excited by two NIR photons. Two-photon excitation could be also applied to FRET-based networks in living organisms by representing information on the external gateway with short pulses of NIR light in a single-exciton encoding scheme.

6.4 Applications

FRET does not necessitate a specific environment, e.g., fluidic medium or free space, to be realizable; however, the efficiency of the energy transfer, thus the performance of the FRET-based communications, depends on the refractive index of the medium where the fluorophore network is deployed, as will be theoretically modeled in Section 6.5. The network nodes can be mobile or immobile depending on the application and the medium.

In this section, we review some prospective applications and deployment scenarios

of FRET-based nanocommunications. We investigate the applications under three main categories: *i*) molecular information processing; *ii*) collaborative sensing and actuating; and *iii*) molecular communications. Specifically, molecular information processing can be considered for immobile deployments, since the intermolecular distances between fluorophore-based logic nodes should be fixed to produce stable logical outputs. FRET-based information processing networks can be deployed on prescribed locations over organic scaffolds like DNA or inorganic scaffolds like zeolite L, and can be integrated into future lab-on-a-chip devices. They can be utilized for *in vivo* information processing, or for *in vitro* applications regarding to molecular computers. FRET-based collaborative sensing and actuating is considered particularly for mobile ad hoc deployments in fluidic medium towards medical and environmental applications, where sensing and actuating molecules search for and act upon the target location. For the application to molecular communications (MC), FRET-based fluorophore networks are considered to be deployed on MC transmitter and receiver nanomachines. The scenarios are detailed in the following subsections.

6.4.1 Molecular Information Processing

In recent years, a great deal of effort has been devoted to the development of molecular scale binary logic gates which can handle optical or chemical signals [Raymo and Giordani, 2001]-[Pischel et al., 2013]. An extensive number of simple molecular switches which are able to generate binary 1 or 0 depending on the input signals have been already developed and proven feasible indicating that digital information processing with molecules even in living cells is not a far-fetched idea [Credi, 2007], [De Silva and Uchiyama, 2007]. Towards the long-standing goal of molecular computers, there is also an ongoing research aimed at development of efficient and reliable techniques to connect these switches with each other to enable more advanced processing. Current approaches in this context are mostly based on the use of chemical signals to carry the output information of one logic gate to the input of another [Erbas-Cakmak and Akkaya, 2013], [Ecik et al., 2014]. However, communication with chemical signals is

a very slow process, and its reliability is also another challenge. FRET-based communication can be an alternative solution to this problem, if the switches are made of fluorophores. Examples of fluorophore-based switches handling several form of control inputs have been discussed in Section 6.3.2, as they can also allow the routing of information flow at nanonetworks. Establishing a FRET-based communication link, an exciton on a fluorophore-based switch generated as a result of a logic operation can be carried to the input of another gate in a fast and reliable manner. If the switches are based on the operation of photochromic molecules controlled by optical signals [Cusido et al., 2009], communication through FRET could enable rapid all-optical molecular information processing which is limited only by the photoisomerization speed of photochromic compounds. Integrated sensing and processing is also possible if biological or chemical switches are used as logic gates [LaBoda et al., 2014]. These logic networks can be implemented on a single supramolecular structure like DNA allowing a controllable spacing and orientation of molecules, which is important for the reliability of information transfer. Individual gates can also be attached to separate molecules such that the communication of logic gates is enabled when these molecules bind to each other, which can bring another dimension to the molecular information processing.

6.4.2 Collaborative Sensing and Actuating

Fluorophores are widely used in bioimaging applications as molecular beacons due to their intrinsic interface capability. Their use as molecular beacons is mainly based on switching of fluorescence due to the conformational changes on the conjugated molecule upon the binding of another molecule or a chemical reaction sensitizing the fluorophore as reviewed in Section 6.3.2. Most of the sensing applications require for a high number of molecular sensors to be deployed in a large area. This complicates the decoding of sensing information at the macroscale because of the high number of fluorescence signals, the release times and propagation directions of which are random. Reducing the number of interface channels without comprising the range

of sensing application can be possible, if individual sensing data which are intrinsically encoded into excitons are collected by central nodes, i.e., sink nodes, possessing more advanced communication capabilities. This could be enabled by FRET-based communication techniques using sensor nodes as relays in a multihop communication manner [Kuscu and Akan, 2013b], as depicted in Fig. 6.4. The central nodes can transmit the collected information to the macroscale gateways in the form of amplified and directed fluorescence [Ming et al., 2012], [Cosa, 2013]. They can also process the data with FRET-enabled on-chip logic networks before transmitting, for example, by multiplexing data collected from different kind of sensors [LaBoda et al., 2014].

If the employed central nodes are capable of acting on the local environment, then autonomous sensing and acting applications could be enabled. A particular application of FRET-based sensor/actor nanonetworks to the photodynamic therapy of cancer was investigated in [Kuscu and Akan, 2014a], [Kuscu and Akan, 2014b]. Photodynamic therapy is based on the use of photosensitizing agents that can be excited by a light source and sensitize singlet oxygens through the transfer of excited-state energy to an O_2 molecule [Samia et al., 2003], [Dolmans et al., 2003], [Dichtel et al., 2004]. Singlet oxygen is extremely harmful for living cells. This property is exploited to initiate the apoptosis of cancer cells by producing them inside or in close proximity of these targets. However, as in the case of other cancer therapies, photodynamic therapy suffers from the low level selectivity, such that normal cells are also killed through singlet oxygens when they are not produced in target locations. A FRET-based ad hoc networking approach employing sensor nodes that can be excited upon the detection of target, and actor nodes which can synthesize singlet oxygens could substantially improve the targeting [Kuscu and Akan, 2014b]. This could be enabled through multihop communication of these sensor nodes with the actor nodes. Since the excitons are mortal information packets, the information diffuses through a narrow spatial range in a very fast manner, hence, it is almost guaranteed for singlet oxygens to be produced by actor nodes in the close proximity of target cells.

6.4.3 Application to Molecular Communications

Fluorophores and FRET-based nanocommunications can also find use in molecular communications where molecules are used to encode, propagate, and decode information [Nakano et al., 2012]. For example, fluorophore-based biological switches can be used as interface transferring the molecular information in an MC nanonetwork to the macroscale gateways in the form of fluorescence signals. If the specialized bacteria which can express fluorescent proteins [Southward and Surette, 2002] are employed as the communicating nanomachines, then the molecular information can be directly detected by macroscale gateways without requiring a bio-switching mechanism. The reverse case, where the molecular communication is optically controlled through macroscale gateways is also possible, if photoactive molecular compounds that can undergo isomerization based on the wavelength of optical signal are used [Mal et al., 2003], [Browne and Feringa, 2006]. For example, an MC transmitter can be equipped with photoactive molecules that control the molecular release mechanism, such that they transmit an information to the channel upon receiving a control signal from a macroscale gateway. These functionalities can also be diversified with FRET-enabled fast processing capabilities of fluorophores on the transmitter and receiver nanomachines. If the received information molecules are transduced to excitons by the fluorophore bio-switches employed on the receiving unit, the information could be processed in the form of excitons, and then transmitted to the macroscale gateways, or used to release an action. Likewise, the transmitter could process the optical control signals together with the chemical inputs, and act, e.g., transmit a molecular message, according to the result of logic operation.

6.5 Theoretical Modeling Approaches

Communication and information theoretical modeling of FRET-based communications relies mainly on the FRET theory, which is established in Theodor Förster's seminal work [Förster, 1948] for immobile fluorophores, and then, validated by an extensive number of experimental studies [Stryer, 1978]. For the cases where single-

exciton encoding scheme is used, we are able to derive analytical expression for the capacity of the channel [Kuscu and Akan, 2012]. However, for multi-exciton encoding scheme [Kuscu and Akan, 2014c], correlated exciton dynamics take part in the information transfer, which impedes the derivation of analytical models. Fortunately, communication performance metrics for multi-exciton cases can be revealed by conducting realistic Monte Carlo simulations. In this section, we first review the fundamentals of FRET theory, which will be then used for modeling the communication channel for single-exciton schemes. We also elaborate on the simulation algorithms, which were developed based on exciton dynamics to be adapted for various network configurations.

6.5.1 Theory of FRET

As explained earlier, in the absence of any external quenching mechanisms, e.g., FRET, an excited-state donor returns to ground-state after a random short time by fluorescing. The excited-state lifetime, which is also the sojourn time of the corresponding exciton, τ can be expressed as an exponential random variable with mean μ_0 [Lakowicz, 1999]. The reciprocal of the mean excited-state lifetime equals to the natural fluorescence rate k_0 of a fluorophore, i.e., $k_0 = 1/\mu_0$, which is the number of photons released at a unit time while the donor is continuously excited by a stimulation. Involvement of any quenching mechanism creates additional relaxation pathways for the excited-state donor, which reduces the sojourn time of excitons by increasing the overall relaxation rate of the donor. Considering the case when there are k acceptors in close proximity of the excited donor, the reduced mean excited-state lifetime is given as follows

$$\mu = (k_0 + \sum_{j=1}^{k} k_{T,j})^{-1} \tag{6.1}$$

where $k_{T,j}$ is the FRET rate between the excited donor and the jth acceptor surrounding the donor. $k_{T,j}$ in terms of the donor-acceptor spacing can be expressed

by

$$k_{T,j} = k_0 \frac{R_{0,j}^6}{R_j^6} \mathbf{1}_j \tag{6.2}$$

where $R_{0,j}$ is the Förster radius of the donor and the jth acceptor, R_j is the spacing between them, and $\mathbf{1}_j$ is an indicator function which indicates whether the jth acceptor is in the ground-state or not, i.e., $\mathbf{1}_j = 1$ if it is in the ground-state, otherwise $\mathbf{1}_j = 0$. Note that when an acceptor is in the excited-state, it cannot accept further exciton until it relaxes [Berney and Danuser, 2003]. Förster radius is the intermolecular distance at which the FRET rate is equal to the natural fluorescence rate of the donor [Lakowicz, 1999], and incorporates the effect of numerous system parameters on the transfer rate:

$$R_{0,j}^6 = 8.8 \times 10^{22} \kappa_{j,i}^2 n^{-4} J_j(\lambda) \tag{6.3}$$

where $\kappa_{j,i}^2$ is the orientation factor which gives a measure of relative orientation between the transition dipoles of donor and jth acceptor; n is the refractive index of the medium, and $J_j(\lambda)$ is the overlap measure between the emission spectrum of the donor and the absorption spectrum of the jth acceptor. The orientation factor can be given as

$$\kappa^2 = (\cos\theta_T - 3\cos\theta_D \cos\theta_A)^2 \tag{6.4}$$

where θ_T, θ_D and θ_A are the angles related to the geometry of transition dipoles which are demonstrated in Fig. 6.1. From this expression, we can infer that when the transition dipoles are orthogonal to each other, κ^2 will be 0, and FRET does not occur. For the configurations where fluorophores are free to rotate in all there axes, or a FRET pair is self-assembled on a backbone structure without any control over transition dipoles, κ^2 would be a random variable with the following probability

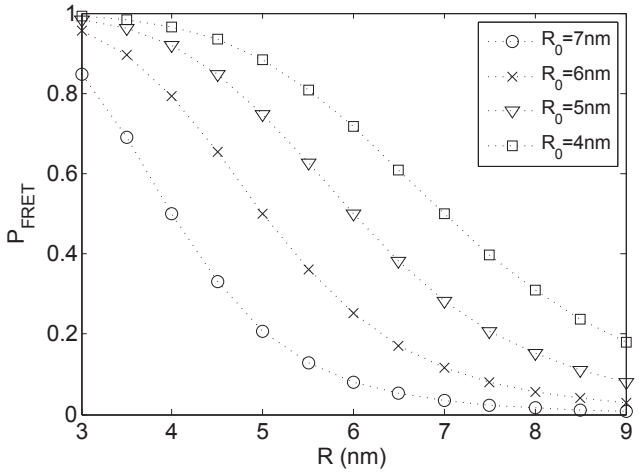


Figure 6.5: Probability of FRET for an excited donor with varying donor-acceptor distance R_0 and Förster radius R_0.

distribution [Badali and Gradinaru, 2011]:

$$p_{\kappa^2}(\kappa^2) = \begin{cases} \frac{1}{2\sqrt{3\kappa^2}} \ln\left(2+\sqrt{3}\right) & 0 \leq \kappa^2 \leq 1 \\ \frac{1}{2\sqrt{3\kappa^2}} \ln\left(\frac{2+\sqrt{3}}{\sqrt{\kappa^2}+\sqrt{\kappa^2-1}}\right) & 1 \leq \kappa^2 \leq 4 \end{cases} \tag{6.5}$$

In many experimental works studying an ensemble of FRET pairs, mean value of κ^2, i.e., 2/3 is used with the assumption of free rotation [Lakowicz, 1999].

Using the process rates, the probability of transfer for an excited donor can be given as

$$P_{FRET,j} = \frac{k_{T,j}}{k_0 + \sum_{l=1}^{k} k_{T,l}} \tag{6.6}$$

When there is only a single pair of donor and acceptor, this expression reduces to:

$$P_{FRET} = \frac{k_T}{k_0 + k_T} \tag{6.7}$$

Probability of FRET between a donor and acceptor fluorophore for different R_0 and R is given in Fig. 6.5, which also reveals the strong distance dependence of FRET.

Now consider that a single exciton is transferred through cascaded FRET channels

in a multihop manner on a one dimensional axis. The cascaded channels are shown to be independent of each other [Heilemann et al., 2004], [Kuscu and Akan, 2012]. Therefore, the probability of exciton transfer through N cascaded FRET channels is given by

$$P_{FRET} = \prod_{i=1}^{N} P_{FRET,i} \tag{6.8}$$

where $P_{FRET,i}$ is the transfer probability on the ith channel.

In most cases, the assumption of immobility can also be applied to mobile fluorophores, because the process rates, i.e., fluorescence and FRET, are generally very much higher than the rate of translational movement, so that the fluorophores are almost immobile during an average lifetime of excited-state [Lakowicz, 1999]. However, when the natural excited-state lifetimes or the diffusion coefficients of fluorophores are high enough that the excited-state molecules move distances comparable to Förster radius, then the mobility cannot be neglected. Averaging over all possible intermolecular distances, a rate expression is derived in [Stryer et al., 1982] for mobile fluorophores as follows

$$k_{T,rd} = \frac{4\pi k_0 R_0^6}{3Va^{-3}} \tag{6.9}$$

where R_0 is the Förster radius when $\kappa^2 = 2/3$, V is the volume of the medium, a is the distance of closest approach of donor and acceptor as measured between their centers. This expression is valid only when the fluorophores meet the rapid-diffusion criterion which is given by

$$\frac{D\mu_0}{s^2} \gg 1 \tag{6.10}$$

where D is the sum of the diffusion coefficients of the donor and acceptor, and s is the mean intermolecular distance [Stryer et al., 1982], [Kinosita Jr et al., 1987]. Lanthanide complexes with lifetimes in the μs-ms range can meet the criterion with

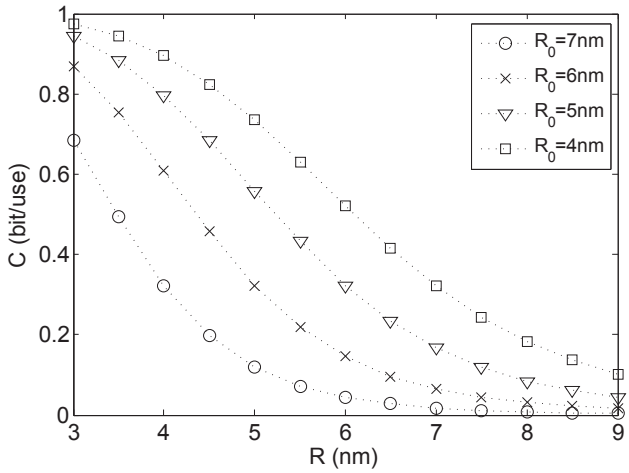


Figure 6.6: Capacity of a point-to-point channel for different Förster radii R_0 and varying internodal distance R.

moderate diffusion coefficients [Vuojola and Soukka, 2014].

6.5.2 Communication with Single-Exciton Encoding

Consider the case when the information is encoded into single exciton with on-off keying modulation such that bit-1 and bit-0 are represented by the excited-state and ground-state of the fluorophores during a predefined bit interval T_b. If there is a single excitation source, bit-0 can be sent to the receiver node without an error assuming the bit interval is large enough to avoid intersymbol interference (ISI). On the other hand, the reliability of bit-1 transmission strongly depends on the dynamics of exciton transfer. Successful transmission probability of bit-1 can be given as equal to the FRET probability [Kuscu and Akan, 2012];

$$p_1 = P_{FRET} \tag{6.11}$$

This expression is valid for all configurations, e.g., point-to-point, multihop and mobile communications, though the probability of FRET is given in terms of different parameters for different configurations.

During an information transfer, when bit-0 is preceded by bit-1, ISI may occur if

the bit interval is not set large enough that the receiver may still remain in excited-state at the time of bit-0 transmission. Thus, the minimum T_b that guarantees no-ISI condition depends on the excited-state lifetimes of both the transmitter and receiver. It should be greater than the maximum possible sojourn time of an exciton on the system;

$$T_{b-min} = \tau_{T,max} + \tau_{R,max} \tag{6.12}$$

where $\tau_{T,max}$ and $\tau_{R,max}$ are the maximum of reduced and natural excited-state lifetimes of transmitter and receiver, respectively. Since the lifetimes are exponential random variables, T_{b-min} goes to infinity. Thus, we can never guarantee no-ISI condition. However, given the lifetimes are independently distributed, setting $T_b = 4 \times (\mu_{\tau_{DA}} + \mu_{\tau_A})$ results in ISI probability lower than 10^{-3}, which might be acceptable depending on the application.

The transition probabilities of bit-1 and bit-0, when no-ISI condition can be assumed, indicate that the channel can be information theoretically modeled as a Z-channel [Cover and Thomas, 2012]. Denoting the binary input and output alphabets as $\mathbf{X}$ and $\mathbf{Y}$, respectively, the mutual information can be expressed by:

$$I(\mathbf{X};\mathbf{Y}) = H(P[1]\ p_1) - P[1]\ H(1-p_1) \tag{6.13}$$

where $H(.)$ is the binary entropy function, and $P[1]$ is the probability of encoding bit-1 on the transmitter. Then the capacity of the channel will be the supremum of $I(\mathbf{X};\mathbf{Y})$ over all input distributions, i.e., $C = \sup_{P_1} I(\mathbf{X};\mathbf{Y})$. As can be seen in Fig. 6.6, the channel capacity strongly depends on the distance between the communicating nodes, and reduces to unacceptable levels when the distance is greater than the Förster radius.

6.5.3 Communication with Multi-Exciton Encoding

When the information is encoded into single exciton, the reliability of the channel substantially decreases when the spacing between communicating nodes exceeds the Förster radius [Kuscu and Akan, 2012]. Reliability can be improved with multi-exciton schemes using longer excitation pulses to represent information [Kuscu and Akan, 2014c]. However, channel modeling for multi-exciton schemes is a highly complex task even for single-hop communications considering that multiple excitons exist on the system at the same time which results in highly random and correlated transfer dynamics. If there are multiple mobile nodes for multihop communications, the problem becomes more complex as the correlation expands over the spatial domain [Kuscu and Akan, 2013b]. For such cases, deriving analytical expressions for performance metrics is almost impractical. However, communication can be simulated to evaluate main performance metrics such as channel capacity, communication rate and delay.

In our previous studies, we developed realistic Monte Carlo algorithms that fully capture the dynamics of excitons during a bit-1 transmission for numerous channel and network configurations such as multihop communications in 1-d and 3-d channels [Kuscu and Akan, 2013b], point-to-multipoint communications [Kuscu and Akan, 2014c], mobile ad hoc sensor/actor networks [Kuscu and Akan, 2014b]. The sample pseudocode given in Algorithm 1 combines all of the previous approaches into a simple one which is written for the transmission of bit-1 in a multihop configuration with mobile relay nodes randomly deployed in 3-d environment containing a single pair of transmitter and receiver nodes. Bit-1 is encoded in the transmitter by a T_p-length excitation pulse. If T_p is set to a value much lower than the excited-state lifetime, then the encoding becomes single-exciton-based. The algorithm can be easily extended for MIMO configurations by setting the number of transmitter and receiver nodes to a value greater than one. The algorithm basically runs a single node at each loop based on their electronic state, and updates their state one by one for each time interval, which is set to a value small enough to guarantee that at most single event,

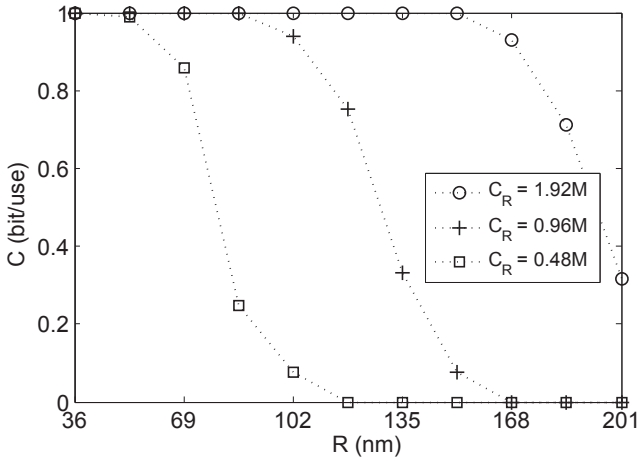


Figure 6.7: Capacity of a multihop communication channel for different relay concentrations C_R and varying transmitter-receiver distance. Data were obtained through Monte Carlo simulations using Algorithm 1 for $T_{pulse} = 1\mu s$ and $R_0 = 6nm$.

e.g., fluoresce or FRET, can occur at a single time step. The nodes are assumed to undergo Brownian motion independently of the exciton dynamics at each time step. Simulations should be run until the observed parameter converges to a finite value. Although the algorithm is highly realistic and accurate, it becomes impractical and time-consuming for systems comprising of high number of nodes.

A simplified version of the algorithm is developed for the cases where the nodes meet rapid-diffusion criterion [Kuscu and Akan, 2014a]. The pseudocode given in Algorithm 2 simulates the bit-1 transmission in a multihop communication between a pair of transmitter and receiver using mobile relays. It is based on a continuous time Markov process model which is given in Fig. 6.8. The numbered states of the process represent the number of excitons on the system, and state-D is the detection state which denotes the reception of information by the receiver. The model comprises of two processes; the first process model is valid during the application of T_p-length excitation pulse which encodes the information on the transmitter. In this process, both the generation and the recombination of excitons, i.e., removal by fluorescence, are possible together with the transfer among nodes, therefore, it denotes a birth-death process. While the excitation continues, the transmitter generates excitons at

a varying rate which depends on the electronic states of other network nodes. The upper limit for the state in the first process is the total number of nodes. When the excitation terminates, the system shifts into the second process model which represents a pure-death process with the initial state N_p denoting the number of excitons on the system at time T_p. In the absence of the excitation pulse, only the recombination and transfer of the previously generated excitons are possible. The simulation terminates when the receiver node detects an exciton, which is possible in both processes. The state-dependent transition rates for the processes are given by

$$\alpha_i = ik_0 \tag{6.14}$$

$$\theta_i = i(N_h - i)k_T \tag{6.15}$$

$$\mu_i = ik_T \tag{6.16}$$

$$\beta_i = k_0 + k_T(N_h - i) \tag{6.17}$$

where i is number of excitons on the network, k_T denotes the transfer rates between nodes calculated using (6.9). Assuming that the time is divided into sufficiently small intervals Δt, the transition probabilities at each time step are calculated by multiplying the corresponding transition rates by Δt.

Markov process modeling approach simplifies the algorithm by averaging out the mobility and fixing the transfer rates, which should be determined at each time step in the previous algorithm. Although it is preferable for calculating the parameters that can be derived from transmission probabilities and delay, it is not possible using this algorithm to obtain spatial performance metrics such as communication coverage [Kuscu and Akan, 2014a].

6.6 Experimental Approaches and Implementation Challenges

FRET is a well-known phenomenon which is extensively experimented for its widespread use in bioimaging applications [Jares-Erijman and Jovin, 2003]. It has an already

Algorithm 1 Algorithm for Multi-Exciton Encoding

Given N: total number of network nodes (one transmitter-receiver pair, $N-2$ relay nodes); E: length-N vector of electronic states ($E_j = 1$ if excited-state, $E_j = 0$ if ground-state); E_1, state of the transmitter; E_N: state of the receiver; T_{sim}: stop time of simulation; T_{pulse}: length of pulse representing bit-1; D: diffusion coefficient.

Deploy network nodes in 3D;
$t = 0$;
while $(t < T_{sim} \wedge E_N == 0\ )$ **do**
  if $t < T_{pulse}$ **then**
    $E_1 = 1$;
  end if
  for $(j = 1;\ j < N; j++)$ **do**
    if $E_j == 1$ **then**
      for All nodes $i \neq j$ with $R_{j,i} < R_{th}$ **do**
        Calculate $k_{T,j,i}$ using (6.2);
      end for
      Construct PMF for the next jump;
      Randomly select a relaxation pathway, move the exciton;
      Update E;
    end if
  end for
  if Nodes are mobile **then**
    Move the nodes ($dx_{\Delta t} \sim dy_{\Delta t} \sim dz_{\Delta t} \sim \mathcal{N}(0, \sqrt{2D\Delta t})$);
    Move the collided nodes to their previous positions;
    Remove excitons from the collided particles;
  end if
  $t = t + \Delta t$;
end while

Algorithm 2 Algorithm for Rapid Diffusion Case

Given i: state of Markov process (Fig. 6.8) at time t; T_{sim}: stop time of simulation; T_{pulse}: length of pulse representing bit-1.

$i = 1$; $t = 0$;
while $t < min(T_{pulse}, T_{sim}) \wedge i \neq D$ **do**
  Calculate PMF using (6.14)-(6.17) based on the model in Fig. 6.8(a);
  Find i_{new}; $i = i_{new}$; $t = t + \Delta t$;
end while
while $i \neq D \wedge i \neq 0 \wedge t < T_{sim}$ **do**
  Calculate PMF using (6.14)-(6.17) based on the model in Fig. 6.8(b);
  Find i_{new}; $i = i_{new}$; $t = t + \Delta t$;
end while

validated theory for both ensemble (ensembleFRET) and single molecular cases (smFRET) [Ha, 2001]. From the aspect of communications, well-documented experimental methodologies together with the intrinsic interface capability of fluorophore nodes provide an easier pathway for the validation of the theoretical models com-

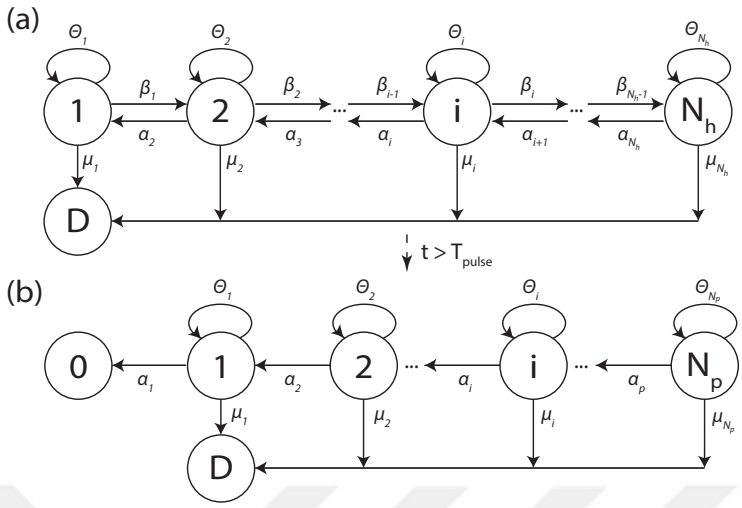


Figure 6.8: Markov process model of bit-1 transmission for rapid-diffusion case: (a) Birth-death Markov process model valid for $t \leq T_{pulse}$; (b) Pure-death Markov process model valid for $t > T_{pulse}$.

pared to other nanocommunications approaches. However, the experimental opportunities for single molecular cases, on which the most of the envisioned applications of FRET-based communication are based, are limited by the low sampling frequencies of state-of-the-art laboratory instruments, which are on the order of 1-10kHz for fluorescence measurements [Roy et al., 2008]. This would restrict the empirical studies of FRET-based communications, at best, to the rates below 10kbps. On the transmitter side, however, it is possible to encode the information even into single excitons using femtosecond-length lasers [Quentmeier et al., 2008].

On the other hand, using an ensemble of molecular channels increases the intensity of output fluorescence; therefore, ensemble measurements are not subject to the strict limitations of smFRET [Vogel et al., 2006]. In this way, recently, we have demonstrated the first real-time and high-rate information transmission between organic dyes, i.e., Fluorescein and Rhodamine B, in a FRET-based MIMO configuration, proving the feasibility of FRET-based nanoscale communications [Kuscu et al., 2015]. We transmitted 5Mbit pseudorandom binary data at 50, 150 and 250kbps rates with acceptable BER values, i.e., 1.91×10^{-6}, 5.72×10^{-5}, 3.05×10^{-2}, respectively. We

used a simple experimental setup including a Ar-Ion laser, the output of which is modulated based on OOK scheme by an electro-optical modulator. The transferred information is measured optically through a conventional photodetector after passing appropriate optical filters. One challenge associated with the observation of the received information is the spectral bleed-through (SBT) resultant from the contamination of the observation channel by the direct fluorescence of receiver molecules [Gordon et al., 1998]. This is due to the fact that the receivers can be excited directly by the excitation pulse of laser if their absorption spectra overlap the excitation wavelength. Another reason of contamination is the direct fluorescence of the transmitters with wavelengths at the spectral range of the observation channel. These unintended contributions result in the contamination of the observed signal which should only contain the fluorescence of receivers due to FRET. Therefore, in most cases, post signal processing is required to obtained the purified FRET signal. 3-cube method is the most prevalent technique to purify the observed signal, which is based on processing of measurements obtained from three samples containing only donor, only acceptor, and the mix of donor and acceptor [Elangovan et al., 2003], [Gordon et al., 1998].

Another challenge associated with implementing a FRET-based nanonetwork may be the photostability of fluorophores. Most fluorophores, especially organic dyes and fluorescent proteins, undergo photobleaching, i.e., lose their fluorescence and FRET capabilities, after a number of excitation-relaxation cycles, e.g., 10^5-10^6 for organic dyes [Lakowicz, 1999]. Reducing oxygen concentration in the environment increases the resistance of fluorophores to photobleaching [Roy et al., 2008]; however, it may not always be possible to remove oxygen from the communication medium, especially considering *in vivo* applications. Alternatively, the problem can be overcome by using intrinsically stable fluorophores such as semiconductor QDs and Nitrogen-vacancy (NV) centers [Clapp et al., 2006], [Tisler et al., 2011], which have almost infinite resistance to photobleaching. Another way could be the use of single-exciton encoding schemes, which increases the service time of organic dyes because of the reduced intensity of irradiation.

Additionally, fluorescent proteins and semiconductor fluorophores under strong illumination could show random blinking whose origin has not been fully understood yet [Roy et al., 2008]. When they are used on the transmitter side, the node could lose its ability to generate exciton for short random intervals due to photoinduced blinking, which may hinder reliable communication. Blinking can be chemically suppressed with the addition of auxiliary compounds to the communication environment [Rasnik et al., 2006]. Using single-exciton scheme, in which the transmitter nodes are exposed to low-intensity illumination, can also reduce the probability of blinking [Roy et al., 2008].

For *in vivo* applications, another challenge is to optically connect the nanonodes with macroscale gateways because of the limited penetration length of visible light in tissue. As discussed in Section 6.3.2, this problem can be overcome by using two-photon excitation scheme which enables the use of NIR light, that allows much more tissue penetration exploiting the near-infrared window in biological tissues, for the downlink transmission [Pawlicki et al., 2009]. To decrease the attenuation using NIR light for transmission in the uplink from nanonetwork to macroscale gateways, the transmitting nodes can be selected from near-infrared emitting fluorophores [Hilderbrand and Weissleder, 2010].

6.7 Conclusion

Developing networks of molecular-scale devices possessing very limited operational capabilities necessitates radically different communication strategies than the prominent nanonetworking approaches. In this chapter, we review the theoretical and experimental positions toward realizing the internet of fluorophore-based molecular devices based on FRET. We present an overview of the basic principles and design requirements of FRET-based nanocommunications, its networking opportunities and prospective applications including molecular-scale information processing and cooperative sensing/actuating for disease treatment. Main implementation challenges, e.g., low photostability of fluorophores and sampling rate limitations of single molecular

experiments, along with the possible solution pathways are discussed. Theoretical modeling approaches, simulation algorithms and experimental opportunities together with networking strategies provided in this chapter will pave the way for the development of unprecedented applications making use of high-rate, reliable and controllable information transfer between molecular devices.

Chapter 7

ON THE PHYSICAL DESIGN OF MOLECULAR COMMUNICATION RECEIVER BASED ON NANOSCALE BIOSENSORS

7.1 Introduction

Designing fully functional nanoscale devices with sensing, computing and actuating capabilities has been a long-standing goal of science and engineering community. Recent advances in nanotechnology including the inventions of novel nanomaterials like carbon nanotube and graphene have enabled the miniaturization of various functional devices like computing units, memories, and batteries into nanoscale dimensions. This exciting progress has led to a thorough investigation on feasibility of enabling different nanomachines to communicate with each other, thus to form nanonetworks, to realize more complex tasks for ground breaking applications ranging from collaborative in-body drug delivery to continuous health monitoring, and water quality control [Akyildiz et al., 2008] [Kuscu and Akan, 2016a].

Since implementing conventional electromagnetic communications among nanoscale devices are obstructed by the limitations of antenna sizes, researches have started a quest for finding alternative communication methods. Among the several paradigms that have been proposed for use in nanonetworks, molecular communications (MC) is the most promising one because it is already implemented in nature as the main communication mechanism of living cells and other microorganisms, and thus, its feasibility in nanoscale domain is readily proven. The paradigm uses molecules to encode, transmit and receive information. One of the physical characteristics of molecules, such as type or concentration, is modulated to be transferred either through active

propagation or diffusion-based passive propagation in a fluid medium [Nakano et al., 2012] [Kuran et al., 2011].

There is a substantial body of theoretical work that provides signal propagation and noise models for both active and passive propagation with various modulation schemes [Atakan and Akan, 2008] [Pierobon and Akyildiz, 2013]. Many aspects of molecular communications like addressing, routing, synchronization, localization, have been widely investigated; and advanced communication protocols for transport, network and link layers have just begun to be designed [Nakano et al., 2014]. However, so far, little attention has been given to the physical design of transmitter and receiver devices compatible with molecular communications.

A limited number of works have focused on the signal processing aspects of molecular receiver with the aim of developing optimal detection schemes generally being adapted from the conventional communication theoretical tools [Kilinc and Akan, 2013] [Meng et al., 2014]. However, these studies ignore the design of the receiver antenna and the characteristics of the antenna's output signal which is to be processed. They implicitly assume that the output signal is already suitable, in terms of physical form, amplitude and resolution, for the proposed detection schemes, all of which require fast and complex signal processing with high computational resources. On the other hand, the current predictions on the design of nanomachines that are capable of communicating through molecules are based on the synthetic biology approaches, and a widespread consensus is established on this completely bio-inspired vision [Nakano et al., 2012] [Nakano et al., 2014]. However, synthetic biology is currently far away from taking the full control over the functionality of a biological cell, and designing artificial cells that are capable of operating in an envisioned nanonetwork application which employs the proposed communication tools including the optimal detection schemes. Moreover, relying only on synthetic cells limits the application range of molecular communications to *in vivo* operations. It is clear that novel approaches are required to remove the discrepancy between the envisioned applications and the device architectures. At this point, this paper aims to pave the way for the physical

design of a nanoscale molecular receiver compatible with the proposed communication schemes that generally require high computational capacity.

A molecular receiver should be capable of *in-situ*, continuous, label-free and selective detection of molecular messages that arrive in the close vicinity of the nanomachine on which it is implemented. It can be considered to consist of a biorecognition unit that selectively recognizes the information molecules; a transducer unit that converts biorecognition events into a processable signal; and a processor unit that analyzes the output of the transducer to extract the transmitted information based on a preset scheme. The expected functionality of a molecular receiver is very similar to the one of biosensors, which are also designed for the aim of quantifying analyte concentrations in a solution [Scheller et al., 2001]. Therefore, in this paper, we first review the state-of-the-art biosensing approaches to determine whether and in what extent they satisfy the design requirements of an MC receiver.

A careful examination of biosensing options, ranging from optical to mechanical and electrical methods, reveals that field-effect transistor-based electrical biosensors (bioFETs) are quite promising for the design of molecular receiver [Poghossian and Schöning, 2014]. Hence, in the second part of the paper, we focus on a conceptual FET-based molecular receiver. We provide a comprehensive design guideline comprising of the operation principles and the performance metrics of the device. We also examine the noise sources originating from the defects in the transducer unit, and from the stochastic nature of molecular bindings in the recognition unit. Moreover, we elaborate on the design options of recognition and transducer units for the optimization of the overall performance from the communication theoretical perspective. Furthermore, we develop a deterministic model of signal flow in a SiNW FET-based MC receiver, and evaluate the receiver performance in terms of sensitivity under different scenarios. We examine integrability of the proposed receiver design into more advanced communication schemes including molecular division multiple access (MDMA), molecular shift keying (MoSK), spatial diversity combining. Lastly, we discuss the challenges before the implementation of the device from a practical aspect,

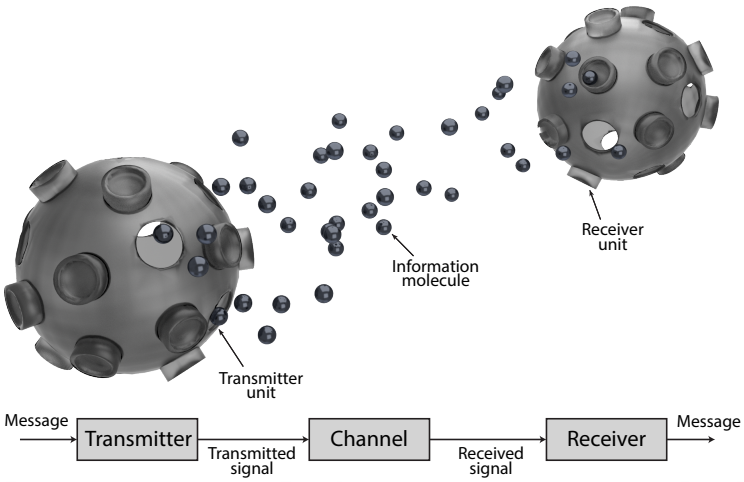


Figure 7.1: Molecular communications between a pair of nanomachines.

and state the future research directions.

7.2 Molecular Communications Receiver

A molecular communication system between a single pair of nanomachines can be depicted as in Fig. 7.1, where the molecular messages encoded into concentration propagate through molecular diffusion from the transmitting nanomachine to the receiving nanomachine. Receiver of a nanomachine in an MC system is responsible for detecting the incoming molecular messages, converting them into a processable signal, and processing the signal for extracting the encoded information. The decoded information may then be used by the nanomachine to realize a prespecified operation. Therefore, the performance of the receiver is critical for the proper functioning of the nanomachine, and thus of the nanonetwork application.

MC receiver slightly differs from a receiver of a conventional electromagnetic communications. Fig. 7.2 demonstrates the block diagram of its envisioned architecture. An MC receiver basically consists of two subunits, namely, a molecular antenna, and a processing unit which is coupled to the output of the antenna. The molecular antenna is comprised of a recognition unit and a transducer. The recognition unit is the interface between the communication channel and the receiver. Its main functionality

is to establish the selectivity only to the molecules that carry information, and thus to minimize the interference from other molecules in the communication environment. The transducer works intimately with the recognition unit, and converts the molecular recognition events into a processable form by means of electrical, optical or chemical signals. The transduced signals, i.e., the output of the antenna, are simultaneously collected by the processing unit which then may amplify and demodulate the signal to recover the transmitted information based on a preset modulation scheme.

To be operable in an MC application, the receiver should basically satisfy the following requirements:

- ***In situ* operation and in-device processing:** Envisaged nanonetwork applications require for nanomachines to operate in a physically independent manner. If nanomachines are required to be controlled through an external device, the communication interface between them should not interrupt the system operation. In the same manner, an MC receiver integrated into a nanomachine should be capable of *in situ* operation. A wired connection to an external device for controlling or powering the receiver is not acceptable. Receiver should detect molecular messages through in-device processing, i.e., without requiring a post-processing of the transduced signals by an external macroscale device or a human controller.

- **Label-free detection:** Receiver should be able to recognize the information carrying molecules based on their intrinsic characteristics, i.e., without requiring a molecular labelling procedure or any other preparation stage.

- **Continuous operation:** Detection should be continuous. This requires for the recognition and the transduction mechanisms to be reversibly responsive, i.e., they should be capable of returning to the initial state after the detection to be able to accept the succeeding molecular messages without causing a communication error.

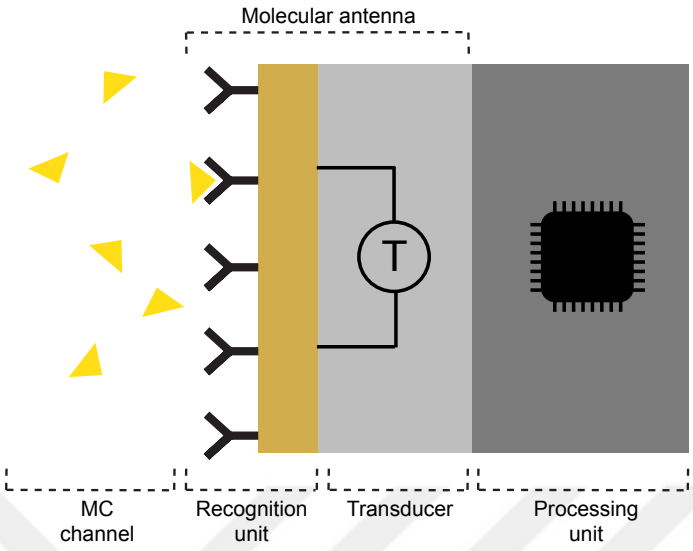


Figure 7.2: Functional units of a molecular communications receiver.

- **Nanoscale dimensions:** The components of the receiver should have nanoscale dimensions for the integration of the overall receiver into a nanomachine.

In addition to these requirements, for *in vivo* applications, the receiver should also be biocompatible. In other words, the operation of the receiver should not have any detrimental effect on the biological environment, or its performance should not be degraded by the environmental conditions.

7.3 Overview of Biosensing Mechanisms

Developing a biosensor capable of detecting the existence of a target molecule in an environment or quantifying the concentration of a molecular specie has been a long-standing goal of analytical chemistry. For this aim, many different biosensing approaches have been proposed for a plethora of target molecular species ranging from proteins to oligonucleotides, as well as small molecules like glucose [Perumal and Hashim, 2014] [Senveli and Tigli, 2013].

A biosensor generally consists of a biorecognition layer and a transducer which converts the recognition events into a processable form [Perumal and Hashim, 2014].

It is not surprising that a biosensor and a molecular receiver have common design principles, since they both aim to analytically recognize the molecules. However, there are also fundamental differences between them. First, it is not sufficient for an MC receiver just to detect the presence of a molecule in an equilibrium state as for the case of a biosensor. The receiver should be capable of detecting the information, which is encoded into a physical property related to the molecules, such as concentration, type, or arrival time, by continuously observing the environment. This requires the communication theoretical tools to be applied. Another critical difference arises from the application domain. The biosensor literature is mostly directed to the design of biosensing approaches suitable for laboratory applications that necessitate the operation of macroscale readout devices and human observers due to the lack of an integrated processor. Moreover, biosensors have not yet been completely scaled down to nanoscale dimensions to be integrated into an envisioned nanomachine. Nevertheless, we can still design a molecular receiver inspired from a biosensing method; but first we need to examine all of the biosensing approaches to determine the most promising one.

Biosensors proposed so far, in general, can be classified into three categories based on the transduction mechanism: electrical, optical, and mechanical biosensors. Electrical biosensing is based on the alterations in the current, voltage, or conductance in the transducer resultant from a chemical reaction or a binding event realized in the recognition unit [Thévenot et al., 2001] [Grieshaber et al., 2008]. Similarly, optical sensing exploits the changes in one of the optical characteristics of the transducer upon the recognition. Optical transduction and recognition are generally realized on the same unit. Several optical sensing mechanisms are developed based on surface plasmon resonance (SPR), chemiluminescence, fluorescence and FRET [Fan et al., 2008]. On the other hand, mechanical sensing benefits from the modulation of the mechanical resonance with the binding of a molecule to the surface of the transducer [Tamayo et al., 2013]. A comprehensive review on different sensing approaches can be found in [Perumal and Hashim, 2014].

In addition to these engineered sensing methods, a fourth mechanism which is called biochemical or molecular transduction is prevalent in nature as part of the cellular communications [Cantrell, 1996] [Weiss and Littman, 1994]. The mechanism converts the biorecognition events on the cellular membrane into an ion flux through the membrane pores of the cell to trigger a function with the potential change, or the events activate the secondary messengers in the cytoplasm to realize cellular functions.

Considering the basic requirements of the molecular receiver, we suggest focusing on electrical biosensing approaches. The reason for eliminating the optical and mechanical biosensing options is that they rely on macroscale detectors that cannot be accepted for an MC receiver considering the requirement of *in situ* operation. Although the biorecognition and transduction units can be downsized to nanoscale, these units should be excited by optical lasers, and the resultant signals, for both optical and mechanical sensing, should be observed through optical detectors to extract the sensing information. Even for bioluminescence-based methods which do not require excitation of the transducer, there is currently no approach towards realizing *in situ* processing of the resultant optical signals mainly due to the diffraction limit of light.

To compare the suitability of electrical and biochemical sensing for an MC receiver, we also need to consider the corresponding nanomachine architectures which are in the nanobioelectronic and synthetic-cell domain, respectively. In this context, the advantages of electrical sensing are several. First, there is a clear trend towards the miniaturization of electrical processing units into nanoscale. Since electrical biosensors intrinsically provide processable inputs for these devices, they can be readily integrated in nanobioelectronic domain. On the other hand, the assumption of synthetic cell-based nanomachines, which is based on combination of the biochemical transduction and high processing capabilities, seems very vague. Biochemical sensing implies also biochemical processing. The speed of electrical operations is incomparably higher than the biochemical processes, thus, we can certainly assert that electrical sensing also promises for fast processing of the transduced signals. More-

over, electrical sensing can provide the receiver with much more diverse functionality which can be tuned and controlled electrically in a similar way with the conventional counterparts. Also, interfacing with macroscale equipments in a wireless manner is more feasible for the electrical domain. Although synthetic-cell based nanomachines intrinsically provide ultimate biocompatibility; with the advances in bioelectronics, it is not a difficult problem also for the nanobioelectronic devices. Therefore, comparing the state-of-the-art in the two research domains, obviously electrical nanomachines seem more suitable and feasible for the envisaged nanonetwork applications. This leads us to investigate the electrical sensing approaches in more details to be adapted for an MC receiver.

Electrical biosensors can be grouped into two classes according to their recognition method: biocatalytic and affinity-based sensors [Ronkainen et al., 2010]-[Sadik et al., 2009]. Biocatalytic recognition employs specific enzymes immobilized on a layer to detect the targets based on enzymatic reactions [Wang, 2008]. When a target is bound to an enzyme, an electroactive specie, e.g., hydrogen ion, is generated as a result of the reaction. If the specie achieves to diffuse into the working electrode of the transducer, it modulates one of the electrical characteristics of the device. Commercialized macroscale glucose sensors can be given as example to the biocatalytic electrical sensors. On the other hand, affinity-based sensing is based on the selective binding of certain receptor-ligand pairs on the recognition layer [Rogers, 2000].

Biocatalytic techniques require two-step reaction, i.e., enzymatic reaction and consecutive detection of the produced electroactive species. This complicates the procedure as the device gets smaller. Also, generation of additional products may not be desired during the operation. Additionally, the method is limited to specific analytes that generate the electroactive species upon the reaction with the corresponding enzymes. Therefore, the method does not provide flexibility in selection of the target molecules. On the other hand, affinity-based sensing uses the nature's approach for recognition offering a more direct detection scheme. Also the method has proven feasible for a larger range of target molecules with higher sensitivity and

selectivity. Moreover, affinity-based biorecognition is more convenient for the current molecular communication models which are mostly based on ligand-receptor binding, thus, provides an easier path to be adapted into the receiver models. Therefore, we focus our attention into affinity-based electrical sensing.

Affinity-based sensing is also classified depending on the detection format in the transducer unit: amperometric, potentiometric, conductometric, and impedance-based. Briefly, amperometric detection is based on the changes in the current [Wang, 1999]; potentiometric detection relies on the change of the potential between two reference electrodes [Koncki, 2007]; conductometric detection is based on the modulation of the conductance by the recognition events [Jaffrezic-Renault and Dzyadevych, 2008]; and impedance-based detection is a frequency-domain method benefitting from the impedance variations as the result of molecule binding events [Daniels and Pourmand, 2007]. All of these methods are developed primarily for *ex situ* analysis in laboratory conditions; thus, they do not promise for portable and *in situ* applications. Fortunately, the advances in nanotechnology in the last decade have led to the design of a new method for affinity-based electrical sensing which is based on FET technology with the use of novel nanomaterials, such as nanowires, nanotubes, organic polymers, and graphene, as the transducer unit [Schöning and Poghossian, 2002]-[Curreli et al., 2008]. It is based on the modulation of transducer conductivity by the electrostatic effects resultant from the molecular bindings on the recognition layer. FET-based biosensors (bioFETs) promises for label-free, continuous and *in situ* operation in nanoscale dimensions, thus, the design of a bioFET stands as a good starting point for the design of an MC receiver. Hence, in the remaining of the paper, we elaborate on the FET-based molecular receiver.

7.4 FET-Based Molecular Receiver

In conventional FET type transistors, current flows between source and drain electrodes through a semiconductor channel whose conductance is controlled via a perpendicular electric field created by a gate electrode. Conductivity is proportional to

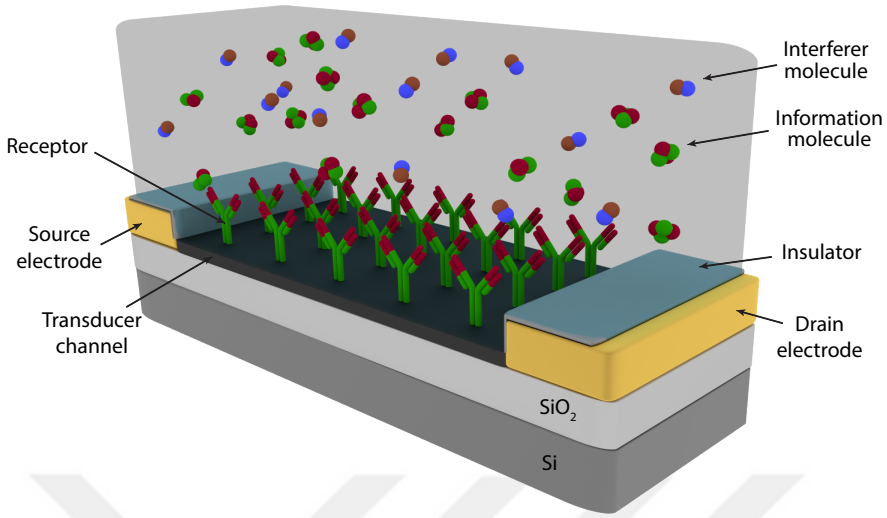


Figure 7.3: Conceptual design of FET-based MC receiver.

the carrier density accumulated in the channel by the electric field, and reflected to the changes in the voltage-current characteristics. Replacing the gate electrode with a biofunctionalized surface through the immobilization of affinity-based receptors directly on top of the channel as depicted in Fig. 7.3, the device becomes a biosensor, namely bioFET.

Binding of charged analytes to the surface receptors results in accumulation or depletion of the carriers on the semiconductor channel, and modulates the channel conductivity; thus, the conductivity becomes a function of the analyte density and the amount of analyte charges. For example, if the channel is p-type doped, negatively charged analytes accumulate the positive hole carriers in the channel when they bind to the receptors; as a result, the conductivity increases depending on the density of the bound analytes as shown in Fig. 7.4. The conductivity change is reflected to the current (I_{ds}) flowing through the channel if a constant source-to-drain potential (V_{ds}) is maintained. For applications in ionic solutions, usually, a reference electrode is immersed in the solution to stabilize the surface potential of the channel on its base level which may be highly fluctuated due to undesirable ionic adsorptions complicating the detection of target analytes [Nair and Alam, 2007]. It is clear that FET-based

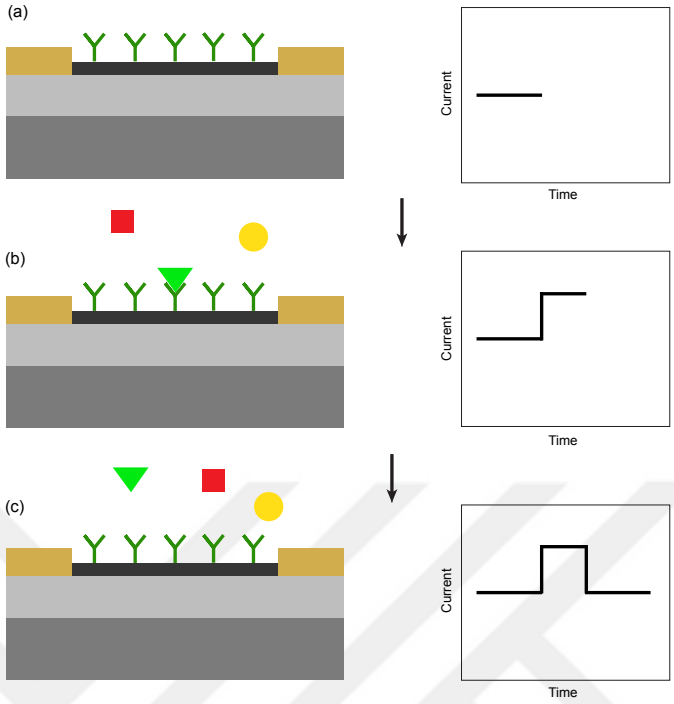


Figure 7.4: Expected time domain response of a p-type doped FET-based MC receiver in terms of drain-to-source current in the transducer channel, when (a) no information molecule is present in the reception space, (b) a negatively charged information molecule binds to a surface receptor, (c) the bound molecule leaves the recognition unit.

biosensing enables direct, label-free, continuous and *in situ* sensing of the molecules by not requiring any complicated processes like labelling of the molecules or the use of any macroscale equipment for readout and processing operations.

Simple operation principles together with the extensive literature on FETs established through many years, electrical controllability of the main device parameters, high-level integrability, and plethora of optimization options for varying applications make FET-based biosensing technology also a quite promising approach for electrical MC receiver. Therefore, we direct our attention to devise a molecular receiver based on the principles of affinity-based bioFETs.

7.4.1 Signal Flow and Noise Sources

To characterize the operation of a FET-based molecular receiver, we need to investigate the input-output signal relations together with the expected contributions of the noise sources. Noise results in random fluctuations in the electrical output signal; hence, it is critical to determine its detrimental effects on the detection performance. Noise sources for a FET-based molecular receiver can be divided into three categories [Hassibi et al., 2007], which are briefly explained as follows:

Reception Noise

A molecule in the reception space undergoes random motion which is governed by Brownian dynamics, and stochastically binds to the receptors on the recognition layer. The uncertainty in the location and the binding state of the molecules results in random fluctuations of the transduced signal and may severely hamper the instant detection of the concentration, and thus, the molecular messages [Hassibi et al., 2005]. This type of reception noise is well-studied from the molecular communications perspective [Pierobon and Akyildiz, 2011].

Transducing noise

Transducing operation also includes contributions from noise sources which can be classified into two types: thermal noise and $1/f$ (flicker) noise [Rajan et al., 2013], [Deen et al., 2006]. Thermal noise is resultant from the thermal fluctuations of the charge carriers both on the transducer channel and on the bound ligands. On the other hand, $1/f$ noise is caused by the traps and defects in the semiconductor channel, and it could be very effective at low frequencies [Rajan et al., 2010a]. Since molecular diffusion and binding kinetics are generally low-frequency processes, we expect that the receiver will also operate at low frequencies. Hence, the $1/f$ noise may dominate all the other noise sources, and thus, need a careful investigation.

Biological Interference

The function of the recognition layer is to selectively bind to the target molecules, which are the information carriers. The selectivity is governed by the binding affinity between the information molecules and the receptors. However, for crowded environments, it is possible that molecules of other species, which show similar affinities for the receptors, exist in the reception space, thus, occasionally bind to the receptors and complicate the detection. This biological interference, which is also termed the background noise, could severely deteriorate the detection performance as the concentration and the charge of the interferers are comparably high [Hassibi et al., 2005]. Biological interference should not be confused with the intersymbol interference (ISI) or co-channel interference which have been already investigated in [Pierobon and Akyildiz, 2012], [Pierobon and Akyildiz, 2014], from the aspect of molecular communications. Note that the randomness of interferers' motion and binding to the receptors also contributes to the total reception noise of the receiver.

Incorporating the contribution of noise sources, a simplified signal flow diagram of the system can be given as in Fig. 7.5, assuming that the binding of interferer molecules and messenger molecules are uncorrelated. In fact, this is a loose assumption; because the receptor-ligand binding kinetics is expected to be affected by the number of bound interferer molecules. However, when the concentration of the receptors in the recognition layer is high enough compared to the total concentration of ligand and interferer molecules in the reception space, this assumption holds true. Then, the electrical output signal can be expressed as follows:

$$s(t) = T\overline{X(t)} + Tu_x(t) + u_T(t) + \sum_{i}^{m} T_i \left(\overline{X_{(i)}(t)} + u_{x(i)} \right), \tag{7.1}$$

where $X(t)$ is a stochastic state matrix which represents the locations of the ligands, including the conjugated ones, in the reception space [Hassibi et al., 2007]. The matrix relates the molecular density of the reception space to the occupancy rate of the receptors on the recognition layer. T is the transducing vector which operates on

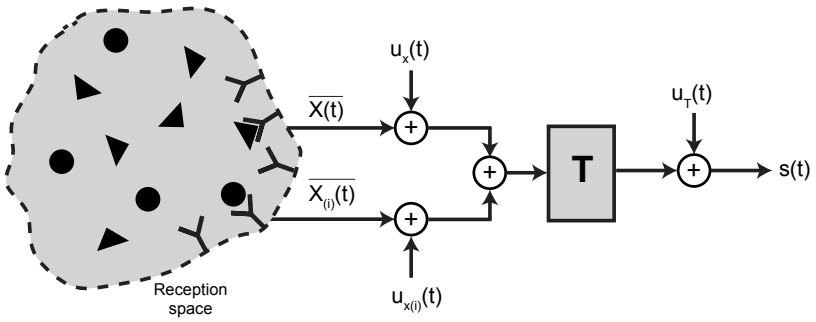


Figure 7.5: Signal flow diagram of an MC receiver antenna. The triangles and circles denote the information and interferer molecules, respectively.

the state matrix, and $\overline{X(t)}$ is the ensemble average of the state matrix. The $u_x(t)$ and $u_T(t)$ denote the reception noise and the total transducing noise, respectively. $\overline{X_{(i)}(t)}$ is the ensemble average of the state matrix of the ith interferer molecule, and $u_{x(i)}$ is the corresponding reception noise. T_i is the transducing vector for the ith interferer. Note that, the reception noise resultant from the stochastic binding events is amplified by the transducing operation.

7.4.2 Performance Metrics

This section aims to define the performance metrics for an electrical MC receiver, and explain the effects of main system parameters on the receiver performance.

Sensitivity

Sensitivity is the capability of the receiver to perceive the small differences in the molecular concentration [Nair and Alam, 2007]. It is a critical performance metric, especially for the design of MC systems which encodes the information into molecular concentrations, e.g., MC with Concentration Shift Keying (CSK). It can be defined as the change in the transducer current per change in the molecular concentration in the reception space of the receiver for a concentration range where linear operation can be assumed. Linear operation corresponds to the operation range where the receptors on the receiver surface are not saturated by the information molecules.

Selectivity

The capability of the receiver to uniquely detect the information molecules in the reception space, which is probably crowded with interferers, is the measure of its selectivity [Nair and Alam, 2007]. It is clear that the recognition unit is directly in charge of the selectivity as it sets the affinity with the messenger ligands and with the possible interferers. Higher selectivity implies that the probability of the interferer molecules to bind the receptors is lower than the one of the information carrying molecules. Selectivity is a critical design consideration especially for MoSK-based MC systems [Kuran et al., 2011]. The receptor molecules as well as the messenger ligands should be carefully selected considering the coexisting molecular species in the communication environment.

Signal-to-Noise Ratio (SNR)

Signal-to-noise ratio at the antenna output determines how easy the receiver can recover the transmitted signal in the presence of noise sources that are explained in Section 7.4.1. It is the most crucial parameter to evaluate the reliability of the detection. It can be simply calculated as the ratio of the received signal power to the total noise power, i.e., $SNR = P_{signal}/P_{noise}$, in a given operation bandwidth of the receiver.

Limit of Detection

The minimum molecular concentration in the reception space required for the receiver to detect the existence of an information molecule is termed the limit of detection (LoD) [Rajan et al., 2014]. It is not to be confused with the minimum concentration required for the exact determination of the concentration. Once the limit is determined, it can be exploited by the transmitter nanomachine to save on the number of molecules transmitted to the channel, especially when the information is encoded into the type of the molecules as in the case of MoSK [Kuran et al., 2011]. The limit of detection is mainly set by the noise level of the overall reception process and the

flow conditions of the environment, and can be given as $LoD = 1/SNR$ [Rajan et al., 2013].

Temporal Resolution

Temporal resolution defines how fast the receiver is able to sample the molecular concentration in the reception space. Considering that electrical processes are very fast compared to molecular processes, the limiting factor for the temporal resolution of the receiver is expected to be the molecular diffusion and binding kinetics. In order for the receiver to be able to detect all the messages carried by the molecules into the reception space regardless of the modulation type, the recognition should be realized in transport-limited manner. In other words, the binding kinetics should not be a limiting factor on the sampling rate. We further discuss the effect of binding kinetics on the temporal resolution in Section 7.5.2.

In addition to these metrics, there are some other measures that can be required to quantify the performance of the electrical MC receiver. For example, how much information about the incoming molecular signal is contained in the electrical output of the receiver is a quite important metric to determine the detection performance. In the information theory, this is represented by the mutual information between the receiver output and the incoming molecular signals. Mutual information is determined based on the conditional entropy, i.e., equivocation, of the received signal given the receiver's electrical output. These information theoretical metrics would be especially important for the design of optimal detection algorithms. They are needed for determining the end-to-end communication capacity of an MC system and developing encoding schemes that can achieve this capacity. However, they require a probabilistic model of the overall reception process combined with the random propagation of the information signals in MC channel. Likewise, if the receiver is implemented along with a differential amplifier, Common Mode Rejection Ratio (CMRR), which measures the capability of the device to reject the common modes in the incoming signals, will become an important metric to determine the receiver performance.

7.5 Design Options

The performance of the receiver should be optimized by the design parameters under different application scenarios. This section elaborates on the main parameters corresponding to the two main receiver components, which are the transducer and the biorecognition unit.

7.5.1 Semiconductor Channel

The semiconductor channel located between the source and the drain electrodes is the main transducing element of the receiver. Binding of the charged information molecules modulates the conductance or potential of the channel through depletion or accumulation of the carriers within the channel. Therefore, its electrical characteristics like conductance and electron mobility are critical for the sensitivity performance of the transduction, thus, of the receiver. Also, $1/f$ noise, which is very effective in low frequency applications is mainly resultant from the inevitable defects and traps on the channel generated during the fabrication process. Moreover, the channel geometry is directly relevant to the surface coverage of the receiver, and affects its integrability to the overall circuitry of a nanomachine [Nair and Alam, 2007].

Many nanomaterials have proven suitable for use in bioFET channel, such as silicon nanowires (SiNWs) [Patolsky and Lieber, 2005], single walled carbon nanotubes (SWCNTs) [Allen et al., 2007], graphene [Kochmann et al., 2012], molybdenum disulfide (MoS_2) [Sarkar et al., 2014], and organic materials like conducting polymers [Torsi et al., 2013]. These materials, some of which are demonstrated in Fig. 7.6, are also feasible candidates for the transducing channel of a molecular receiver. It is to be noted here that use of different materials does not change the operation principles of the receiver, and does not bring any fundamental constraint on the design of other parts of the receiver such as the biorecognition unit.

First generation bioFETs rely on the use of one dimensional materials like SWCNT and SiNW as the channel in a bulk form. However, use in the form of single material or aligned arrays have proved to surpass the performance of the bulk channels in terms of

sensitivity and reduced noise [Curreli et al., 2008], [Allen et al., 2007]. SWCNT-based bioFETs have attracted more attention due to the excellent electrical characteristics of carbon nanotubes which lead to higher sensitivity; however, clean fabrication of SWCNT without defects is the most challenging among all of the candidates, which may hamper its proper practice in an MC receiver [Maehashi and Matsumoto, 2009]. On the other hand, SiNWs can be fabricated in a relatively easy and controlled manner, with adjustable length, diameter, and doping levels which have direct influence on the material conductance [Chen et al., 2011]. However, SiNWs still possess substantial production challenges due to their 1D nature [Wang et al., 2012].

Graphene has emerged as an alternative with its 2D planar structure providing higher spatial coverage in a single device with the possibility of immobilizing higher number of receptors [Park et al., 2012]. The same 2D structure also leads to a higher sensitivity compared to 1D materials, since all of its atoms are able to closely interact with the bound molecules on the recognition layer. Moreover, intrinsic flexibility of graphene provides higher chance of integration into devices with non-planar surfaces which can be more suitable for the design of nanomachines in an MC application [Yang et al., 2010]. Another 2D alternative for the transduction channel is MoS_2 which has been very recently shown to be more sensitive than the graphene channel [Sarkar et al., 2014]. The possession of a bandgap which is not the case for graphene has been pointed out as the reason for the higher sensitivity of MoS_2-based bioFETs.

Organic conductive polymers also have been shown to provide similar electronic performances with the inorganic counterparts when used as the semiconducting channel. They can be utilized in both 1D and 2D forms [Lin and Yan, 2012]. In addition, they provide ultimate biocompatibility which make them more preferable for *in vivo* applications of MC.

The selection among these materials should be carefully made according to the performance requirements of the MC application [Yang et al., 2010], [Li et al., 2011]. Also, the architecture of the overall nanomachine can mandate the use of flexible planar materials. On the other hand, some applications may require more complex

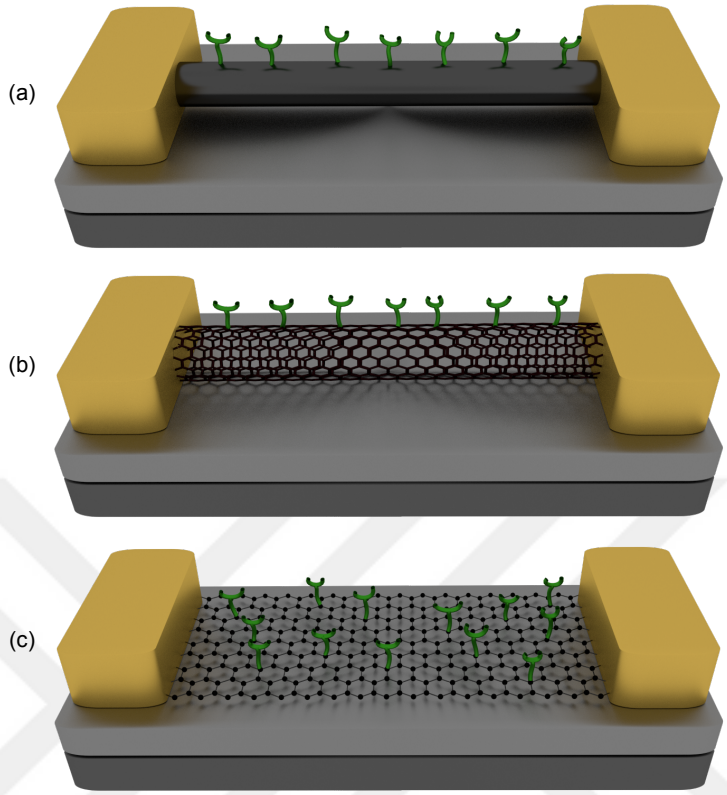


Figure 7.6: FET-based MC receiver with different type of transducer channels: (a) SiNW channel, (b) SWCNT chanel, (c) graphene channel.

receivers with more than one channels for multiplexing purposes which will be discussed in Section 7.7; and for such cases, 1D materials may be more suitable allowing dense channel deployments.

7.5.2 Bioreceptors and Ligands

Bioreceptor is another design fundamental which is the principal determinant of the receiver's selectivity. The array of receptors constitutes the interface between the receiver and the MC channel, being the active components of the recognition unit. The design considerations on the receptor molecules cannot be isolated from the information molecules, i.e., ligands; since the modulation of the transducer current is realized as a result of the binding of the ligands and the receptors to each other. The

binding reaction can be simply represented by the following relation

$$\mathrm{N_R} + \mathrm{N_L} \underset{k_-}{\overset{k_+}{\rightleftharpoons}} \mathrm{N_B} \tag{7.2}$$

where N_R, N_L, and N_B denote the number of unbounded receptor, ligand, and receptor-ligand complexes, respectively; k_+ and k_- are the association and dissociation reaction rates. The affinity between the ligands and the receptors is quantized by the dissociation constant which can be given by $K_D = k_-/k_+$. Affinity is inversely proportional to the dissociation constant K_D. In order for the receiver to be selective only to the ligands that represent the information, the affinity of the receptors for the ligands should be significantly higher than their affinity for the interferer molecules that may exist in the reception space.

Mainly three types of recognition pairs used in affinity-based FET-type biosensors are feasible for an MC application: antibody/antigen (Ab/Ag), natural receptor/ligand, and aptamer/ligand [Poghossian and Schöning, 2014] [Rogers, 2000]. These pairs are suitable because they bind to each other reversibly, and their sizes are small enough to be utilized in an MC application.

Antibodies are Y-shaped immune system proteins that are generated to bind to specific antigens which are perceived as the proteins of an harmful microorganism inside the body. Antibodies generally operate with lock-and-key principle, thus, provide high level selectivity for the corresponding antigens. Hence, incorporation of them as receptors has provided highly selective bioFETs [Schöning and Poghossian, 2002, Curreli et al., 2008]. Antibodies are usually generated by introducing antigens into an animal. Therefore, the utilization of Ab/Ag may face certain production challenges and biocompatibility risks for *in vivo* applications.

Natural receptors are cellular proteins that are immobilized within the plasma membrane. They enable the cell to interact and communicate with its surroundings, e.g., neighboring cells, by binding to corresponding ligands which can be a sort of ions or complex molecules like proteins that represent the information relevant to the cell. Binding of a ligand to a receptor opens a membrane pore resulting in a subsequent

ion flux through the pore. Because of the ion flux, the potential across the plasma membrane changes. The potential change is then followed by a relevant activity of the cell [Cantrell, 1996, Weiss and Littman, 1994]. The cellular receptors including neuroreceptors, taste and olfactory receptors, have proved to be successfully implemented on the recognition unit of bioFETs to detect neurotransmitters [Kim et al., 2013], taste molecules, and odorants [Song et al., 2014]. Since these receptors naturally operate in living organisms, their utilization in *in vivo* applications do not bring up any biocompatibility problem. Moreover, their ability to detect odorants promises for long range MC applications that have been reviewed in [Giné and Akyildiz, 2009].

Additionally, aptamers, which are artificial single-stranded DNAs and RNAs, have also been widely utilized as recognition elements in bioFETs to detect a wide range of targets, i.e., ligands, including small molecules, proteins, ions, aminoacids, or other oligonucleotides [Willner and Zayats, 2007]. An aptamer for a specific ligand is selected through a SELEX (systematic evolution of ligands by exponential enrichment) process which is based on scanning a large library of DNAs and RNAs to determine a convenient nucleic acid sequence that has the desired affinity with the ligand. There already exist in the literature numerous aptamer libraries determined for a plethora of ligands, which reduce the fabrication challenges [Luzi et al., 2003, Lee et al., 2008]. Availability of almost infinite number of different aptamer-ligand combinations with varying affinities makes aptamer-based recognition promise for highly selective MC receivers.

In the MC studies published so far, the effect of the affinity between the receptor-ligand pairs, and thus, the effect of the association and the dissociation reaction rates on the communication performance have been neglected, assuming perfect recognition and transduction units which are capable of continuously detecting the overall ligand concentration in the reception space. However, these reaction rates may be critical limiting factors on the maximum sampling rate of the receiver, and thus, may lead to detection errors if they are not optimized for varying communication rates. To gain more insight on this issue, we need to investigate the relation between the transport

dynamics of the ligands and the binding kinetics on the receptors. Unfortunately, in the literature, there is not an analytical model that achieves to fully capture this relation, but the two compartment model is usually able to provide with a qualitative examination of the behavior [Goldstein et al., 1999, Das et al., 2009]. The model divides the space into two virtual compartments assuming that the ligand concentration is homogenous in each of them, but the amount of the concentration may change with time in individual compartments. For a spherical receiver, the resultant compartments are two spheres inside each other; and for a planar receiver, they can be considered as two planar layers, one on the top of the other. Inner space, which is adjacent to the receiver, corresponds to the reception space whose volume is small enough to assume that receptors and ligands are homogenously distributed. The model expresses the correlation between the ligand concentrations in each compartment by the following differential equations:

$$V\frac{dc_L^R}{dt} = k_M\left(c_L - c_L^R\right) - k_+ c_L^R\left(N_R - N_B\right) + k_- N_B, \tag{7.3a}$$

$$\frac{dN_B}{dt} = k_+ c_L^R\left(N_R - N_B\right) - k_- N_B, \tag{7.3b}$$

where V is the volume of reception space; c_L^R and c_L denote the ligand concentration inside and outside the reception space, respectively; N_R and N_B are the number of free and bound receptors on the surface of the recognition layer, respectively [Duan et al., 2012]. The transport dynamics of the ligands from the outer space to the reception space are governed by a transport parameter k_M which quantizes the rate of the ligand transport into the reception space. This parameter is intended for capturing the molecular diffusion due to a concentration difference between the outer space and the reception space, and the transport dynamics resultant from the flows in the fluid environment. The relation between k_M and the reaction rates is critical for determining whether the sampling rate of the device is sufficient to capture all the concentration changes in the reception space. It is clear that the binding reaction rates k_+ and k_- should be high enough for the recognition to be diffusion-limited, or

in a more general sense, transport-limited, and not reaction-limited. If the recognition is reaction-limited, then, the concentration changes in the reception space may not be fully captured; thus, successive signals cannot be discriminated from each other, which may result in intersymbol interference (ISI). For the recognition to be transport-limited, the following inequality must be satisfied: $k_+ \times (N_R - N_B) \geq k_M$. This requires that both k_+ and k_- have to be sufficiently high. There are in the literature analytical estimates of k_M for different geometries of the receiver and for different flow conditions [Jokić et al., 2012], which are not included in this paper; but, they can be incorporated into the analytical models that will be developed to capture the full dynamics of both molecular transport and binding reactions.

The characteristics of the ligand-receptor pairs also affect the performance of the receiver, especially its sensitivity. The range of distance from the surface of the receiver where the transducer can detect a recognition event is limited because of the screening of the ligand charges by the ions existing in the communication environment [Nair and Alam, 2008]. The mean effective charge of a free electron on a ligand as observed by the transducer is degraded as the distance between the ligand and the transducer increases. The relation is given by

$$q_{eff} = qe^{-\frac{r}{\lambda_D}}, \tag{7.4}$$

where q is the elementary charge, and r is the average distance of the ligand electrons to the transducer's surface [Rajan et al., 2013]. λ_D is the Debye length which quantizes the ionic strength of the solution according to the following relation

$$\lambda_D = \sqrt{\frac{\epsilon_R k_B T}{2N_A q^2 c_{ion}}}, \tag{7.5}$$

where ϵ_R is the permittivity of the solvent, k_B is the Boltzmann's constant, T is the temperature, and N_A is Avogadro's number, c_{ion} is the ionic concentration of the medium [Rajan et al., 2013]. Debye length is a key parameter in determining an appropriate receptor-ligand pair. The distance of the receptor part where the charged

ligand binds from the transducer surface should not exceed the Debye length. Otherwise, charges of the bound ligands cannot be effectively reflected into the transducer current [Stern et al., 2007]. Therefore, receptors with lengths exceeding the Debye length should be avoided to develop a sensitive receiver. Aptamers and natural receptors having lengths typically smaller than 2nm are advantageous compared to antibodies, and have proven effective even in solutions with high concentration of ions [Luzi et al., 2003]. On the other hand, antibodies can be shortened using only their fab fragments which are the main recognition elements [Elnathan et al., 2012].

The intrinsic charge of the ligands also should be high enough for the proper functioning of the receiver. Most of the biomolecules like proteins and nucleic acids are highly charged in solutions, but the amount of molecular charges may significantly change depending on the pH level of the environment [Nair and Alam, 2007].

Additionally, density of the receptors can remarkably affect the performance of the receiver [Elias et al., 2013, Caré and Soula, 2011]. It is obvious that dense deployment of the receptors on the receiver surface increases the chance of binding to a ligand. However, the receptor density should be optimized together with the concentration of the ligands used for communication. On one hand, if the ligand concentration is very low compared to the receptor density, then, most of the receptors will be unbounded; and thus, prone to the binding of the interferers, which may result in higher background noise. On the other hand, if the information is represented by very high concentrations of ligands compared to the receptor density, then, the recognition unit may face saturation, and the linear operation range may be disturbed, which then complicates the detection.

7.6 A Modeling Approach for SiNW FET-Based MC Receiver

In Section 7.4.1, we gave an expression in (7.1) to describe the signal flow for the operation of a general MC receiver. That expression includes a transducer vector and a stochastic state matrix denoting the random locations and binding/unbinding states of information molecules. Although it gives an intuition for the receiver operation, it

is only useful for simulation-based approaches, and it does not lead to the derivation of analytical expressions for deterministic signal flow to evaluate the performance of the receiver.

In this section, based on the existing modeling efforts in the literature [Berezhkovskii and Szabo, 2013, Kuscu and Akan, 2015], we present an analytical model of molecular signal reception for a SiNW FET-based MC receiver and evaluate its performance in terms of mean electrical response, sensitivity and SNR. For modulation of molecular signals, we assume that CSK is utilized such that the messages are represented by different levels of ligand concentration. The receiver detects the concentration-encoded messages by observing the transducer channel current.

7.6.1 Model of Biorecognition Unit

We start by deriving the dynamics between the information-carrying ligand molecules and the receptor molecules tethered on the surface of the NW transducer channel. To be able to derive analytical expressions for performance metrics, we make the following assumptions: *i*) Diffusion of ligands are assumed to be fast enough such that the reception is not mass transport limited. Therefore, the ligands are assumed to be homogenously distributed in the reception space, and all of the receptors are always exposed to the same concentration of ligands. *ii*) Concentration of ligand molecules are assumed to be significantly higher than the surface concentration of receptor molecules such that the ligand concentration remains almost constant despite the ligand-receptor reactions taking place. *iii*) Biological interference of any chemically similar molecule is neglected; therefore, the only molecules that can bind to the receptors are the information-carrying ligands. These assumptions are prevalent in molecular communications and biosensor studies [Pierobon and Akyildiz, 2013, Pierobon and Akyildiz, 2011], and lead to a pseudo-first order ligand-receptor dynamics, where the first time derivative of the mean number of bound receptors at time t can

be expressed through the following differential equation:

$$\frac{d\overline{N_B(t)}}{dt} = k_+ c_L^R(t)(N_R - \overline{N_B(t)}) - k_- \overline{N_B(t)}, \tag{7.6}$$

where k_+ and k_- are the intrinsic association and dissociation rate constants of the receptor-ligand complex, respectively. N_R is the total number of receptors on the bioFET surface, and $c_L^R(t)$ is the ligand concentration in the vicinity of the recognition layer, i.e., in the reception space.

Since the diffusion effects on the reaction dynamics are neglected, we can assume that a concentration change in the bulk due to successively transmitted messages from information source is immediately reflected to the concentration in the reception space. Thus, we can neglect the transient phase between different levels of ligand concentration such that $c_L^R(t) = c_i$ for $t \in [t_i, t_i + 1/B)]$, where c_i is the ligand concentration corresponding to the ith message, t_i is the transition time from the $(i-1)$th message to the ith message in reception space, and $1/B$ is the symbol duration with B being the symbol transmission rate. In other words, biorecognition layer of the receiver is assumed to be exposed to a constant concentration c_i representing the ith symbol for $t \in [t_i, t_i + 1/B)]$.

Given the initial condition $\overline{N_B(t_i - \epsilon)} = N_{B,i-1}$ with $\epsilon \to 0$, the solution of (7.6) can be given as [Berezhkovskii and Szabo, 2013] [Kuscu and Akan, 2015]

$$\overline{N_B(t)} = \overline{N_{B,i}^{ss}} + \left(N_{B,i-1} - \overline{N_{B,i}^{ss}}\right) e^{-(k_+ c_i + k_-)(t - t_i)} \quad \text{for } t \in [t_i, t_i + 1/B), \tag{7.7}$$

where $\overline{N_{B,i}^{ss}}$ is the mean number of bound receptors at steady-state, i.e., when $d\overline{N_B(t)}/dt = 0$. We can infer from this equation that although the ligand concentration level immediately changes in the reception space, it takes a certain time for the receptors to adapt the concentration level of the new message. The time to reach steady-state is governed by the reaction timescale $\tau_B = (k_+ c_i + k_-)^{-1}$; thus, for higher ligand concentrations, the adaptation time of the recognition layer decreases. The mean number

of bound receptors at steady-state is given by

$$N_{B,i}^{ss} = \frac{k_+ c_i}{k_+ c_i + k_-} N_R = \frac{c_i}{c_i + K_D} N_R, \tag{7.8}$$

Receiver is assumed to sample the state of receptors at steady-state; thus, the mean number of occupied receptors corresponding to the ith message can be given as $\overline{N_{B,i}} = \overline{N_{B,i}^{ss}}$. The occupation states of the receptors fluctuate around the mean value even in the steady-state. This phenomenon is referred to as receptor noise, which we discussed in Section 7.4.1. As being a summation of Bernoulli random variables, the number of bound receptors at steady-state follows the well-known binomial distribution, variance of which is given by

$$Var(N_{B,i}) = \frac{k_- k_+ c_i}{(k_+ c_i + k_-)^2} N_R. \tag{7.9}$$

The autocorrelation function for the stationary fluctuations of the number of bound receptors at steady-state can be approximated with a single exponential [Bialek and Setayeshgar, 2005]:

$$R(\tau) = Var(N_{B,i}) e^{-\frac{\tau}{\tau_B}}, \tag{7.10}$$

where the characteristic timescale of ligand-receptor binding τ_B is also being the correlation time of binding noise. The Fourier Transform of (7.10) gives the Power Spectral Density (PSD) of the fluctuations:

$$S_{\Delta N_B}(f) = Var(N_{B,i}) \frac{2\tau_B}{1 + (2\pi f \tau_B)^2}. \tag{7.11}$$

7.6.2 Model of Transducer Unit

The charged ligands bound to the surface receptors induce opposite charges on the NW surface to some extent depending on their intrinsic charge. The mean amount of charge generated by the bound ligands for the ith message is given by $Q_i =$

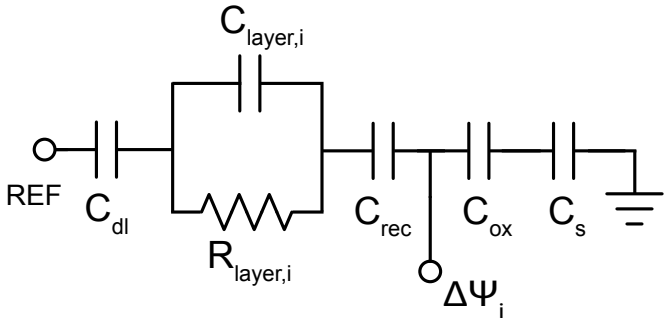


Figure 7.7: Equivalent circuit model for the transducer of the SiNW FET-based MC receiver [Deen et al., 2006] [Kuscu and Akan, 2015] [Georgakopoulou et al., 2015]. *REF* denotes the reference electrode, which stabilizes the gate voltage V_G.

$\overline{N_{B,i}}\, N_e\, q_{eff}$, where N_e is the average number of free electrons per ligand molecule. q_{eff} is the mean effective charge induced by a single electron on a ligand molecule which is given in (7.4), where the mean vertical distance of ligand electrons at the bound state to the transducer surface is assumed equal to the length of the receptor molecule $r = L_R$.

The induced charges on the NW surface are translated into the variation of the surface potential through the equivalent circuit of the transducer [Deen et al., 2006, Kuscu and Akan, 2015, Georgakopoulou et al., 2015], which is demonstrated in Fig. 8.5. By neglecting the current through R_{layer}, i.e., resistance of the layer of bound ligands, which is on the order of tens of $G\Omega$s [Georgakopoulou et al., 2015, Bang et al., 2008], the mean potential difference resulting from the bound ligands can be written as

$$\overline{\Delta\Psi_i} = \frac{Q_i}{C_{eq,i}}, \tag{7.12}$$

where $C_{eq,i}$ is the overall capacitance of the equivalent circuit:

$$C_{eq,i} = \left((C_{ox}WL)^{-1} + (C_sWL)^{-1}\right)^{-1} + \left(C_{rec}^{-1} + C_{layer,i}^{-1} + (C_{dl}WL)^{-1}\right)^{-1}. \tag{7.13}$$

Here, C_{ox}, C_s and C_{dl} are the silicon oxide (SiO_2), the semiconductor, i.e. SiNW,

and the double layer capacitances per unit area, respectively; C_{rec} and $C_{layer,i}$ are the capacitances of the receptor layer and the layer of bound ligands when the ith message is received, respectively; and W and L are the width and length of the transducer's active region. $C_{ox} = \epsilon_{ox}/t_{ox}$ with ϵ_{ox} and t_{ox} being the permittivity and the thickness of the oxide layer. $C_{rec} = N_R \times C_{mol,R}$, $C_{layer,i} = \overline{N_{B,i}} \times C_{mol,L}$ with $C_{mol,R}$ and $C_{mol,L}$ being the capacitance of a single receptor and a single ligand molecule, respectively.

The deviation of the surface potential is reflected into a change in the FET device threshold as $\overline{\Delta V_{TH,i}} = \overline{\Delta \Psi_i}$. We know that the drain-to-source current of FETs in the linear operation regime can be written as

$$I_{DS} = \frac{W}{L} \mu_{eff} C_{ox} (V_{GS} - V_{TH}) V_{DS}, \tag{7.14}$$

where μ_{eff} is the effective carrier mobility in the transducer channel, and V_{DS} is the drain-to-source voltage, which is held constant [Rajan, 2013], V_{GS} is the gate-to-source voltage, which is stabilized by the reference electrode. In case the threshold voltage is shifted, the mean variation reflected to I_{DS} can be given by

$$\overline{\Delta I_{DS,i}} = \overline{\Delta V_{TH,i}} \frac{W}{L} \mu_{eff} C_{ox} V_{DS}, \tag{7.15}$$

Table 7.1: Simulation Parameters

Size of active region ($W \times L$)	0.1×5 (μm) [Rajan et al., 2011]
Temperature (T)	298 (K)
Relative permittivity of SiO_2 layer (ϵ_{ox}/ϵ_0)	3.9 [Deen et al., 2006]
Thickness of SiO_2 layer (t_{ox})	17.5 (nm) [Deen et al., 2006]
Effective mobility (μ_{eff})	16×10^{-3} ($m^2V^{-1}s^{-1}$) [Deen et al., 2006]
Drain-source voltage (V_{DS})	0.1 (V) [Rajan, 2013]
Relative permittivity of solvent (ϵ_R/ϵ_0)	78 [Hediger et al., 2012]
Ionic concentration of medium (c_{ion})	70 (mM) [Okada et al., 1990]
Trap density (N_t)	2.3×10^{24} ($eV^{-1}m^{-3}$) [Rajan et al., 2011]
Tunneling distance (λ)	0.05 (nm) [Deen et al., 2006]
Average net charge of ligands (N_e)	4 [Fritz et al., 2002]
Length of receptor (L_R)	4 (nm) [Song et al., 2008]
Binding rate (k_+)	2×10^{-18} (m^3s^{-1}) [Pierobon and Akyildiz, 2011]
Unbinding rate (k_-)	10 (s^{-1}) [Pierobon and Akyildiz, 2011]
Ligand concentration in reception space (c_i)	$4K_D$
Concentration of receptors on the surface (c_R)	2×10^{16} (m^{-2}) [Rajan, 2013]
Molecular capacitance ($C_{mol,L}, C_{mol,R}$)	2×10^{-20} (F) [Shorokhov et al., 2011]
Capacitance of dielectric layer (C_{dl})	5×10^{-2} (F/m^2) [Landheer et al., 2005]
Capacitance of silicon (C_s)	2×10^{-3} (F/m^2) [Landheer et al., 2005]

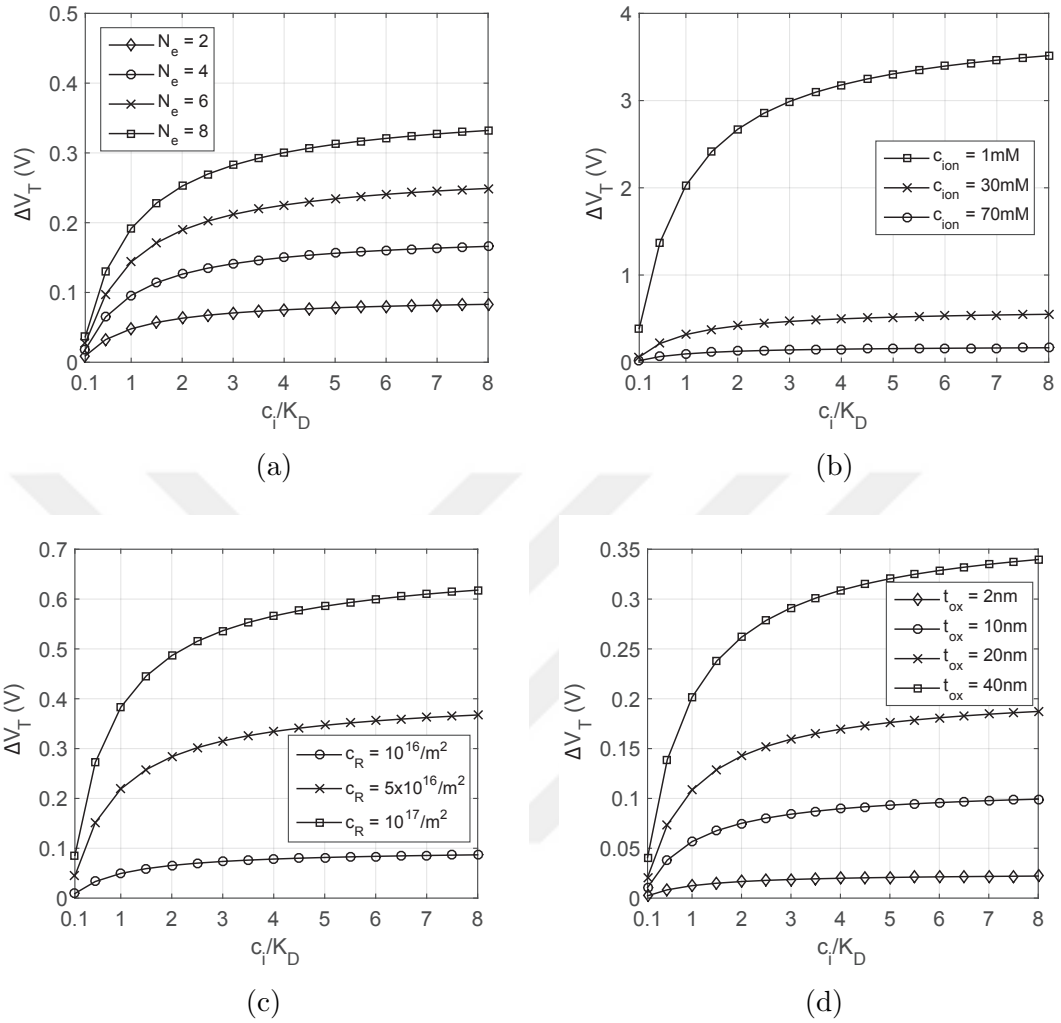


Figure 7.8: Receiver response in terms of difference in threshold voltage, i.e., $\Delta V_T = \Delta I_{DS}/g_m$, as a function of ligand concentration c_i for (a) different mean number of electrons per ligand N_e, (b) different ionic concentration c_{ion}, (c) different concentration of surface receptors c_R (note that $N_R = c_R WL$), (d) different oxide layer thickness t_{ox}.

We can simply express the mean current variation by $\overline{\Delta I_{DS,i}} = g_m \overline{\Delta V_{TH,i}} = g_m \Delta\Psi_i$, where g_m is the transconductance of the device, which can be given as

$$g_m = \frac{W}{L} \mu_{eff} C_{ox} V_{DS}, \tag{7.16}$$

The processor unit of the receiver uses the signal $\Delta I_{DS,i}$, to infer the incoming ligand concentration c_i; and thus the molecular message i, based on a predefined CSK scheme.

As discussed in Section 7.4.1, random diffusion of free electrons results in thermal noise on the resistive layer of bound ligands. The uncertainty in the location of electrons are reflected to fluctuations in the threshold voltage of bioFET antenna. Using the thermal noise model derived in [Georgakopoulou et al., 2015], the PSD of voltage fluctuations on the layer of bound ligands can be expressed by $S_{\Delta V_{TH,i}^{T,layer}} = 4kTR_{layer,i}$, where $R_{layer,i}$ is the mean resistance of the layer of bound ligands when the ith message is received, k is the Boltzmann constant, T is the temperature. The fluctuations in the voltage across $R_{layer,i}$ are reflected to the threshold voltage through the RC network shown in Fig. 8.5. Using the transfer function of the RC network, the PSD of the resultant thermal noise contribution on the threshold voltage can be written as [Kuscu and Akan, 2015] [Georgakopoulou et al., 2015]

$$S_{\Delta V_{TH,i}^{T}}(f) = S_{\Delta V_{TH,i}}^{T,layer} \left(1 + \left[2\pi R_{layer,i} C'_{eq} f\right]^2\right)^{-1}, \tag{7.17}$$

where

$$C'_{eq} = C_{layer,i} + \left[(C_{dl}^{-1} + C_{ox}^{-1} + C_{s}^{-1})(WL)^{-1} + C_{rec}^{-1}\right]^{-1}. \tag{7.18}$$

In addition to the receptor and thermal noise, the low-frequency operation of bioFET-based molecular antenna is also suffered from $1/f$ noise. Using the well-known number fluctuation model [Kuscu and Akan, 2015] [Rajan, 2013], the PSD of $1/f$ noise can be written as follows

$$S_{\Delta V_{TH}^{F}}(f) = \frac{\lambda k T q^2 N_t}{WLC_{ox}^2 f}, \tag{7.19}$$

where λ is the characteristic tunneling distance, and N_t is the trap density of the NW channel. $1/f$ noise is independent of the received signals, and shows an additive

behavior on the overall threshold voltage fluctuations [Georgakopoulou et al., 2015].

7.6.3 Performance Analysis

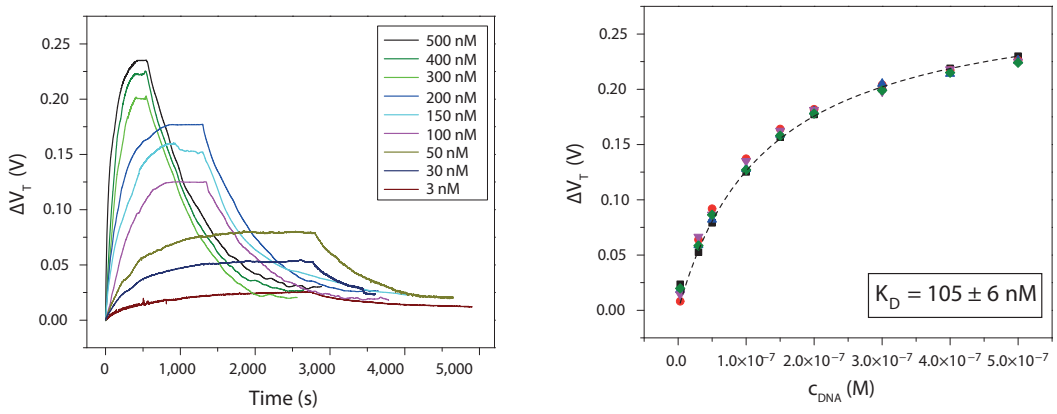
In this section, using the models of biorecognition and transducer units developed in the previous sections, we analyze the expected response of the receiver to varying concentration of information molecules in the reception space under different system settings. Table 9.1 lists the default parameter values used in the analysis. Considering that most of the nanonetwork applications are envisioned for *in vivo* scenarios, the parameter values pertaining to medium characteristics are selected based on the physiological conditions. For example, the default value of ionic concentration, c_{ion}, is selected according to the reported value for bovine serum (70mM) [Okada et al., 1990]; but in the sensitivity and SNR analyses, we investigate the performance for ionic concentrations ranging from the one of highly diluted solutions (1mM) to the one of human blood plasma (>100mM) [Duan et al., 2012]. The solvent is water by default in physiological conditions, which implies the relative permittivity, $\epsilon_R/\epsilon_0 = 78$ [Hediger et al., 2012]. The employed receptors on the FET surface are considered to be aptamers, the production process of which provides full control over the selection of length, binding and unbinding rates, as well as the type of corresponding ligand molecules (see Section 7.5.2). The default length of receptors is set to 4nm, which corresponds to 12 base pair-aptamers. Binding and unbinding rates, k_+ and k_-, are set, considering the accepted values in the MC literature [Pierobon and Akyildiz, 2011] and the range of rates that aptamers can provide [Luzi et al., 2003]. Aptamers can bind to a large set of ligands, such as, aptamers, small proteins, RNA and DNA, and even non-organic molecules, which can attain a broad range of elementary charges, as will be discussed in Section 7.6.3. The capacitance of receptors and ligands, $C_{mol,R}$ and $C_{mol,L}$, are selected based on the reported values for oligonucleotides and small molecules [Lu and Zhang, 2008], which correspond to a mean value of 2×10^{-20}F. The relative permittivity of SiO_2 layer is reported as $\epsilon_{ox}/\epsilon_0 = 3.9$ [Deen et al., 2006]. The thickness of the SiO_2 layer, t_{ox}, is a design parameter, for which we select a

default value of 17.5nm corresponding to the design in [Deen et al., 2006]. However, we carry out the analyses for a wide range of t_{ox} values considering that the thickness can be reduced to below 5nm, as reported in [Kobayashi et al., 1998]. Depending on the fabrication, the tunneling distance for SiO_2 is on the order of 0.01-0.1nm [Rajan et al., 2011]. We set $\lambda = 0.05$nm as reported in [Deen et al., 2006], which also reports the effective mobility as $16 \times 10^{-3}\text{m}^2/\text{Vs}$. The capacitance of dielectric layer, C_{dl}, and silicon substrate, C_s are design parameters for which we set the default values as reported in [Deen et al., 2006]. The trap density N_t depends on the quality of fabrication, and can attain a wide range of values [Rajan et al., 2011]. As default, we set a moderate value of $2.3 \times 10^{24}\text{eV}^{-1}\text{m}^{-3}$. In the analyses, we also discuss the experimental results obtained in [Duan et al., 2012] and compare them with our numerical results.

Receiver Response

Fig. 7.8a, presents the receiver response in terms of the expected variation in the threshold voltage ΔV_T, which is the mean variation of the channel current normalized by the device transconductance g_m, as a function of the average number of elementary charges that ligands possess. As is seen, the net charge of ligands critically affects the receiver response, since the transducer operation is based on the field effect generated by the ligand charges. As reviewed in Section 7.5.2, oligonucleotides are negatively charged in physiological conditions, i.e., at pH 7.4, due to their highly charged phosphate backbone. For example, a DNA sequence with 4 base-pairs at pH 7.4 can attain a net charge of $-8e$. Likewise, small proteins and antigens, depending on the pH of the environment, can attain a net charge of up to $\pm$4e [Tsai, 2007].

Employing highly charged ligands as information molecules is not sufficient to obtain a proper receiver performance, since the ligand charges are substantially screened by the ions present in the surrounding medium. The major determinant of this so-called Debye screening is the ionic concentration of the medium, i.e., c_{ion}. In Fig. 7.8b, we present the receiver response for different values of c_{ion}. As it is clear,



(a) (b)

Figure 7.9: The results of experiments conducted in [Duan et al., 2012] for the detection of DNA concentration by a SiNW FET functionalized with HMGB1 proteins: (a) Threshold voltage ΔV_T vs. time data for the detection of DNA with HMGB1 receptors on the same SiNW bioFET device for different concentrations of DNA. Each DNA delivery is followed by 1 M NaCl buffer to accelerate the desorption of bound DNAs from the surface. (b) ΔV_T as a function of DNA concentration. The dissociation constant K_D for DNA-HMGB1 ligand-receptor pair is determined by the authors as 105 ± 6 nM.

the shift in the threshold voltage significantly increases with decreasing ionic concentration. 20-fold increase in the threshold voltage is obtained when the ions in the solution is diluted to 1mM from 70mM concentration, which is the ionic concentration of bovine serum [Okada et al., 1990]. Note that physiological conditions for human body generally imply ionic concentrations higher than 100mM [Rajan et al., 2013].

Third analysis is performed for varying concentration of surface receptors. As is seen from Fig. 7.8c, deploying receptor molecules more densely on the surface of the semiconductor channel, increases the receiver response almost linearly. However, size restrictions and possible correlations among densely deployed receptors, which are not captured by this model, should be accounted for in a real world implementation.

Lastly, we analyze the effect of oxide layer thickness t_{ox}, which is the main determinant of the oxide capacitance C_{ox}, on the receiver response. Fig. 7.8d demonstrates the results for conventional values of t_{ox}. As can be inferred, higher t_{ox} implies a

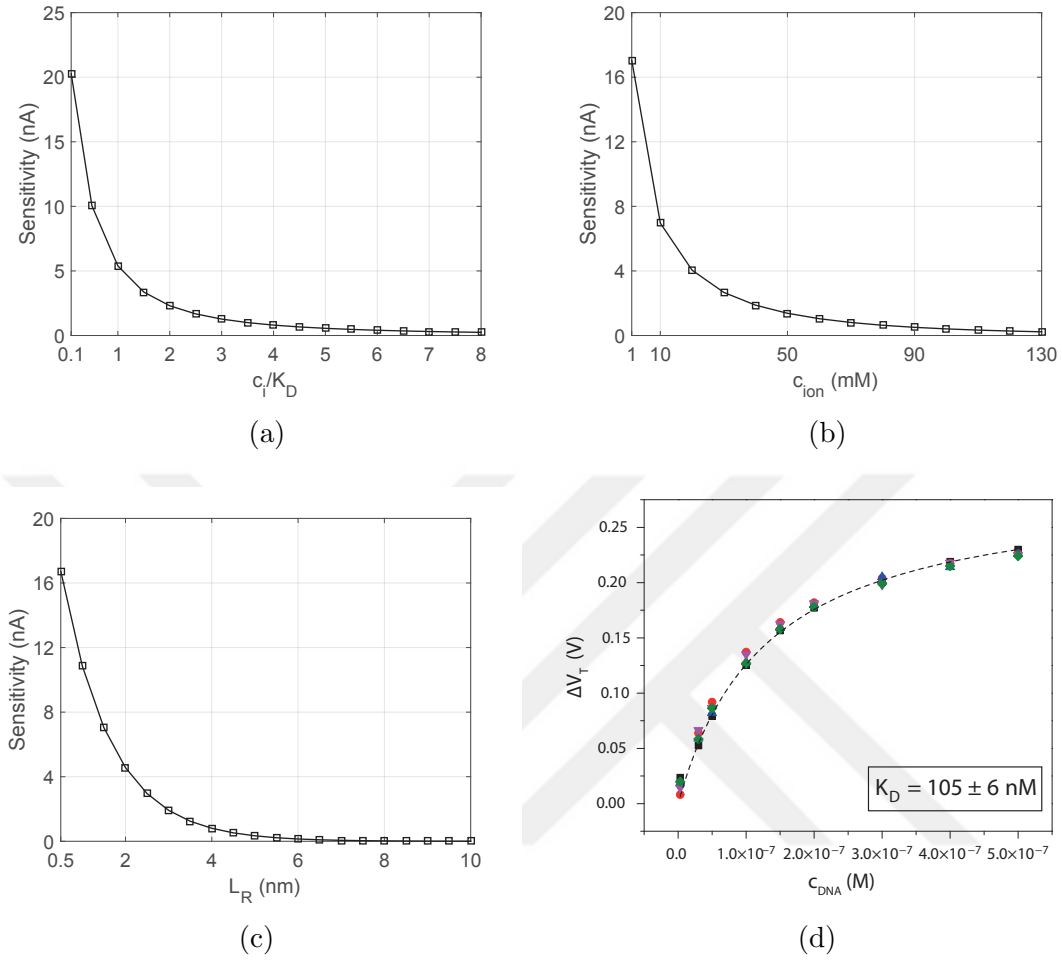


Figure 7.10: Receiver sensitivity with input concentration c_i normalized by K_D. Sensitivity with (a) varying concentration c_i of information-carrying ligands, (b) varying ionic concentration c_{ion}, (c) varying receptor length L_R, and (d) varying oxide layer thickness t_{ox}.

better receiver performance.

The response of a typical SiNW bioFET, which is the base of the developed receiver model, to the varying ligand concentration can also be observed from the experimental results presented in Fig. 7.9. These results have been acquired from [Duan et al., 2012], where the authors employed a SiNW bioFET to quantify the affinity of DNA sequences with HMGB1 proteins in terms of their dissociation constant K_D. HMBG1 proteins of an unspecified concentration were deployed on the SiNW surface, and

varying concentration of DNAs as the charged ligands at pH 7.4 were introduced into the reception space of the bioFET through a microfluidic system. The association on the surface through the ligand-receptor binding dynamics as the DNAs were supplied at a constant rate with different concentrations, and the dissociation after the steady-state was reached, can be observed from Fig. 7.9a. The binding dynamics of DNA and HMGB1 were confirmed to be reaction-limited; thus, it does not violate the well-mixed assumption made for the analytical model of biorecognition layer. Unfortunately, many of the critical system parameters, such as the concentration of the surface receptors, the average ligand charge, the average receptor length, each of which substantially affects the device response, were not provided in that study. Thus, we are not able to make a one-to-one comparison of the response given in Fig. 7.9b with the numerical results obtained using the model provided in this paper. Nevertheless, the experimental results clearly show the same saturation trend observed for the device response and very well fall into the range of the numerical results obtained in our analysis.

7.6.4 Sensitivity Analysis

Sensitivity is one of the key metrics that can reveal the performance of the proposed MC receiver. It gives the responsivity of the receiver to the varying concentration of ligands; thus, it determines how successful the receiver is in discriminating the different messages encoded into different levels of ligand concentration. The sensitivity of the receiver can be found by taking the derivative of (9.11) with respect to the input concentration c_i:

$$S(c_i) = \frac{K_D N_e q_{eff} g_m}{(K_D + c_i)^2 C_{mol,L} C_{eq,i}^2 C_{p,i}^2} (N_R C_{mol,L} C_{eq,i} C_{p,i}^2 - 1), \tag{7.20}$$

where $C_{p,i} = C_{rec}^{-1} + C_{layer,i}^{-1} + (C_{dl} W L)^{-1}$. Note that $C_{eq,i}$ and $C_{p,i}$ are functions of input concentration c_i.

Fig. 8.13 demonstrates the receiver sensitivity with the input concentration nor-

malized by the dissociation constant K_D, such that the normalized sensitivity in the results correspond to the amount of increase in the output current due to a unit increase in the normalized concentration c_i/K_D at a given system setting. As can be inferred from the results in Fig. 7.10a, the sensitivity substantially decreases as the concentration level in the reception space increases. This is because the receptors on the biorecognition layer are saturated at higher ligand concentrations, thus become insensitive to the changes in the input. The results presented in Fig. 7.10b and Fig. 7.10c reveal the effect of Debye screening, which is mathematically given by (9.9), such that the sensitivity decreases with increasing ion concentration in the medium and with the increasing length of receptors. Since it is not always possible to control the ionic concentration of the medium, it is critical to employ surface receptors with lengths smaller than the Debye length to obtain a highly sensitive receiver antenna. Physiological conditions generally imply ionic concentrations higher than $100 mol/m^3$, which decrease the Debye length below $1nm$. As discussed in Section 7.5.2, aptamers and natural receptors with smaller sizes are advantageous compared to antibodies to be employed as receptors in *in vivo* applications. The last sensitivity analysis in Fig. 7.10d demonstrates that the thickness of the oxide layer t_{ox} has also a significant effect on the sensitivity. As t_{ox} increases, the oxide capacitance C_{ox} decreases, which directly reduces the channel transconductance g_m as given in (8.35). Fortunately, control over the oxide layer thickness is possible, and t_{ox} values lower than $5nm$ are reported in the literature [Kobayashi et al., 1998].

7.6.5 SNR Analysis

The receptor noise, which is the fluctuations in the number of bound receptors at steady-state, is reflected to the threshold voltage fluctuations by the relation $S_{\Delta V_{TH}^B}(f) = S_{\Delta N_B}(f) V_m^2$, where $V_m = (N_e q_{eff})/C_{eq,i}$ is the mean deviation in the threshold voltage resulting from the binding of a single ligand. The receptor and thermal noise can be assumed uncorrelated, since they are largely separated in the frequency domain [Georgakopoulou et al., 2015]. Therefore, including the additive

$1/f$ noise, the overall PSD of the threshold voltage-referred noise can be given by [Kuscu and Akan, 2015]

$$S_{\Delta V_{TH}}(f) = S_{\Delta V_{TH}^{B}}(f) + S_{\Delta V_{TH}^{T}}(f) + S_{\Delta V_{TH}^{F}}(f). \tag{7.21}$$

The additive noise effective on the threshold voltage is reflected to channel current noise via $S_{\Delta I_{DS}}(f) = S_{\Delta V_G}(f) g_m^2$. Assuming a resistance of 1Ω for the channel, we formulate the receiver SNR as follows

$$SNR = \frac{I_{DS}^2}{\int_{-\infty}^{\infty} S_{\Delta I_{DS}}(f) df}. \tag{7.22}$$

Using (8.43), we investigate the effect of different system parameters on the SNR of the receiver's electrical output. SNR for varying ligand concentration corresponding to different symbols is plotted in Fig. 7.11a, which clearly shows that SNR is significantly improved with increasing concentration. However, it begins to saturate at around 25dB due to the saturation of the surface receptors for high ligand concentrations. The effect of ionic strength of the fluidic medium on the output SNR is given in Fig. 7.11b. When the ionic concentration increases above 100mol/m^3, the Debye length decreases below 1nm resulting in substantial screening of ligand charge. Therefore, SNR significantly decreases with increasing ionic strength. Physiological conditions imply ionic concentrations higher than 100mol/m^3. To compensate the attenuation of SNR, receptors with lengths comparable to Debye length should be selected. We also investigate the effect of receptor length on the SNR when the ionic strength is 70mM which makes the Debye length equal to 1.15nm. As seen in Fig. 7.11c, SNR in dB decreases linearly as the receptor length increases. Lastly, we analyze the SNR for varying trap density which is inversely proportional to the purity of the transducer channel. Trap density increases the $1/f$ noise, which is very effective in the frequency range of the antenna's operation. As is shown in Fig. 7.11d, the effect of trap density on the $1/f$ noise, and thus, on the SNR, is evident especially for $N_t > 10^{24}\text{eV}^{-1}\text{m}^{-3}$. Fortunately, experimentally reported trap densities for SiNW bioFETs are on the

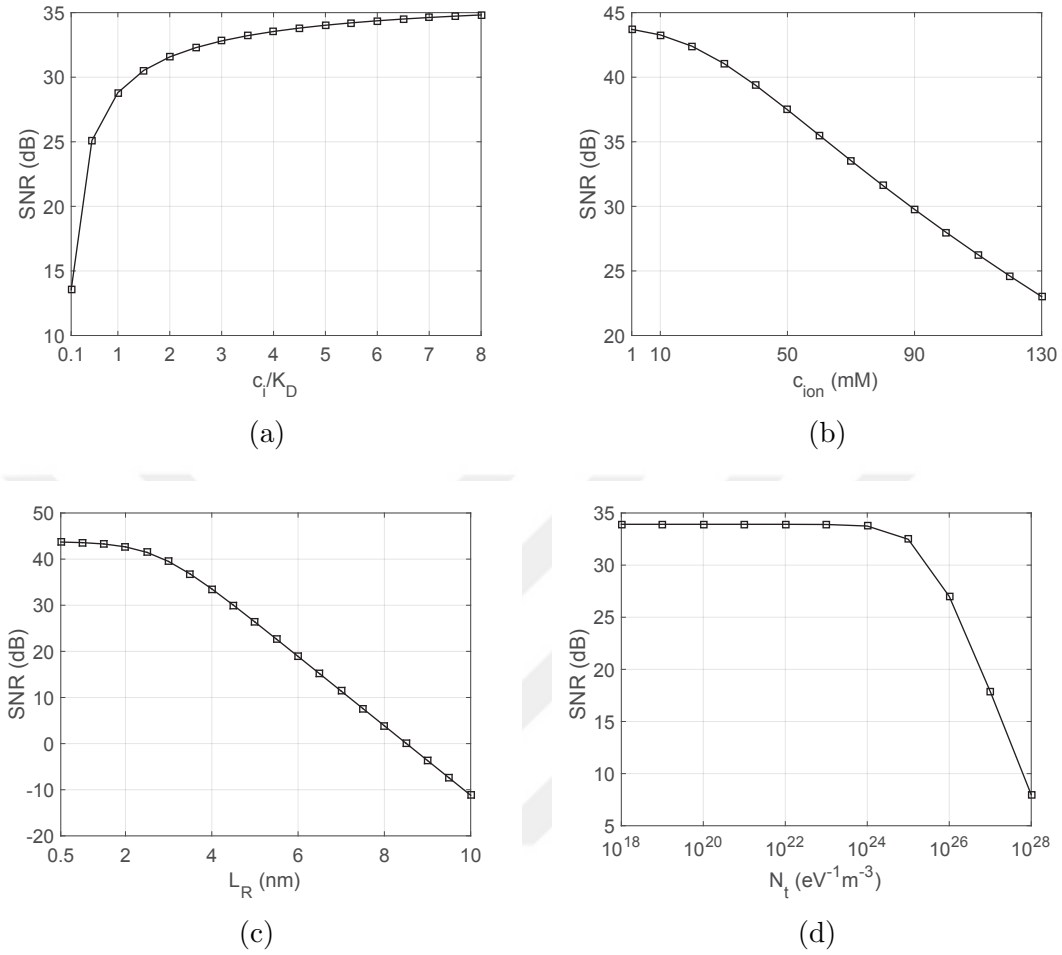


Figure 7.11: SNR as a function of (a) ligand concentration c_i, (b) ionic concentration c_{ion}, (c) receptor length L_R, and (d) trap density N_t.

order of $10^{22}\text{eV}^{-1}\text{m}^{-3}$ [Rajan et al., 2011].

7.7 Advanced Design Issues

7.7.1 Molecular Division Multiple Access (MDMA) and MoSK

Use of different types of molecules brings up several opportunities to increase the functionality and improve the performance of MC. MoSK where messages are encoded into the type of molecules is one of the two robust modulation techniques envisioned for MC applications [Kuran et al., 2011]. Combining MoSK scheme with CSK, i.e., repre-

senting messages by both molecular concentration and type, multiplies the alphabet size, thus, can boost the communication rate. Moreover, employing various types of molecules for encoding can enable a particular code division multi-access scheme which is termed Molecular Division Multiple Access (MDMA) [Giné and Akyildiz, 2009].

All of these modulation and multiple access schemes require for different messages to be discriminated by the receiver. The receiver architecture based on bioFETs can be adapted to each of these schemes through one of the following modifications:

- Employing multiple antennas with different types of receptors each corresponding to a different type of ligand as shown in Fig. 7.12(a), receiver can separately process the electrical outputs of different antennas, and thus, can easily decode different messages. Therefore, this architecture does not require a complex signal processing for detection; however, it implies a larger area of deployment, and more energy consumption which multiplies with the number of antennas.

- Employing a single antenna is convenient if a significant diversity exists among the efficient charges, i.e., $N_e q_{eff}$, for different types of molecules. The receptors can be of the same type if the ligands have similar affinity to the same receptor; otherwise, for each of the ligand type, different receptors should be deployed on the recognition layer as shown in Fig. 7.12(b). It is clear that employing a single antenna is more energy-efficient and space-saving compared to the other architecture. However, for the case of MDMA where different signals received at the same time are superposed at the output, this architecture requires more complex signal processing on the electrical signal to discriminate the contributions of different messages [Horesh et al., 2011].

In Fig. 7.13, we demonstrate the results of the experiment conducted in [Zheng et al., 2005] for multiplexed detection of cancer biomarkers with SiNW bioFETs. As shown in Fig. 7.13a, three bioFETs are constructed in parallel on a common substrate, and each SiNW channel is functionalized with different bioreceptors that have affinities

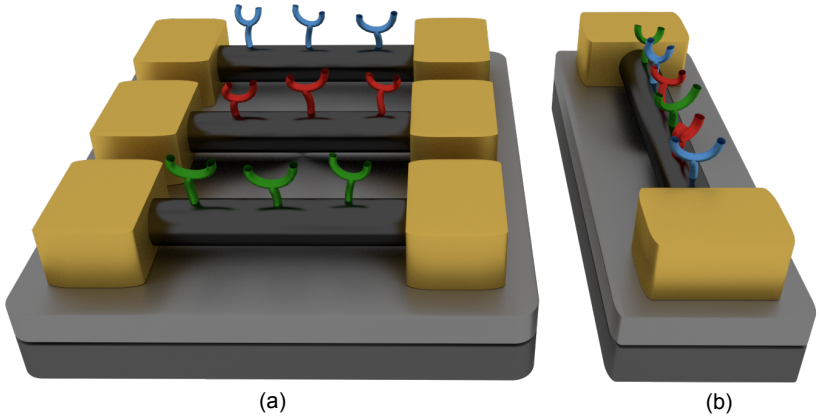
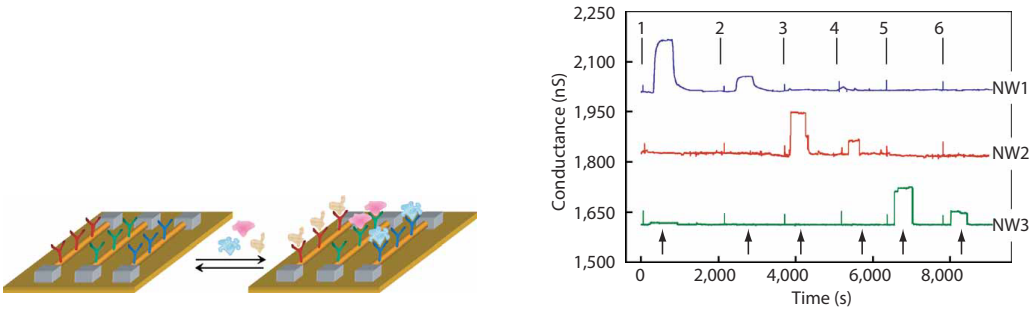


Figure 7.12: Receiver antennas for MDMA and MoSK schemes.

to specific ligands, i.e., biomarkers. The study reports negligible interference among the bioFETs in the array, as is clear from the conductance measurements shown in Fig. 7.13b, justifying the feasibility of MDMA schemes for MC with bioFET-based receivers.

7.7.2 Diversity Combining

The size of nanomachines could be significantly larger compared to a single receiver or transmitter antenna, and they are generally envisioned as motile undergoing both translational and rotational motion, which means that the distance between the transmitter and the receiver antennas of communicating nanomachines may alter notably during the operation. The distance between transmitter and receiver antennas has strong effect on the attenuation of molecular signals [Pierobon and Akyildiz, 2013]. Hence, employing multiple receiver antennas with spatial diversity on a single nanomachine can lead to important diversity gains and reductions of the transmission delays. Several diversity combining schemes like selective combining, maximum ratio combining are applicable for the electrical receiver [Meng et al., 2012].



(a) (b)

Figure 7.13: (a) Multiplexed detection of cancer biomarkers with three SiNW bioFETs constructed on a common substrate [Zheng et al., 2005]. Each bioFET is functionalized with distinct monoclonal antibody receptors (**NW1** with PSA antibody, **NW2** with CEA antibody, **NW3** with mucin-1 antibody) specific to the three different biomarkers (PSA, CEA, mucin-1). (b) Conductance measurements for the simultaneous detection of biomarkers which are sequentially delivered to the array as follows: (1) 0.9 ng/ml PSA, (2) 1.4 pg/ml PSA, (3) 0.2 ng/ml CEA, (4) 2 pg/ml CEA, (5) 0.5 ng/ml mucin-1, (6) 5 pg/ml mucin-1. The biomarker solutions are followed by buffer solutions which are delivered at the time points indicated by black arrows.

7.7.3 Energy Efficiency Schemes

Nanomachines are envisioned to have limited power; thus, energy consumption of the receiver should be minimized. This objective can be realized by optimizing the hardware, or employing energy-efficient scheduling algorithms. Since the receiver is electrically powered, a nanomachine has the control on its operation times and sampling periods. Therefore, most of the conventional energy-efficient schemes in the literature can also be incorporated to the molecular receiver [Akyildiz et al., 2002]. However, power saving modes of receiver's operation like sleep, idle, standby, and active modes, need to be defined in the context of the nanocommunications application.

7.7.4 Tunable Kinetics

The voltage applied to the solution gate, i.e., the reference electrode, creates, to some extent, an electrical field between the transducer channel and the reference electrode. This electrical field is shown to induce electrophoretic forces on the charged ligands in the reception space and manipulate their motion in perpendicular to the recognition layer [Jayant et al., 2013]. It has been speculated that this effect can be exploited to attract or repel the ligands from the recognition layer, thus, to increase or decrease their probability of binding to the receptors depending on the magnitude and polarity of the applied electrical field [Rajan et al., 2013, Jayant et al., 2013]. From the receiver perspective, this phenomenon can be used to increase the power of the received signal by applying an attracting electric field in the reception space when very low concentrations of ligands are expected to be received. Moreover, if the receptors become saturated as a result of high-concentration signals, then the receiver can periodically use a repelling electric field to decrease the binding rates of the molecules. This adaptive scheme with tunable binding kinetics clearly brings important functionalities to the receiver; however, the application of electrophoresis to the binding kinetics is quite new concept, and analytical models that fully capture its effects on the binding rates are still missing.

7.7.5 EM-Molecular Hybrid Operation

Graphene and CNT, with extraordinary electromagnetic (EM) properties, have also proven to be promising candidates for the design of transceiver antennas in nanoscale EM communications, especially in THz [Jornet and Akyildiz, 2013] and optical frequencies [Gulbahar and Akan, 2012]. Designing the MC receiver with graphene or CNT-based transducer channels can allow a hybrid receiver architecture that can operate both in MC and EM nanocommunications. This hybrid design could bring up novel applications for both nanocommunication paradigms. For example, the hybrid receiver can act as a nanoscale gateway that connects an *in vivo* molecular nanonetwork to an external macroscale network, e.g., Internet, through an EM-based

communication channel to enable Internet of Nano Things (IoNT) [Akyildiz and Jornet, 2010b, Akyildiz et al., 2015, Kuscu and Akan, 2016a]. In a similar manner, two distant molecular nanonetwork can be connected with an EM link. To design a hybrid receiver, additional challenges should be addressed. For example if the intention is to design a single hybrid receiver antenna, the effect of biofunctionalization on the electromagnetic characteristics of the transducer channel should be analyzed.

7.8 Challenges

There are unique challenges of making the proposed architecture operational for MC. In this section, we discuss the most important ones together with possible solution approaches.

7.8.1 Fabrication Challenges

Nanoscale semiconductors, such as graphene, CNT and SiNW, which constitute the transducer channel of the proposed bioFET-based MC receiver, can be fabricated following any of the two fundamental approaches: bottop-up or top-down [Lu et al., 2013]. Bottom-up techniques are mostly based on the production, i.e., synthesis, of semiconductors through chemical vapor deposition (CVD). Top-down approaches, on the other hand, are generally based on lithographic fabrication methods. Both approaches impose unique challenges to the proper fabrication of semiconductors. Although top-down methods are more costly compared to bottom-up synthesis, they provide more advanced control enabling mass production and compatibility with CMOS fabrication technologies promising for large-scale integration. However, top-down methods are known to be more amenable to producing defects and traps on channel surface, leading to higher level of $1/f$ noise [Rajan, 2013]. On the other hand, bottom-up methods mostly rely on stochastic processes and do not allow an entire control over fabrication, leading to reproducibility problems, which is the main challenge to produce bioFETs with homogeneous characteristics.

Immobilization of bioreceptors on the semiconductor channel can be realized through

covalent or non-covalent binding, depending on the type of semiconductor and receptor molecules [Lu et al., 2013]. Surface binding of receptors is a random process, and it is not possible with the current state-of-the-art technologies to exactly control the number of immobilized receptors and their orientation on the surface. This implies another reproducibility problem that should be accounted for while implementing a bioFET-based receiver.

The effect of imperfect fabrication and the inevitable randomness in main system parameters, such as the concentration of surface receptors and the net charge of ligands, could be reflected as noise processes into an analytical model that would be derived based on the deterministic model provided in this paper.

7.8.2 Scaling and Integration Challenges

As discussed in Section 7.2, one of the main design requirements for the MC receiver is to consist of nanoscale components so that it could be integrated into a nanomachine, e.g., a medical nanorobot. Although nanotechnology has not yet enabled the implementation of fully functional nanomachines with integrated processing, energy harvesting, memory, and communication units, we should consider the challenges to reduce the size of bioFET-based receivers to nanoscale and integrate them into envisioned nanomachines.

Main functional units of the bioFET-based MC receiver, which are the biorecognition layer and the semiconductor channel, are already made of nanoscale materials; and thus, they do not pose a problem for scaling of the receiver. The major components that set the limitation for the receiver size are the source and drain contacts together with the reference electrode which is generally used for the aim of stabilizing the surface potential for improved detection performance [Rajan, 2013].

It is an ongoing challenge to miniaturize the reference electrode by keeping its stable operation. For the aim of integrating bioFETs to small scale on-chip devices, pseudo reference electrodes has been introduced with smaller sizes compared to a true reference electrode. However, they compromise voltage stability to some extent,

and need to be further scaled down to work on a nanoscale device [Rajan, 2013]. Recently, a promising approach has been proposed to completely remove the need for a reference electrode [Jain et al., 2012]. Combining the piezoelectric effect with the bioFET concept, the authors came up with a novel architecture named Flexure-FET which achieves to detect molecular concentration with high sensitivity, even by not requiring for ligands to be charged [Jain and Alam, 2014].

Another size limitation arises from the planar design of metal contacts on substrate. To overcome this for SiNW bioFETs, [Tian et al., 2010] has proposed a kinked design, in which the channel and the source/drain contacts are placed on the same SiNW. The source and drain contacts are defined over the arms on either side of the kink by heavy n^{++}-type doping. This design approach removes the need for implementing additional metallic contacts nearby the sensing unit; thus, it may be a promising solution for integrating the envisioned bioFET receivers with the other components of the nanomachines.

Apart from these attempts focusing on the miniaturization of individual components, there is a continuing trend towards the integration of biosensors with the CMOS technology, which have already yielded SiNW bioFETs fabricated through CMOS compatible processes [Gao et al., 2011]. Hand in hand with the relentless efforts towards the miniaturization of CMOS technology to sub-10nm regime, we can expect nanoscale machines having a high computational capacity with CMOS integrated bioFET-based MC receivers to be employed in nanonetwork applications of near future.

7.8.3 Application Challenges

A major challenge arises when the receiver is employed in an *in vivo* application. The physiological conditions imply solutions with high ionic concentrations, abundance of interferers and contaminants, and existence of disruptive flows and fluctuating temperature, which may degrade the receiver's performance in several aspects. First, high ionic concentration, which is $\sim$100mM for physiological conditions, creates a

strong screening effect reducing the Debye length to ∼1nm, and thus, impedes the sensitivity of the receiver [Rajan et al., 2013]. Moreover, interferers that have affinities for the receptors could create strong background noise; and contaminants and disruptive flows may alter the binding kinetics, impede the stability of the receptors, even separate them from the dielectric layer. The disruptive flows may also strongly fluctuate the concentration of the ligands in the reception space.

Even though using highly charged ligands and very small size receptors like aptamers can solve the screening problem in theory, recently proposed frequency domain techniques promise for much more realistic solutions. In [Zheng et al., 2010], the authors have shown that the power spectrum of binding events is Lorentzian-shaped, and easy to distinguish from the $1/f$ noise in frequency domain, because of the weakening of $1/f$ noise at high frequencies. They reveal that frequency domain detection outperforms the conventional time domain technique in terms of sensitivity in highly ionic solutions. The second method proposed in [Kulkarni and Zhong, 2012] is based on applying a high-frequency alternating current between the source and the drain electrodes, instead of a DC current, to weaken the double layer capacitance generated by the solution ions. They show that the effective charges of the ligands become inversely dependent on the Debye length instead of the exponential dependence. As a result, the screening effect on the bound ligands is significantly reduced, and the FET-based biosensing becomes feasible even for physiological conditions.

7.9 Future Research Avenues

Progress in biosensor research has been mostly based on empirical studies. Therefore, the proposed designs generally lack the complementary analytical models that mathematically represent the operation incorporating the effects of the system parameters on the performance. This leads to a problem for reproducibility of experimental results, and thus, to a plethora of studies that are not consistent with each other [Matsumoto and Miyahara, 2013].

There are only a few attempts to analytically model a biosensor, most of which

are cited in this paper [Hassibi et al., 2007, Rajan et al., 2013, Rajan et al., 2014] [Kuscu and Akan, 2015]. However, these works together with our model assume that the ligands to be detected are in equilibrium with the receptors at the time of detection. This is an acceptable assumption in the context of biosensors, because they are usually envisioned to be operated in laboratory conditions as being immersed in pre-prepared solutions with long incubation times. However, for the case of communications, considering the continuous and *in situ* operation of the envisioned nanonetwork applications, this assumption could be violated when the bandwidth of the incoming signal is comparably high or the diffusion effects cannot be neglected. Therefore, the first research avenue should be development of comprehensive analytical models both for time and frequency domains that capture the transient dynamics without the dynamic equilibrium assumption, the effects of environmental conditions, also the mobility of the nanomachines. This requires a careful incorporation of the molecular transport dynamics into the recognition and transduction characteristics of the receiver. The model should be able to provide closed-form analytical expressions for the main performance metrics, e.g., sensitivity, SNR, LoD, in terms of system parameters including receiver geometry and molecule types used in the channel and recognition layer.

The analytical models that will be developed in the first phase can be incorporated into simulation frameworks for the optimization of the models under different communication scenarios and for the design of optimal detection schemes and communication protocols. There are a few attempts towards establishing realistic simulation frameworks for diffusion-based MC and bioFETs. The current MC simulators are designed based on widely used network simulator NS-3, and they are mainly focused on the communication channels and network architectures [Gul et al., 2010, Llatser et al., 2014]. The models used in the simulators assume ideal MC receivers with perfect sampling of the molecular concentration in the reception space. On the other hand, bioFET simulators are web-based and developed mainly for the purpose of proper evaluation and classification of the experimental results [Hediger et al., 2012]

[Heitzinger et al., 2008]. These frameworks lack underlying analytical models, thus, are not able to provide required design and optimization tools. At this point, a simulation framework for bioFET-based MC receivers needs to be developed using the analytical models; and then, the framework should be combined with the MC simulators, which are continuously being improved, to provide a realistic simulation environment for end-to-end molecular communications.

Analytical models and simulation frameworks should be accompanied by experimental validations. This requires the development of receiver prototypes based on bioFET architectures optimized for communication purposes. Microfluidics provides an invaluable platform to transport molecules in a controlled fashion. It has proven feasible for conducting MC experiments with controllable system parameters [Bicen and Akyildiz, 2013], which makes microfluidics a promising means of further optimizing the MC receiver prototypes in real communication scenarios. Following experimental validations, receiver antenna should be integrated with nanoscale processors which have the capability of performing the optimal detection with the processing rates sufficient for the envisioned MC applications.

7.10 Conclusion

In this chapter, physical design of a molecular receiver is elaborated for the first time in the literature. Detection of messages in a molecular communication system mandates the label-free and *in situ* sensing of molecules. A comprehensive review of the state-of-the-art biosensing methods reveal that the basic requirements of a molecular receiver can be met only with a design in nanobioelectronic domain. FET-based biosensing mechanism is particularly favoured as the underlying mechanism of a nanobioelectronic molecular receiver due to the fast, reversible and simple operation with a plethora of engineering options. We conceptually present the main operation principles of a FET-based molecular receiver together with the performance metrics and design parameters. We provide a deterministic model for a SiNW FET-based MC receiver, and evaluate the reception performance in terms of sensitivity. These

preliminary results demonstrating the reliable reception of molecular messages are encouraging for the further development of MC receiver in nanobioelectronic domain. We address the practical challenges with possible solution approaches. Future research avenues include the derivation of an improved analytical model for the receiver operation comprising the transient kinetics of molecular binding and transportation dynamics, optimization of the receiver performance for the envisioned applications through simulations and experiments, development of optimal detection schemes, and the integration of the receiver into a nanomachine.

Chapter 8

MODELING AND ANALYSIS OF SINW FET-BASED MOLECULAR COMMUNICATION RECEIVER

8.1 Introduction

Molecular communication (MC) defines the technology where molecules are used to encode, transmit, and receive information. MC is a biocompatible communication method providing efficient and reliable information transfer between living entities at nanoscale. Hence, it has been regarded as the most promising paradigm to realize nanonetworks by enabling the communication among nanoscale devices, i.e., nanomachines [Akan et al., 2017], [Kuscu et al., 2015].

MC paradigm has been extensively studied from various aspects. A large body of work has been devoted to modeling the MC channel from information theoretical perspective [Pierobon and Akyildiz, 2013] [Atakan and Akan, 2008], designing modulation schemes [Kuran et al., 2011] and developing communication protocols [Nakano et al., 2014] and optimal detection algorithms compatible with MC [Kilinc and Akan, 2013]. While adapting the tools of conventional communication techniques to MC, these studies have mostly ignored the physical design of system components such as transmitter and receiver. Besides these contributions, there are only a few studies focusing on the physical design of communicating units. For example, in [Unluturk et al., 2015], the authors propose a biotransceiver architecture which can realize transmitting, receiving and basic processing operations based on the functionalities of genetically engineered bacteria. Similarly, a layered architecture for MC based on functionalities that can be acquired from bio-nanomachines, such as molecular motors, is presented in [Nakano et al., 2014]. Furthermore, numerous studies

have investigated MC-based networks of bacteria colonies [Balasubramaniam et al., 2014], [Petrov et al., 2015]. Common to these studies is the assumption that the MC nanonetwork consists of nanomachines, which are entirely made up of biological components.

Although designing nanomachines with only biological components provides the advantage of biocompatibility, which is crucial for biomedical applications, it has also numerous disadvantages that restrict the application domain of nanonetworks. First of all, very low computational capacities of biological devices, which are evident from [Unluturk et al., 2015], limit the speed of information processing, and thus, the extent of the tasks that these nanomachines can undertake in a nanonetwork application. This limitation points out a major discrepancy between the envisaged applications of nanonetworks [Akan et al., 2017], most of which require the implementation of complex communication protocols and algorithms, and the very limited processing capabilities of the biological devices. Another critical drawback of the entirely biological device architectures is that they are operational only in *in vivo* applications, i.e., applications within living organisms like human body. Moreover, they do not allow the incorporation of a noninvasive and seamless interface between molecular nanonetworks and macroscale cyber networks such as the Internet. This is one of the key challenges to realization of Internet of nanothings (IoNT), which is a visionary concept that promises for ground-breaking medical and environmental applications [Akyildiz et al., 2015], [Kuscu and Akan, 2016a]. Furthermore, the current state-of-the-art of synthetic biology research is not advanced enough to take the full control over the functionalities of living cells to design engineered cells that can operate in one of the envisioned nanonetwork applications [Church et al., 2014].

The discrepancies and the challenges pertaining to the entirely biological architectures have led us to consider different design solutions. In our recent review of design options [Kuscu and Akan, 2016c], interfacing the biochemical environment, where molecular messages propagate, with a nanobioelectronic architecture, that can provide fast information processing and wireless interface with macroscale networks

has been revealed to be the most promising and feasible solution. This nanobioelectronic design approach implies transmitters that can release molecular messages upon being triggered by electrical signals, and receivers that can detect molecular messages and transduce them into electrical signals for further processing.

In [Kuscu and Akan, 2016c], for implementing a nanobioelectronic MC receiver, we have proposed the use of FET-based biosensors, i.e., bioFETs, optimized from MC theoretical perspective. BioFETs have emerged as promising analytical tools, which enable the label-free electrical sensing of target molecules [Poghossian and Schöning, 2014]. We have shown that they satisfy the basic requirements of an MC receiver such as the capability of precise, continuous and noninvasive detection of molecular concentrations. Use of novel nanomaterials, such as nanowires, carbon nanotube (CNT) and graphene, has enabled them to be designed with nanoscale dimensions [Schöning and Poghossian, 2002], [Curreli et al., 2008]. Transduction of biochemical concentrations into electrical signals in bioFETs could provide a fast in-device information processing for the MC receiver. It could also enable the design of a seamless interface between the nanobioelectronic receiver and macroscale networks by means of electromagnetic signals.

Towards the goal of optimizing bioFETs as MC receivers, one of the major challenges pointed out in [Kuscu and Akan, 2016c] is the lack of a comprehensive analytical model for bioFETs. Although there are a vast number of experimental works reported for bioFETs and a few theoretical studies focusing on the noise processes effective on their operation [Deen et al., 2006], [Rajan et al., 2013], none of them is able to entirely capture the physical processes in stochastic sensing of molecular concentrations.

In [Kuscu and Akan, 2015], we introduced deterministic and noise models for SiNW FET-based MC receiver antenna, and derived the SNR at the antenna output by neglecting the effects of the ligand transport dynamics. In this study, we revisit and extend this model by accounting for the effects of the MC channel on the receiver operation. The resultant unified model capturing all of the stochastic processes regarding the MC and biosensing enables the derivation of closed-form expressions for

the decision statistics at the electrical end of the receiver, and thus, provides a complete analytical framework for the performance analysis and design optimization of bioFETs as MC receivers. The major contributions of this study can be explained as follows:

- We present a comprehensive model of SiNW bioFETs by integrating the contributions of all the noise processes affecting the electrical output of the devices. As such, the model also contributes to the nanobiosensor literature.

- Based on the recent findings in biophysics literature, we incorporate the spatial and temporal correlation effects resulting from finite-rate diffusion into the stochastic ligand-receptor binding process, and obtain the statistics of the diffusion-influenced binding noise at the receiver side. This development leads to a combined channel and receiver noise model, which can be applicable for MC systems with various receiver architectures, including the entirely biological ones, and channel geometries. The current studies in MC investigates the reception problem only in diffusion-limited or reaction-limited regime. Up to now, a vast majority of MC studies focus on the diffusion-limited regime by assuming that the receiver with infinite reaction rates could perfectly count the number of molecules in an arbitrarily defined reception space [Pierobon and Akyildiz, 2013, Meng et al., 2014, Noel et al., 2014b]. There are also a few studies, such as [Pierobon and Akyildiz, 2011, ShahMohammadian et al., 2013], that focus on the reaction-limited case and derive the statistics of ligand-receptor binding process, which is Markovian in this regime. However, both approaches neglect the extended correlations in the reception process resulting from the finite transport and reaction rates. There is another modeling approach based on reaction-diffusion master equation (RDME), which divides the channel into discrete voxels and provides a combined channel-receiver model by taking the propagation and ligand-receptor binding process as a continuous-time Markov process (CTMP) [Chou, 2013, Chou, 2015]. Although the derived model is

more comprehensive in its approach to small-scale systems (limited in size and number of information molecules), it does not allow the derivation of closed-form expressions for the statistics of transport-influenced reception noise. The unified noise model developed in this paper overcomes this limitation with a steady-state assumption in the received concentration signal.

- We provide the first unified channel and receiver model by incorporating the SiNW bioFET into an MC system as a receiver. The use of electronic chemical sensors, similar to bioFETs, for MC receiver has been previously addressed in [Farsad et al., 2013]. In that study, the authors have designed an experimental testbed for MC with macroscale dimensions and use a metal oxide semiconductor sensor for detecting chemical messages encoded into isopropyl alcohol. Based on the experimental data obtained using the testbed, they developed a combined channel and receiver model [Kim et al., 2015]. Although similar trends are observed in receiver detection performance, the analytical framework developed in this study is based on a more comprehensive and unified approach, thus, better suited for the purpose of optimizing biosensors from MC theoretical perspective.

- We obtain closed-form expressions for the deterministic response of the receiver, the statistics of the noise processes and the SNR at the receiver output. We also investigate an MC system that utilizes M-ary Concentration Shift Keying (M-CSK) [Kuran et al., 2011] for modulation at the transmitter side and Maximum Likelihood (ML) method for detection at the receiver side, and derive an analytical expression for the corresponding SEP.

- Evaluating the receiver in terms of SNR and SEP, we reveal the effects of individual system parameters on the detection performance. The obtained results underline the feasible optimization pathways that can be targeted to improve the receiver.

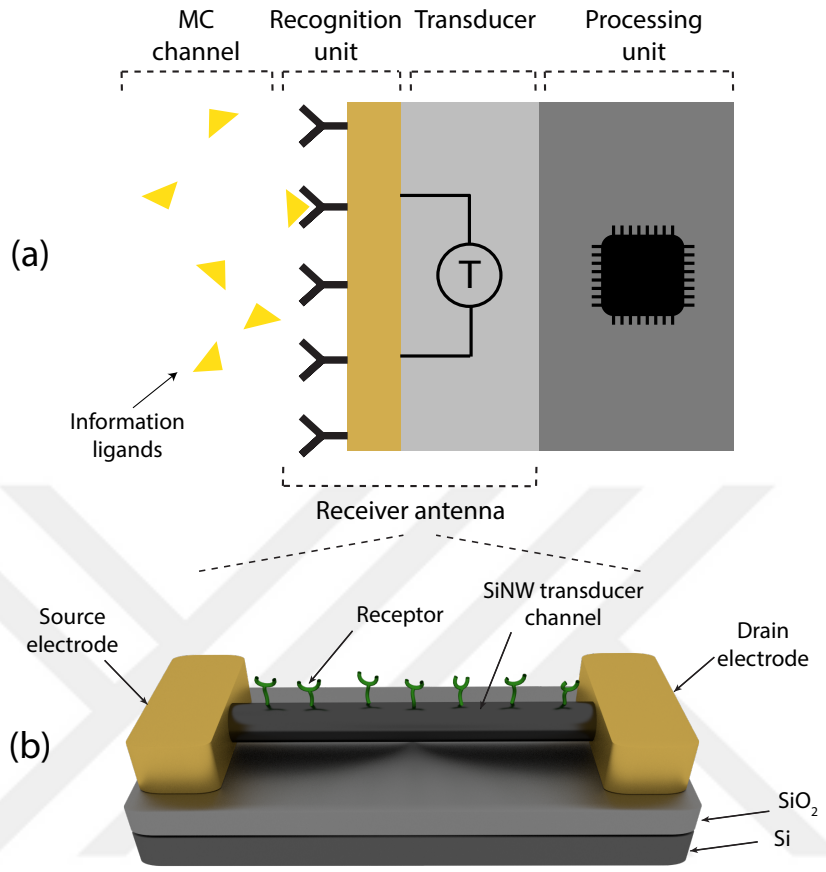


Figure 8.1: (a) Functional units of an MC receiver, and (b) SiNW FET-based MC receiver antenna. Insulating SiO_2 layer entirely covering the SiNW is not shown in (b) for better visualization of the transducer.

The remainder of the paper is organized as follows. In Section II, we describe bioFETs and explain their operation principles. We develop the model of SiNW FET-based MC receivers in Section III. In Section IV, we derive the SEP for an MC system that employs the nanobioelectronic receiver and utilizes M-CSK scheme for modulation. The performance evaluation results are presented in Section V. Finally, the concluding remarks are given in Section VI.

8.2 Principles of BioFETs

Operation principles of bioFET, which is the basis of the nanobioelectronic MC receiver architecture, are similar to the ones of the conventional FETs. In conventional FET type transistors, current flows from the source electrode to the drain electrode through a semiconductor channel, conductance of which is controlled by the electric field created by the potential applied on the gate electrode. Conductivity is proportional to the density of the carriers accumulated in the channel, and the variations of the electric field resulting from the additional surface potential is reflected to the changes in the voltage-current characteristics between the drain and the source electrodes.

BioFETs slightly differ from the conventional FETs by including an additional biorecognition layer that is capable of selectively binding the target molecules [Poghossian and Schöning, 2014]. This layer is composed of a high number of receptor molecules tethered on the surface of the FET channel, and replaces the gate electrode of conventional FETs, as shown in Fig. 8.1. Binding of ligands to the surface receptors results in accumulation or depletion of the carriers in the semiconductor channel due to the field effect generated by the intrinsic charges of the bound ligands. Hence, the ligand binding modulates the channel conductance and current, and thus, the output current becomes a function of the ligand density and the amount of ligand charges. Label-free, continuous and in situ sensing of the molecules by not requiring any complicated processes such as the use of macroscale equipments for readout and processing operations makes bioFETs a natural candidate for the architecture of MC receivers.

Several ligand-receptor pairs, e.g., antibody-antigen, aptamer-natural ligand, natural receptor/ligand, have proven suitable for bioFETs [Rogers, 2000]. Various types of semiconductors, such as SiNW, Carbon NanoTube (CNT) and graphene, can be used as the FET channel, i.e., transducer channel [Poghossian and Schöning, 2014]. The basics of biorecognition and transducing operations and the noise processes do not fundamentally differ based on the type of the ligand-receptor pair and the semiconduc-

tor channel. However, the literature is currently dominated by the studies focusing on SiNW bioFETs. One inherent drawback of SiNW bioFETs is the thin oxide layer built up around the SiNW surface, which deteriorates its detection performance [Senveli and Tigli, 2013]. Therefore, researchers are in search for other nanomaterials suitable for application in biosensing. For example, metal-oxide nanowires, such as SnO_2, ZnO, In_2O_3, are rapidly proving to be useful in nanoscale biosensing applications as the active channels of thin film biotransistors [Huang and Wan, 2009]. Though, in several cases, they could outperform the SiNW counterparts in terms of sensitivity and limit of detection, their fabrication is currently constrained by bottom-up methods, which limits the controllability of their size and doping characteristics [Senveli and Tigli, 2013]. In contrast, SiNW provides a wider range of fabrication options including well-developed lithographic top-down methods, which allows their seamless integration into the current fabrication technologies [Chen et al., 2011]. Together with a more established literature, easier and controllable fabrication of SiNWs lead us to focus on SiNW bioFETs in this study to develop a model for bioFET-based MC receiver.

8.3 SiNW FET-Based Receiver Model

8.3.1 Model Description

We consider a time-slotted molecular communication system between a single transmitter receiver pair, which are assumed to be perfectly synchronized with each other in terms of time. The system utilizes M-ary concentration shift keying (M-CSK) modulation such that information is encoded into the concentration, i.e., the number, of molecules. Given that the input alphabet is $\mathcal{M} = \{0, 1, ..., M-1\}$, to send the symbol $m \in \mathcal{M}$ for the k^{th} time slot, the transmitter releases N_m molecules at the beginning of the signaling interval, i.e., at time $t_k = kT_s$, where T_s is the slot duration, i.e., the symbol period.

For the propagation medium, we consider a simple straight microfluidic channel with a rectangular cross-section, as shown in Fig. 8.2. The transmitter is assumed to

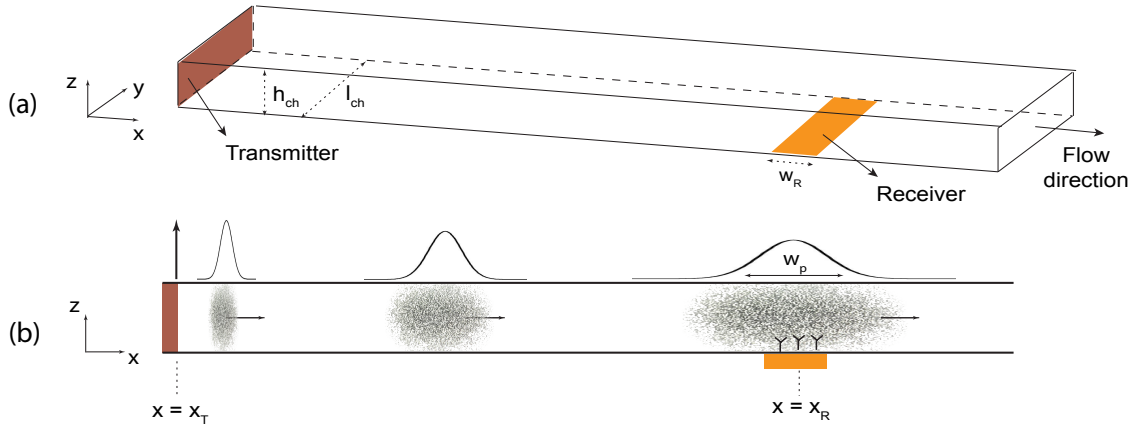


Figure 8.2: (a) 3D and (b) 2D dimensional view of microfluidic propagation channel. The locations of the transmitter and receiver, and the plug of ligands, which is dispersed as it flows towards the receiver location, are shown.

be located at the entrance of the channel. A SiNW FET-based MC receiver is considered to be located at the bottom of the microfluidic channel at position $x = x_R$, with its SiNW transducing channel covered by the oxide layer and surface receptors, which are directly exposed to the information molecules, i.e., ligands, of varying concentration. The receiver samples the concentration of ligands flowing over its surface based on ligand-receptor binding kinetics [Pierobon and Akyildiz, 2011]. A fluid flows unidirectionally from the transmitter to the receiver location in the microfluidic channel such that the transmitted ligands are propagated towards the receiver through advection and diffusion. The trajectories of each molecule along the propagation channel are assumed to be independent of each other.

Employing microfluidic channels for the propagation medium is prevalent in both MC [Bicen and Akyildiz, 2013, Bicen and Akyildiz, 2014], and biosensing literature [Sheehan and Whitman, 2005, Karsenty et al., 2014]. We will frequently make use of the results obtained in these studies to derive analytical expressions for the performance metrics of the SiNW receiver.

In the considered scenario, ligands are not absorbed by the receiver, instead they temporarily bind to the surface receptors and unbind after a random amount of time.

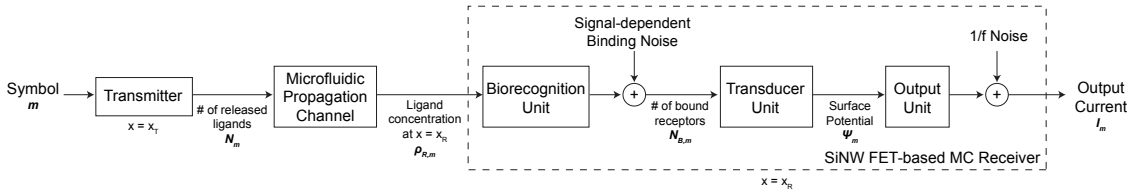


Figure 8.3: Block diagram of microfluidic MC system with SiNW FET-based MC receiver.

This characteristic of the ligands together with their long propagation times and spread over the x-axis through diffusion make the propagation channel have a memory, that may result in intersymbol interference (ISI) [Bicen and Akyildiz, 2015]. ISI can be overcome by selecting the symbol period T_s sufficiently long, or employing auxiliary enzymes in the channel that degrade the information molecules in the environment after the detection, as proposed in [Noel et al., 2014a]. To simplify the derivation of the receiver model, without loss of generality, we assume that the propagation channel is memoryless, thus, we neglect ISI.

The block diagram of the communication system including the SiNW FET-based MC receiver is shown in Fig. 8.3. The receiver's operation can be described by the operations of three consecutive functional units. The Biorecognition Unit (BU) constitutes the interface of the receiver with the communication channel and is responsible for selectively sensing the concentration of ligands. In the Transducer Unit (TU), the ligands, which stochastically bind the surface receptors, modulate the gate potential of the FET through the field effect resultant from their intrinsic charges. In the Output Unit (OU), the modulated gate potential is immediately reflected into the current flowing through the SiNW channel between the drain and the source electrodes of the FET.

In the following, we determine the characteristics of the receiver input signal by modeling the propagation inside the microfluidic channel, and then model each functional unit of the receiver individually to obtain the input-output relations and derive the statistics of the additive noise processes effective on the output current.

8.3.2 Molecular Transport in Microfluidic Channel

Transport dynamics of ligands inside the microfluidic channel can be described by the advection-diffusion equation. The fluid flow, which may be created by a pressure difference between the two ends of the channel, is taken as laminar, steady, and unidirectional along the channel's longitudinal axis, i.e., x-axis [Bicen and Akyildiz, 2014]. Assuming that a relatively low number of ligands reversibly react with the surface receptors and do not substantially change the concentration in the channel, the propagation of the ligands throughout the channel is handled as a one-dimensional advection-diffusion problem such that the ligand concentration ρ and the fluid velocity u are represented by their average over the channel's cross section [Karsenty et al., 2014]. Therefore, the concentration and fluid flow are invariant along the y- and z-axis. One dimensional advection-diffusion equation along the direction of the fluid flow, $\vec{x}$, can be written as

$$\frac{\partial \rho(x,t)}{\partial t} = D\frac{\partial^2 \rho(x,t)}{\partial x^2} - u\frac{\partial \rho(x,t)}{\partial x}, \tag{8.1}$$

where $\rho(\vec{x},t)$ is the average ligand concentration at position $\vec{x}$ and time t, and u is the x-axis fluid flow velocity averaged over the channel's cross section. D is the effective diffusion coefficient that accounts for the effect of Taylor-Aris type dispersion of ligands [Bruus, 2007]. For a channel with rectangular cross-section, it is given by

$$D = \left(1 + \frac{8.5u^2 h_{ch}^2 l_{ch}^2}{210 D_0^2 (h_{ch}^2 + 2.4 h_{ch} l_{ch} + l_{ch}^2)}\right) D_0, \tag{8.2}$$

where the intrinsic diffusion coefficient is denoted by D_0 [Bicen and Akyildiz, 2014]. h_{ch} and l_{ch} are the cross-sectional height and length of the channel, respectively. Transmitter is assumed to be a planar ligand source located at $x = x_T$ and release a preset number of ligands N_m at time $t_k = kT_s$ into the channel for representing symbol m. Assuming that the ligands are uniformly distributed over the channel's cross-section at the instant of release, the transmitter signal can be represented by

an impulse scaled by the surface concentration:

$$\rho_m(x,t) = \frac{N_m}{A_{ch}}\delta(x - x_T, t - t_k), \tag{8.3}$$

where $A_{ch} = h_{ch} \times l_{ch}$ is the cross-sectional area of the channel. Since we neglect ISI, to model the propagation, it is sufficient to consider only one signaling interval, say $k = 0$. Taking the transmitter location as $x_T = 0$, with the given initial condition (8.3), the solution of one dimensional advection-diffusion equation (8.1) is given by [Bruus, 2007] as follows

$$\rho_m(x,t) = \frac{N_m/A_{ch}}{\sqrt{4\pi Dt}} \exp\left(-\frac{(x-ut)^2}{4Dt}\right). \tag{8.4}$$

Note that although the initial condition is represented by a surface concentration, the resulting solution is given in terms of volumetric concentration of ligands.

8.3.3 Received Signal

The SiNW FET-based receiver is considered to be placed at the bottom of the microfluidic channel and located along the transverse axis perpendicular to fluid flow. We assume that the length of the SiNW, l_R, is equal to the cross-sectional length of the channel, i.e., $l_R = l_{ch}$, and the drain, source and gate electrodes of the receiver are buried inside the channel walls and do not affect the fluid flow and ligand propagation. The radius of the SiNW is denoted by r_R, and the position of the radial axis of the SiNW is taken as the center position of the receiver and denoted by x_R.

As can be inferred from (8.4), the concentration profile of the ligand plug is Gaussian at any observation time. The plug disperses and its peak concentration attenuates as the plug is transported by the fluid flow along the channel. We define the delay between the transmitter and the receiver as the time it takes for the plug's peak concentration to arrive at the center position of the receiver $x = x_R$:

$$t_D = \frac{x_R}{u}. \tag{8.5}$$

Following [Karsenty et al., 2014], we define an effective plug width w_p in the spatial domain, as the width that encloses 95% of the Gaussian area of $\rho_m(x, t_D)$. This corresponds approximately to the four times the standard deviation of the distribution, and can be given by

$$w_p = 4\sqrt{2Dt_D}, \tag{8.6}$$

which is independent of the ligand concentration released from the transmitter.

We neglect the attenuation and dispersion of the ligand plug during its passage over the receiver surface, as in [Karsenty et al., 2014]. We also assume that all of the points on the receiver surface are exposed to the same concentration of ligands. This assumption is reasonable since the effective width of the receiver, $w_R \approx \pi l_R$, along the flow direction is very small, i.e., typically on the order of 30 nm, compared to the effective plug width w_p, typical values of which are on the order of 100 μm (for example, in the case of $x_R = 1$ mm and $u = 10$ μm/s, $w_p \simeq 565$ μm). Thus, the ligand concentration seen by the receiver at time t can be given by

$$\rho_m(x_R, t) = \rho_{R,m}^{max} \exp\left(-8\frac{(x_R - ut)^2}{w_p^2}\right), \tag{8.7}$$

where $\rho_{R,m}^{max}$ is the peak concentration at time t_D at the receiver location

$$\rho_{R,m}^{max} = \rho_m(x_R, t_D) = \sqrt{\frac{8}{\pi}}\frac{N_m}{A_{ch} w_p}. \tag{8.8}$$

Given the effective plug width w_p, the ligand plug is assumed to complete its passage in a time duration of w_p/u. During the passage of the plug, we assume, as in [Karsenty et al., 2014], that the receiver is exposed to a stationary concentration

$\rho_{R,m}$,

$$\begin{aligned}\rho_{R,m} = \langle \rho_m(x_R,t) \rangle &= \int_{t_D - w_p/2u}^{t_D + w_p/2u} \rho_m(x_R,t)dt \\ &= \rho_{R,m}^{max} \sqrt{\frac{\pi}{8}} \operatorname{erf}(\sqrt{2}), \\ &= \frac{N_m}{A_{ch} w_p} \operatorname{erf}(\sqrt{2}), \\ &\text{for } t \in [t_D - w_p/2u, t_D + w_p/2u],\end{aligned} \tag{8.9}$$

which is the time average. In the considered scenario, the receiver samples the ligand concentration at a single time instant in this interval, e.g., at $t = t_D$. Therefore, the received signal is taken as equal to $\rho_{R,m}$, when the transmitter sends symbol m.

8.3.4 Biorecognition Block and Binding Noise

We start modeling the biorecognition block by first investigating the ligand flux to the receiver surface. In some MC studies, the transport of ligands is assumed to be fast enough to assure that the ligand-receptor binding kinetics is reaction-limited, i.e., governed simply by the intrinsic binding and unbinding rates of the reactants, thus, the successive samples of the concentration taken by the receptors becomes uncorrelated [Pierobon and Akyildiz, 2011]. The opposite case, i.e., transport-limited kinetics, is more prominently accepted in MC studies which assume that the receiver is perfect observer that counts every single molecule that enters into a defined reception volume. This corresponds to an infinite binding and unbinding rates, thus, a continuous sampling of the concentration signals brings along an additive counting noise (rather than the ligand-receptor binding noise), correlation of which is governed only by the transport rate, e.g, diffusion coefficient, of the ligands [Pierobon and Akyildiz, 2013]. However, this is not always the case, because we usually observe binding/unbinding and transport rates comparable to each other, i.e., the receptor-ligand binding kinetics is neither reaction-limited nor transport-limited. This problem has been recently addressed by several studies [Berezhkovskii and Szabo, 2013, Kaizu et al., 2014], which

arrive at the same correlation time depending on both transport and reaction rates. To make use of the analytical results obtained in these studies, we first investigate the transport of ligands to the receiver surface.

Since the SiNW resides on the surface of bulk SiO_2, which occludes the ligand flux from the bottom, the ligands flowing over the receiver can be assumed to interact only with the receptors tethered to the top surface of the SiNW, which is covered by a SiO_2 layer, as shown in Fig. 8.4. Thus, we can consider that the receiver has a hemicylindrical interface to the fluid. The transport rate, i.e., flux, of ligands, flowing with a stationary concentration, to a hemicylindrical surface, placed at the bottom of a microfluidic channel with rectangular cross-section is investigated in [Sheehan and Whitman, 2005]. The authors show that it can be approximated (with an error of $\sim 5\%$) by the flux to a sensor rectangular surface with the same length and the width $w_R = \pi r_R$, providing a closed-form expression [Sheehan and Whitman, 2005]:

$$k_T = Dl_r \times \begin{cases} \left(0.8075 P_s^{1/3} + 0.7058 P_s^{-1/6} - 0.1984 P_s^{-1/3}\right), & \text{if } P_s > 1 \\ \frac{2\pi}{4.885 - \ln(P_s)} \left(1 - \frac{0.09266 P_s}{4.885 - \ln(P_s)}\right), & \text{if } P_s < 1 \end{cases} \tag{8.10}$$

where P_s is defined as

$$P_s = \frac{6 Q w_R^2}{D l_{ch} h_{ch}^2}, \tag{8.11}$$

where Q is the volumetric flow rate, which is given by $Q = u \times A_{ch}$.

The ligands flowing over the receiver surface interact with the surface receptors through ligand-receptor binding mechanism. Assuming that the surface receptors are kinetically non-interacting, i.e., there is no cooperativity among them, the number of bound receptors can be described by the following kinetic scheme,

$$0 \underset{\beta_1}{\overset{\alpha_0}{\rightleftharpoons}} 1 \underset{\beta_2}{\overset{\alpha_1}{\rightleftharpoons}} 2 \quad \ldots \quad \mathrm{N_R} - 1 \underset{\beta_{N_R}}{\overset{\alpha_{N_R-1}}{\rightleftharpoons}} \mathrm{N_R}, \tag{8.12}$$

where N_R is the number of surface receptors. In the case that the ligand-receptor binding process is reaction-limited (no influence of ligand transport with infinite transport rate), the state-dependent rates α_n and β_{n+1} can be given as follows

$$\alpha_n = (N_R - n)k_1\rho_{R,m}, \tag{8.13}$$

$$\beta_{n+1} = nk_{-1}, \tag{8.14}$$

where k_1 and k_{-1} are the intrinsic binding and unbinding rates of ligand-receptor pair, respectively, and n denotes the number of bounded receptors. In this reaction-limited case, $\rho_{R,m}$, which is the concentration of ligands flowing over the receiver location, is equal to the concentration of ligands at contact with the surface receptors. When the transport rate cannot be assumed to be infinite, the binding statistics are affected by the transport dynamics. This effect is captured by [Berezhkovskii and Szabo, 2013], which obtains the transport-influenced state-dependent rates, based on the detailed balance conditions at equilibrium, as follows

$$\alpha_n^T = \frac{k_T(N_R - n)k_1\rho_{R,m}}{k_T + (N_R - n)k_1}, \tag{8.15}$$

$$\beta_{n+1}^T = \frac{k_T(n+1)k_{-1}}{k_T + (N_R - n)k_1}, \tag{8.16}$$

where k_T is the transport rate adjusted based on the channel and sensor geometry, which is given in (8.10).

For the kinetic scheme in (8.12) updated by the transport-influenced rates α_n^T and β_{n+1}^T, the equilibrium probability distribution P_n^{eq} of having n number of bound receptors is given in [Berezhkovskii and Szabo, 2013] as a Binomial distribution:

$$P_n^{eq} = P(N_B = n) = \binom{N_R}{n} P_{on|m}^n (1 - P_{on|m})^{N_R - n}, \tag{8.17}$$

where N_B is a random variable representing the number of bound receptors, and $P_{on|m}$

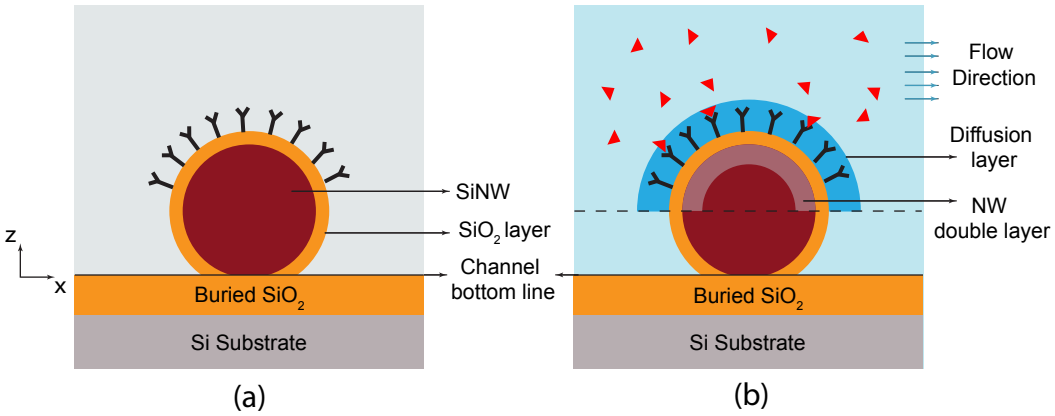


Figure 8.4: Cross-sectional view of SiNW FET-based MC receiver buried at the bottom of the microfluidic channel, (a) when the channel is empty; (b) when the receiver is exposed to the electrolyte solution with ligands flowing along the x-axis. We show only the receptors at the top surface of the SiNW, since we assume that the ligands can bind only to these receptors. The top part of the diffusion layer resulting from the counterions attracted to the insulating SiO_2 layer, and the corresponding SiNW double layer emerged inside the SiNW are also shown in (b). The region of interest is the zone lying above the dashed line, which is the effective part of the receiver for ligand detection.

is the probability of finding a single receptor in the ON (bound) state, given by

$$P_{on|m} = \frac{k_1 \rho_{R,m}}{k_1 \rho_{R,m} + k_{-1}} = \frac{\rho_{R,m}}{\rho_{R,m} + K_D}, \tag{8.18}$$

where $K_D = k_{-1}/k_1$ is the dissociation constant of receptor-ligand pair. Note that the equilibrium probability is a function of only the intrinsic reaction rates and not affected by the transport rate of ligands. The mean and variance of the number of occupied receptors at equilibrium can be written as follows

$$\mu_{N_{B,m}} = P_{on|m} N_R, \tag{8.19}$$

$$\sigma^2_{N_{B,m}} = P_{on|m}(1 - P_{on|m}) N_R. \tag{8.20}$$

Following [Berezhkovskii and Szabo, 2013], the autocorrelation function (ACF) of the ligand-receptor binding fluctuations at equilibrium is approximated with a single

exponential as follows

$$R_m(t, t+\tau) = R_m(\tau) \simeq \sigma^2_{N_{B,m}} e^{-\frac{\tau}{\tau_{B,m}}}, \quad \text{for } t, t+\tau \in [t_D - w_p/2u, t_D + w_p/2u], \quad (8.21)$$

where $\tau_{B,m}$ is the correlation time of the binding fluctuations influenced by the finite diffusion rate, given by [Berezhkovskii and Szabo, 2013] as follows

$$\tau_{B,m} = \frac{1}{k_1 \rho_{R,m} + k_{-1}} + \frac{k_1(k_1 \rho_{R,m} + N_R k_{-1})}{k_T (k_1 \rho_{R,m} + k_{-1})^2}. \quad (8.22)$$

For high values of k_T, i.e., in the reaction-limited case, the second term in the RHS of (8.22), which incorporates the effect of ligand transport rate, would vanish, and in this case, the correlation would be governed only by the reaction terms. Also note that the correlation time increases with increasing number of receptors N_R. The exact same correlation time has been obtained by [Kaizu et al., 2014] for the single receptor case, i.e., $N_R = 1$.

The power spectral density (PSD) for the random fluctuations of the number of bound receptors, which we call *the binding noise*, can be found by taking the Fourier transform (FT) of the ACF given in (8.21)

$$S_{N_{B,m}}(f) = \mathcal{F}\{R_m(\tau)\} = \sigma^2_{N_{B,m}} \frac{2\tau_{B,m}}{1 + (2\pi f \tau_{B,m})^2}. \quad (8.23)$$

8.3.5 Transducer Block

As the charged ligands bind to the surface receptors on the insulating SiO_2 layer, which covers the SiNW, the carrier distribution of SiNW near the SiO_2/SiNW interface is disturbed. The amount of ligand charge effective on the SiNW, when the symbol m is transmitted, is given by

$$Q_m = N_{B,m}\, q_{eff}\, N_{e^-}, \quad (8.24)$$

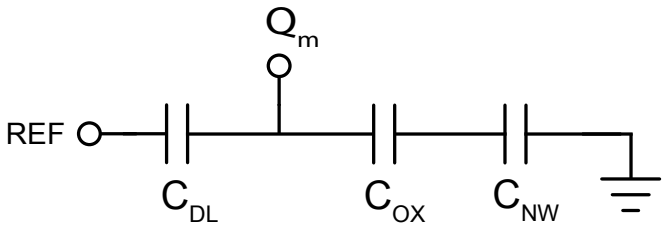


Figure 8.5: Equivalent circuit model for the transducer of the SiNW FET-based MC receiver [Gao et al., 2009], [Shoorideh and Chui, 2014]. *REF* denotes the reference electrode.

where N_{e^-} is the number of free electrons per ligand molecule. q_{eff} is the mean effective charge that can be reflected to the NW surface by a single electron of a ligand molecule in the presence of ionic screening in the medium, which is also known as the Debye screening [Stern et al., 2007]. The mean effective charge of a free ligand electron is degraded as the distance between the ligand electron and the transducer increases. The relation is given by

$$q_{eff} = q \times exp(-r/\lambda_D), \tag{8.25}$$

where q is the elementary charge, and r is the average distance of ligand electrons in the bound state to the transducer's surface [Rajan et al., 2013], which is assumed to be equal to the average surface receptor length, i.e., $r = l_{SR}$. The Debye length, λ_D, quantizes the ionic strength of the medium according to

$$\lambda_D = \sqrt{\frac{\epsilon_M k_B T}{2 N_A q^2 c_{ion}}}, \tag{8.26}$$

where ϵ_M is the dielectric permittivity of the medium, k_B is the Boltzmann's constant, T is the temperature, N_A is Avogadro's number, and c_{ion} is the ionic concentration of the medium [Rajan et al., 2013].

The effective ligand charges on the surface are transduced into a surface potential

as follows [Deen et al., 2006],

$$\Psi_m = \frac{Q_m}{C_{eq}}, \tag{8.27}$$

where C_{eq} is the equivalent capacitance of the transducer. As demonstrated in Fig. 8.5, mainly three capacitances are effective on the transduction of the surface charges: (i) Diffusion layer capacitance, C_{DL}, resulting from the double layer created by the medium counterions accumulated at the interface between oxide layer, i.e., SiO_2 layer, and the electrolyte medium; (ii) the capacitance of the oxide layer; (iii) the SiNW capacitance, C_{NW}, which is again a double layer capacitance caused by the accumulation of carriers to the SiO_2/SiNW interface [Gao et al., 2009], [Shoorideh and Chui, 2014]. Therefore, the equivalent capacitance can be given by

$$C_{eq} = \left(\frac{1}{C_{OX}} + \frac{1}{C_{NW}}\right)^{-1} + C_{DL}. \tag{8.28}$$

As we assume a nanowire-on-insulator (NWoI) configuration for the receiver design, individual capacitances can be obtained by considering the SiNW as a hemicylinder with an oxide layer of thickness t_{OX} covering the SiNW, and a diffusion layer of thickness λ_D covering the oxide layer [Shoorideh and Chui, 2014]. Accordingly, the diffusion layer capacitance can be written as

$$C_{DL} = (\epsilon_M/\lambda_D) w_R l_R. \tag{8.29}$$

Similarly, the oxide layer capacitance can be given by

$$C_{OX} = (\epsilon_{OX}/t_{OX}) w_R l_R, \tag{8.30}$$

where ϵ_{OX} and t_{OX} are the permittivity of the oxide layer. For high values of hole density, e.g., $p \sim 10^{18}$ cm^{-3}, corresponding to the linear operation regime of the FET, the double layer capacitance emerged in the NW channel can be obtained as follows

[Gao et al., 2009]

$$C_{NW} = (\epsilon_{Si}/\lambda_{Si}) w_R l_R, \tag{8.31}$$

where ϵ_{Si} is the dielectric permittivity of SiNW, and λ_{NW} is the thickness of the double layer created in the inner surface of the NW, which is given by [Gao et al., 2009]

$$\lambda_{NW} = \sqrt{\frac{\epsilon_{Si} k_B T}{pq^2}}. \tag{8.32}$$

8.3.6 Output Block and $1/f$ Noise

In the output block, the potential induced at the SiNW/oxide layer interface is reflected into a variation in the current flowing through the SiNW transducer channel. We assume that the p-type FET is operated in the linear (Ohmic) region, with the electrode voltage values satisfying the following conditions [Sze and Ng, 2006]:

$$V_{SG} > |V_T|; \quad V_{SD} \leq V_{SG} - |V_T|, \tag{8.33}$$

where $V_{SG} = -V_{GS}$ is source to gate voltage, $V_{SD} = -V_{DS}$ is the source to drain voltage, and V_T is the threshold voltage of the SiNW FET. The voltage values are assumed to be held constant during the receiver operation. In the linear region, the current flowing between the source and drain electodes is given by

$$I_{SD} = \mu_p C_{OX} \frac{w_R}{l_R} \left[(V_{SG} - |V_T|) V_{SD} - \frac{V_{SD}^2}{2} \right], \tag{8.34}$$

where μ_p is the carrier (hole) mobility, which depends on the impurity density of the transducer channel [Sze and Ng, 2006], and $l_R = l_{ch}$ as stated before. The partial derivative of the source-drain current with respect to source-gate voltage gives the

transconductance of the FET:

$$g_{FET} = \frac{\partial I_{SD}}{\partial V_{SG}} = \mu_p C_{OX} \frac{w_R}{l_R} V_{SD}, \tag{8.35}$$

A potential created at the electrolyte/oxide layer interface due to the bound ligands acts upon the FET channel in the same way as the gate voltage does in a conventional FET. Therefore, the part of the channel current, I_m, generated by the surface potential, Ψ_m, can be written in terms of transconductance as follows

$$I_m = g_{FET} \times \Psi_m, \tag{8.36}$$

Combining the equations (8.9), (8.18), (8.19), (8.36), the mean of the generated output current can be given by

$$\mu_{I_m} = g_{FET} \Psi_L N_R \left(1 + \frac{K_D A_{ch} w_p}{N_m \operatorname{erf}(\sqrt{2})}\right)^{-1}, \tag{8.37}$$

where Ψ_L is defined as the surface potential created by the binding of a single ligand:

$$\Psi_L = (q_{eff} \times N_e^-)/C_{eq}. \tag{8.38}$$

As in all transistor devices, low-frequency operation of bioFET-based MC receiver is suffered from $1/f$ noise. Although the origin of flicker noise and its full analytical model are still open issues, there are several models, including the well-known Hooge's model, that approximate the noise power in frequency domain [Rajan, 2013].

In this paper, we use *the correlated carrier number and mobility fluctuation model*, which provides a more accurate description of the $1/f$ noise for FET type devices, compared to the Hooge's model and the carrier number fluctuation model, attributing the source of $1/f$ noise to the random generation and recombination of charge carriers due to the defects and traps in the SiNW channel resulting from imperfect fabrication. It also accounts for the correlation of the carrier mobility with the carrier number fluctuations [Sze and Ng, 2006]. The model expresses the resulting output current-

referred noise PSD as

$$S_{I_m^F}(f) = S_{V,FB}(f) g_{FET}^2 \left[1 + \alpha_s \mu_p C_{OX} (V_{SG} - |V_{TH}|)\right]^2, \tag{8.39}$$

where α_s is the Coulomb scattering coefficient which depends on the temperature, and μ_p is the mobility of the hole carriers, which depends on the impurity concentration of the SiNW channel [Rajan et al., 2010b]. $S_{V,FB}$ is the PSD of the flatband-voltage noise, given as

$$S_{V,FB}(f) = \frac{\lambda k_B T q^2 N_{ot} g_m^2}{w_R l_R C_{OX}^2 |f|}, \tag{8.40}$$

where λ is the characteristic tunneling distance, N_{ot} is the oxide trap density, i.e., impurity concentration, of the SiNW channel [Rajan et al., 2010b]. $1/f$ noise is independent of the received signals, and shows an additive behavior on the overall output current fluctuations [Georgakopoulou et al., 2015]. Theoretically, $1/f$ noise does not have a low frequency cutoff, and has infinite power at zero frequency. However, in experimental studies with a finite measurement time, a finite variance for $1/f$ noise is observed. The reason is related to the low frequency cutoff set by the observation time T_{obs} [Keshner, 1982], [Niemann et al., 2013]. Considering that the received molecular signals are at the baseband, to be able to calculate the total noise power, we assume one-year operation time, i.e., $\sim \pi \times 10^7$ s, for the antenna such that the low cutoff frequency is $f_L = 1/T_{obs} \approx 1/\pi \times 10^{-7}$ Hz. At frequencies lower than f_L, the noise is assumed to show the white noise behavior, i.e., $S_{I_m^F}(f) = S_{\Delta I_m^F}(f_L)$ for $|f| < f_L$.

8.3.7 Overall Noise PSD and Output SNR

The PSD for the output current fluctuations due to the additive binding noise $S_{I_m^B}$ can be written as

$$S_{I_m^B}(f) = S_{N_{B,m}}(f) \times \Psi_L^2 \times g_{FET}^2. \tag{8.41}$$

Including the additive $1/f$ noise, the overall PSD of the output current referred noise is given by

$$S_{I_m}(f) = S_{I_m^B}(f) + S_{I_m^F}(f). \tag{8.42}$$

Given the noise PSD, the output SNR of the receiver can be computed by

$$SNR_{out,m} = \frac{\mu_{I_m}^2}{\sigma_{I_m}^2}, \tag{8.43}$$

where $\sigma_{I_m}^2$ is the output current variance, obtained as follows

$$\sigma_{I_m}^2 = \int_{-\infty}^{\infty} S_{I_m}(f) df. \tag{8.44}$$

8.4 Gaussian Approximation and Symbol Error Probability

8.4.1 Gaussian Approximation for Noise Processes

To analytically derive the symbol error probability (SEP), we make some reasonable approximations for the noise statistics. We can expect that a significant number of receptors, e.g. > 1000, are tethered to the top surface of a SiNW channel. For large number of surface receptors, the binomial distribution given in (8.17) can be approximated as Gaussian, i.e., $N_{B,m} \sim \mathcal{N}\left(\mu_{N_{B,m}}, \sigma_{N_{B,m}}^2\right)$, with $\mu_{N_{B,m}}$ and $\sigma_{N_{B,m}}^2$ given in (8.19) and (8.20), respectively. Thus, the zero-mean additive binding noise follows the normal distribution $\mathcal{N}\left(0, \sigma_{N_{B,m}}^2\right)$. The binding noise keeps the zero-mean Gaussian characteristics when it is passed through the linear filter in the transducing block.

$1/f$ noise is resulting from the bias current flowing through SiNW channel, therefore, it is independent of the binding noise. Although, there has been a long-standing discussion about the $1/f$ noise statistics [Milotti, 2002], in many well-accepted experimental studies in the literature, it has been reported that $1/f$ noise can be approximated to follow a Gaussian distribution [Bell, 1955]-[Hooge and Hoppenbrouwers,

1969]. In this paper, we rely on these reports to provide an analytical expression for the SEP.

Therefore, the overall noise process effective on the output current is the sum of two additive stationary noise processes that independently follow Gaussian statistics; thus, it is a stationary Gaussian process with a colored PSD.

8.4.2 Derivation of SEP for M-CSK Modulation

Let H_m be the hypothesis that the symbol $m \in \mathcal{M}$ is transmitted at the beginning of k^{th} time slot, and Z_k be the output current sampled by the receiver for the k^{th} slot. Then, with the Gaussian approximation of the additive noises, the conditional probability of Z_k given that the hypothesis H_m is true can be written as

$$P(Z_k|H_m) = \frac{1}{\sqrt{2\pi\sigma_{I_m}^2}} e^{-\frac{(Z_k-\mu_{I_m})^2}{2\sigma_{I_m}^2}}, \tag{8.45}$$

where μ_{I_m} is the mean of the output current given by (9.10), and $\sigma_{I_m}^2$ is the output current variance given by (8.44). Assuming that maximum likelihood (ML) detection is applied by the receiver, the decision rule can be expressed by

$$\hat{m}_k = \arg\max_m P(Z_k|H_m), \tag{8.46}$$

where $\hat{m}_k$ is the symbol decided at the receiver for the k^{th} transmission. The ML decision rule divides the entire range of the output current into M decision regions corresponding to the M symbols in the source alphabet. Decision region D_m for the transmitted symbol m can be defined as

$$\begin{aligned} D_m = &\{Z_k : P(Z_k|H_m) > P(Z_k|H_j), \forall j \neq m\}, \\ &\text{for} \quad m = 0, ..., M-1. \end{aligned} \tag{8.47}$$

Assuming $N_0 < N_1 < ... < N_{M-1}$, from (8.19) and (9.10), we know that the symbols satisfy the following condition

$$\mu_{I_0} < \mu_{I_1} < ... < \mu_{I_{M-1}}. \tag{8.48}$$

Given this condition, the decision thresholds λ_x separating the decision regions D_{m-1} and D_m can be obtained by comparing the conditional probabilities of adjacent symbols [Singhal et al., 2015]

$$\frac{1}{\sqrt{2\pi\sigma_{I_m}^2}} e^{-\frac{(\lambda_m - \mu_{I_m})^2}{2\sigma_{I_m}^2}} = \frac{1}{\sqrt{2\pi\sigma_{I_{m-1}}^2}} e^{-\frac{(\lambda_m - \mu_{I_{m-1}})^2}{2\sigma_{I_{m-1}}^2}}, \quad \text{for} \;\; m = 1, ..., M-1. \tag{8.49}$$

Solving we obtain the decision thresholds as

$$\lambda_m = \frac{1}{\sigma_{I_m}^2 - \sigma_{I_{m-1}}^2} \left(\sigma_{I_m}^2 \mu_{I_{m-1}} - \sigma_{I_{m-1}}^2 \mu_{I_m} + \sigma_{I_m} \sigma_{I_{m-1}} \sqrt{(\mu_{I_m} - \mu_{I_{m-1}})^2 + 2(\sigma_{I_m}^2 - \sigma_{I_{m-1}}^2) \ln \frac{\sigma_{I_m}}{\sigma_{I_{m-1}}}} \right), \quad \text{for} \;\; m = 1, ..., M-1. \tag{8.50}$$

The error probability of detection based on the decision thresholds given in (8.50) can be computed as

$$P(e|H_m) = \int_{z \notin D_m} P(z|H_m) dz. \tag{8.51}$$

Assuming that a priori probabilities for all symbols are equal, SEP can be given

as follows

$$\begin{aligned} P_e =& \frac{1}{M}\sum_{m=0}^{M-1} P(e|H_m) \\ =& \frac{1}{2M}\left[\text{erfc}\left(\frac{\lambda_1-\mu_{I_0}}{\sigma_{I_0}\sqrt{2}}\right)+\text{erfc}\left(\frac{\mu_{I_{M-1}}-\lambda_{M-1}}{\sigma_{I_{M-1}}\sqrt{2}}\right)\right. \\ &\left.+\sum_{m=1}^{M-2}\left(\text{erfc}\left(\frac{\mu_{I_m}-\lambda_m}{\sigma_{I_m}\sqrt{2}}\right)+\text{erfc}\left(\frac{\lambda_{m+1}-\mu_{I_m}}{\sigma_{I_m}\sqrt{2}}\right)\right)\right], \\ &\text{for} \quad m=0,...,M-1, \end{aligned} \tag{8.52}$$

where $\text{erfc}(z)=\frac{2}{\sqrt{\pi}}\int_z^\infty e^{-y^2}dy$ is the complementary error function.

8.5 Performance Analysis

In this section, we present the numerical results obtained based on the developed model under different settings to reveal the performance of the SiNW FET-based MC receiver. The default values for the controllable parameters used in the analyses are listed in Table 9.1.

We assume that the microfluidic channel is filled up with an electrolyte, which is moderate in its ionic concentration (with $c_{ion} = 30$ mol/m^3) compared to the diluted solutions (with $c_{ion} < 1$ mol/m^3) used in *in vitro* biosensing experiments [Duan et al., 2012] and physiological solutions (with $c_{ion} > 70$ mol/m^3) [Compton and O'Grady, 1991], [Okada et al., 1990]. The employed receptors on the FET surface are considered to be aptamers, the production process of which provides full control over the selection of length, binding and unbinding rates, as well as the type of corresponding ligand molecules [Kuscu and Akan, 2016c]. The default length of receptors is set to 2 nm, which corresponds to 6 base pair-aptamers. Binding and unbinding rates, k_+ and k_-, are set, considering the accepted values in the MC literature [Pierobon and Akyildiz, 2011] and the range of rates that aptamers can provide [Luzi et al., 2003]. Aptamers can bind to a large set of ligands, such as, aptamers, small proteins, RNA and DNA, and even non-organic molecules, which can attain a broad range of elementary charges,

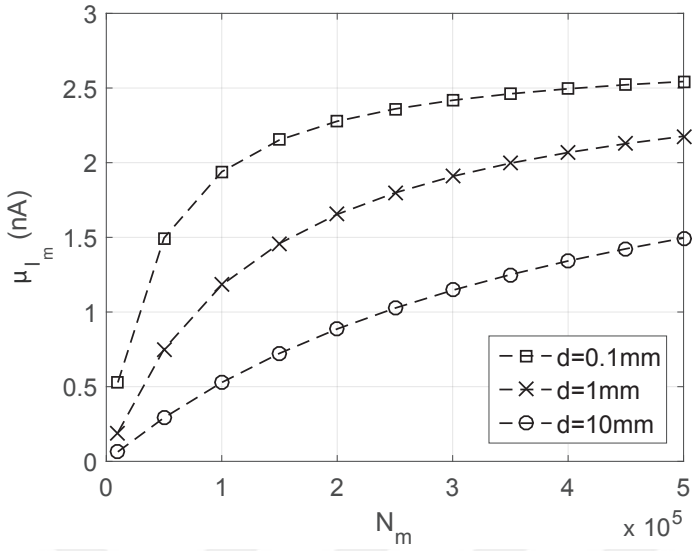


Figure 8.6: Expected output current μ_{I_m} as a function of number of ligands N_m released by transmitter and transmitter-receiver distance d.

as reviewed in [Kuscu and Akan, 2016c]. The relative permittivity of SiO_2 layer is reported as $\epsilon_{ox}/\epsilon_0 = 3.9$ [Deen et al., 2006]. The thickness of the SiO_2 layer, t_{ox}, is a design parameter, for which we select a default value of 2 nm. Depending on the fabrication, the tunneling distance for SiO_2 is on the order of 0.01-0.1nm [Rajan et al., 2011]. We set $\lambda = 0.05$ nm as reported in [Deen et al., 2006]. We assume the use of a p-type SiNW, which is moderately clean with the impurity density $N_{ot} = 10^{16}$ $eV^{-1}cm^{-3}$. This corresponds to a low-field mobility of $\mu_p = 500$ cm^2/Vs for hole carriers in SiNW (see Fig. 15 in [Sze and Ng, 2006]). The Coulomb scattering coefficient is taken as $\alpha_s = 1.9 \times 10^{14}$ Vs/C, which is the value at $T = 300$ K [Rajan et al., 2010b]. We assume that a shallow microfluidic channel with cross-sectional height $h_{ch} = 3$ μm and length $l_{ch} = 15$ μm, resulting in a laminar and steady flow [Bicen and Akyildiz, 2013]. The fluid flow velocity can be adjusted through the pressure difference between the two ends of the microfluidic channel. We assume an average flow velocity of $u = 10$ μm/s, a moderate value widely observed in microfluidic literature [Bicen and Akyildiz, 2013], [Karsenty et al., 2014].

8.5.1 Receiver Response and Noise Power

Receiver Response

We first investigate the expected response of the receiver to varying number N_m of ligands released by the transmitter. The mean output current generated in the SiNW channel for several transmitter-receiver distances $d = x_R - x_T$ is plotted in Fig. 8.6. For each distance setting, we observe that the output current increases as the transmitter releases more ligands. However, at some value of N_m, the current begins to saturate. This is because as the receptors on the biorecognition layer are occupied by higher number of ligands; the receptors lose their sensitivity to the varying ligand concentration.

From the same figure, we can also infer that for the investigated range of number of released ligands, the receiver is most sensitive to the concentration variations when $d = 1$ mm. Since the attenuation of the concentration is proportional to $\sqrt{d}$ (see

Table 8.1: Default Values of Simulation Parameters

Microfluidic channel height (h_{ch})	3 μm
Microfluidic channel width (l_{ch})	15 μm
Number of transmitted ligands for symbol m (N_m)	10^5
Max number of ligands TN transmits (K)	2×10^4
Transmitter-receiver distance (d)	1 mm
Average flow velocity (u)	10 μm/s
Intrinsic diffusion coefficient of ligands (D_0)	10^{-10} m^2/s
Binding rate (k_1)	2×10^{-18} m^3/s
Unbinding rate (k_{-1})	10 s^{-1}
Average number of electrons in a ligand (N_e^-)	3
SiNW radius (r_R)	10 nm
Concentration of receptors on the surface (ρ_{SR})	4×10^{16} m^{-2}
Length of a surface receptor (l_{SR})	2 nm
Temperature (T)	300K
Relative permittivity of oxide layer (ϵ_{ox}/ϵ_0)	3.9
Relative permittivity of SiNW (ϵ_{NW}/ϵ_0)	11.68
Relative permittivity of medium (ϵ_R/ϵ_0)	78
Ionic strength of electrolyte medium (c_{ion})	30 mol/m^3
Source-drain voltage (V_{SD})	0.1 V
Source-gate voltage (V_{SG})	0.4 V
Threshold voltage (V_{TH})	0 V
Hole density in SiNW (p)	10^{18} cm^{-3}
Tunneling distance (λ)	0.05 nm
Thickness of oxide layer (t_{ox})	2 nm
Oxide trap density (N_{ot})	10^{16} eV^{-1}cm^{-3}
Effective mobility of hole carriers (μ_p)	500 cm^2/Vs
Coulomb scattering coefficient (α_s)	1.9×10^{14} Vs/C

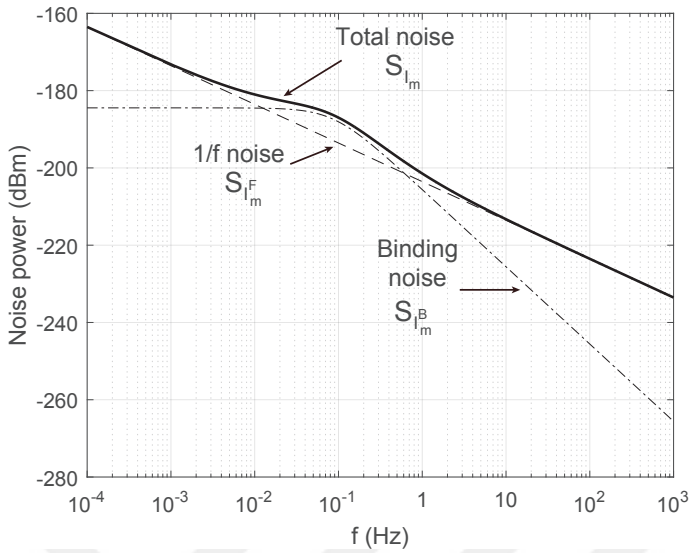


Figure 8.7: PSD of noise effective on the output current of SiNW FET-based MC receiver. The plot reveals the individual contributions of binding and $1/f$ noise.

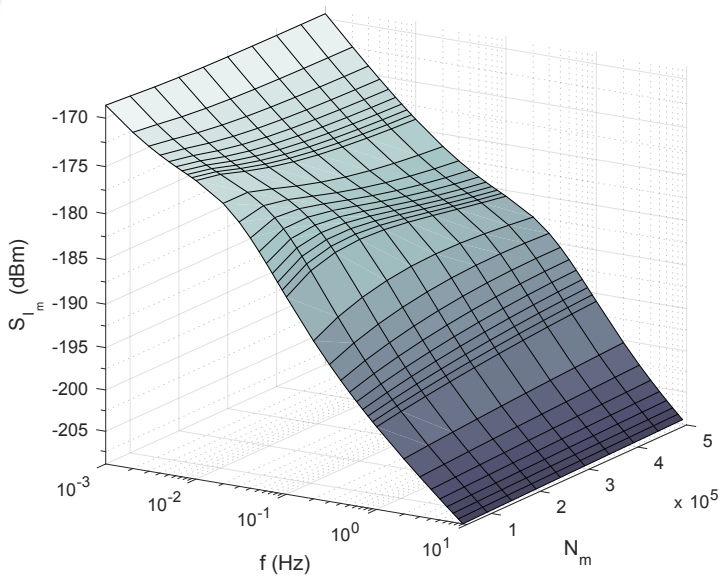


Figure 8.8: Output current noise PSD at the frequency range of receiver's operation with varying N_m.

Equations (8.5)-(8.9)); in the minimum distance case, i.e., when $d = 0.1$ mm, the

ligand concentration observed at the receiver location is expected to be much higher compared to the other settings. On the other hand, higher concentration of ligands in the receiver location leads to a more rapid saturation of the biorecognition unit, as evident from Fig. 8.6. When the distance is increased to 10 mm, the ligand concentration over the receiver significantly decreases for the whole range of N_m, so that the variations of N_m do not result in significant differences in the output current. Therefore, the dynamic range of the receiver and the attenuation of the concentration signals in the channel should be carefully considered while designing the overall MC system.

Noise Power

To analyze the effect of noise on the receiver operation, we plot the individual PSDs of binding and output noises as well as the overall noise PSD effective on the output current. As seen in Fig. 8.7, the frequency domain is virtually divided into three regions, in each of which one of the two noise sources is prevailing. At very low frequencies, e.g., $f \ll 0.1$ Hz for the default setting here, $1/f$ noise is dominating over the binding noise, since the binding noise has a flat power density for frequencies below a critical value determined by the correlation time, i.e., $f_B = 1/\tau_B$, whereas the power of $1/f$ noise is increasing as proportional to $1/f$. Around f_B, the binding noise may become dominant, depending on the total variance of the binding process. At frequencies higher than f_B, the power of binding noise is attenuated more rapidly than the $1/f$ noise. Although $1/f$ noise is dominating again at high frequencies, its power decreases under -220 dBm, thus, the overall noise power is negligible in this frequency range.

As the bandwidth of the received signal is expected to be at most on the order of Hz [Pierobon and Akyildiz, 2011], contributions of both binding noise and $1/f$ noise at low frequencies should be accounted for while designing the MC receiver.

The overall noise PSD is analyzed also for varying number of ligands released by the transmitter. As can be seen from Fig. 8.8, the contribution of $1/f$ noise

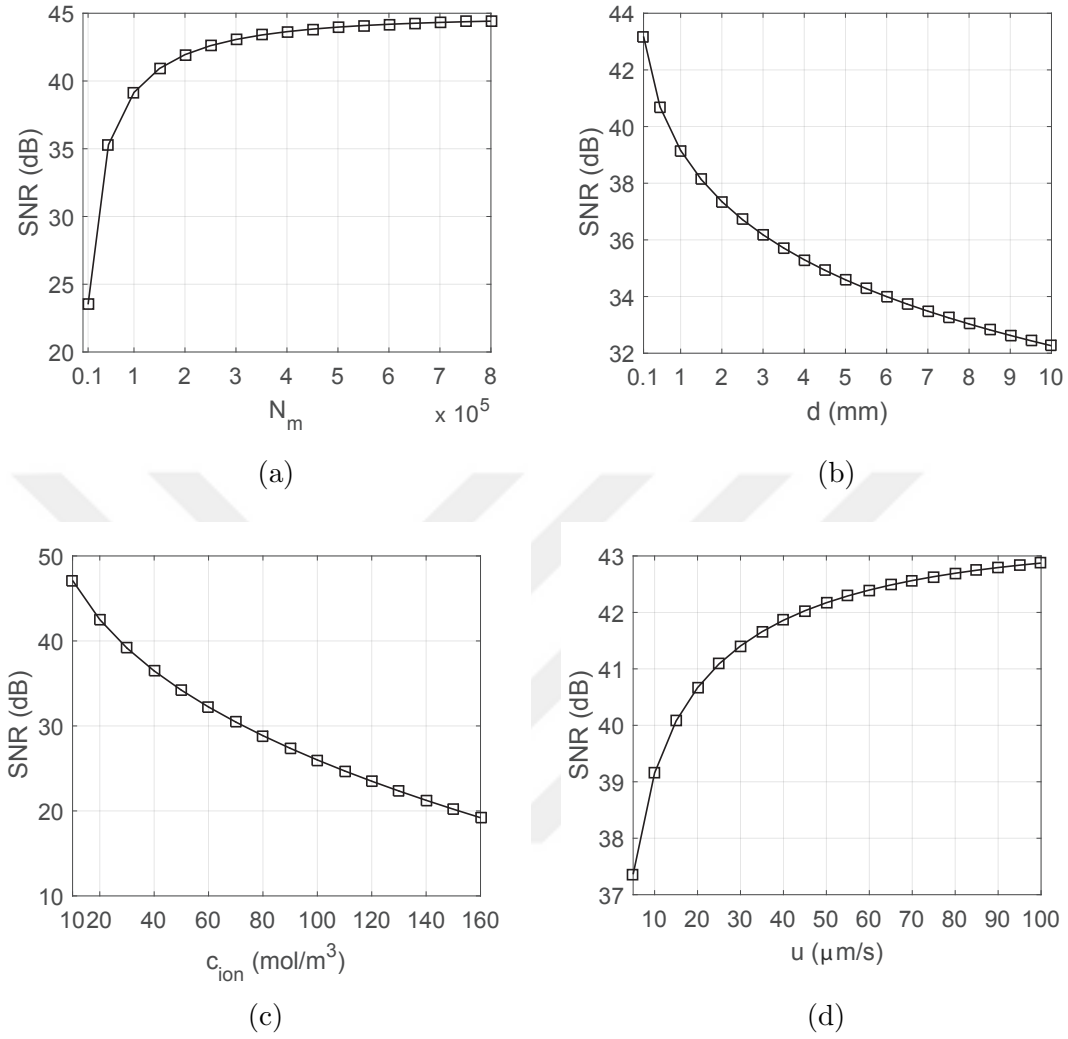


Figure 8.9: Effect of the communication system parameters on the SNR at the electrical output of the receiver. SNR as a function of (a) number of transmitted ligands N_m, (b) transmitter-receiver distance $d = x_R - x_T$, (c) ion concentration c_{ion} of the electrolyte medium, (d) average flow velocity u inside the microfluidic channel.

dominating at very low frequencies does not vary as N_m is changed; however, the contribution of the binding noise at low frequencies becomes more prevailing for lower ligand concentrations. This is originating from the fact that the correlation time of the binding fluctuations increases with decreasing ligand concentration, which decreases the critical frequency; see (8.22).

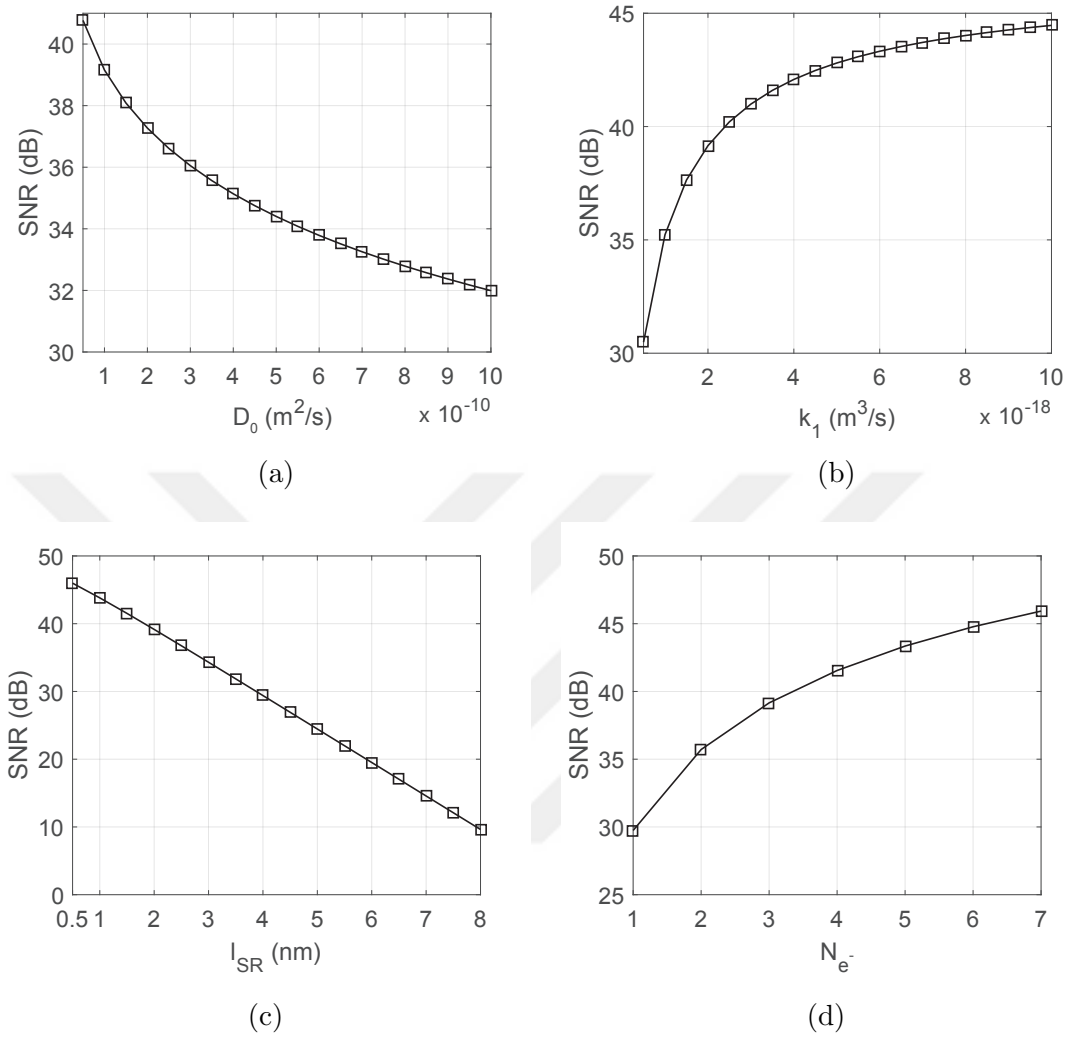


Figure 8.10: Effect of the molecular parameters on the SNR at the electrical output of the receiver. SNR as a function of (a) intrinsic diffusion coefficient of ligands D_0, (b) intrinsic binding rate of ligands k_1, (c) surface receptor length l_{SR}, (d) number of free electrons per ligand molecule N_e^-.

8.5.2 SNR Analysis

In this section, we investigate the effect of main system parameters on the receiver's output SNR, which is formulated in (8.43). We group the system parameters under three main categories: (i) communication system parameters related to the transmitter and communication channel, (ii) molecular parameters related to the character-

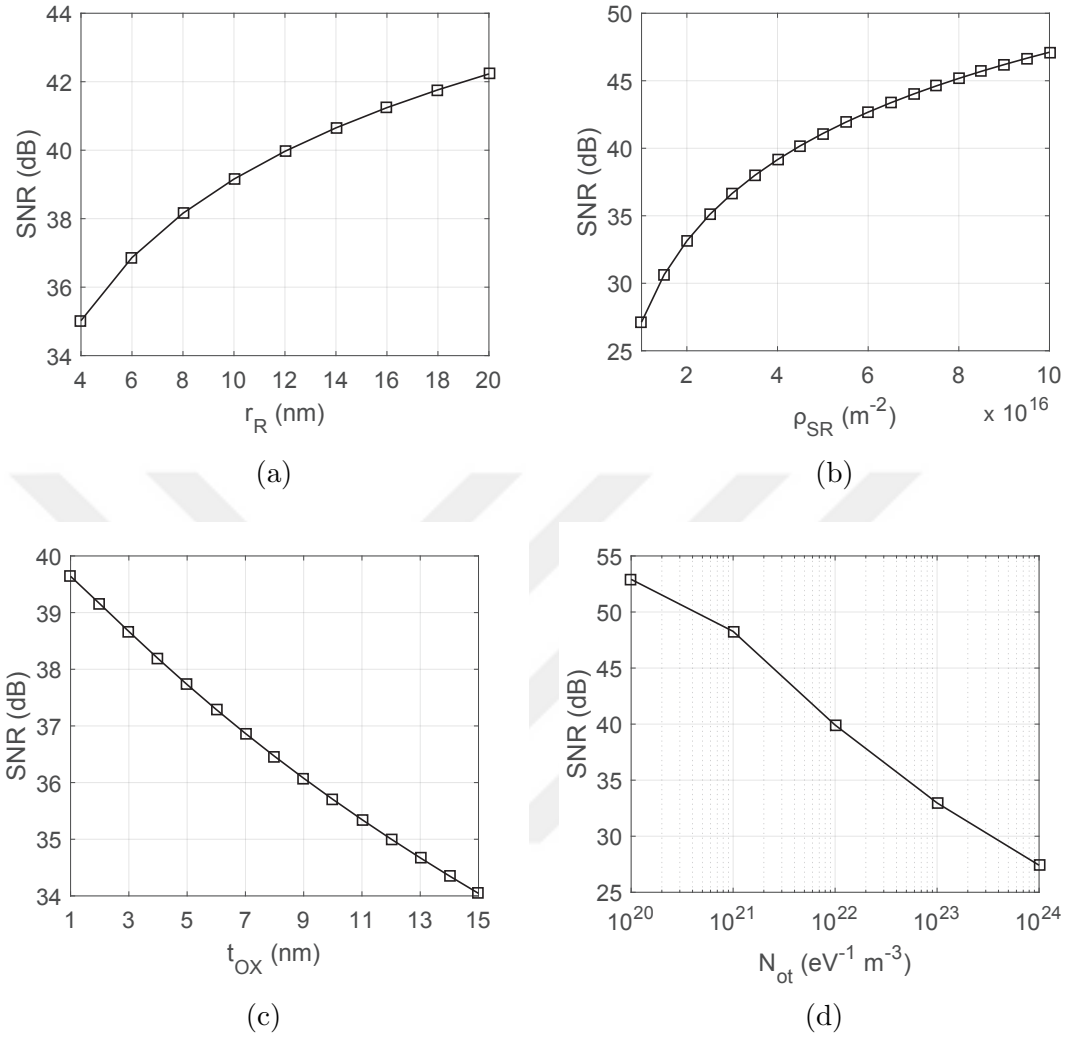


Figure 8.11: Effect of the receiver design parameters on the SNR at the electrical output of the receiver. SNR as a function of (a) SiNW radius r_R, (b) surface receptor concentration ρ_{SR} (c) SiO_2 layer thickness t_{OX}, and (d) oxide trap density N_t in SiNW.

istics of information carriers and corresponding receptors, (iii) receiver parameters related to the design of the SiNW FET-based MC receiver.

Effect of Communication System Parameters

SNR of the output current for varying number of ligands released by the transmitter is plotted in Fig. 8.9a, which clearly shows that SNR is significantly improved with increasing number of ligands. However, it begins to saturate at around 45 dB for the default setting due to the saturation of the surface receptors for very high concentrations of ligands. Given a number of ligands released by the transmitter, the output SNR decreases with increasing transmitter-receiver distance d, as demonstrated in Fig. 8.9b. This is because the ligand concentration is attenuated (proportional to $\sqrt{d}$) as the distance increases.

The effect of ionic strength of the fluidic medium on the receiver SNR is demonstrated in Fig. 8.9c. When the ionic concentration increases above 100 mol/m^3, the Debye length decreases below 1 nm resulting in substantial screening of ligand charges. Therefore, SNR significantly decreases with increasing ionic strength. Physiological conditions generally imply ionic concentrations higher than 100 mol/m^3. To compensate the attenuation of SNR, receptors with lengths comparable to Debye length should be selected.

The velocity of the fluid flow u also has a remarkable effect on the SNR, as is seen Fig. 8.9d. As the velocity increases, the plug arrives more rapidly at the receiver location, resulting in less attenuation. Therefore, higher velocity means higher ligand concentration at the receiver side, and this implies continuously improved SNR until it leads to the saturation of the surface receptors.

Effect of Molecular Parameters

Diffusion coefficient D_0 is an important characteristic of the information ligands although it also depends on the temperature and the viscosity of the fluid. Its effect on the SNR is shown in Fig. 8.10a. As is seen, the SNR decreases with increasing D_0. This is mainly caused by the increased dispersion of the concentration plug, which decreases the average ligand concentration that the receiver observes.

The effect of binding constant, k_1, is plotted in Fig. 8.10b. Increasing k_1 means

that more ligands can bind to the surface receptors as the plug flows over the receiver, this obviously results in an improved SNR.

We also investigate the effect of receptor length, l_{SR}, when the ionic strength is set to 30 mol/m^3 which makes the Debye length equal to 1.75 nm. As seen in Fig. 8.10c, SNR in dB decreases linearly with the increasing length. Considering also the results plotted in Fig. 8.9c, l_{SR} have a substantial effect on the receiver performance.

The number of free charges per ligand also critically affects the receiver response, since the operation the SiNW transducer is mainly based on the field effect generated by the ligand charges. As demonstrated in 8.10d, employing highly charged ligands would improve the receiver SNR. As reviewed by [Kuscu and Akan, 2016c], oligonucleotides are negatively charged in physiological conditions, i.e., at pH 7.4, due to their highly charged phosphate backbone. For example, a DNA sequence with 4 base-pairs at pH 7.4 can attain a net charge of $-8e$. Likewise, small proteins and antigens, depending on the pH of the environment, can attain a net charge of up to $\pm$4e.

Effect of Receiver Parameters

An important parameter of the receiver design is the size of the SiNW, which has a direct impact on the the ligand flux to the receiver, the number of surface receptors, and the capacitance values of the oxide layer, the SiNW double layer and the diffusion layer. Since we fixed the length of the SiNW as equal to the cross-sectional length of the microfluidic channel, we only change its radius r_R, and thus, its effective width w_R (recall that $w_R \simeq \pi \times r_R$). The effect of SiNW radius is demonstrated in Fig. 8.11a. Increasing the radius also increases the SNR. This is mainly because the transport rate of the ligands k_T and the number of surface receptors N_R increase with the radius.

Given that the SiNW radius is fixed to its default value $r_R = 10$ nm, increasing the concentration of receptors on the receiver surface ρ_{SR}, which means increasing the number of surface receptors (note that $N_R = w_r \times \rho_{SR}$), is another way of improving SNR, as can be inferred from Fig. 8.11b. However, size restrictions imposed by

the receptor size and possible interactions among densely deployed receptors, such as negative cooperativity, which are not captured by this model, should be accounted for in a real world implementation.

We also analyze the effect of oxide layer thickness t_{OX}, which determines the oxide layer capacitance $C_{OX} = \epsilon_{OX}/t_{OX}$. Fig. 8.11c demonstrates the results for conventional values of t_{OX}. As can be inferred, lower t_{OX} implies an improved SNR for the default system settings used in our analysis. This is mainly because increasing C_{OX} results in higher values of transconductance g_{FET}, which means more effective transduction of the surface potential to the output current. On the other hand, the effect of C_{OX} on the equivalent capacitance of the transducer is usually negligible compared to the substantial effect of the diffusion layer capacitance C_{DL}.

Lastly, we analyze the SNR for varying oxide trap density N_{ot}, which is proportional to the impurity of the SiNW. Trap density affects the carrier mobility, and increases the $1/f$ noise, which is very effective in the frequency range of the receiver's operation. The negative effect of increasing trap density on the SNR is evident from Fig. 8.11d.

8.5.3 SEP Analysis

In the last analysis, we evaluate the performance of the receiver when M-CSK is utilized for the modulation. We find the SEP for binary, 4-ary, 8-ary, 16-ary cases for different system settings. For better visualization, we present the results for each setting in two different plots separating the binary case from the 4-, 8-, 16-ary cases.

For the constellation design of M-CSK, we assume

$$N_m = \lceil (m+1)^s \times (K/M^s) \rceil, \tag{8.53}$$

where K is the maximum number of molecules that TN can release in a single transmission, s is the exponent defined to obtain a non-uniform constellation, and $m \in \mathcal{M} = \{0, 1, ..., M-1\}$ with $M \in \{2, 4, 8, 16\}$. Except for the analysis where we

investigate the effect of distance, we set $K = 2 \times 10^4$ and $s = 1$, so that we obtain a uniform constellation where the adjacent symbols are separated by K/M number of ligands. For the distance analysis, to be able to reveal the correlated effect of the distance and maximum number of ligands, we set $K = 2 \times 10^5$.

Figs. 8.12a and 8.12d show the SEP as a function of transmitter-receiver distance d. As is seen, for all modulation schemes, the SEP is minimum for intermediate distances, e.g., $1 - 2$ mm, and begins to increase when the distance is below or above this range. The reason can be explained as follows. As the distance gets smaller, the receiver operates near saturation because the concentration of ligands at the receiver location significantly increases when the transmitter and receiver are close to each other. This is reflected to the output current, and results in a decrease in the sensitivity of the receiver so that it cannot discriminate different levels of ligand concentration corresponding to different symbols. In a similar way, when the distance is increased, the ligand concentration is substantially attenuated until the plug reaches to the receiver location, which also leads to a degradation in the receiver sensitivity. Hence, we can conclude that there is an optimal range of distance for a given maximum number of ligands K.

Next, we analyze the effect of maximum number of ligands that the transmitter can release. As can be inferred from the results presented in Figs. 8.12b and 8.12e, increasing K up to 2×10^5 decreases the SEP for binary CSK. However, when we further increase K above this range, the SEP begins to get higher. Similar trends can be observed for 4-, 8-, and 16-ary cases. The reason is closely related to the reasons that lead to the results obtained with varying distance in the previous analysis. As the transmitter releases higher number of ligands for each symbol, the receiver begins to operate near saturation, which degrades its ability to discriminate different symbols.

The nontrivial results obtained for varying distance and maximum number of transmitted ligands are the consequences of the dynamic range imposed by the receiver, which has a limited reception capacity set by the number of surface receptors. Similar trends also have been noted in the MC experiments conducted with metal ox-

ide semiconductor alcohol sensors [Farsad et al., 2013], [Kim et al., 2015]. Although these sensors are not operating based on ligand-receptor binding mechanism, they result in saturation when they are exposed to a high concentration of alcohol molecules, since the devices have an active channel limited in size.

Since the response of the receiver is nonlinear as obvious from Fig. 8.6, utilizing a uniform constellation for M-CSK modulation obviously is not optimal. Particularly, there is a need to place more symbols on the lower half of the modulation range, for which the receiver is more sensitive to concentration variations, regardless of the maximum number of ligands that TN can transmit. We analyze the performance of the receiver employing a simple non-uniform M-ary modulation scheme by varying the exponent s in (8.53). For binary CSK case, rising the exponent significantly decreases the SEP, as demonstrated in Fig. 8.12c. However, when more than two symbols are transmitted as in cases of 4-, 8-, and 16-ary CSK, different trends are observed in Fig. 8.12f. After some threshold, the SEP begins to increase again. This is because the low level symbols are approaching to each other when we increase s, which complicates the detection in the receiver. Hence, there is a need for a more complex constellation design that can properly exploit the nonlinear response of the receiver. The results of these analyses reveal that there is plenty of room for optimization of the MC settings to obtain lower values of SEP.

Second set of analyses is performed for controllable parameters related mostly to the receiver and propagation medium, i.e., ionic concentration of the medium c_{ion}, receptor length l_{SR}, and oxide trap density in SiNW N_{ot}. The same trends observed in the SNR analyses are also seen for the SEP. For example, in Figs. 8.13a and 8.13d, we can see that increasing the ionic concentration substantially degrades the receiver performance for all M-CSK modulation schemes. As previously discussed in the SNR analysis, screening of the ligand charges by the medium counterions near the biorecognition layer leads to a lower signal power at the receiver output. In the presence of signal-independent $1/f$ noise, this is reflected to a degraded detection performance of the receiver. The same reason leads to the results obtained for varying

receptor lengths, which are presented in Figs. 8.13b and 8.13e. As can be inferred, it is possible to obtain a SEP lower than 10^{-10} for binary CSK case by utilizing receptors with lengths smaller than 2 nm. The trap density of the SiNW channel is also a critical parameter for the receiver performance, as it influences the extent of the $1/f$ noise. Accordingly, lower values of N_{ot} indicate a clean semiconductor channel, and thus, lead to an improved receiver performance, as evident from Figs. 8.13c and 8.13f.

8.6 Conclusion

In this chapter, as the first step towards implementing a human-made MC system with nanobioelectronic devices, we develop a communication theoretical model for SiNW FET-based MC receivers integrating all the underlying processes in MC and bioFET operation. Focusing on a microfluidic MC system, we derive closed-form expressions for fundamental performance metrics, such as SNR and SEP, to provide an analysis and optimization framework for MC with nanobioelectronic receivers. The results of performance evaluation point out several optimization pathways that need to be taken to improve the detection performance of the receiver. The developed model can be extended to incorporate the transient dynamics of MC and bioFETs for enabling analysis also in the frequency domain. Open issues include the design of optimal constellations and optimal receiver detection schemes for MC systems equipped with bioFET receivers. Further research on devising nanobioelectronic MC receivers could enable the implementation of all the theoretical protocols and algorithms designed for reliable and efficient MC and the development of seamless interfaces between MC nanonetworks and macroscale networks towards realizing IoBNT.

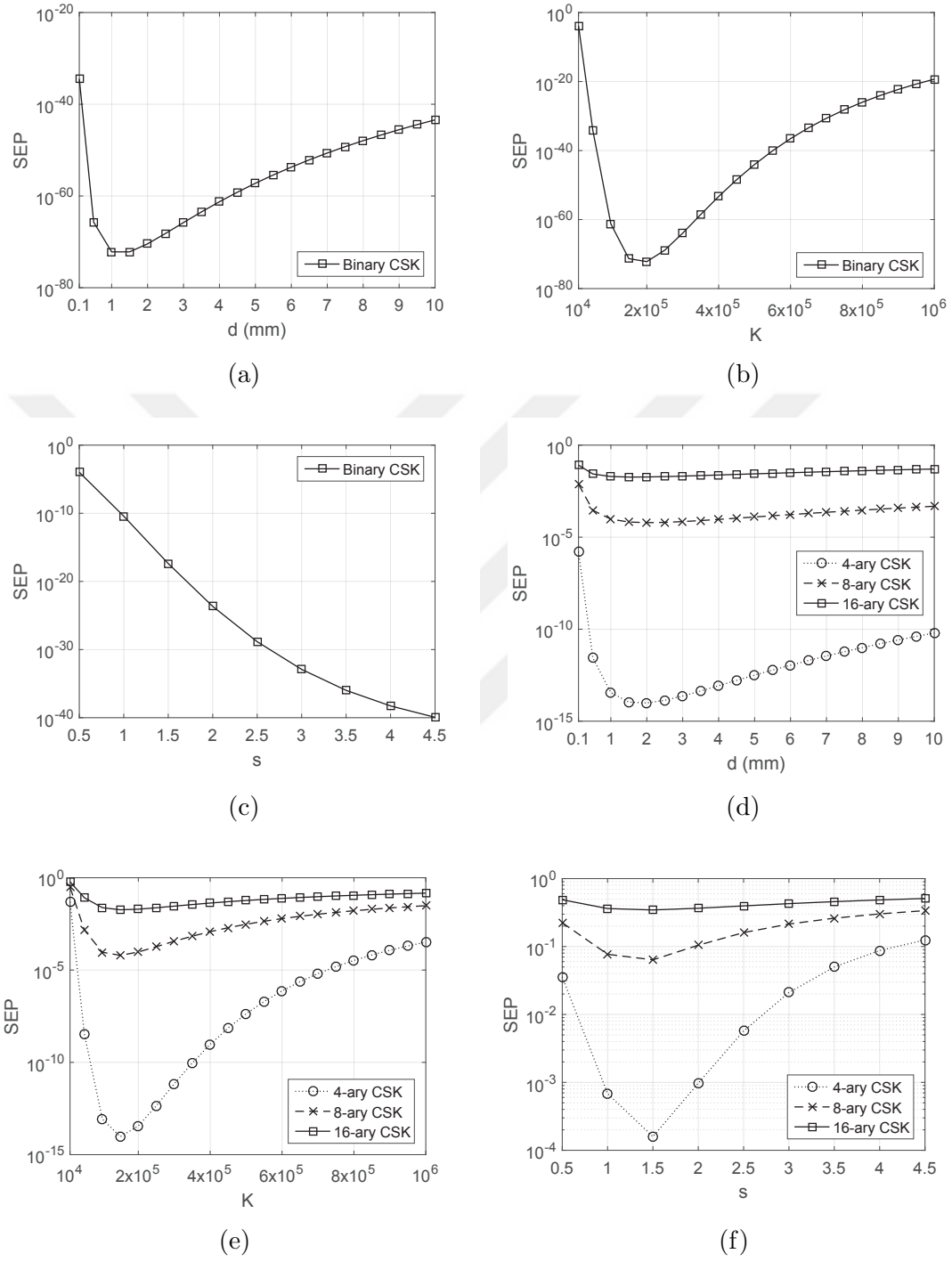


Figure 8.12: Symbol error probability (SEP) for M-CSK modulation. SEP as a function of (a, c) transmitter-receiver distance d, (b, e) maximum number K of ligands that transmitter can release, (c, f) constellation exponent s.

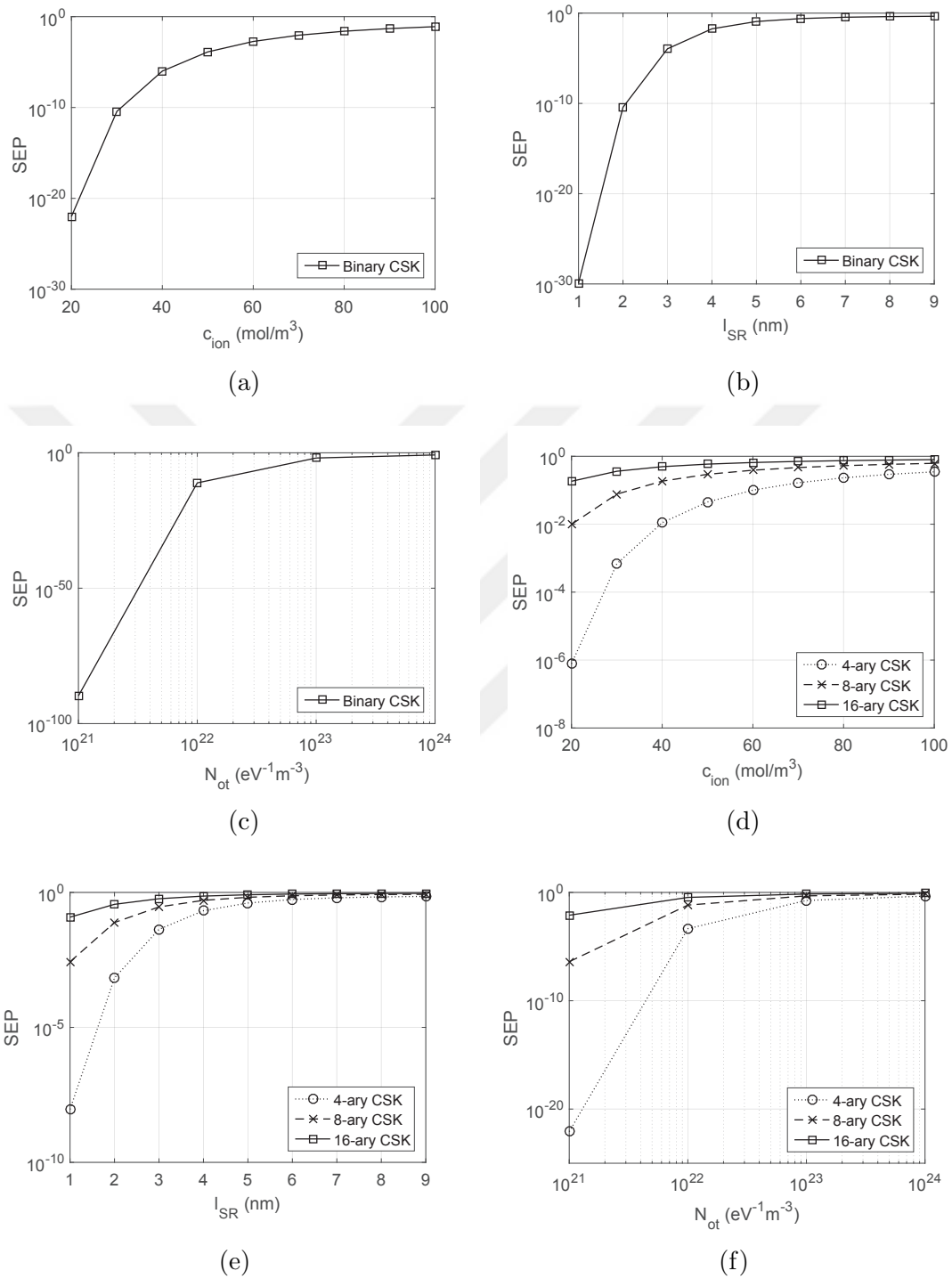


Figure 8.13: Symbol error probability (SEP) for M-CSK modulation. SEP as a function of (a, c) ion concentration c_{ion} of the electrolyte medium, (b, e) receptor length l_{SR}, (c, f) oxide trap density N_{ot} in SiNW.

Chapter 9

ON THE CAPACITY OF DIFFUSION-BASED MOLECULAR COMMUNICATIONS WITH SINW FET-BASED RECEIVER

9.1 Introduction

Molecular communication (MC) is a promising means of realizing nanonetworks and the Internet of nano-bio things (IoBNT), which could find breakthrough applications in several domains, such as continuous health monitoring and smart drug delivery [Akan et al., 2017], [Kuscu and Akan, 2016a]. This bio-inspired method is mainly based on the use of molecules to encode, transmit and receive information.

MC has been studied from several perspectives, including that of information theory [Pierobon and Akyildiz, 2013], [Nakano et al., 2012]. However, except for a few studies, the design of transceiving units and corresponding physical limitations have been largely neglected in the literature. There exist mainly two approaches to design MC transceivers. The first approach is to use synthetic biology techniques for designing artificial cells capable of transmitting and receiving molecular messages [Unluturk et al., 2015]. The second one is based on nanobioelectronic architectures which exploit the extraordinary properties of novel nanomaterials, such as nanowires and graphene, with a bio-inspired approach. In our recent review of design options for the MC receiver, we justify that nanobioelectronic designs are feasible and more convenient in most cases [Kuscu and Akan, 2016c]. Electrical output of a nanobioelectronic receiver provides the advantage of high-speed information processing, making the design more suitable for the complex communication schemes and protocols developed for MC [Nakano et al., 2012].

In [Kuscu and Akan, 2016b], we develop a communication theoretical model for a SiNW FET-based MC receiver and obtain the noise statistics. This nanobioelectronic design, shown in Fig. 9.1, is based on SiNW FET biosensors (bioFETs), which operate in a similar way to the conventional FETs. A SiNW bioFET consists of a biorecognition layer of surface receptors capable of binding the target ligands and a SiNW transducer channel which transduces the intrinsic charges of bound ligands into an electrical current flowing between the source and drain electrodes. In this paper, we develop an information theoretical model for a memoryless MC system equipped with the proposed SiNW FET-based MC receiver. We derive analytical closed-form expressions for the MC capacity and capacity-achieving input distribution, following the methodology of [Marzen et al., 2013]. The resulting expressions incorporate the effect of transmitter, channel and receiver parameters, and could be used for optimizing the information flow in MC systems including nanobioelectronic receivers.

The remainder of the paper is organized as follows. In Section II, we present the existing model of MC system with a SiNW FET-based receiver. The capacity is derived in Section III, and the results are provided in Section IV. Finally, the concluding remarks are given in Section V.

9.2 MC System Model

We consider a time-slotted MC system between a single transmitter nanomachine (TX) and a single receiver nanomachine (RX). TX and RX are assumed to be perfectly synchronized with each other in terms of time. Information is encoded into the number of molecules, i.e., ligands, released by the TX. The channel is assumed to be memoryless. This can be practically realized with a low symbol rate or using auxiliary enzymes degrading the residual molecules that cause inter-symbol interference (ISI).

The channel is assumed to be a free diffusion channel, where the trajectories of individual ligands are independent of each other. Thus, the ligand concentration as

a function of time and space can be expressed by the Fick's equation

$$\frac{\partial \rho(\vec{r},t)}{\partial t} = D\nabla^2 \rho(\vec{r},t), \tag{9.1}$$

where $\rho(\vec{r},t)$ is the ligand concentration at location $\vec{r}$ and time t, and D is the diffusion coefficient of the ligands. TX is assumed to be a point source located at the origin of 3D Cartesian coordinate system, i.e., $\vec{r_T} = (0,0,0)$. It releases N_{tx} number of molecules at the very beginning of a time slot. Thus, we can express the initial condition as $\rho(\vec{r},0) = N_{tx}\delta(\vec{r})$. Assuming that the distance d between the TX and RX surface is much higher than the largest dimension of the RX surface, we can consider that all of the surface receptors are at equal distance from TX, and thus, are exposed to the same ligand concentration, which can be obtained by solving the Fick's equation at the RX location with the initial condition imposed by the TX:

$$\rho(d,t) = \frac{N_{tx}}{(4\pi Dt)^{3/2}} \exp\left(-\frac{d^2}{4Dt}\right). \tag{9.2}$$

We assume that RX samples the occupation states of the receptors when the ligand concentration at the receiver location is at its maximum, which is the case when $t = \frac{d^2}{6D}$ [Llatser et al., 2011]. The corresponding maximum ligand concentration at the RX location is then given by

$$\rho_R = \left(\frac{3}{2\pi e}\right)^{3/2} \frac{N_{tx}}{d^3} = \alpha_{ch} \times N_{tx}, \tag{9.3}$$

where we define $\alpha_{ch} = (3/2\pi e)^{3/2} d^{-3}$ as the channel attenuation parameter.

The interaction of ligands with the surface receptors is governed by the ligand-receptor binding kinetics. Assuming steady-state conditions, the probability of finding a single receptor at the bound state is given by

$$P_b = \frac{k_1 \rho_R}{k_1 \rho_R + k_{-1}} = \frac{k_1 \alpha_{ch} N_{tx}}{k_1 \alpha_{ch} N_{tx} + k_{-1}}, \tag{9.4}$$

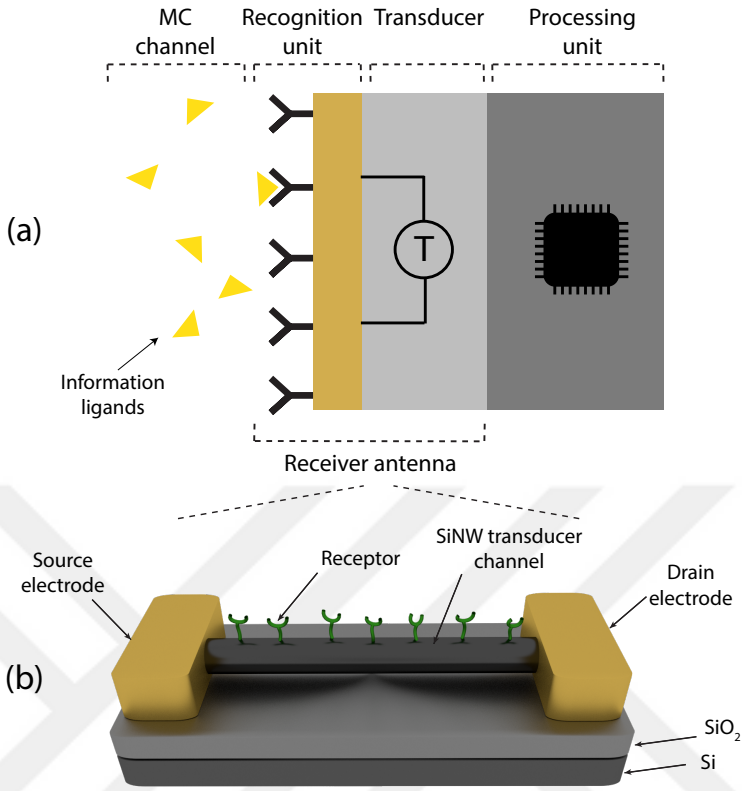


Figure 9.1: (a) Functional units of an MC receiver, and (b) SiNW FET-based MC receiver antenna.

where k_{-1} is the unbinding rate constant for the receptor-ligand pair; and k_1 is the binding rate constant in $m^3 s^{-1}$. Generalizing the results to the case with N_r receptors, and assuming that all of the receptors observe independent concentrations, the distribution of number of bound receptors becomes binomial [Berezhkovskii and Szabo, 2013]:

$$P(N_b = k) = \binom{N_r}{k} (P_b)^k (1 - P_b)^{N_r - k}, \tag{9.5}$$

with mean and variance given by

$$\mu_{N_b} = P_b N_r, \quad \sigma^2_{N_b} = P_b(1 - P_b)N_r. \tag{9.6}$$

Surface potential created on the NW-electrolyte interface as a result of binding of a single ligand is given as

$$\psi_L = (q_{eff} \times N_e^-)/C_{eq}, \tag{9.7}$$

where N_{e^-} is the number of free electrons per ligand molecule, and C_{eq} is the equivalent capacitance of the transducer. q_{eff} is the mean effective charge of a free ligand electron, which is degraded as the distance between the ligand electron and the transducer increases due to the Debye screening. The relation is given by $q_{eff} = q \times exp(-r/\lambda_D)$, where q is the elementary charge, and r is the average distance of ligand electrons in the bound state to the transducer's surface [Rajan et al., 2013], which is assumed to be equal to the average surface receptor length, i.e., $r = l_{SR}$. The Debye length, λ_D, quantizes the ionic strength of the medium according to

$$\lambda_D = \sqrt{\frac{\epsilon_M k_B T}{2 N_A q^2 c_{ion}}}, \tag{9.8}$$

where ϵ_M is the dielectric permittivity of the medium, k_B is the Boltzmann's constant, T is the temperature, N_A is Avogadro's number, and c_{ion} is the ionic concentration of the medium [Rajan et al., 2013]. The transducer capacitance is given by

$$C_{eq} = \left(\frac{1}{C_{ox}} + \frac{1}{C_{nw}}\right)^{-1} + C_{dl}, \tag{9.9}$$

where C_{dl} is the diffusion layer capacitance resulting from the double layer created by the medium counterions accumulated at the interface between oxide layer, i.e., SiO_2 layer, and the electrolyte medium; C_{ox} is the capacitance of the oxide layer; and C_{nw} is the SiNW capacitance, which is again a double layer capacitance caused by the accumulation of carriers to the SiO_2/SiNW interface [Gao et al., 2009], [Shoorideh and Chui, 2014].

For a nanowire-on-insulator (NWoI) configuration of RX, we can consider the SiNW as a hemicylinder with an oxide layer of thickness t_{ox} covering the surface, and

a diffusion layer of thickness λ_D covering the oxide layer [Shoorideh and Chui, 2014]. Accordingly, the diffusion layer capacitance can be given by $C_{dl} = (\epsilon_M/\lambda_D)w_R l_R$., where $w_R = \pi r_R$ is the effective width of SiNW with radius r_R, and l_R is the SiNW length. The oxide capacitance is given by $C_{ox} = C^s_{ox} w_R l_R = (\epsilon_{ox}/t_{ox})w_R l_R$, where ϵ_{ox} is the permittivity and the thickness of the oxide layer, respectively. We will use C^s_{ox} to denote the oxide capacitance per area. For high values of hole density, e.g., $p \sim 10^{18}$ cm^{-3}, corresponding to the linear operation regime of the FET, the C_{nw} is obtained as $C_{nw} = (\epsilon_{Si}/\lambda_{nw})w_R l_R$ [Gao et al., 2009] , where ϵ_{Si} is the dielectric permittivity of SiNW, and λ_{nw} is the thickness of the double layer created in the inner surface of the NW, which is given by $\lambda_{nw} = \sqrt{\epsilon_{Si} k_B T/pq^2}$.

The potential induced at the SiNW/oxide layer interface is reflected into the output current of the RX. We assume that the p-type FET is operated in the linear (Ohmic) region; thus, its transconductance is expressed by $g_{FET} = \mu_p C^s_{ox} V_{SD} w_R/l_R$, where $V_{SD} = -V_{DS}$ is the source to drain voltage of the SiNW FET. Given the transconductance, the output current, I_{rx}, resulting from the surface potential generated by the bound ligands is given as $I_{rx} = g_{FET}\psi_L N_b$, which has the mean

$$\mu_{I_{rx}} = g_{FET} \times \psi_L \times \mu_{N_b}. \tag{9.10}$$

The operation of bioFET-based MC receiver is suffered from $1/f$ noise. Based on *the correlated carrier number and mobility fluctuation model*, power spectral density (PSD) of the $1/f$ noise at the output current can be written as

$$S_{I^F_{rx}}(f) = S_{V,FB}(f) g^2_{FET} \left[1 + \alpha_s \mu_p C^s_{ox}(V_{SG} - |V_{TH}|)\right]^2, \tag{9.11}$$

where $V_{SG} = -V_{GS}$ is source to gate voltage, and V_T is the threshold voltage of the SiNW FET. α_s is the Coulomb scattering coefficient, and μ_p is the mobility of the hole carriers [Rajan et al., 2010b]. The PSD of the flatband-voltage noise $S_{V,FB}$ is

given by

$$S_{V,FB}(f) = \frac{\lambda k_B T q^2 N_{ot} g_{FET}^2}{w_R l_R (C_{ox}^s)^2 |f|}, \tag{9.12}$$

where λ is the characteristic tunneling distance, N_{ot} is the oxide trap density, i.e., impurity concentration, of the SiNW channel [Rajan et al., 2010b]. $1/f$ noise is independent of the received signals, and shows an additive behavior on the overall output current fluctuations. Theoretically, $1/f$ noise does not have a low frequency cutoff, and has infinite power at zero frequency. However, in experimental studies with a finite measurement time, a finite variance for $1/f$ noise is observed. The reason is related to the low frequency cutoff set by the observation time T_{obs} [Niemann et al., 2013]. Considering that the received molecular signals are at the baseband, to be able to calculate the total noise power, we assume one-year operation time, i.e., $\sim \pi \times 10^7$ s, for the antenna such that the low cutoff frequency is $f_L = 1/T_{obs} \approx 1/\pi \times 10^{-7}$ Hz. At frequencies lower than f_L, the noise is assumed to show the white noise behavior, i.e., $S_{I_{rx}^F}(f) = S_{I_{rx}^F}(f_L)$ for $|f| < f_L$.

$$\sigma_F^2 = \int_{-\infty}^{\infty} S_{I_{rx}^F}(f) df. \tag{9.13}$$

We can expect that a significant number of receptors, e.g. > 1000, are tethered to the top surface of a SiNW channel. For large number of surface receptors, the binomial distribution given in (9.5) can be approximated as Gaussian, i.e., $N_b \sim \mathcal{N}\left(\mu_{N_b}, \sigma_{N_b}^2\right)$. $1/f$ noise is resulting from the bias current flowing through SiNW channel, thus, it is independent of the binding noise. It can be approximated to follow a Gaussian distribution [Hooge and Hoppenbrouwers, 1969]. Therefore, the overall noise process effective on the output current becomes a stationary Gaussian process with the variance

$$\sigma_{I_{rx}}^2 = \sigma_F^2 + \sigma_{N_b}^2 g_{FET}^2 \psi_L^2. \tag{9.14}$$

9.3 Capacity

We consider the overall system as a continuous-input continuous-output memoryless channel. Although information is encoded into discrete number of molecules, we can assume that the input is continuous given that it takes values from a very large input range. Then, the mutual information between the transmitted signal N_{tx} and the received signal I_{rx} can be written as

$$\begin{aligned} I(N_{tx};I_{rx}) = &\int_{N_{tx}^{min}}^{N_{tx}^{max}} f_{N_{tx}}(x) \int_{-\infty}^{\infty} f_{I_{rx}|N_{tx}}(y|x) \log_2 f_{I_{rx}|N_{tx}}(y|x) dy dx \\ &- \int_{N_{tx}^{min}}^{N_{tx}^{max}} f_{N_{tx}}(x) \int_{-\infty}^{\infty} f_{I_{rx}|N_{tx}}(y|x) \log_2 f_{I_{rx}}(y) dy dx \end{aligned} \tag{9.15}$$

where N_{tx}^{min} and N_{tx}^{max} denote the minimum and maximum number of molecules that TX can transmit. The input probability distribution satisfies the condition $\int_{N_{tx}^{min}}^{N_{tx}^{max}} f_{N_{tx}}(x)dx = 1$. Based on the discussion at the end of Section 9.2, overall channel transition pdf $f_{I_{rx}|N_{tx}}$ can be given by

$$f_{I_{rx}|N_{tx}}(y|x) = \frac{1}{\sqrt{2\pi\sigma_{I_{rx}}^2}} e^{-\frac{\left(y-\mu_{I_{rx}}\right)^2}{2\sigma_{I_{rx}}^2}} \tag{9.16}$$

where $\mu_{I_{rx}}$ and $\sigma_{I_{rx}}^2$ are functions of $N_{tx} = x$, as given in (9.10) and (9.14). Given the Gaussian pdf, the first integral on the RHS of (9.15) is obtained as [Marzen et al., 2013]

$$\int_{-\infty}^{\infty} f_{I_{rx}|N_{tx}}(y|x) \log_2 f_{I_{rx}|N_{tx}}(y|x) dy = -\frac{1}{2} \log_2(2\pi e \sigma_{I_{rx}}^2). \tag{9.17}$$

We approximate the second integral on the RHS of (9.15) using Taylor series expansion of $\log_2 p(\mu_{I_{rx}})$ up to the second order [Marzen et al., 2013]:

$$\begin{aligned}
&\int_{-\infty}^{\infty} f_{I_{rx}|N_{tx}}(y|x) \log_2 f_{I_{rx}}(y) dy \\
&= \int_{-\infty}^{\infty} f_{I_{rx}|N_{tx}}(y|x) \log_2 f_{\mu}(\mu_{I_{rx}}) dy \\
&+ \int_{-\infty}^{\infty} f_{I_{rx}|N_{tx}}(y|x) \left. \frac{\partial \log_2 f_{I_{rx}}(y)}{\partial y} \right|_{\mu_{I_{rx}}} (I_{rx} - \mu_{I_{rx}}) dy \\
&+ \frac{1}{2} \int_{-\infty}^{\infty} f_{I_{rx}|N_{tx}}(y|x) \left. \frac{\partial^2 \log_2 f_{I_{rx}}(y)}{\partial y^2} \right|_{\mu_{I_{rx}}} (I_{rx} - \mu_{I_{rx}})^2 dy.
\end{aligned} \tag{9.18}$$

The first integral in (9.18) becomes

$$\begin{aligned}
&\int_{-\infty}^{\infty} f_{I_{rx}|N_{tx}}(y|x) \log_2 f_{\mu}(\mu_{I_{rx}}) dy \\
&\quad = \log_2 f_{\mu}(\mu_{I_{rx}}) \int_{-\infty}^{\infty} f_{I_{rx}|N_{tx}}(y|x) dy = \log_2 f_{\mu}(\mu_{I_{rx}}),
\end{aligned} \tag{9.19}$$

and the second integral translates into

$$\begin{aligned}
&\int_{-\infty}^{\infty} f_{I_{rx}|N_{tx}}(y|x) \left. \frac{\partial \log_2 f_{I_{rx}}(y)}{\partial y} \right|_{\mu_{I_{rx}}} (y - \mu_{I_{rx}}) dy \\
&= \left. \frac{\partial \log_2 f_{I_{rx}}(y)}{\partial y} \right|_{\mu_{I_{rx}}} \int_{-\infty}^{\infty} f_{I_{rx}|N_{tx}}(y - \mu_{I_{rx}}) dy = 0.
\end{aligned} \tag{9.20}$$

The third integral is simplified as follows

$$\begin{aligned}
&\int_{-\infty}^{\infty} f_{I_{rx}|N_{tx}}(y|x) \frac{1}{2} \left. \frac{\partial^2 \log_2 f_{I_{rx}}(y)}{\partial y^2} \right|_{\mu_{I_{rx}}} (y - \mu_{I_{rx}})^2 dy \\
&\quad = \frac{1}{2} \left. \frac{\partial^2 \log_2 f_{I_{rx}}(y)}{\partial y^2} \right|_{\mu_{I_{rx}}} \int_{-\infty}^{\infty} f_{I_{rx}|N_{tx}}(y|x)(y - \mu_{I_{rx}})^2 dy \\
&\quad = \frac{1}{2} \left. \frac{\partial^2 \log_2 f_{I_{rx}}(y)}{\partial y^2} \right|_{\mu_{I_{rx}}} \sigma^2_{I_{rx}} \approx 0.
\end{aligned} \tag{9.21}$$

The approximation in (9.21) follows from the fact that the variance is very small compared to the mean for the high values of the number of surface receptors [Kuscu and Akan, 2016b], [Marzen et al., 2013]. Using (9.19)-(9.21) we can approximate the second integral on the RHS of (9.15) as follows

$$\int_{-\infty}^{\infty} f_{I_{rx}|N_{tx}}(y|x) \log_2 f_{I_{rx}}(y) dy \approx \log_2 f_{\mu}(\mu_{I_{rx}}). \tag{9.22}$$

Since $\mu_{I_{rx}}$ is a deterministic and single valued function of N_{tx}, $f_{\mu}(\mu_{I_{rx}})$ can be written in terms of the input distribution $f_{N_{tx}}(x)$ as follows

$$f_{\mu}(\mu_{I_{rx}}) = f_{N_{tx}}(x) \frac{(x\alpha_{ch}k_1 + k_{-1})^2}{N_r M}, \tag{9.23}$$

where $M = \alpha_{ch} k_1 k_{-1} g_{FET} \psi_L$, and the mutual information becomes

$$\begin{aligned} I(N_{tx}; I_{rx}) = -\int_{N_{tx}^{min}}^{N_{tx}^{max}} f_{N_{tx}}(x) \Bigg(& \log_2 \sqrt{2\pi e \sigma^2_{I_{rx}}} \\ & + \log_2 f_{N_{tx}}(x) + \log_2 \left(\frac{(x\alpha_{ch}k_1 + k_{-1})^2}{N_r M} \right) \Bigg) dx. \end{aligned} \tag{9.24}$$

To find the capacity, the mutual information should be maximized over all in-

Table 9.1: Default Values of Simulation Parameters

Max number of ligands TN transmits (N_{tx}^{max})	10^9
Min number of ligands TN transmits (N_{tx}^{min})	10^8
Transmitter-receiver distance (d)	250 μm
Binding rate (k_1)	2×10^{-18} m^3/s
Unbinding rate (k_{-1})	10 s^{-1}
Average number of electrons in a ligand (N_e^-)	3
SiNW radius (r_R)	10 nm
Concentration of receptors on the surface (ρ_{SR})	4×10^{16} m^{-2}
Length of a surface receptor (l_{SR})	2 nm
Temperature (T)	300K
Relative permittivity of oxide layer (ϵ_{ox}/ϵ_0)	3.9
Relative permittivity of SiNW (ϵ_{NW}/ϵ_0)	11.68
Relative permittivity of medium (ϵ_R/ϵ_0)	78
Ionic strength of electrolyte medium (c_{ion})	30 mol/m^3
Source-drain voltage (V_{SD})	0.1 V
Source-gate voltage (V_{SG})	0.4 V
Threshold voltage (V_{TH})	0 V
Hole density in SiNW (p)	10^{18} cm^{-3}
Tunneling distance (λ)	0.05 nm
Thickness of oxide layer (t_{ox})	2 nm
Oxide trap density (N_{ot})	10^{16} eV^{-1}cm^{-3}
Effective mobility of hole carriers (μ_p)	500 cm^2/Vs
Coulomb scattering coefficient (α_s)	1.9×10^{14} Vs/C

put distributions satisfying $\int_{N_{tx}^{min}}^{N_{tx}^{max}} f_{N_{tx}}(x)dx = 1$. We use the method of Lagrange multipliers defining the Lagrange function as

$$I_L \equiv I(N_{tx}; I_{rx}) - \lambda \left(\int_{N_{tx}^{min}}^{N_{tx}^{max}} f_{N_{tx}}(x)dx - 1 \right), \tag{9.25}$$

where λ is the Lagrange multiplier. The input distribution $f_{N_{tx}}^*$ maximizing I_L is then found by functional derivative

$$\left. \frac{\partial I_L}{\partial f_{N_{tx}}(x)} \right|_{f_{N_{tx}} = f_{N_{tx}}^*} = 0, \tag{9.26}$$

which gives

$$f_{N_{tx}}^*(x) \times \sqrt{2\pi e \sigma_{I_{rx}}^2} \times \frac{(x\alpha_{ch}k_1 + k_{-1})^2}{N_r M} \times e \times 2^{\lambda} = 1. \tag{9.27}$$

Combining the terms independent of x into a normalization factor K, we can write the optimal distribution as follows

$$f_{N_{tx}}^*(x) = \frac{1}{K\sigma_{I_{rx}}(\alpha_{ch}k_1 x + k_{-1})^2}. \tag{9.28}$$

The normalization factor K can then be obtained as

$$\begin{aligned} K =& \int_{N_{tx}^{min}}^{N_{tx}^{max}} \frac{dx}{\sigma_{I_{rx}}(\alpha_{ch}k_1 x + k_{-1})^2} \\ =& \frac{1}{M\sqrt{N_r}} \left[\sin^{-1}\left(L \frac{N_{tx}^{max} - k_D/\alpha_{ch}}{N_{tx}^{max} + k_D/\alpha_{ch}} \right) \right. \\ & \left. - \sin^{-1}\left(L \frac{N_{tx}^{min} - k_D/\alpha_{ch}}{N_{tx}^{min} - k_D/\alpha_{ch}} \right) \right], \end{aligned} \tag{9.29}$$

where we define

$$L = \sqrt{\frac{g_{FET}^2 \psi_L^2 N_r}{4\sigma_F^2 + g_{FET}^2 \psi_L^2 N_r}}. \tag{9.30}$$

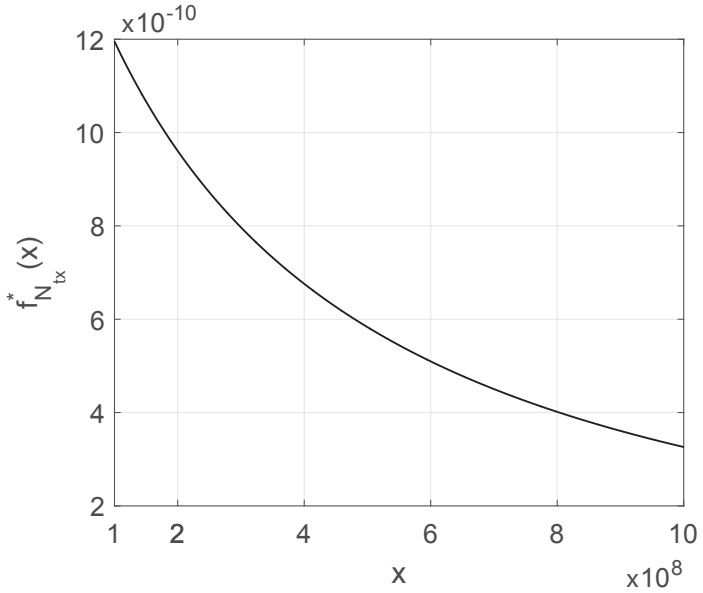


Figure 9.2: Capacity-achieving input distribution with $N_{tx}^{min} = 10^8$ and $N_{tx}^{max} = 10^9$.

Substituting $f^*_{N_{tx}}(x)$ into (9.24), we obtain the capacity, in bits per use, as follows

$$\begin{aligned} C =& \frac{1}{2}\log_2\frac{N_r}{2\pi e} + \log_2\Bigg[\sin^{-1}\left(L\frac{N_{tx}^{max} - k_D/\alpha_{ch}}{N_{tx}^{max} + k_D/\alpha_{ch}}\right) \\ & - \sin^{-1}\left(L\frac{N_{tx}^{min} - k_D/\alpha_{ch}}{N_{tx}^{min} - k_D/\alpha_{ch}}\right)\Bigg]. \end{aligned} \tag{9.31}$$

9.4 Results

In this section, we investigate the characteristics of the capacity-achieving input distribution and the effect of main system parameters on the capacity. The default values for the controllable parameters used in the analyses are listed in Table 9.1. The overall setting is the same as that used in [Kuscu and Akan, 2016b].

The capacity-achieving input distribution $f^*_{N_{tx}}$ is demonstrated in Fig. 9.2. As expected, the distribution is more focused around the minimum number of molecules N_{tx}^{max} TX transmits, which results in a less amount of noise in the receiver's electrical output.

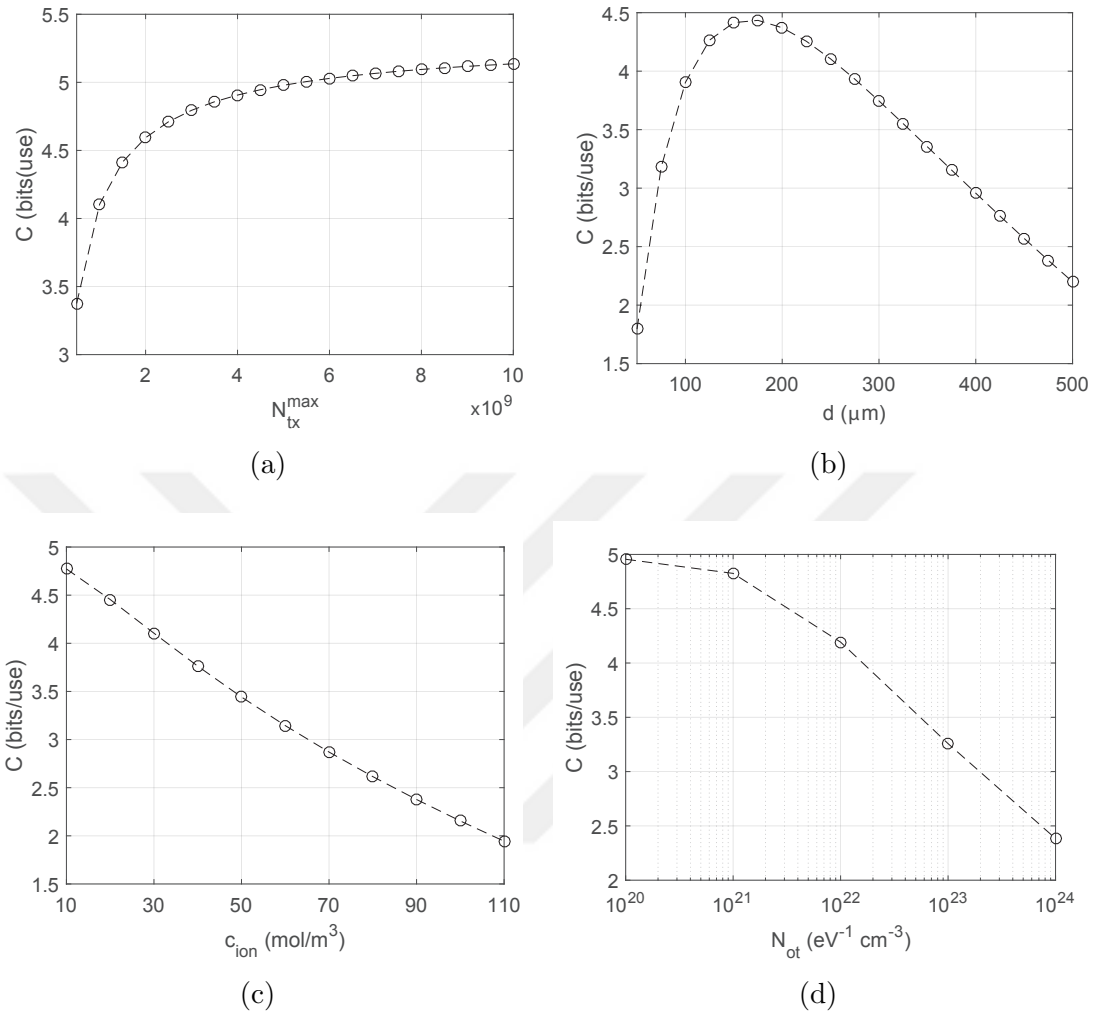


Figure 9.3: Capacity with (a) varying maximum number N_{tx}^{max} of transmitted molecules, (b) varying TX-RX distance d, (c) varying ionic concentration c_{ion}, and (d) varying oxide trap density N_{ot}.

Next, we analyze the relation between the upper limit N_{tx}^{max} of transmitted molecules and the capacity. As is seen in Fig. 9.3a, the capacity significantly increases with the increasing N_{tx}^{max} until it begins to saturate around 5 bits/use. This is originating from the fact that the receiver has a finite number of molecules; thus, it becomes saturated when $\rho_R \gg K_D$, resulting in a reduced receiver sensitivity. Therefore, transmitting more molecules to increase the ligand concentration at the receiver location is not favorable when the receiver is saturated.

The second analysis is carried out for varying TX-RX distance. As demonstrated in Fig. 9.3b, the capacity is maximum at intermediate distances, e.g., $d \approx 150$ μm, and begins to decrease when the distance is below or above this range. For a given N_{tx}^{max}, as the distance gets smaller, the receiver begins to operate near saturation because ρ_R significantly increases when the transmitter and receiver are close to each other. This is reflected to the output current, and results in a decrease in the sensitivity of the receiver so that it cannot discriminate different levels of ligand concentration corresponding to different symbols. As a result, the capacity decreases. For large distances, the ligand concentration gets significantly attenuated in the channel, thus, the signal-to-noise ratio (SNR) decreases [Kuscu and Akan, 2016b], resulting in a lower capacity.

The ionic strength of the fluidic medium also substantially affects the capacity, as is seen in Fig. 9.3c. The Debye length λ_D decreases with the increasing ionic concentration, implying more effective screening of ligand charges. This in turn reduces the SNR, and thus, the capacity. Physiological conditions generally imply ionic concentrations higher than 100 mol/m^3. To compensate the attenuation of capacity, surface receptors with lengths comparable to Debye length should be selected.

Lastly, we analyze the capacity for varying oxide trap density N_{ot}, which is proportional to the impurity of the SiNW. Trap density affects the carrier mobility, and increases the $1/f$ noise. The negative effect of increasing trap density on the capacity is evident from Fig. 9.3d.

9.5 Conclusion

In this chapter, we develop an information theoretical model for a memoryless MC system equipped with a SiNW FET-based MC receiver, and derive analytical closed-form expressions for the capacity and capacity-achieving input distribution. The provided expressions enable the analysis of the effect of nanobioelectronic receiver parameters on the MC system capacity, and reveal the optimization pathways that can be targeted to improve reliability of the overall communication system.

Chapter 10

CONCLUSION

This thesis is focused on a wide range of topics in the emerging field of nanoscale communications and nanonetworks and Internet of Bio-Nano Things. A novel nanoscale communication method, which is based on the well known photophysical phenomenon of Fr̈ster Resonance Energy Transfer (FRET), is thoroughly studied as a communication mechanism between fluorophore-based molecular devices through encoding information into the electronic states of molecules. Two different FRET-based mobile ad hoc sensor-actor nanonetwork architectures are proposed, and their coverage and throughput performances are examined. The use of Graphene Plasmons as mediators of FRET-based information transfer between two Quantum Dots (QDs) is proposed, and an end-to-end channel model for its information theoretical analysis is developed. In another part of the thesis, wireless high-rate data transfer between fluorescent molecules is experimentally demonstrated, proving the feasibility of wireless communications at nanoscale, for the first time in the literature. These studies underlined the potential and practicality of FRET as a high-rate and reliable nanocommunication method among molecular scale devices, and all of them have opened new research avenues in this emerging field.

This thesis is also focused on a bio-inspired nanoscale communication technique: molecular communications, with a particular emphasis on the design of bio-cyber interfaces between the molecular domain of nanonetworks and the electrical domain of macroscale conventional networks towards realizing the Internet of Bio-Nano Things. The state-of-the-art nanoscale biosensing methods suitable for the implementation of a molecular receiver antenna is reviewed and the fundamental design criteria along with corresponding challenges and future research avenues in this direction is out-

lined. Moreover, a comprehensive analytical model for Silicon Nanowire Field Effect Transistor (SiNW FET)-based molecular receiver antenna is developed to provide an optimization framework for molecular communications with bioFET receivers. Furthermore, the information theoretical capacity of a molecular communication system with a SiNW bioFET receiver is analytically derived and analyzed.

The detailed conclusion reached in the chapters is given in the following.

10.1 A Communication Theoretical Analysis of FRET-Based Mobile Ad Hoc Molecular Nanonetworks

In this chapter, based on our recent studies, we introduce FRET-based mobile molecular nanonetworks for the first time in the literature. We present continuous time Markov chain models for FRET-based mobile molecular sensor and actor networks (FRET-MSAN) and FRET-based mobile ad hoc molecular networks (FRET-MAMNET) benefiting from birth-death processes. We analyze the performance of both nanonetworks in terms of reliable transmission probability, message transmission delay, system throughput, mutual information, information theoretical channel capacity and achievable rates assuming that the network nodes satisfy the rapid-diffusion criterion. The simulation results reveal that it is possible to achieve reliable communication at high-rates with FRET-based mobile molecular networks.

10.2 Coverage and Throughput Analysis for FRET-Based Mobile Molecular Sensor/Actor Nanonetworks

In this chapter, we analyze the fundamental spatial properties of information propagation in FRET-MSAN performing extensive Monte Carlo simulations. We investigate the effect of main system parameters on the coverage, network throughput and propagation rate, and conclude that the exciton mobility can be described by the FRET mechanism rather than the diffusion of network nodes. We show that excitons signaling the existence of a single target molecule can rapidly propagate and activate actor nodes over significant distances compared to their sizes when the system parameters

are properly set.

10.3 An Information-Theoretic Model and Analysis of Graphene Plasmon-Assisted FRET-Based Nanocommunication Channel

In this chapter, we propose and analysis an FRET-based nanocommunication channel exploiting graphene plasmons as the intermediaries for information transfer. We analyze the performance of the channel with varying channel parameters by means of information theoretical capacity, and theoretically prove that the reliable communication range can be extended to distances over 500nm with an acceptable communication rates by properly selecting configuring the system parameters.

10.4 Fluorescent Molecules as Transceiver Nanoantennas: The First Practical and High-Rate Information Transfer over a Nanoscale Communication Channel based on FRET

In this chapter, we realise the first data transfer exploiting FRET as a communication means at nanoscale. We implemente a practical communication system in which macroscale devices are connected over a nanoscale MIMO communication channel between fluorophore-based nanoantennas. The performance of the channel is evaluated by transmitting pseudorandom binary bit sequences and observing the resultant BER and SNR for different transmission rates. The experiments reveal that the FRET-based communication channel provides acceptable reliability for nanonetworks up to 150kbps transmission rates, even when the location of nanoantennas are not fully controllable.

10.5 The Internet of Molecular Things Based on FRET

Developing networks of molecular-scale devices possessing very limited operational capabilities necessitates radically different communication strategies than the prominent nanonetworking approaches. In this chapter, we review the theoretical and

experimental positions toward realizing the internet of fluorophore-based molecular devices based on FRET. We present an overview of the basic principles and design requirements of FRET-based nanocommunications, its networking opportunities and prospective applications including molecular-scale information processing and cooperative sensing/actuating for disease treatment. Main implementation challenges, e.g., low photostability of fluorophores and sampling rate limitations of single molecular experiments, along with the possible solution pathways are discussed.

10.6 On the Physical Design of Molecular Communication Receiver Based on Nanoscale Biosensors

In this chapter, physical design of a molecular receiver is elaborated for the first time in the literature. Detection of messages in a molecular communication system mandates the label-free and *in situ* sensing of molecules. A comprehensive review of the state-of-the-art biosensing methods reveal that the basic requirements of a molecular receiver can be met only with a design in nanobioelectronic domain. FET-based biosensing mechanism is particularly favoured as the underlying mechanism of a nanobioelectronic molecular receiver due to the fast, reversible and simple operation with a plethora of engineering options. We conceptually present the main operation principles of a FET-based molecular receiver together with the performance metrics and design parameters. We provide a deterministic model for a SiNW FET-based MC receiver, and evaluate the reception performance in terms of sensitivity. These preliminary results demonstrating the reliable reception of molecular messages are encouraging for the further development of MC receiver in nanobioelectronic domain. We address the practical challenges with possible solution approaches. Future research avenues include the derivation of an improved analytical model for the receiver operation comprising the transient kinetics of molecular binding and transportation dynamics, optimization of the receiver performance for the envisioned applications through simulations and experiments, development of optimal detection schemes, and the integration of the receiver into a nanomachine.

10.7 Modeling and Analysis of SiNW FET-Based Molecular Communication Receiver

In this chapter, as the first step towards implementing a human-made MC system with nanobioelectronic devices, we develop a communication theoretical model for SiNW FET-based MC receivers integrating all the underlying processes in MC and bioFET operation. Focusing on a microfluidic MC system, we derive closed-form expressions for fundamental performance metrics, such as SNR and SEP, to provide an analysis and optimization framework for MC with nanobioelectronic receivers. The results of performance evaluation point out several optimization pathways that need to be taken to improve the detection performance of the receiver. The developed model can be extended to incorporate the transient dynamics of MC and bioFETs for enabling analysis also in the frequency domain. Open issues include the design of optimal constellations and optimal receiver detection schemes for MC systems equipped with bioFET receivers. Further research on devising nanobioelectronic MC receivers could enable the implementation of all the theoretical protocols and algorithms designed for reliable and efficient MC and the development of seamless interfaces between MC nanonetworks and macroscale networks towards realizing IoBNT.

10.8 On the Capacity of Diffusion-Based Molecular Communications with SiNW FET-Based Receiver

In this chapter, we develop an information theoretical model for a memoryless MC system equipped with a SiNW FET-based MC receiver, and derive analytical closed-form expressions for the capacity and capacity-achieving input distribution. The provided expressions enable the analysis of the effect of nanobioelectronic receiver parameters on the MC system capacity, and reveal the optimization pathways that can be targeted to improve reliability of the overall communication system.

BIBLIOGRAPHY

[Ackermann et al., 2010] Ackermann, D., Schmidt, T. L., Hannam, J. S., Purohit, C. S., Heckel, A., and Famulok, M. (2010). A double-stranded dna rotaxane. *Nature nanotechnology*, 5(6):436–442.

[Akan et al., 2017] Akan, O. B., Ramezani, H., Khan, T., Abbasi, N. A., and Kuscu, M. (2017). Fundamentals of molecular information and communication science. *Proceedings of the IEEE*, 105(2):306–318.

[Akyildiz et al., 2015] Akyildiz, I., Pierobon, M., Balasubramaniam, S., and Koucheryavy, Y. (2015). The internet of bio-nano things. *IEEE Communications Magazine*, 53(3):32–40.

[Akyildiz et al., 2008] Akyildiz, I. F., Brunetti, F., and Blázquez, C. (2008). Nanonetworks: A new communication paradigm. *Computer Networks*, 52(12):2260–2279.

[Akyildiz and Jornet, 2010a] Akyildiz, I. F. and Jornet, J. M. (2010a). Electromagnetic wireless nanosensor networks. *Nano Communication Networks*, 1(1):3–19.

[Akyildiz and Jornet, 2010b] Akyildiz, I. F. and Jornet, J. M. (2010b). The internet of nano-things. *IEEE Wireless Communications*, 17(6).

[Akyildiz et al., 2011] Akyildiz, I. F., Jornet, J. M., and Pierobon, M. (2011). Nanonetworks: A new frontier in communications. *Communications of the ACM*, 54(11):84–89.

[Akyildiz et al., 2002] Akyildiz, I. F., Su, W., Sankarasubramaniam, Y., and Cayirci, E. (2002). A survey on sensor networks. *IEEE Communications magazine*, 40(8):102–114.

[Allen et al., 2007] Allen, B. L., Kichambare, P. D., and Star, A. (2007). Carbon nanotube field-effect-transistor-based biosensors. *Advanced Materials*, 19(11):1439–1451.

[Allen and Blinks, 1978] Allen, D. G. and Blinks, J. R. (1978). Calcium transients in aequorin-injected frog cardiac muscle. *Nature*, 273(5663):509–513.

[Ashton et al., 1998] Ashton, P. R., Ballardini, R., Balzani, V., Baxter, I., Credi, A., Fyfe, M. C., Gandolfi, M. T., Gómez-López, M., Martínez-Díaz, M.-V., Piersanti, A., et al. (1998). Acid- base controllable molecular shuttles. *Journal of the American Chemical Society*, 120(46):11932–11942.

[Atakan and Akan, 2008] Atakan, B. and Akan, Ö. B. (2008). On channel capacity and error compensation in molecular communication. *Trans. Computational Systems Biology*, 10:59–80.

[Badali and Gradinaru, 2011] Badali, D. and Gradinaru, C. C. (2011). The effect of brownian motion of fluorescent probes on measuring nanoscale distances by förster resonance energy transfer. *The Journal of chemical physics*, 134(22):06B604.

[Balasubramaniam and Kangasharju, 2013] Balasubramaniam, S. and Kangasharju, J. (2013). Realizing the internet of nano things: challenges, solutions, and applications. *Computer*, 46(2):62–68.

[Balasubramaniam et al., 2014] Balasubramaniam, S., Lyamin, N., Kleyko, D., Skurnik, M., Vinel, A., and Koucheryavy, Y. (2014). Exploiting bacterial properties for multi-hop nanonetworks. *IEEE Communications Magazine*, 52(7):184–191.

[Bang et al., 2008] Bang, G. S., Chang, H., Koo, J.-R., Lee, T., Advincula, R. C., and Lee, H. (2008). High-fidelity formation of a molecular-junction device using a thickness-controlled bilayer architecture. *Small*, 4(9):1399–1405.

[Becker et al., 2006] Becker, K., Lupton, J. M., Müller, J., Rogach, A. L., Talapin, D. V., Weller, H., and Feldmann, J. (2006). Electrical control of förster energy transfer. *Nature materials*, 5(10):777–781.

[Bell, 1955] Bell, D. (1955). Distribution function of semiconductor noise. *Proceedings of the Physical Society. Section B*, 68(9):690.

[Berezhkovskii and Szabo, 2013] Berezhkovskii, A. M. and Szabo, A. (2013). Effect of ligand diffusion on occupancy fluctuations of cell-surface receptors. *The Journal of chemical physics*, 139(12):09B610_1.

[Berney and Danuser, 2003] Berney, C. and Danuser, G. (2003). Fret or no fret: a quantitative comparison. *Biophysical journal*, 84(6):3992–4010.

[Bialek and Setayeshgar, 2005] Bialek, W. and Setayeshgar, S. (2005). Physical limits to biochemical signaling. *Proceedings of the National Academy of Sciences of the United States of America*, 102(29):10040–10045.

[Bicen and Akyildiz, 2013] Bicen, A. O. and Akyildiz, I. F. (2013). System-theoretic analysis and least-squares design of microfluidic channels for flow-induced molecular communication. *IEEE Transactions on Signal Processing*, 61(20):5000–5013.

[Bicen and Akyildiz, 2014] Bicen, A. O. and Akyildiz, I. F. (2014). End-to-end propagation noise and memory analysis for molecular communication over microfluidic channels. *IEEE Transactions on Communications*, 62(7):2432–2443.

[Bicen and Akyildiz, 2015] Bicen, A. O. and Akyildiz, I. F. (2015). Interference modeling and capacity analysis for microfluidic molecular communication channels. *IEEE Transactions on Nanotechnology*, 14(3):570–579.

[Bonnett, 1995] Bonnett, R. (1995). Photosensitizers of the porphyrin and phthalocyanine series for photodynamic therapy. *Chemical Society Reviews*, 24(1):19–33.

[Browne and Feringa, 2006] Browne, W. R. and Feringa, B. L. (2006). Making molecular machines work. *Nature nanotechnology*, 1(1):25–35.

[Bruus, 2007] Bruus, H. (2007). *Theoretical microfluidics*. Oxford university press Oxford.

[Bulgarini et al., 2012] Bulgarini, G., Reimer, M. E., Hocevar, M., Bakkers, E. P., Kouwenhoven, L. P., and Zwiller, V. (2012). Avalanche amplification of a single exciton in a semiconductor nanowire. *Nature Photonics*, 6(7):455–458.

[Cantrell, 1996] Cantrell, D. (1996). T cell antigen receptor signal transduction pathways. *Annual review of immunology*, 14(1):259–274.

[Caré and Soula, 2011] Caré, B. R. and Soula, H. A. (2011). Impact of receptor clustering on ligand binding. *BMC Systems Biology*, 5(1):48.

[Chen et al., 2011] Chen, K.-I., Li, B.-R., and Chen, Y.-T. (2011). Silicon nanowire field-effect transistor-based biosensors for biomedical diagnosis and cellular recording investigation. *Nano Today*, 6(2):131–154.

[Chou, 2013] Chou, C. T. (2013). Extended master equation models for molecular communication networks. *IEEE transactions on nanobioscience*, 12(2):79–92.

[Chou, 2015] Chou, C. T. (2015). A markovian approach to the optimal demodulation of diffusion-based molecular communication networks. *IEEE Transactions on Communications*, 63(10):3728–3743.

[Church et al., 2014] Church, G. M., Elowitz, M. B., Smolke, C. D., Voigt, C. A., and Weiss, R. (2014). Realizing the potential of synthetic biology. *Nature Reviews Molecular Cell Biology*, 15(4):289–294.

[Cinlar, 2013] Cinlar, E. (2013). *Introduction to stochastic processes*. Courier Corporation.

[Clapp et al., 2006] Clapp, A. R., Medintz, I. L., and Mattoussi, H. (2006). Förster resonance energy transfer investigations using quantum-dot fluorophores. *ChemPhysChem*, 7(1):47–57.

[Compton and O'Grady, 1991] Compton, B. J. and O'Grady, E. A. (1991). Role of charge suppression and ionic strength in free zone electrophoresis of proteins. *Analytical chemistry*, 63(22):2597–2602.

[Contag and Bachmann, 2002] Contag, C. H. and Bachmann, M. H. (2002). Advances in in vivo bioluminescence imaging of gene expression. *Annual review of biomedical engineering*, 4(1):235–260.

[Cosa, 2013] Cosa, G. (2013). Single-molecule fluorescence: Assembling nanoantennas. *Nature chemistry*, 5(3):159–160.

[Cover and Thomas, 2012] Cover, T. M. and Thomas, J. A. (2012). *Elements of information theory*. John Wiley & Sons.

[Credi, 2007] Credi, A. (2007). Molecules that make decisions. *Angewandte Chemie International Edition*, 46(29):5472–5475.

[Curreli et al., 2008] Curreli, M., Zhang, R., Ishikawa, F. N., Chang, H.-K., Cote, R. J., Zhou, C., and Thompson, M. E. (2008). Real-time, label-free detection of biological entities using nanowire-based fets. *IEEE Transactions on Nanotechnology*, 7(6):651–667.

[Cusido et al., 2009] Cusido, J., Deniz, E., and Raymo, F. M. (2009). Fluorescent switches based on photochromic compounds. *European Journal of Organic Chemistry*, 2009(13):2031–2045.

[Daniels and Pourmand, 2007] Daniels, J. S. and Pourmand, N. (2007). Label-free impedance biosensors: Opportunities and challenges. *Electroanalysis*, 19(12):1239–1257.

[Das et al., 2009] Das, S., Vikalo, H., and Hassibi, A. (2009). On scaling laws of biosensors: a stochastic approach. *Journal of Applied Physics*, 105(10):102021.

[de Silva et al., 2001] de Silva, A. P., Fox, D. B., Moody, T. S., and Weir, S. M. (2001). The development of molecular fluorescent switches. *TRENDS in Biotechnology*, 19(1):29–34.

[De Silva et al., 1997] De Silva, A. P., Gunaratne, H. N., Gunnlaugsson, T., Huxley, A. J., McCoy, C. P., Rademacher, J. T., and Rice, T. E. (1997). Signaling recognition events with fluorescent sensors and switches. *Chemical Reviews*, 97(5):1515–1566.

[De Silva and Uchiyama, 2007] De Silva, A. P. and Uchiyama, S. (2007). Molecular logic and computing. *Nature Nanotechnology*, 2(7):399–410.

[Deen et al., 2006] Deen, M., Shinwari, M., Ranuárez, J., and Landheer, D. (2006). Noise considerations in field-effect biosensors. *Journal of applied physics*, 100(7):074703.

[Dichtel et al., 2004] Dichtel, W. R., Serin, J. M., Edder, C., Fréchet, J. M., Matuszewski, M., Tan, L.-S., Ohulchanskyy, T. Y., and Prasad, P. N. (2004). Singlet oxygen generation via two-photon excited fret. *Journal of the American Chemical Society*, 126(17):5380–5381.

[Dolmans et al., 2003] Dolmans, D. E., Fukumura, D., and Jain, R. K. (2003). Photodynamic therapy for cancer. *Nature reviews cancer*, 3(5):380–387.

[Duan et al., 2012] Duan, X., Li, Y., Rajan, N. K., Routenberg, D. A., Modis, Y., and Reed, M. A. (2012). Quantification of the affinities and kinetics of protein interactions using silicon nanowire biosensors. *Nature nanotechnology*, 7(6):401–407.

[Ecik et al., 2014] Ecik, E. T., Atilgan, A., Guliyev, R., Uyar, T. B., Gumus, A., and Akkaya, E. U. (2014). Modular logic gates: cascading independent logic gates via metal ion signals. *Dalton Transactions*, 43(1):67–70.

[Elangovan et al., 2003] Elangovan, M., Wallrabe, H., Chen, Y., Day, R. N., Barroso, M., and Periasamy, A. (2003). Characterization of one-and two-photon excitation fluorescence resonance energy transfer microscopy. *Methods*, 29(1):58–73.

[Elias et al., 2013] Elias, D. R., Poloukhtine, A., Popik, V., and Tsourkas, A. (2013). Effect of ligand density, receptor density, and nanoparticle size on cell targeting. *Nanomedicine: nanotechnology, biology and medicine*, 9(2):194–201.

[Elnathan et al., 2012] Elnathan, R., Kwiat, M., Pevzner, A., Engel, Y., Burstein, L., Khatchtourints, A., Lichtenstein, A., Kantaev, R., and Patolsky, F. (2012). Biorecognition layer engineering: overcoming screening limitations of nanowire-based fet devices. *Nano letters*, 12(10):5245–5254.

[Empedocles and Bawendi, 1997] Empedocles, S. A. and Bawendi, M. G. (1997). Quantum-confined stark effect in single cdse nanocrystallite quantum dots. *Science*, 278(5346):2114–2117.

[Erbas-Cakmak and Akkaya, 2013] Erbas-Cakmak, S. and Akkaya, E. U. (2013). Cascading of molecular logic gates for advanced functions: A self-reporting, activatable photosensitizer. *Angewandte Chemie International Edition*, 52(43):11364–11368.

[Fan et al., 2008] Fan, X., White, I. M., Shopova, S. I., Zhu, H., Suter, J. D., and Sun, Y. (2008). Sensitive optical biosensors for unlabeled targets: A review. *analytica chimica acta*, 620(1):8–26.

[Farsad et al., 2013] Farsad, N., Guo, W., and Eckford, A. W. (2013). Tabletop molecular communication: Text messages through chemical signals. *PloS one*, 8(12):e82935.

[Förster, 1948] Förster, T. (1948). Zwischenmolekulare energiewanderung und fluoreszenz. *Annalen der physik*, 437(1-2):55–75.

[Fritz et al., 2002] Fritz, J., Cooper, E. B., Gaudet, S., Sorger, P. K., and Manalis, S. R. (2002). Electronic detection of dna by its intrinsic molecular charge. *Proceedings of the National Academy of sciences*, 99(22):14142–14146.

[Gao et al., 2011] Gao, A., Lu, N., Dai, P., Li, T., Pei, H., Gao, X., Gong, Y., Wang, Y., and Fan, C. (2011). Silicon-nanowire-based cmos-compatible field-effect transistor nanosensors for ultrasensitive electrical detection of nucleic acids. *Nano letters*, 11(9):3974–3978.

[Gao et al., 2009] Gao, X. P., Zheng, G., and Lieber, C. M. (2009). Subthreshold regime has the optimal sensitivity for nanowire fet biosensors. *Nano letters*, 10(2):547–552.

[Georgakopoulou et al., 2015] Georgakopoulou, K., Birbas, A., and Spathis, C. (2015). Modeling of fluctuation processes on the biochemically sensorial surface of silicon nanowire field-effect transistors. *Journal of Applied Physics*, 117(10):104505.

[Giné and Akyildiz, 2009] Giné, L. P. and Akyildiz, I. F. (2009). Molecular communication options for long range nanonetworks. *Computer Networks*, 53(16):2753–2766.

[Goldstein et al., 1999] Goldstein, B., Coombs, D., He, X., Pineda, A. R., and Wofsy, C. (1999). The influence of transport on the kinetics of binding to surface receptors: Applications to cells and biacore. *Journal of Molecular Recognition*, 12(5):293–299.

[Gordon et al., 1998] Gordon, G. W., Berry, G., Liang, X. H., Levine, B., and Herman, B. (1998). Quantitative fluorescence resonance energy transfer measurements using fluorescence microscopy. *Biophysical journal*, 74(5):2702–2713.

[Grieshaber et al., 2008] Grieshaber, D., MacKenzie, R., Voeroes, J., and Reimhult, E. (2008). Electrochemical biosensors-sensor principles and architectures. *Sensors*, 8(3):1400–1458.

[Gul et al., 2010] Gul, E., Atakan, B., and Akan, O. B. (2010). Nanons: A nanoscale network simulator framework for molecular communications. *Nano Communication Networks*, 1(2):138–156.

[Gulbahar and Akan, 2012] Gulbahar, B. and Akan, O. B. (2012). A communication theoretical modeling of single-layer graphene photodetectors and efficient multireceiver diversity combining. *IEEE Transactions on Nanotechnology*, 11(3):601–610.

[Ha, 2001] Ha, T. (2001). Single-molecule fluorescence resonance energy transfer. *Methods*, 25(1):78–86.

[Hardin et al., 2009] Hardin, B. E., Hoke, E. T., Armstrong, P. B., Yum, J.-H., Comte, P., Torres, T., Fréchet, J. M., Nazeeruddin, M. K., Grätzel, M., and McGehee, M. D. (2009). Increased light harvesting in dye-sensitized solar cells with energy relay dyes. *Nature Photonics*, 3(7):406–411.

[Hassibi et al., 2007] Hassibi, A., Vikalo, H., and Hajimiri, A. (2007). On noise processes and limits of performance in biosensors. *Journal of applied physics*, 102(1):014909.

[Hassibi et al., 2005] Hassibi, A., Zahedi, S., Navid, R., Dutton, R. W., and Lee, T. H. (2005). Biological shot-noise and quantum-limited signal-to-noise ratio in affinity-based biosensors. *Journal of Applied Physics*, 97(8):084701.

[Hediger et al., 2012] Hediger, M. R., Jensen, J. H., and De Vico, L. (2012). Biofetsim web interface: Implementation and two applications. *PloS one*, 7(10):e45379.

[Heilemann et al., 2004] Heilemann, M., Tinnefeld, P., Sanchez Mosteiro, G., Garcia Parajo, M., Van Hulst, N. F., and Sauer, M. (2004). Multistep energy transfer in single molecular photonic wires. *Journal of the American Chemical Society*, 126(21):6514–6515.

[Heitzinger et al., 2008] Heitzinger, C., Kennell, R., Klimeck, G., Mauser, N., McLennan, M., and Ringhofer, C. (2008). Modeling and simulation of field-effect biosensors (biofets) and their deployment on the nanohub. In *Journal of Physics: Conference Series*, volume 107, page 012004. IOP Publishing.

[Hell, 2009] Hell, S. W. (2009). Microscopy and its focal switch. *Nature methods*, 6(1):24–32.

[Hilderbrand and Weissleder, 2010] Hilderbrand, S. A. and Weissleder, R. (2010). Near-infrared fluorescence: application to in vivo molecular imaging. *Current opinion in chemical biology*, 14(1):71–79.

[Hogg and Freitas Jr, 2012] Hogg, T. and Freitas Jr, R. A. (2012). Acoustic communication for medical nanorobots. *Nano Communication Networks*, 3(2):83–102.

[Hooge and Hoppenbrouwers, 1969] Hooge, F. and Hoppenbrouwers, A. (1969). Amplitude distribution of 1/f noise. *Physica*, 42(3):331–339.

[Horesh et al., 2011] Horesh, M., Lidich, N., Yitzchaik, S., and Hanein, Y. (2011). A temperature-differential affinity biosensor: Model and d-optimal performance limits. *IEEE Sensors Journal*, 11(9):2007–2015.

[Huang and Wan, 2009] Huang, J. and Wan, Q. (2009). Gas sensors based on semiconducting metal oxide one-dimensional nanostructures. *Sensors*, 9(12):9903–9924.

[Huidobro et al., 2012] Huidobro, P. A., Nikitin, A. Y., González-Ballestero, C., Martín-Moreno, L., and García-Vidal, F. J. (2012). Superradiance mediated by graphene surface plasmons. *Physical Review B*, 85(15):155438.

[Hwang et al., 2009] Hwang, J., Pototschnig, M., Lettow, R., Zumofen, G., Renn, A., Götzinger, S., and Sandoghdar, V. (2009). A single-molecule optical transistor. *Nature*, 460(7251):76–80.

[Ibraheem and Campbell, 2010] Ibraheem, A. and Campbell, R. E. (2010). Designs and applications of fluorescent protein-based biosensors. *Current opinion in chemical biology*, 14(1):30–36.

[Im Jun et al., 2000] Im Jun, S., Lee, J. W., Sakamoto, S., Yamaguchi, K., and Kim, K. (2000). Rotaxane-based molecular switch with fluorescence signaling. *Tetrahedron Letters*, 41(4):471–475.

[Jablan et al., 2013] Jablan, M., Soljačić, M., and Buljan, H. (2013). Plasmons in graphene: fundamental properties and potential applications. *Proceedings of the IEEE*, 101(7):1689–1704.

[Jaffrezic-Renault and Dzyadevych, 2008] Jaffrezic-Renault, N. and Dzyadevych, S. V. (2008). Conductometric microbiosensors for environmental monitoring. *Sensors*, 8(4):2569–2588.

[Jain and Alam, 2014] Jain, A. and Alam, M. A. (2014). Intrinsic low pass filtering improves signal-to-noise ratio in critical-point flexure biosensors. *Applied Physics Letters*, 105(8):084106.

[Jain et al., 2012] Jain, A., Nair, P. R., and Alam, M. A. (2012). Flexure-fet biosensor to break the fundamental sensitivity limits of nanobiosensors using nonlinear electromechanical coupling. *Proceedings of the National Academy of Sciences*, 109(24):9304–9308.

[Jares-Erijman and Jovin, 2003] Jares-Erijman, E. A. and Jovin, T. M. (2003). Fret imaging. *Nature biotechnology*, 21(11):1387–1395.

[Jayant et al., 2013] Jayant, K., Auluck, K., Funke, M., Anwar, S., Phelps, J. B., Gordon, P. H., Rajwade, S. R., and Kan, E. C. (2013). Programmable ion-sensitive transistor interfaces. ii. biomolecular sensing and manipulation. *Physical Review E*, 88(1):012802.

[Jokić et al., 2012] Jokić, I., Djurić, Z., Frantlović, M., Radulović, K., Krstajić, P., and Jokić, Z. (2012). Fluctuations of the number of adsorbed molecules in biosensors due to stochastic adsorption–desorption processes coupled with mass transfer. *Sensors and Actuators B: Chemical*, 166:535–543.

[Joo et al., 2008] Joo, C., Balci, H., Ishitsuka, Y., Buranachai, C., and Ha, T. (2008). Advances in single-molecule fluorescence methods for molecular biology. *Annu. Rev. Biochem.*, 77:51–76.

[Jornet and Akyildiz, 2013] Jornet, J. M. and Akyildiz, I. F. (2013). Graphene-based plasmonic nano-antenna for terahertz band communication in nanonetworks. *IEEE Journal on selected areas in communications*, 31(12):685–694.

[Kaizu et al., 2014] Kaizu, K., de Ronde, W., Paijmans, J., Takahashi, K., Tostevin, F., and ten Wolde, P. R. (2014). The berg-purcell limit revisited. *Biophysical journal*, 106(4):976–985.

[Karsenty et al., 2014] Karsenty, M., Rubin, S., and Bercovici, M. (2014). Acceleration of surface-based hybridization reactions using isotachophoretic focusing. *Analytical chemistry*, 86(6):3028–3036.

[Kawata and Kawata, 2000] Kawata, S. and Kawata, Y. (2000). Three-dimensional optical data storage using photochromic materials. *Chemical reviews*, 100(5):1777–1788.

[Keshner, 1982] Keshner, M. S. (1982). 1/f noise. *Proceedings of the IEEE*, 70(3):212–218.

[Kilinc and Akan, 2013] Kilinc, D. and Akan, O. B. (2013). Receiver design for molecular communication. *IEEE Journal on Selected Areas in Communications*, 31(12):705–714.

[Kim et al., 2013] Kim, B., Song, H. S., Jin, H. J., Park, E. J., Lee, S. H., Lee, B. Y., Park, T. H., and Hong, S. (2013). Highly selective and sensitive detection of neurotransmitters using receptor-modified single-walled carbon nanotube sensors. *Nanotechnology*, 24(28):285501.

[Kim et al., 2015] Kim, N.-R., Farsad, N., Chae, C.-B., and Eckford, A. W. (2015). A universal channel model for molecular communication systems with metal-oxide detectors. In *Communications (ICC), 2015 IEEE International Conference on*, pages 1054–1059. IEEE.

[Kinosita Jr et al., 1987] Kinosita Jr, K., Kouyama, T., and Ikegami, A. (1987). Criteria for the rapid diffusion limit of fluorescence energy transfer. *The Journal of chemical physics*, 86(6):3273–3282.

[Kobayashi et al., 1998] Kobayashi, H., Kubota, T., Kawa, H., Nakato, Y., and Nishiyama, M. (1998). Oxide thickness dependence of energy shifts in the si 2p levels for the sio 2/si structure, and its elimination by a palladium overlayer. *Applied physics letters*, 73(7):933–935.

[Kochmann et al., 2012] Kochmann, S., Hirsch, T., and Wolfbeis, O. S. (2012). Graphenes in chemical sensors and biosensors. *TrAC Trends in Analytical Chemistry*, 39:87–113.

[Komarala et al., 2008] Komarala, V. K., Bradley, A. L., Rakovich, Y. P., Byrne, S. J., Gun?ko, Y. K., and Rogach, A. L. (2008). Surface plasmon enhanced förster resonance energy transfer between the cdte quantum dots. *Applied Physics Letters*, 93(12):123102.

[Koncki, 2007] Koncki, R. (2007). Recent developments in potentiometric biosensors for biomedical analysis. *Analytica chimica acta*, 599(1):7–15.

[Kulkarni and Zhong, 2012] Kulkarni, G. S. and Zhong, Z. (2012). Detection beyond the debye screening length in a high-frequency nanoelectronic biosensor. *Nano letters*, 12(2):719–723.

[Kuran et al., 2011] Kuran, M. S., Yilmaz, H. B., Tugcu, T., and Akyildiz, I. F. (2011). Modulation techniques for communication via diffusion in nanonetworks. In *Communications (ICC), 2011 IEEE International Conference on*, pages 1–5. IEEE.

[Kurian et al., 2005] Kurian, A., George, S. D., Nampoori, V., and Vallabhan, C. (2005). Study on the determination of molecular distance in organic dye mixtures using dual beam thermal lens technique. *Spectrochimica Acta Part A: Molecular and Biomolecular Spectroscopy*, 61(13):2799–2802.

[Kuscu, 2014] Kuscu, M. (2014). An information-theoretic model and analysis of graphene plasmon-assisted fret-based nanocommunication channel. In *Proceedings of ACM The First Annual International Conference on Nanoscale Computing and Communication*, page 8. ACM.

[Kuscu and Akan, 2011] Kuscu, M. and Akan, O. B. (2011). A nanoscale communication channel with fluorescence resonance energy transfer (fret). In *Computer Communications Workshops (INFOCOM WKSHPS), 2011 IEEE Conference on*, pages 425–430. IEEE.

[Kuscu and Akan, 2012] Kuscu, M. and Akan, O. B. (2012). A physical channel model and analysis for nanoscale molecular communications with förster resonance energy transfer (fret). *IEEE Transactions on Nanotechnology*, 11(1):200–207.

[Kuscu and Akan, 2013a] Kuscu, M. and Akan, O. B. (2013a). Fret-based mobile molecular nanonetworks. In *Ad Hoc Networking Workshop (MED-HOC-NET), 2013 12th Annual Mediterranean*, pages 120–127. IEEE.

[Kuscu and Akan, 2013b] Kuscu, M. and Akan, O. B. (2013b). Multi-step fret-based long-range nanoscale communication channel. *IEEE Journal on Selected Areas in Communications*, 31(12):715–725.

[Kuscu and Akan, 2014a] Kuscu, M. and Akan, O. B. (2014a). A communication theoretical analysis of fret-based mobile ad hoc molecular nanonetworks. *IEEE transactions on nanobioscience*, 13(3):255–266.

[Kuscu and Akan, 2014b] Kuscu, M. and Akan, O. B. (2014b). Coverage and throughput analysis for fret-based mobile molecular sensor/actor nanonetworks. *Nano Communication Networks*, 5(1):45–53.

[Kuscu and Akan, 2014c] Kuscu, M. and Akan, O. B. (2014c). Fret-based nanoscale point-to-point and broadcast communications with multi-exciton transmission and channel routing. *IEEE transactions on nanobioscience*, 13(3):315–326.

[Kuscu and Akan, 2015] Kuscu, M. and Akan, O. B. (2015). Modeling and analysis of sinw biofet as molecular antenna for bio-cyber interfaces towards the internet of bio-nanothings. In *Internet of Things (WF-IoT), 2015 IEEE 2nd World Forum on*, pages 669–674. IEEE.

[Kuscu and Akan, 2016a] Kuscu, M. and Akan, O. B. (2016a). The internet of molecular things based on fret. *IEEE Internet of Things Journal*, 3(1):4–17.

[Kuscu and Akan, 2016b] Kuscu, M. and Akan, O. B. (2016b). Modeling and analysis of sinw fet-based molecular communication receiver. *IEEE Transactions on Communications*, 64(9):3708–3721.

[Kuscu and Akan, 2016c] Kuscu, M. and Akan, O. B. (2016c). On the physical design of molecular communication receiver based on nanoscale biosensors. *IEEE Sensors Journal*, 16(8):2228–2243.

[Kuscu et al., 2015] Kuscu, M., Kiraz, A., and Akan, O. B. (2015). Fluorescent molecules as transceiver nanoantennas: The first practical and high-rate information transfer over a nanoscale communication channel based on fret. *Scientific reports*, 5:7831.

[LaBoda et al., 2014] LaBoda, C., Duschl, H., and Dwyer, C. L. (2014). Dna-enabled integrated molecular systems for computation and sensing. *Accounts of chemical research*, 47(6):1816–1824.

[Lakowicz, 1999] Lakowicz, J. R. (1999). *Principles of Fluorescence Spectroscopy*. Kluwer Academic/Plenum Publishers, second edition.

[Landheer et al., 2005] Landheer, D., Aers, G., McKinnon, W., Deen, M., and Ranuarez, J. (2005). Model for the field effect from layers of biological macromolecules on the gates of metal-oxide-semiconductor transistors. *Journal of applied physics*, 98(4):044701.

[Lee et al., 2008] Lee, J.-O., So, H.-M., Jeon, E.-K., Chang, H., Won, K., and Kim, Y. H. (2008). Aptamers as molecular recognition elements for electrical nanobiosensors. *Analytical and bioanalytical chemistry*, 390(4):1023–1032.

[Li et al., 2011] Li, J., Zhang, Y., To, S., You, L., and Sun, Y. (2011). Effect of nanowire number, diameter, and doping density on nano-fet biosensor sensitivity. *ACS nano*, 5(8):6661–6668.

[Li et al., 2005] Li, Y., Li, H., Li, Y., Liu, H., Wang, S., He, X., Wang, N., and Zhu, D. (2005). Energy transfer switching in a bistable molecular machine. *Organic letters*, 7(22):4835–4838.

[Li et al., 2007] Li, Y., Zheng, H., Li, Y., Wang, S., Wu, Z., Liu, P., Gao, Z., Liu, H., and Zhu, D. (2007). Photonic logic gates based on control of fret by a solvatochromic perylene bisimide. *The Journal of organic chemistry*, 72(8):2878–2885.

[Lin and Yan, 2012] Lin, P. and Yan, F. (2012). Organic thin-film transistors for chemical and biological sensing. *Advanced materials*, 24(1):34–51.

[Llatser et al., 2011] Llatser, I., Alarcón, E., and Pierobony, M. (2011). Diffusion-based channel characterization in molecular nanonetworks. In *Computer Communications Workshops (INFOCOM WKSHPS), 2011 IEEE Conference on*, pages 467–472. IEEE.

[Llatser et al., 2014] Llatser, I., Demiray, D., Cabellos-Aparicio, A., Altilar, D. T., and Alarcón, E. (2014). N3sim: Simulation framework for diffusion-based molecular communication nanonetworks. *Simulation Modelling Practice and Theory*, 42:210–222.

[Lu and Zhang, 2008] Lu, J.-Q. and Zhang, X.-G. (2008). Nucleotide capacitance calculation for dna sequencing. *Biophysical journal*, 95(9):L60–L62.

[Lu et al., 2013] Lu, N., Gao, A., Dai, P., Li, T., Wang, Y., Gao, X., Song, S., Fan, C., and Wang, Y. (2013). Ultra-sensitive nucleic acids detection with electrical nanosensors based on cmos-compatible silicon nanowire field-effect transistors. *Methods*, 63(3):212–218.

[Luo et al., 2013] Luo, X., Qiu, T., Lu, W., and Ni, Z. (2013). Plasmons in graphene: recent progress and applications. *Materials Science and Engineering: R: Reports*, 74(11):351–376.

[Luzi et al., 2003] Luzi, E., Minunni, M., Tombelli, S., and Mascini, M. (2003). New trends in affinity sensing: aptamers for ligand binding. *TrAC Trends in Analytical Chemistry*, 22(11):810–818.

[Maehashi and Matsumoto, 2009] Maehashi, K. and Matsumoto, K. (2009). Label-free electrical detection using carbon nanotube-based biosensors. *Sensors*, 9(7):5368–5378.

[Mal et al., 2003] Mal, N. K., Fujiwara, M., and Tanaka, Y. (2003). Photocontrolled reversible release of guest molecules from coumarin-modified mesoporous silica. *Nature*, 421(6921):350–353.

[Marzen et al., 2013] Marzen, S., Garcia, H. G., and Phillips, R. (2013). Statistical mechanics of monod–wyman–changeux (mwc) models. *Journal of molecular biology*, 425(9):1433–1460.

[Matsumoto and Miyahara, 2013] Matsumoto, A. and Miyahara, Y. (2013). Current and emerging challenges of field effect transistor based bio-sensing. *Nanoscale*, 5(22):10702–10718.

[Medintz et al., 2003] Medintz, I. L., Clapp, A. R., Mattoussi, H., Goldman, E. R., Fisher, B., and Mauro, J. M. (2003). Self-assembled nanoscale biosensors based on quantum dot fret donors. *Nature materials*, 2(9):630–638.

[Meng et al., 2012] Meng, L.-S., Yeh, P.-C., Chen, K.-C., and Akyildiz, I. F. (2012). Mimo communications based on molecular diffusion. In *Global Communications Conference (GLOBECOM), 2012 IEEE*, pages 5380–5385. IEEE.

[Meng et al., 2014] Meng, L.-S., Yeh, P.-C., Chen, K.-C., and Akyildiz, I. F. (2014). On receiver design for diffusion-based molecular communication. *IEEE Transactions on Signal Processing*, 62(22):6032–6044.

[Milotti, 2002] Milotti, E. (2002). 1/f noise: a pedagogical review. *arXiv preprint physics/0204033*.

[Ming et al., 2012] Ming, T., Chen, H., Jiang, R., Li, Q., and Wang, J. (2012). Plasmon-controlled fluorescence: beyond the intensity enhancement. *The Journal of Physical Chemistry Letters*, 3(2):191–202.

[Nair and Alam, 2007] Nair, P. R. and Alam, M. A. (2007). Design considerations of silicon nanowire biosensors. *IEEE Transactions on Electron Devices*, 54(12):3400–3408.

[Nair and Alam, 2008] Nair, P. R. and Alam, M. A. (2008). Screening-limited response of nanobiosensors. *Nano letters*, 8(5):1281–1285.

[Nakano et al., 2012] Nakano, T., Moore, M. J., Wei, F., Vasilakos, A. V., and Shuai, J. (2012). Molecular communication and networking: Opportunities and challenges. *IEEE transactions on nanobioscience*, 11(2):135–148.

[Nakano et al., 2005] Nakano, T., Suda, T., Moore, M., Egashira, R., Enomoto, A., and Arima, K. (2005). Molecular communication for nanomachines using intercellular calcium signaling. In *Nanotechnology, 2005. 5th IEEE Conference on*, pages 478–481. IEEE.

[Nakano et al., 2014] Nakano, T., Suda, T., Okaie, Y., Moore, M. J., and Vasilakos, A. V. (2014). Molecular communication among biological nanomachines: A layered architecture and research issues. *IEEE transactions on nanobioscience*, 13(3):169–197.

[Newman, 2002] Newman, M. E. (2002). Spread of epidemic disease on networks. *Physical review E*, 66(1):016128.

[Niemann et al., 2013] Niemann, M., Kantz, H., and Barkai, E. (2013). Fluctuations of 1/f noise and the low-frequency cutoff paradox. *Physical review letters*, 110(14):140603.

[Noel et al., 2014a] Noel, A., Cheung, K. C., and Schober, R. (2014a). Improving receiver performance of diffusive molecular communication with enzymes. *IEEE Transactions on NanoBioscience*, 13(1):31–43.

[Noel et al., 2014b] Noel, A., Cheung, K. C., and Schober, R. (2014b). Optimal receiver design for diffusive molecular communication with flow and additive noise. *IEEE transactions on nanobioscience*, 13(3):350–362.

[Okada et al., 1990] Okada, M., Watanabi, T., Imamura, K., Tsurumi, T., Suma, Y., and Sakai, K. (1990). Ionic strength affects diffusive permeability to an inorganic phosphate ion of negatively charged dialysis membranes. *ASAIO Journal*, 36(3):M324–326.

[Park et al., 2012] Park, S. J., Kwon, O. S., Lee, S. H., Song, H. S., Park, T. H., and Jang, J. (2012). Ultrasensitive flexible graphene based field-effect transistor (fet)-type bioelectronic nose. *Nano letters*, 12(10):5082–5090.

[Patolsky and Lieber, 2005] Patolsky, F. and Lieber, C. M. (2005). Nanowire nanosensors. *Materials today*, 8(4):20–28.

[Pawlicki et al., 2009] Pawlicki, M., Collins, H. A., Denning, R. G., and Anderson, H. L. (2009). Two-photon absorption and the design of two-photon dyes. *Angewandte Chemie International Edition*, 48(18):3244–3266.

[Pease et al., 2001] Pease, A. R., Jeppesen, J. O., Stoddart, J. F., Luo, Y., Collier, C. P., and Heath, J. R. (2001). Switching devices based on interlocked molecules. *Accounts of chemical research*, 34(6):433–444.

[Perumal and Hashim, 2014] Perumal, V. and Hashim, U. (2014). Advances in biosensors: Principle, architecture and applications. *Journal of Applied Biomedicine*, 12(1):1–15.

[Petrov et al., 2015] Petrov, V., Moltchanov, D., Balasubramaniam, S., and Koucheryavy, Y. (2015). Incorporating bacterial properties for plasmid delivery in nano sensor networks. *IEEE Transactions on Nanotechnology*, 14(4):751–760.

[Pierobon and Akyildiz, 2011] Pierobon, M. and Akyildiz, I. F. (2011). Noise analysis in ligand-binding reception for molecular communication in nanonetworks. *IEEE Transactions on Signal Processing*, 59(9):4168–4182.

[Pierobon and Akyildiz, 2012] Pierobon, M. and Akyildiz, I. F. (2012). Intersymbol and co-channel interference in diffusion-based molecular communication. In *Communications (ICC), 2012 IEEE International Conference on*, pages 6126–6131. IEEE.

[Pierobon and Akyildiz, 2013] Pierobon, M. and Akyildiz, I. F. (2013). Capacity of a diffusion-based molecular communication system with channel memory and molecular noise. *IEEE Transactions on Information Theory*, 59(2):942–954.

[Pierobon and Akyildiz, 2014] Pierobon, M. and Akyildiz, I. F. (2014). A statistical–physical model of interference in diffusion-based molecular nanonetworks. *IEEE Transactions on communications*, 62(6):2085–2095.

[Pinto da Silva and Esteves da Silva, 2012] Pinto da Silva, L. and Esteves da Silva, J. C. (2012). Firefly chemiluminescence and bioluminescence: efficient generation of excited states. *ChemPhysChem*, 13(9):2257–2262.

[Pischel et al., 2013] Pischel, U., Andréasson, J., Gust, D., and Pais, V. F. (2013). Information processing with molecules?quo vadis? *ChemPhysChem*, 14(1):28–46.

[Poghossian and Schöning, 2014] Poghossian, A. and Schöning, M. J. (2014). Label-free sensing of biomolecules with field-effect devices for clinical applications. *Electroanalysis*, 26(6):1197–1213.

[Proakis and Salehi, 2007] Proakis, J. and Salehi, M. (2007). *Digital Communications, 5th Edition*. McGraw-Hill Science/Engineering/Math, 5th edition.

[Quentmeier et al., 2008] Quentmeier, S., Denicke, S., Ehlers, J.-E., Niesner, R. A., and Gericke, K.-H. (2008). Two-color two-photon excitation using femtosecond laser pulses. *The Journal of Physical Chemistry B*, 112(18):5768–5773.

[Rajan, 2013] Rajan, N. K. (2013). *Limit of detection of silicon bioFETs*. Yale University.

[Rajan et al., 2014] Rajan, N. K., Brower, K., Duan, X., and Reed, M. A. (2014). Limit of detection of field effect transistor biosensors: Effects of surface modification and size dependence. *Applied Physics Letters*, 104(8):084106.

[Rajan et al., 2013] Rajan, N. K., Duan, X., and Reed, M. A. (2013). Performance limitations for nanowire/nanoribbon biosensors. *Wiley Interdisciplinary Reviews: Nanomedicine and Nanobiotechnology*, 5(6):629–645.

[Rajan et al., 2010a] Rajan, N. K., Routenberg, D. A., Chen, J., and Reed, M. A. (2010a). 1/f noise of silicon nanowire biofets. *IEEE Electron Device Letters*, 31(6):615–617.

[Rajan et al., 2010b] Rajan, N. K., Routenberg, D. A., Chen, J., and Reed, M. A. (2010b). Temperature dependence of 1/f noise mechanisms in silicon nanowire biochemical field effect transistors. *Applied physics letters*, 97(24):243501.

[Rajan et al., 2011] Rajan, N. K., Routenberg, D. A., and Reed, M. A. (2011). Optimal signal-to-noise ratio for silicon nanowire biochemical sensors. *Applied physics letters*, 98(26):264107.

[Ramachandra et al., 2011] Ramachandra, S., Schuermann, K. C., Cucinotta, F., Calzaferri, G., De Cola, L., et al. (2011). Förster resonance energy transfer in quantum dot–dye-loaded zeolite l nanoassemblies. *Small*, 7(10):1488–1494.

[Rasnik et al., 2006] Rasnik, I., McKinney, S. A., and Ha, T. (2006). Nonblinking and long-lasting single-molecule fluorescence imaging. *Nature methods*, 3(11):891–894.

[Raymo and Giordani, 2001] Raymo, F. M. and Giordani, S. (2001). Signal processing at the molecular level. *Journal of the American Chemical Society*, 123(19):4651–4652.

[Raymo and Tomasulo, 2005] Raymo, F. M. and Tomasulo, M. (2005). Electron and energy transfer modulation with photochromic switches. *Chemical Society Reviews*, 34(4):327–336.

[Ritz et al., 2002] Ritz, T., Damjanović, A., and Schulten, K. (2002). The quantum physics of photosynthesis. *ChemPhysChem*, 3(3):243–248.

[Rogers, 2000] Rogers, K. R. (2000). Principles of affinity-based biosensors. *Molecular biotechnology*, 14(2):109–129.

[Ronkainen et al., 2010] Ronkainen, N. J., Halsall, H. B., and Heineman, W. R. (2010). Electrochemical biosensors. *Chemical Society Reviews*, 39(5):1747–1763.

[Roy et al., 2008] Roy, R., Hohng, S., and Ha, T. (2008). A practical guide to single-molecule fret. *Nature methods*, 5(6):507–516.

[Sadik et al., 2009] Sadik, O. A., Aluoch, A. O., and Zhou, A. (2009). Status of biomolecular recognition using electrochemical techniques. *Biosensors and Bioelectronics*, 24(9):2749–2765.

[Samia et al., 2003] Samia, A. C., Chen, X., and Burda, C. (2003). Semiconductor quantum dots for photodynamic therapy. *Journal of the American Chemical Society*, 125(51):15736–15737.

[Sarkar et al., 2014] Sarkar, D., Liu, W., Xie, X., Anselmo, A. C., Mitragotri, S., and Banerjee, K. (2014). Mos2 field-effect transistor for next-generation label-free biosensors. *ACS nano*, 8(4):3992–4003.

[Scheller et al., 2001] Scheller, F. W., Wollenberger, U., Warsinke, A., and Lisdat, F. (2001). Research and development in biosensors. *Current Opinion in Biotechnology*, 12(1):35–40.

[Schöning and Poghossian, 2002] Schöning, M. J. and Poghossian, A. (2002). Recent advances in biologically sensitive field-effect transistors (biofets). *Analyst*, 127(9):1137–1151.

[Senveli and Tigli, 2013] Senveli, S. U. and Tigli, O. (2013). Biosensors in the small scale: methods and technology trends. *IET nanobiotechnology*, 7(1):7–21.

[ShahMohammadian et al., 2013] ShahMohammadian, H., Messier, G. G., and Magierowski, S. (2013). Modelling the reception process in diffusion-based molecular communication channels. In *Communications Workshops (ICC), 2013 IEEE International Conference on*, pages 782–786. IEEE.

[Sheehan and Whitman, 2005] Sheehan, P. E. and Whitman, L. J. (2005). Detection limits for nanoscale biosensors. *Nano letters*, 5(4):803–807.

[Shoorideh and Chui, 2014] Shoorideh, K. and Chui, C. O. (2014). On the origin of enhanced sensitivity in nanoscale fet-based biosensors. *Proceedings of the National Academy of Sciences*, 111(14):5111–5116.

[Shorokhov et al., 2011] Shorokhov, V., Soldatov, E., and Gubin, S. (2011). Self-capacitance of nanosized objects. *Journal of Communications Technology and Electronics*, 56(3):326–341.

[Singhal et al., 2015] Singhal, A., Mallik, R. K., and Lall, B. (2015). Performance analysis of amplitude modulation schemes for diffusion-based molecular communication. *IEEE Transactions on Wireless Communications*, 14(10):5681–5691.

[Song et al., 2014] Song, H. S., Jin, H. J., Ahn, S. R., Kim, D., Lee, S. H., Kim, U.-K., Simons, C. T., Hong, S., and Park, T. H. (2014). Bioelectronic tongue using heterodimeric human taste receptor for the discrimination of sweeteners with human-like performance. *ACS nano*, 8(10):9781–9789.

[Song et al., 2008] Song, S., Wang, L., Li, J., Fan, C., and Zhao, J. (2008). Aptamer-based biosensors. *TrAC Trends in Analytical Chemistry*, 27(2):108–117.

[Southward and Surette, 2002] Southward, C. M. and Surette, M. G. (2002). The dynamic microbe: green fluorescent protein brings bacteria to light. *Molecular microbiology*, 45(5):1191–1196.

[Stein et al., 2011] Stein, I. H., Steinhauer, C., and Tinnefeld, P. (2011). Single-molecule four-color fret visualizes energy-transfer paths on dna origami. *Journal of the American Chemical Society*, 133(12):4193–4195.

[Stern et al., 2007] Stern, E., Wagner, R., Sigworth, F. J., Breaker, R., Fahmy, T. M., and Reed, M. A. (2007). Importance of the debye screening length on nanowire field effect transistor sensors. *Nano letters*, 7(11):3405–3409.

[Stryer, 1978] Stryer, L. (1978). Fluorescence energy transfer as a spectroscopic ruler. *Annual review of biochemistry*, 47(1):819–846.

[Stryer et al., 1982] Stryer, L., Thomas, D. D., and Meares, C. F. (1982). Diffusion-enhanced fluorescence energy transfer. *Annual review of biophysics and bioengineering*, 11(1):203–222.

[Sze and Ng, 2006] Sze, S. M. and Ng, K. K. (2006). *Physics of semiconductor devices*. John wiley & sons.

[Tallini et al., 2002] Tallini, L. G., Al-Bassam, S., and Bose, B. (2002). On the capacity and codes for the z-channel. In *Information Theory, 2002. Proceedings. 2002 IEEE International Symposium on*, page 422. IEEE.

[Tamayo et al., 2013] Tamayo, J., Kosaka, P. M., Ruz, J. J., San Paulo, Á., and Calleja, M. (2013). Biosensors based on nanomechanical systems. *Chemical Society Reviews*, 42(3):1287–1311.

[Thévenot et al., 2001] Thévenot, D. R., Toth, K., Durst, R. A., and Wilson, G. S. (2001). Electrochemical biosensors: recommended definitions and classification. *Biosensors and Bioelectronics*, 16(1):121–131.

[Thomas et al., 1978] Thomas, D. D., Carlsen, W. F., and Stryer, L. (1978). Fluorescence energy transfer in the rapid-diffusion limit. *Proceedings of the National Academy of Sciences*, 75(12):5746–5750.

[Tian et al., 2010] Tian, B., Cohen-Karni, T., Qing, Q., Duan, X., Xie, P., and Lieber, C. M. (2010). Three-dimensional, flexible nanoscale field-effect transistors as localized bioprobes. *Science*, 329(5993):830–834.

[Tisler et al., 2011] Tisler, J., Reuter, R., La?mmle, A., Jelezko, F., Balasubramanian, G., Hemmer, P. R., Reinhard, F., and Wrachtrup, J. (2011). Highly efficient fret from a single nitrogen-vacancy center in nanodiamonds to a single organic molecule. *ACS nano*, 5(10):7893–7898.

[Toppari et al., 2013] Toppari, J. J., Wirth, J., Garwe, F., Stranik, O., Csaki, A., Bergmann, J., Paa, W., and Fritzsche, W. (2013). Plasmonic coupling and long-range transfer of an excitation along a dna nanowire. *ACS nano*, 7(2):1291–1298.

[Torsi et al., 2013] Torsi, L., Magliulo, M., Manoli, K., and Palazzo, G. (2013). Organic field-effect transistor sensors: a tutorial review. *Chemical Society Reviews*, 42(22):8612–8628.

[Tsai, 2007] Tsai, C. S. (2007). *Biomacromolecules: Introduction to structure, function and informatics*. John Wiley & Sons.

[Tsujioka and Kondo, 2003] Tsujioka, T. and Kondo, H. (2003). Organic bistable molecular memory using photochromic diarylethene. *Applied physics letters*, 83(5):937–939.

[Unluturk et al., 2015] Unluturk, B. D., Bicen, A. O., and Akyildiz, I. F. (2015). Genetically engineered bacteria-based biotransceivers for molecular communication. *IEEE Transactions on Communications*, 63(4):1271–1281.

[Van Amerongen et al., 2000] Van Amerongen, H., Van Grondelle, R., and Valkunas, L. (2000). *Photosynthetic excitons*. World Scientific.

[Velizhanin and Efimov, 2011] Velizhanin, K. A. and Efimov, A. (2011). Probing plasmons in graphene by resonance energy transfer. *Physical Review B*, 84(8):085401.

[Velizhanin and Shahbazyan, 2012] Velizhanin, K. A. and Shahbazyan, T. V. (2012). Long-range plasmon-assisted energy transfer over doped graphene. *Physical Review B*, 86(24):245432.

[Vogel et al., 2006] Vogel, S. S., Thaler, C., and Koushik, S. V. (2006). Fanciful fret. *Sci. STKE*, 2006(331):re2–re2.

[Vuojola and Soukka, 2014] Vuojola, J. and Soukka, T. (2014). Luminescent lanthanide reporters: new concepts for use in bioanalytical applications. *Methods and Applications in Fluorescence*, 2(1):012001.

[Wang et al., 2012] Wang, B., Stelzner, T., Dirawi, R., Assad, O., Shehada, N., Christiansen, S., and Haick, H. (2012). Field-effect transistors based on silicon nanowire arrays: effect of the good and the bad silicon nanowires. *ACS applied materials & interfaces*, 4(8):4251–4258.

[Wang et al., 2010] Wang, C.-X., Hong, X., Ge, X., Cheng, X., Zhang, G., and Thompson, J. (2010). Cooperative mimo channel models: A survey. *IEEE Communications Magazine*, 48(2).

[Wang, 1999] Wang, J. (1999). Amperometric biosensors for clinical and therapeutic drug monitoring: a review. *Journal of pharmaceutical and biomedical analysis*, 19(1):47–53.

[Wang, 2008] Wang, J. (2008). Electrochemical glucose biosensors. *Chemical reviews*, 108(2):814–825.

[Weiss and Littman, 1994] Weiss, A. and Littman, D. R. (1994). Signal transduction by lymphocyte antigen receptors. *Cell*, 76(2):263–274.

[Willner and Zayats, 2007] Willner, I. and Zayats, M. (2007). Electronic aptamer-based sensors. *Angewandte Chemie International Edition*, 46(34):6408–6418.

[Wunsch et al., 2006] Wunsch, B., Stauber, T., Sols, F., and Guinea, F. (2006). Dynamical polarization of graphene at finite doping. *New Journal of Physics*, 8(12):318.

[Yang et al., 2010] Yang, W., Ratinac, K. R., Ringer, S. P., Thordarson, P., Gooding, J. J., and Braet, F. (2010). Carbon nanomaterials in biosensors: should you use nanotubes or graphene? *Angewandte Chemie International Edition*, 49(12):2114–2138.

[Zheng et al., 2010] Zheng, G., Gao, X. P., and Lieber, C. M. (2010). Frequency domain detection of biomolecules using silicon nanowire biosensors. *Nano letters*, 10(8):3179–3183.

[Zheng et al., 2005] Zheng, G., Patolsky, F., Cui, Y., Wang, W. U., and Lieber, C. M. (2005). Multiplexed electrical detection of cancer markers with nanowire sensor arrays. *Nature biotechnology*, 23(10):1294–1301.

[Zhou et al., 2008] Zhou, Z., Yu, M., Yang, H., Huang, K., Li, F., Yi, T., and Huang, C. (2008). Fret-based sensor for imaging chromium (iii) in living cells. *Chemical Communications*, (29):3387–3389.